

8-2017

## A Numerical Study of the Interaction Between one Dimensional Carbyne Chain and Single Stranded DNA

Zeina Salman  
*University of Arkansas, Fayetteville*

Follow this and additional works at: <https://scholarworks.uark.edu/etd>



Part of the [Biophysics Commons](#), [Condensed Matter Physics Commons](#), and the [Molecular Biology Commons](#)

---

### Citation

Salman, Z. (2017). A Numerical Study of the Interaction Between one Dimensional Carbyne Chain and Single Stranded DNA. *Graduate Theses and Dissertations* Retrieved from <https://scholarworks.uark.edu/etd/2506>

This Dissertation is brought to you for free and open access by ScholarWorks@UARK. It has been accepted for inclusion in Graduate Theses and Dissertations by an authorized administrator of ScholarWorks@UARK. For more information, please contact [uarepos@uark.edu](mailto:uarepos@uark.edu).

A Numerical Study of the Interaction Between One Dimensional Carbyne Chain  
and Single Stranded DNA

A dissertation submitted in partial fulfillment  
of the requirements for the degree of  
Doctor of Philosophy in Microelectronics-Photonics

by

Zeina Salman  
University of Baghdad, 2003  
Master of Science in Physics  
University of Arkansas, 2014  
Master of Science in Physics

August 2017  
University of Arkansas

This dissertation is approved for recommendation to the Graduate Council.

---

Dr. Steve Tung  
Dissertation Director

---

Dr. Arun Nair  
Dissertation Co-Director

---

Dr. Jin Woo Kim  
Committee Member

---

Dr. Jali Li  
Committee Member

---

Dr. Rick Wise  
Ex-Officio Member

The following signatories attest that all software used in this dissertation was legally licensed for use by Zeina Salman for research purposes and publication.

---

Ms. Zeina Salman, Student

---

Dr. Steve Tung, Dissertation Director

---

Dr. Arun Nair, Dissertation Co-Director

This dissertation was submitted to <http://www.turnitin.com> for plagiarism review by the TurnItIn company's software. The signatories have examined the report on this dissertation that was returned by TurnItIn and attest that, in their opinion, the items highlighted by the software are incidental to common usage and are not plagiarized material.

---

Dr. Steve Tung, Dissertation Director

---

Dr. Arun Nair, Dissertation Co-Director

---

Dr. Rick Wise, Program Director

## ABSTRACT

The interactions between two-dimensional carbon-based materials and biomolecules have been an active area of research recently. Such interactions are beneficial in many applications such as biosensors and DNA sequencers. For such practical applications, the electrical response of the sensing elements to the presence of different ssDNA bases plays a crucial role, and it is affected by its interaction with different DNA bases. The width of the sensing element influences the spatial resolution at the single nucleotide level when developing DNA sequencers.

The purpose of this research was to numerically study the electrical properties associated with the interaction between 1D carbon chain, known as carbyne, and ssDNA. First, the electrical properties of the carbyne chain were calculated. Second, the electrical properties of the carbyne chain were calculated in the presence of different ssDNA bases. Analyzing the differences between the two cases led to determining the effects of these different bases on the electrical properties. The numerical simulation approach conducted in this research was based on the first-principle simulation. The first-principle simulation was based on using density functional theory (DFT) and non-equilibrium Green's functions (NEGF). The electrical properties investigated in this study included the density of states and the transmission probability functions that were used to calculate the electrical current. The study showed that the electrical response of the chain in the presence of each base is distinguishable. In particular, the chain current increased by 3.3  $\mu\text{A}$  in the presence of base A at 0.6 V. In contrast, the current decreased by 41.1  $\mu\text{A}$ , 14.7  $\mu\text{A}$ , and 25.6  $\mu\text{A}$  in the presence of bases C, T, and G, respectively. Moving bases A and C to different locations showed different electrical responses due to having O,  $\text{NH}_2$ , and CH at different distances from the chain. A force model was developed to describe the force interaction between the chain and these groups. The force trend showed a similar trend to the electrical current when compared at -0.85 V. Different

orientations of the bases influenced the electrical properties in a different way. For two different orientations, parallel and perpendicular to the chain axis, base A showed 0.0776 mA difference in the electrical current at 0.6 V. Base C, G, and T showed 0.0325 mA, 0.0426 mA, and 0.00305 mA difference, respectively. More importantly, this work contributes to the knowledge of the nano device based DNA sequencing technique and enables further progress toward ultrafast, low cost, label-free, and high-resolution DNA sequencing devices.

@2017 by Zeina Salman  
All Rights Reserved

## **ACKNOWLEDGMENTS**

Many thanks to my parents because I owe it all to them. Without their love, continuous support, and raising me the way they did, I would not have been the person who I have become. I am also grateful for having great siblings who never became tired of caring and motivating me along the way. I would like to thank my other family members and friends for helping and supporting while I was at the University of Arkansas.

Special thanks and sincere recognitions to my advisor, Dr. Steve Tung, and co-advisor, Dr. Arun Nair. I am very appreciative for your support, patience, and guidance through my PhD research at the University of Arkansas. You both have influenced my academic progress and professional career differently for which I will be grateful forever. You worked very hard with me in order for this dissertation to come into the way it is. Dr. Steve Tung, you have not only been my advisor but my mentor who have taught me life lessons. I was lucky to have an advisor as great as you are.

I would like to thank especially microEP director, Dr. Rick Wise, for his support and advice. I am thankful to the microEP management specialist, Renee Jones-Hearson, for her support and assistance along the way. I would like to thank Mrs. Tamara Snyder for her support and care that reminded me of my sister's love and support. Thanks to the physics department for their financial support while I worked as a teaching assistant for them. Thanks to the faculty, students, and staff at the University of Arkansas for their continuous help. Special thanks to AHPCC for their willingness to help even during the weekends. Thanks to all my friends from all countries whom I have been pleased to know. Thank you for your encouragement along the way.

## **DEDICATION**

To my parents who raised me to be an eager and motivated learner who has never become tired of facing new challenges



# TABLE OF CONTENTS

CHAPTER ONE: INTRODUCTION.....	1
1.1. Nanopore Sequencing.....	4
1.2. Carbon Based Materials.....	10
1.2.1 Graphene.....	11
1.2.2 Carbyne .....	15
1.3. Carbon Based Materials and ssDNA.....	21
1.3.1 Carbyne and ssDNA Bases.....	25
1.4. Primary Objectives of this Research.....	26
1.4.1 Specific Tasks .....	27
1.5. Dissertaion Organization .....	28
CHAPTER TWO: SIMULATION METHODS.....	29
2.1. First-Principle Simulation.....	29
2.1.1. Electron Transport in Nanoscale Devices .....	29
2.1.2. Density Functional Theory (DFT).....	30
2.1.3. Non-Equilibrium Green’s Function (NEGF) .....	32
2.1.4. Calculating the Electrical Current.....	33
2.1.4.1. Many Body States.....	33
2.1.4.2. DFT Functional.....	37
2.1.4.3. Pseudopotential.....	39
2.1.4.4. The Plane Waves Basis Set.....	42
2.1.5. DFT Simulation Using QUANTUM ESPRESSO and Wannier90 .....	47
2.1.6. Simulation Details .....	50

CHAPTER THREE: RESULTS AND DISCUSSION .....	53
3.1. First Principle Simulation .....	53
3.1.1. One-Dimensional Carbyne Chain .....	53
3.1.2. Atomic Carbon Chain as a Sensing Element for ssDNA.....	61
3.1.2.1. Current of chain/ssDNA at 0.6 V and -0.85 V.....	71
3.1.2.2. Carbyne/A Model.....	74
3.1.2.3. Carbyne/G Model.....	77
3.1.3. Orientations of the ssDNA Bases .....	82
3.1.3.1. Orientations of Base A.....	82
3.1.3.2. Parallel ssDNA Bases .....	90
3.1.4. Bases A and C at Different Locations from the Chain .....	102
3.1.4.1. Force Model .....	110
3.1.4.2. Current at 0.6 V.....	116
3.1.5. 1D Carbon Chain Between Graphene Nanoribbons .....	120
3.1.5.1. Control Model .....	120
3.1.5.2. 1D Carbon Chain Attached to Graphene Nanoribbons as a Sensing Element for ssDNA.....	127
3.1.6. Graphene and Carbyne.....	136
CHAPTER 4: CONCLUSION .....	149
CHAPTER 5: FUTURE WORK.....	153
REFERENCES .....	154
Appendix A:Example of Input File for QUANTUM ESPRESSO Caculations .....	167
Appendix B: Example of Input File for wannier90 calculations .....	169

Appendix C: Description of Research for Popular Publication .....	183
Appendix D: Executive Summary of Newly Created Intellectual Property .....	186
Appendix E: Potential Patent and Commercialization Aspects of Listed Intellectual Property Items.....	187
E.1. Patentability of Intellectual Property	
E.2. Commercialization Prospects	
E.3 Possible Prior Disclosure of IP	
Appendix F: Broader Impact of Research .....	188
F.1. Applicability of Research Methods to Other Problems.....	188
F.2. Impact of Research Results on U.S. and Global Society.....	188
F.3. Impact of Research Results on the Environment.....	189
Appendix G: Microsoft Project for Ph.D. MicroEP Degree Plan.....	190
Appendix H: Identification of All Software Used in Research and Dissertation Generation .	193
Appendix I: All Publications Published, Submitted and Planned.....	195
Appendix J: Research Abstract in Arabic.....	196

## LIST OF FIGURES

Figure 1.1. Cost per genome accessed from National Human Genome Research Institute.....	2
Figure 1.2. Cost of sequencing million bases using different nanoscale techniques. Red represents the cost in dollars per mega base.....	4
Figure 1.3. Schematic of dsDNA showing the spacing between two sequential base pairs.....	5
Figure 1.4. Schematics of ssDNA showing the different DNA bases.....	5
Figure 1.5. Sensing modality based on charges transport (a) Ionic current as a sensing modality (b) Tunneling current as a sensing modality (c) Transverse current along one single electrode as a sensing modality.....	7
Figure 1.6. Schematic of 3D view of the sensing modality based on charges transport through the sensing element .....	8
Figure 1.7. Schematics of carbon based materials include SWCNT, graphene, and carbyne chain.....	11
Figure 1.8. Graphene sheet showing zigzag and armchair configurations where brown spheres are carbon atoms, blue bonds represent zigzag configurations, and orange bonds represent armchair configurations.....	13
Figure 1.9. Schematics of carbyne composed of 1D chain of carbon atoms. Top sketch is polyyne with alternating single and triple bonds and bottom sketch is cumulene with double bonds.....	16
Figure 1.10. $\sigma$ and $\pi$ bonds are extended along orbitals s and p.....	17
Figure 1.11. Schematics of $\sigma$ bonds and $\pi$ bonds between atoms.....	17
Figure 1.12. Schematics of an example of the simulated models and 3D view of a carbyne DNA sequencer.....	26
Figure 2.1. Schematics of Bloch, Wannier, and the localized states. Black dots represent the lattice vectors. Dashed orange line represents the envelop.....	43
Figure 2.2. Work flow of the simulation process using QE and wannier90 codes.....	51
Figure 3.1. Schematic of the control model (polyyne) that is a chain of 16 carbon atoms along the x direction.....	53
Figure 3.2. Schematic of the control model (polyyne) chain after the relaxation process.....	55

Figure 3.3. Transmission probability functions and DOS at positive and negative energies for the control model.....	56
Figure 3.4. I-V characteristics and electrical conductivity for the control model at positive and negative biasing voltages. ....	59
Figure 3.5. Schematics of the chain/A simulated model systems (top and side views). Schematics of the side view of bases C, G, and T. Gray spheres are the carbon atoms, red are the oxygen, yellow are the phosphorus, light purple are the nitrogen, and the white spheres are the hydrogen atoms .....	63
Figure 3.6. DOS for the chain/ssDNA simulated model systems compared with the control model.....	64
Figure 3.7. The transmission probability functions for the chain/ssDNA simulated model systems compared with the control model.....	64
Figure 3.8. I-V characteristics of the chain/ssDNA model systems compared with the control model at positive and negative biasing voltages .....	65
Figure 3.9. I-V curves for the different simulated models at the positive biasing voltages.....	67
Figure 3.10. The current at 0.6 V for the chain/ssDNA model systems compared with the control model.....	71
Figure 3.11. Change in the current for chain/ssDNA model systems compared with the control model at 0.6 V. Negative numbers refer to a decrease in the electrical current. The blue line is the chain current at 0.6 V (0.1225 mA).....	72
Figure 3.12 (a) Current for the chain/ssDNA model systems compared with the control model at -0.85 V (b) The percentage of change in the chain current with respect to the control model .....	73
Figure 3.13. (a)Transmission probability functions and (b) DOS for chain/A compared with the control model at positive and negative biasing voltages .....	75
Figure 3.14. I-V characteristics of the chain/A model with the base normal to the chain compared with the control model at positive and negative biasing voltages .....	76
Figure 3.15. (a) Transmission probability and (b) DOS for the chain/G model compared with the control model .....	78
Figure 3.16. I-V characteristics of the carbyne/G model with the base normal to the chain compared with the control model at positive and negative biasing voltages .....	80
Figure 3.17. Schematics of the three models for oriented base A.....	82

Figure 3.18. DOS for the models with base A at three different orientations.....	84
Figure 3.19. Transmission probability functions for the models with base A at three different orientations.....	84
Figure 3.20. I-V characteristics for the carbyne/A model at three different orientations with respect to the chain compared with the control model.....	85
Figure 3.21. Geometrical arrangements for $\pi$ - $\pi$ interactions .....	86
Figure 3.22. Geometrical arrangements of the NH <sub>2</sub> and CH groups with respect to the chain....	87
Figure 3.23. Relative current for the chain/A model with base A at three different orientations with respect to the chain at positive and negative voltages.....	89
Figure 3.24. Schematics of the carbyne/ssDNA model systems with each base parallel to the chain.....	91
Figure 3.25. DOS for the models with the bases parallel to the chain.....	92
Figure 3.26. Transmission probability functions for the models with the bases parallel to the chain.....	92
Figure 3.27. I-V characteristics of the models with the bases parallel to the chain compared with the control model at positive and negative voltage.....	93
Figure 3.28. I-V characteristics of the models shows two orientations of ssDNA with respect to the chain compared with the control model at positive and negative voltages.....	96
Figure 3.29. Relative current for the chain/C model with base C parallel (0°) and normal (90°) to the chain at positive and negative biasing voltages .....	97
Figure 3.30. The current for the different model systems with the bases A, C, G, and T at two different orientations (0°, 90°) with respect to the chain at 0.6 V.....	100
Figure 3.31. Schematics show the five different locations of bases A and C with respect to the chain.....	103
Figure 3.32. DOS for the models with base A at five different locations from the chain compared with the control model .....	105
Figure 3.33. Transmission probability functions for the models with base A at five different locations from the chain compared with the control model.....	105
Figure 3.34. I-V characteristics of the model chain/A where the base is placed at five different locations with respect to the chain compared with the control model.....	105

Figure 3.35 DOS for the models with the base C at five different locations from the chain compared with the control model .....	106
Figure 3.36. Transmission probability functions for the models with the base C at five different locations from the chain compared with the control model.....	105
Figure 3.37. I-V characteristics of the model chain/C with the base C placed at five different locations with respect to the chain compared with the control model.....	108
Figure 3.38. Force trend and current for the 1D chain/A model at -0.85 V.....	114
Figure 3.39. Force trend and current for the 1D chain/C model at -0.85 V.....	115
Figure 3.40. I-V curves for the chain/A and chain/C model systems at the five different locations for the positive biasing voltages.....	117
Figure 3.41. Current as a function of the base distances from the chain for the chain/A and chain/C models at 0.6 V.....	117
Figure 3.42. Current as a function of time calculated by assuming bases A and C move with a speed of 0.1 $\mu\text{m/s}$ at 0.6 V.....	119
Figure 3.43. Schematic of the model that has a single chain of carbon atoms attached to graphene nanoribbons on both sides.....	121
Figure 3.44. Electrical properties for a single chain attached to graphene nanoribbons on both sides at positive and negative energies.....	123
Figure 3.45. Electrical current and conductance for the model that has a 1D chain attached to graphene nanoribbons on both sides at positive and negative voltages.....	124
Figure 3.46. Schematic of the model that has single chain of carbon atoms attached to two graphene nanoribbons on both sides with base A placed normal to the chain.....	127
Figure 3.47. DOS for the chain2/ssDNA models compared with the control model.....	128
Figure 3.48. Transmission probability functions for the chain2/ssDNA models compared with the control model.....	129
Figure 3.49. I-V characteristics for the chain2/ssDNA models compared with the model that has carbon chain attached to two graphene ribbons on both sides at positive and negative voltages.....	130
Figure 3.50. (a) The electrical current for the chain/ssDNA models at two different biasing voltages (-0.85 V and 1.3 V) and (b) the percentage increase in current associated with the presence of these ssDNA bases at -0.85 V and 1.3 V.....	133

Figure 3.51. The relative current for the two different models or structures of chain in the presence of ssDNA.....	134
Figure 3.52. Schematics for the top view of the simulated models of graphene with two different widths. Gray spheres are the carbon atoms and the white spheres are the hydrogen atoms.....	138
Figure 3.53. DOS for the two models of graphene compared with the single chain of carbon...	139
Figure 3.54. Transmission probability functions for the two models of graphene compared with the control model.....	139
Figure 3.55. I-V characteristics of the graphene models compared with the carbon chain model in the absence of base A at positive and negative voltages.....	140
Figure 3.56. Schematic of the model with base A placed normal to the graphene nanoribbon with width of 9.3 Å.....	141
Figure 3.57. DOS for the two models of graphene compared with the control model in the presence of base A.....	142
Figure 3.58. Transmission probability functions for the two models of graphene nanoribbons compared with the control model in the presence of base A.....	142
Figure 3.59. I-V characteristics of the graphene models of thickness 7.1 Å and 9.3 Å compared with the carbon chain model in the presence of base A.....	143
Figure 3.60. (a) Current for the models with graphene 1, graphene 2, and carbyne (b) The percentage of the increase in current in the presence of base A compared at -0.6 V.....	145
Figure 3.61. Normalized graphene current with respect to the single chain control model current.....	147



## LIST OF TABLES

Table 3.1. Number of atoms and size of the simulation cell for the model system chain/ssDNA.....	63
Table 3.2. Locations of different groups in base A with respect to the chain.....	111
Table 3.3. Locations of different groups in base C with respect to the chain.....	111
Table 3.4. The simulation parameters for model systems of carbyne and graphene.....	137

## LIST OF SYMBOLS

$\vec{c}$	Chiral vector
$\vec{a}_1$	Basis vectors of the graphene lattice for atom 1
$\vec{a}_2$	Basis vectors of the graphene lattice for atom 2
$n$	Chiral indices
$m$	Chiral indices
$H$	Total Hamiltonian
$E$	Total energy
$\Psi$	Wave function
$\hbar = \frac{h}{2\pi}$	Planck's constant
$m$	Mass of electron
$M$	Mass of ion
$V(r)$	Potential energy
$\nabla^2$	The second derivative with respect to the space coordinates
$Z$	Charge of ion
$e$	Electron Charge
$R$	Ion distance
$r$	Electron distance
$n(r)$	Electron density

$V_H$	Hartree potential energy
$V_{xc}$	Exchange correlation potential energy
$V_x$	Exchange potential energy
$V_c$	Correlation potential energy
$V_{ion-electron}$	Interaction potential energy between electron and ion
$H_{KS}$	Kohn-Sham total Hamiltonian
$f_x(s)$	Exchange enhancement factor
$s$	Reduced density gradient
$V_{pseudo}$	Pseudopotential
$V_{local}$	Local pseudopotential
$V_{non-local}$	Non-local pseudopotential
$k$	Wave number in reciprocal space
$\chi_i^k$	The periodic function of state i
$e^{ikr}$	The oscillating function
$w_{iR}$	Wannier function for state i
$R$	The lattice vector
BZ	Brillion zone
$G(E)$	Green's function
$I$	The identity matrix

$i\eta$	Imaginary part
$G^a$	Advanced Green's function
$G^r$	Retarded Green's function
$\Gamma_L$	Functions of molecule coupling to the left electrode
$\Gamma_R$	Functions of molecule coupling to the right electrode
$G_C^r$	Retarded Green's functions of the molecule
$G_C^a$	Advanced Green's functions of the molecule
$T(E)$	Transmission probability functions
$E_f$	Fermi energy
$C$	Quantum conductance
$\mathcal{G}(E)$	Total quantum conductance
$I(V)$	Electrical current
$V$	Voltage
$f(E)$	Fermi distribution function
$\rho(E)$	Density of states
$G(V)$	Differential conductance
$G_0$	Quanta
$E_{dipole-dipole}$	Dipole-dipole energy
$E_{dispersion}$	Dispersion energy

$E_{dipole-induced\ dipole}$	Dipole-induced dipole energy
$A, B, C, D, O$	Constants
$f(\theta, \phi)$	Function of the angles between atoms in each molecule
$f'(\theta, \phi)$	Function of the angles between atoms in each molecule
$F$	Total interaction force
$F_{dipole-dipole}$	Dipole-dipole interaction force
$F_{dipole-induced\ dipole}$	Dipole-induced dipole force
$A', B', D', O'$	Constants
$\beta$	Constant
$\gamma$	Constant

## LIST OF ABBREVIATIONS

1D	One dimensional
2D	Two dimensional
DFT	Density functional theory
NEGF	Non-equilibrium Green's function
KS-DFT	Kohn-Sham density functional theory
CNT	Carbon nanotube
SWCNT	Single-walled carbon nanotube
QE	QUANTUM ESPRESSO
DNA	Deoxyribonucleic acid
ssDNA	Single stranded DNA
dsDNA	Double stranded DNA
PCR	Polymerase chain reaction
G	Guanine
A	Adenine
T	Thymine
C	Cytosine
BLA	Bond length alternation

TEM	Tunneling electron microscopy
STM	Scanning tunneling microscopy
LDOS	Local density of states
ZPV	Zero-point vibration

## CHAPTER ONE: INTRODUCTION

The term ‘nanotechnology’ refers to the science of the operation and creation of materials at the atomic or molecular level where the material properties are size-dependent [1]. One of the main advantages that nanotechnology offers is the large surface to volume ratio, which can be taken advantage of in many fields of science and engineering. Moreover, the recent drastic growth in nanotechnology has enabled the fabrication of devices at the single nucleotide scale [2]. These devices are capable of identifying and analyzing the electrical and mechanical properties of single molecules. More importantly, the incorporation of nanotechnology in biological science has led to a new field of research known as bio-nanotechnology which has enabled the revision of the interactions between nanometer scale materials and biomolecules via providing the researchers in this field with the finest possible tools for drastic progress [3]–[5]. Nanofluidic devices have emerged as one of the fields that focuses on the fluid flow through nanoscale devices [6]. Several research groups have investigated methods of incorporating nanofluidic devices to sequence the entire human genome. Deoxyribonucleic acid (DNA) has all the genomic information for inherited properties of an organism. In particular, the genetic information is revealed via determining the order of the DNA nucleotides, and it is responsible for deviations among populations [7]. DNA sequencing or the method of determining the sequence of its nucleotides inexpensively and rapidly contributes significantly to the progress of the diagnosis techniques and personalized treatments of diseases based on individuals’ genes. Hence, any rapid advancement in DNA sequencing technology results in new avenues of revolutionized medical tools that benefit human physiology and development [8]. The launch of the Human Genome Project has directed DNA sequencing technology toward drastic development in human genome sequencing research. Figure 1.1 shows the cost per genome



based on National Human Genome Research Institute [9]. At the beginning, the project used the Sanger method or the classical first-generation DNA sequencing method. The accuracy of the Sanger sequencing is 99.999% for a read length within the range 400-900 bp. However, the instrument price is \$95,000 and the cost for sequencing a million bases is \$2400 [10]. The cost and time required are major drawbacks. Therefore, both scientists and companies have considered examining cheaper and faster sequencing methods.

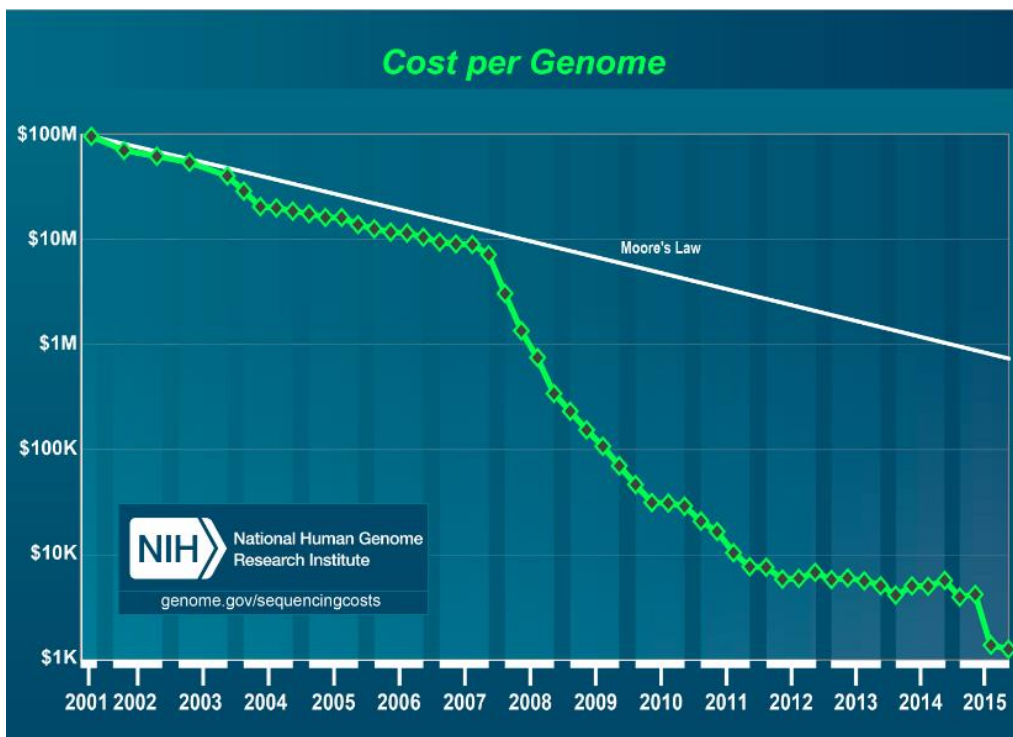


Figure 1.1. Cost per genome accessed from National Human Genome Research Institute [9].

The sequencing methods and time have substantially improved in second-generation sequencing. For example, the price for sequencing a million bases is \$10. In addition, it takes 24 hours for a read length of 700 bp with an accuracy of 99.9% when using the 454 GS FLX Titanium system [10]. This generation is described as a massive parallel sequencing generation.

Nevertheless, the 454 GS FLX instrument price is \$500,000. Thus, the high cost of the instruments is still a major shortcoming for second generation sequencing methods besides it requires the use of PCR. PCR is Polymerase Chain Reaction. It is a reaction used to magnify a single DNA several orders of magnitude by using DNA polymerase [11]. Even though the second generation has led to reducing the cost of sequencing, its low read lengths [8] and high cost are major issues to achieve the ultimate goal of the Human Genome Project. Therefore, a single-molecule, long-read-length, and label free sequencing method has become the subject of intense research.

Third-generation sequencing is the most recent sequencing technology used [10], [12]. It is based on the application of nanoscale devices to achieve ‘direct’ sequencing where the time used for DNA sample pre-processing is minimized. The sequencing methods have two significant advantages over the other two generations. The first advantage is that it does not require the usage of PCR. As a result, the time and cost required to prepare DNA is reduced which leads to reducing any error caused by PCR. The second advantage is the capturing of the output signal in real time throughout the sequencing reactions [10]. As an illustration, hours are needed to run a sequencing instead of days. Also, a read length of 1300 bp has been achieved by the PacBio RS [10]. This read length is longer than any read length reported via using the second-generation sequencing methods.

Therefore, the human genome project has led to tremendous progress toward achieving the ultimate goal of \$1000, label-free, and fast sequencing technology. Figure 1.1 shows the remarkable decline in prices. After the revolution of bio-nanotechnology, the focus of research has been on using quantum mechanics based techniques and nanoscale material properties to achieve the human genome project goal. Figure 1.2 shows the cost of sequencing million bases

using different nanoscale techniques, which clearly demonstrates the efficiency of using quantum sequencing techniques [13]. Fast and cost-effective DNA sequencing would enable the healthcare specialists to provide treatments based on each patient's genome and predict future

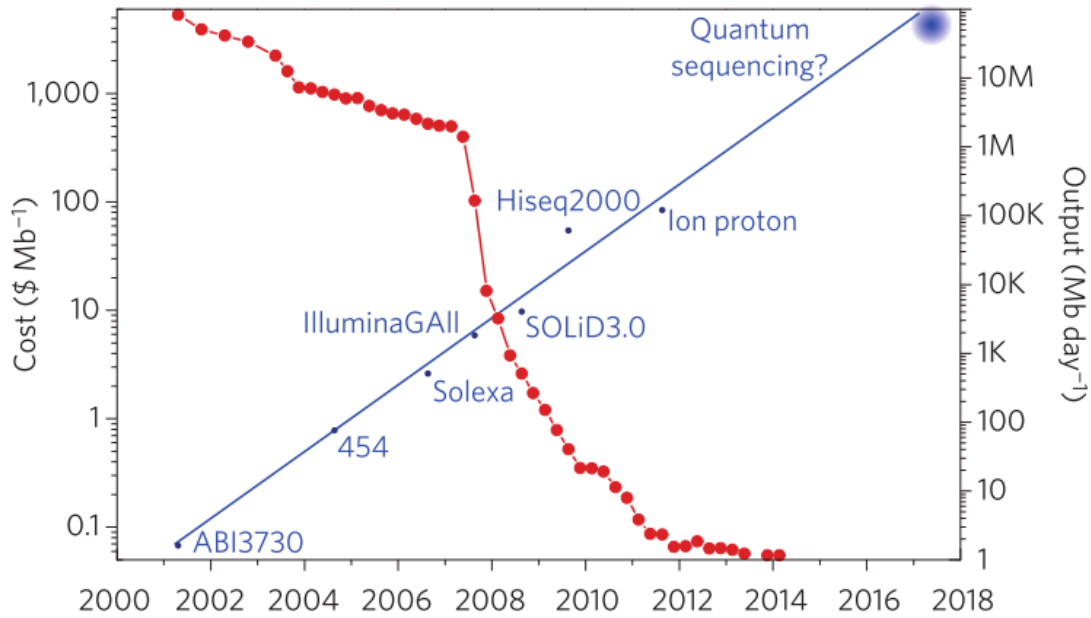


Figure 1.2. Cost of sequencing million bases using different nanoscale techniques [13]. Red represents the cost in dollars per mega base.

diseases to minimize undesirable consequences. In order to reach such goal, human genome sequencing should be part of the normal medical processes in health care systems. However, there are still some challenges to be resolved before human genome sequencing becomes part of the routine medical procedures.

### 1.1. Nanopore Sequencing

Nanopores are the best-known nanoscale devices used in the third-generation sequencing techniques. In nanopore-based sequencing, ssDNA bases are dragged through nanometer scale

openings via applying an external electric field [14]. ssDNA stands for single stranded DNA which forms with another strand the helical structure known as double stranded DNA (dsDNA). In nanopore sequencing technology, the different ssDNA bases are sensed via their blockage to the electrical current while passing through the nanopore. These nucleotide units, or ssDNA bases, are of four types that differ in the base attached to the sugar. The bases are guanine (G), adenine (A), thymine (T), and cytosine (C). The length of a DNA depends on the number of bases included [15]. Each base pair is 0.34 nm spaced from the next pair [15] as shown in Figure 1.3.

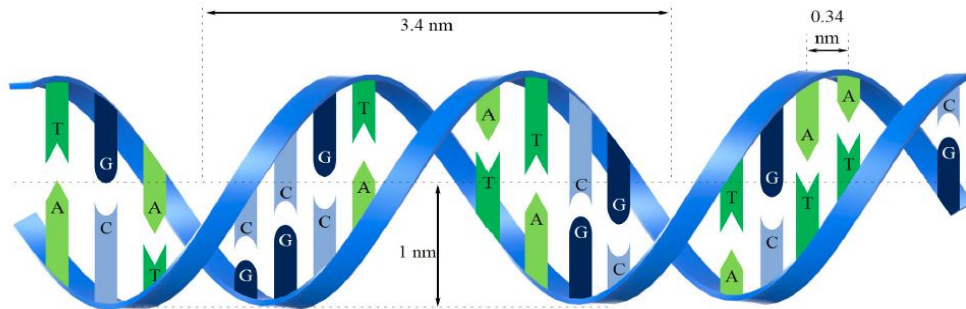


Figure 1.3. Schematic of dsDNA showing the spacing between two sequential base pairs.

The different ssDNA bases are shown in Figure 1.4. When these different bases transport through the nanopore, they block the electrical current differently based on their sizes.

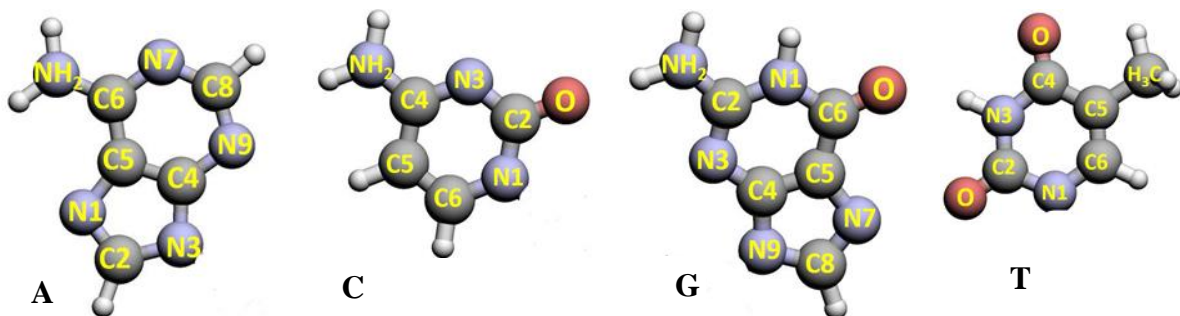


Figure 1.4. Schematics of ssDNA showing the different DNA bases.

The current measured in nanopore sequencing devices can be either ionic current or tunneling current. One of the main issues with using nanopore sequencing is the fast translocation speed of DNA through the nanopore. It has been reported that the average translocation speed of a DNA can be within the range of 0.5-30 mm/s and can speed up to 5 cm/s, which is too high for electrical signal measurement [16], [17]. Several possible solutions have been offered, such as increasing the fluid viscosity, electrolyte temperature, salt concentration, voltage regulation, and inducing magnetic field [16]. There is another technique to lower the DNA translocation speed [18] according to a recent study. The technique is based on using nanochannels and measuring the tunneling current. More importantly, an electrical sensing element is embedded in the channel to sense the changes in the tunneling current when a base of DNA passes through [18]. In both nanopore and nanochannel, sequencing mechanisms rely on the charge transport. However, the direction of measuring the flow of the charge is different.

The sensing modality based on charge flow in nanopore devices can be classified into ionic current and tunneling current as mentioned earlier. In nanopore and nanochannel devices, tunneling current can be measured in two ways. Schematics of side view for the three sensing modalities including the two methods of measuring the tunneling current are shown in Figure 1.5. Ionic current based devices measure the electrical current in the longitudinal directions of DNA axes, whereas the tunneling current based devices measure the electrical current in the perpendicular direction of the DNA axes [14]. Ionic current direction is shown in Figure 1.5 a.

Two different methods can be used to measure the tunneling or transverse current. In the first method, two separate electrodes are embedded in a nanopore or nanochannel [19]–[21]. The sensing modality in this method is based on tunneling the charge carriers between the two electrodes. Tunneling current of this method is clarified in Figure 1.5 b. The second method of

measuring the current in the transverse direction is to have one single electrode where the charge carries flow from one end of the electrode to the other end as shown in Figure 1.5 c. Figure 1.6 shows one example of the recently proposed sequencing devices, which is based on measuring the charge transport in the transverse direction.

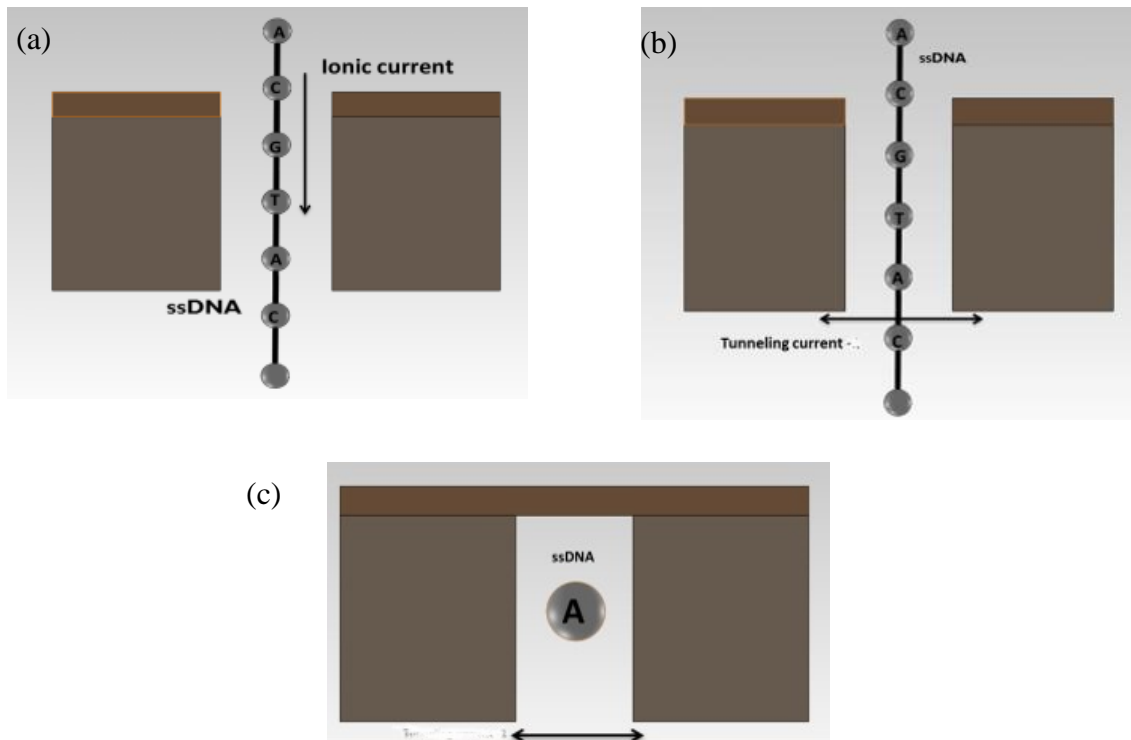


Figure 1.5. Sensing modality based on charges transport. (a) Ionic current as a sensing modality (b) Tunneling current as a sensing modality (c) Transverse current along one single electrode as a sensing modality.

There have been several experimental and theoretical studies to explore devices that are based on the ionic current and tunneling current [14], [19], [21], [22]. However, there are a limited number of studies that investigate the second type of measuring the transverse electrical

current along one single electrode. These studies mainly use graphene nanoribbon as a sensing element. Figure 1.6 demonstrates an example of using graphene nanoribbon as a sensing element where the electrical current is measured.

One of the major drawbacks of the third-generation sequencing methods is the low resolution. The resolution can be either temporal or spatial resolution. The temporal resolution problem is caused by the fast translocation speeds of DNA bases when these bases are translocated through the nanopore, which has been discussed earlier. The spatial resolution problem is caused by the width (or thickness) of the sensing element. Therefore, achieving better temporal and spatial resolutions requires slowing the DNA bases translocation speeds and reducing the width of the sensing element to the smallest possible value. Commercially, Oxford

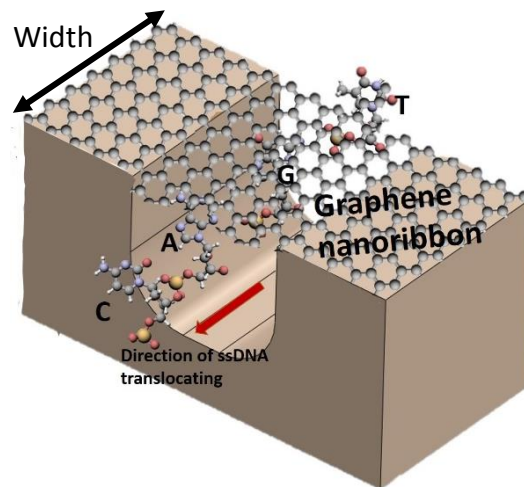


Figure 1.6. Schematic of 3D view of the sensing modality based on charges transport through the sensing element.

Nanopore Technology (ONT) (New York, NY, <https://nanoporetech.com/>) has recently released a biological nanopore DNA sequencer. The DNA sequencer is known as MinION. MinION is a portable sequencer that relies on measuring the ionic current. It is controlled using laptop

computer software. According to the reported data, MinION can sequence M13 phage dsDNA and 48-kb lambda phage [13]. Nevertheless, there are two main challenges. The first challenge is the limited accuracy caused possibly by having many nucleobases contribute to the electrical responses [13], [23]. Another issue is using a biological nanopore, which is known for being unstable and having inconsistent pore size [24]. Although, there are some advantages of the MinION sequencer, the limited accuracy and the use of biological nanopores are still the main challenges for such sequencing devices. Thus, new approaches and materials have been eagerly introduced for new sequencing devices. For example, several groups have used a variety of compound semiconductors as nanowires and nanotubes besides silicon nitride in designing nanopore devices that can be used in sequencing DNA such as ZnO, TiO<sub>2</sub>, CuO, and graphene [7].

Furthermore, the charge transport processes require information about physiological interaction properties between the sensing element and DNA. Thus, developing a robust sequencing device based on the charge transport measurement requires a deep understanding of the electrical properties of the sensing element and its interaction with different ssDNA bases. For example, many studies in the bio-nanotechnology field include the interactions between nanomaterials, such as carbon nanotubes (CNT) and graphene, and ssDNA. Hybrid structures of ssDNA and CNT, or ssDNA hybridizations, are structures that have received remarkable attention and led to significant progress in drug delivery systems, bio-sensing devices, and sensitive detection of ssDNA hybridization via cantilever based biosensors [25], [26]. Graphene is a two dimensional carbon based material that has been investigated intensively due to its physical and chemical properties [27], [28]. Numerous experiments and several numerical studies have been recently performed regarding the interactions between graphene and



biomolecules such as ssDNA. It has been concluded that the interaction between ssDNA and graphene can yield to the adsorption of ssDNA onto the graphene surface [8], [29]–[31]. One promising application in bio-nanotechnology is the use of the graphene-based devices as electrical measurement based sensors for fast DNA sequencing [28], [32].

The interaction of DNA with nanomaterials has not been limited to only CNT and graphene, but it has also included some other nanoparticles to form new materials or improve the properties of the existing ones. For example, the interactions between DNA and gold nanoparticles, where DNA acts as a mediator of a programmable material, have been examined by Kim and coworkers [33]. The term programmable material indicates any self-assembled structure in which the components follow arbitrary functions to align in arbitrary directions. In their work, a technique to control the number, locations, and orientations of DNA linkers on the surface of gold nanoparticles was proposed and is expected to open a wide range of applications in tissue engineering besides the possibility of producing new types of materials and improving the current material properties [33]–[35]. Therefore, knowing the electrical properties associated with the interaction between the sensing element and DNA is mandatory when designing sequencing devices that rely on the charge transport as a sensing modality.

## **1.2. Carbon Based Materials**

Carbon based nanomaterials can be found in variety of chemical forms [36]–[38]. Figure 1.7 is a schematic that shows the different sizes of CNT, graphene, and carbyne. Diamond is a three-dimensional (3D) allotropic form of carbon. Graphite and graphene are two-dimensional (2D) carbon based materials [36], [39], [40]. Carbon based nanomaterials have been investigated intensely by researchers in many fields due to their unusual properties. Furthermore, the

reduction in dimensionality from 3D to 2D has led to the discovery of new physical and mechanical properties of materials and has revealed a wide range of applications in electronic devices [36].

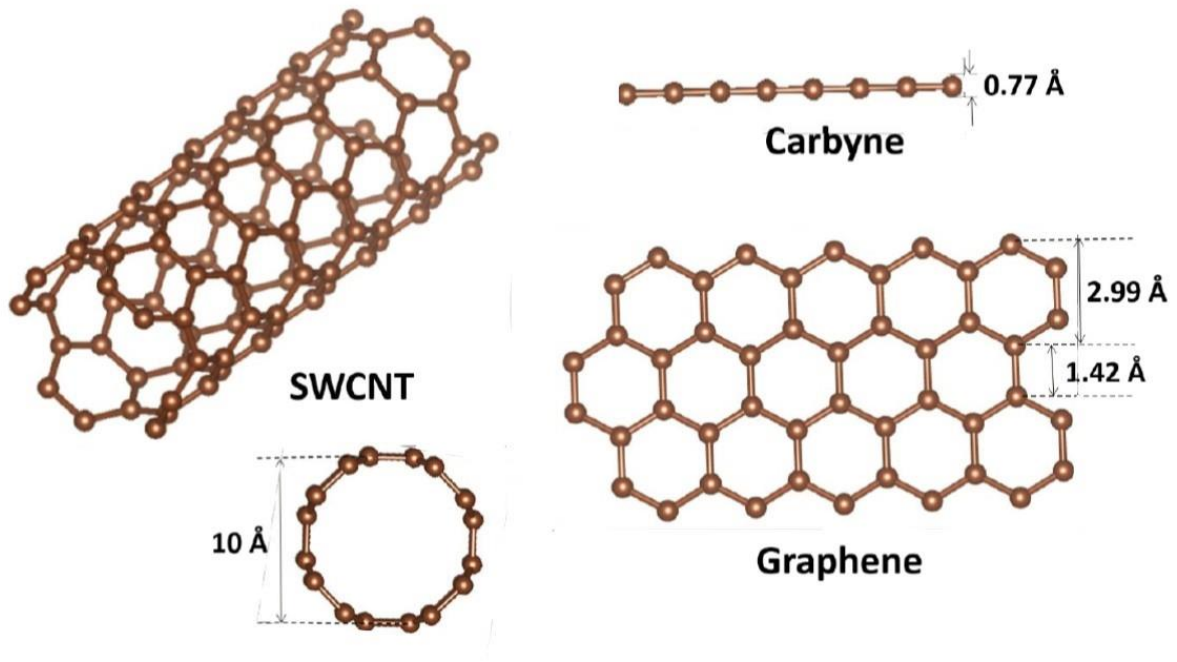


Figure 1.7. Schematics of carbon based materials include SWCNT, graphene, and carbyne chain.

CNT is also considered as a 2D structure of carbon atoms that consists of single layer of graphene wrapped into cylinder as mentioned earlier [39]. In addition, there is another form of carbon known as carbyne. Carbyne is a one-dimensional (1D) chain of carbon [36]–[38], [40], [41]. The variations among carbon based nanomaterials in size and electronic structure are plausible and have played substantial roles in many applications. In fact, each allotrope of carbon materials has its unique mechanical, electrical, thermal, optical, and transport properties [42].

### 1.2.1. Graphene

Graphene is a 2D material and consists of single layer of  $sp^2$  hybridized carbon atoms in the form of a hexagonal structure [8], [18], [43], [44]. There has been a drastically increasing shift in research toward exploring graphene and proposing its potential in many applications at the nanoscale since 2004. More specifically, graphene has been of great interest for numerous electronic devices due to its attractive properties. It has been reported that graphene is elastic, strong and stretchable, translucent, impermeable to ions, an excellent thermal and electrical conductor, one atom thickness, and unique in its optical properties [45]–[49]. More importantly, graphene has revealed a high charge carrier mobility of  $1 \times 10^5$  ( $\text{cm}^2 / \text{V} \cdot \text{s}$ ) at room temperature [50]. The possibility of producing massive area graphene for cheap prices has placed it as a strong candidate for many electronic devices for biomedical applications such as nanoscale DNA sequencers [51]. Due to its large surface area,  $2.630 \text{ m}^2/\text{g}$ , graphene has been embedded as a platform to distinguish different DNA bases [52]. Theoretical and experimental approaches have suggested that graphene nanopore, nanogap, and nanoribbon can be used in label-free and single molecule resolution DNA sequencers. Graphene nanoribbon is described as an open and unzipped CNT. Geometrical formation of graphene nanoribbon can be either armchair or zigzag edges and a mixture of both in some cases depending upon the cutting direction [53], [54]. These two different edges structures lead to different electronic properties. The main difference in these two structures of edges relies on the angles between the edge segment. If the angle between successive edge segments is opposite to the angle of the previous segments, the graphene nanoribbon is considered as zigzag-edged. On the other hand, the graphene nanoribbon has armchair edges if the angle of each pair of segments is  $120^\circ$  or  $-120^\circ$  with respect to the previous pair [54]. Zigzag and armchair graphene sheets are shown in Figure 1.8.

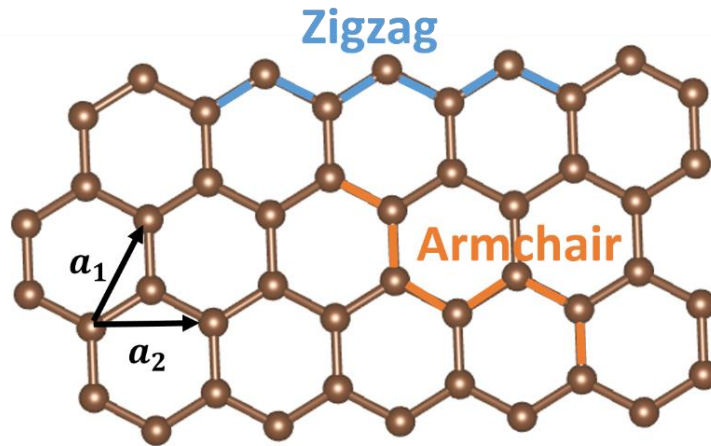


Figure 1.8. Graphene sheet showing zigzag and armchair configurations where brown spheres are carbon atoms, blue bonds represent zigzag configurations, and orange bonds represent armchair configurations.

For graphene sheet to form a cylinder with completed hexagons, there are several ways of rolling it up. The direction of the roll up is known as chiral vector,  $\vec{c}$ , which can be described by Equation 1.1 [55].

$$\vec{c} = n\vec{a}_1 + m\vec{a}_2 \quad (\text{Equation 1.1})$$

Here,  $\vec{a}_1$  and  $\vec{a}_2$  are the basis vectors of the graphene lattice as shown in Figure 1.8.  $n$  and  $m$  are the chiral indices, while 1 and 2 represent atoms 1 and 2, respectively.

Graphene as a 2D material has been proposed in many investigations [8]. The attractive electrical and mechanical properties of graphene have provided new opportunities for DNA sequencing devices as mentioned earlier. The possibility of producing graphene in cost effective manners has encouraged researchers to implement it in different sequencing techniques, such as graphene electrodes, graphene nanopores, and graphene nanoribbons via measuring the ionic current and the tunneling current. Min et al. [18] embedded a graphene nanoribbon of 1 nm width in a nanofluidic channel where ssDNA is pulled. The electrical current was measured

through GNR that played as one single electrode. Figure 1.6 is an example of such a device. According to this study,  $\pi$ - $\pi$  stacking interaction led to probing the different ssDNA bases by the sensing element which was graphene nanoribbon. Specifically, the interaction affected the characteristics of the molecular orbitals of graphene nanoribbon via Fano resonance, which led to change in the electrical properties of graphene. These changes in the electrical properties caused the conductance to change and allowed the bases to be identified. Thus, the possibility of designing a device in which each base is being probed and held firmly at the same time has been approached. Also, measuring the electrical current through one single electrode while ssDNA is pulled through the nanofluidic channel is experimentally feasible and can be used as a sensing mechanism for nanofluidic based ssDNA sequencing devices.

Therefore, 1 nm width provides enough spatial resolution for single nucleotide detection. Nevertheless, sub-nanometer width of a sensing element is suspected to have better spatial resolution. Structuring graphene into nanoribbons can lead to either armchair or zigzag edges with semiconducting and metallic properties, respectively. These edges influence the electrical response of graphene nanoribbons to the existence of ssDNA. In experimental situations, they can co-exist and affect the electrical response. Also, signal-to-noise ratio increases when using multilayer structures of graphene nanoribbons [8].

Song et al. [56] placed each base parallel to the graphene nanoribbons and measured the electrical current through the nanoribbon. According to their study, the adsorption of the different ssDNA bases on the graphene nanoribbon surface resulted in changes of the electrical current of the graphene nanoribbons. These changes were caused by the interactions between the graphene nanoribbon and the different bases. Their proposed device was able to detect bases C, G, and T but not base A at biasing voltages within the range of 0.3 V to 0.6 V. The study

suggested that the oxygen atom in bases C, G, and T interacts with the nanoribbon and, hence, affects the electrical properties of the graphene nanoribbon.

Although graphene has been treated as a one-dimensional carbon material in DNA sequencing devices, graphene is not a true one-dimensional material. The smallest possible width is required for high spatial resolution in DNA sequencing. The interaction between graphene and different ssDNA bases changes the electrical properties of graphene and induces modulations that can be calculated. Moreover, graphene has shown no effect for different ssDNA base orientations [18]. In brief, there are still some issues with graphene nanodevices for DNA sequencing despite its attractive opportunities.

In order to use graphene nanoribbons in DNA sequencing devices, the graphene has to be very thin with defined edges meaning to have either zigzag or armchair edge. Moreover, a way to control the absorption of DNA to graphene nanoribbons is required [8].

### **1.2.2. Carbyne**

Carbyne is a one-dimensional (1D) carbon based materials that is composed of sp-hybridized atoms as shown in Figure 1.9. It has been indicated that carbyne can exist as “shock-compressed graphite, interstellar dust, and meteorites” [37]. Moreover, it has been proven that carbyne is twice as stiff as graphene and diamond. For example, the tensile strength of carbyne is in the range of  $6.0-7.5 \times 10^7$  N·m/kg. For graphene and diamond, it is in the range of  $4.7-5.5 \times 10^7$  N·m/kg and  $2.5-6.5 \times 10^7$  N·m/kg, respectively [37]. This property has placed it as a strong competitor to graphene in several applications including biomedical engineering. More importantly, the width of a carbyne chain is about the thickness of single atom and has been reported to have an effective thickness of  $0.772 \text{ \AA}$  [37]. Thus, carbyne is considered as the

smallest nanowires that can be obtained in nature [57]. Carbyne can be either a cumulene or polyynes based on the chemical bonds throughout the chain. Cumulene is double bonded ( $=C=C=$ ), while polyynes has alternate single and triple bonds ( $-C\equiv C-$ ) [57]. Cumulene is  $sp^2$  hybridized, whereas polyynes is  $sp-sp^3$  hybridized. Schematics of polyynes and cumulene are shown in Figure 1.9.

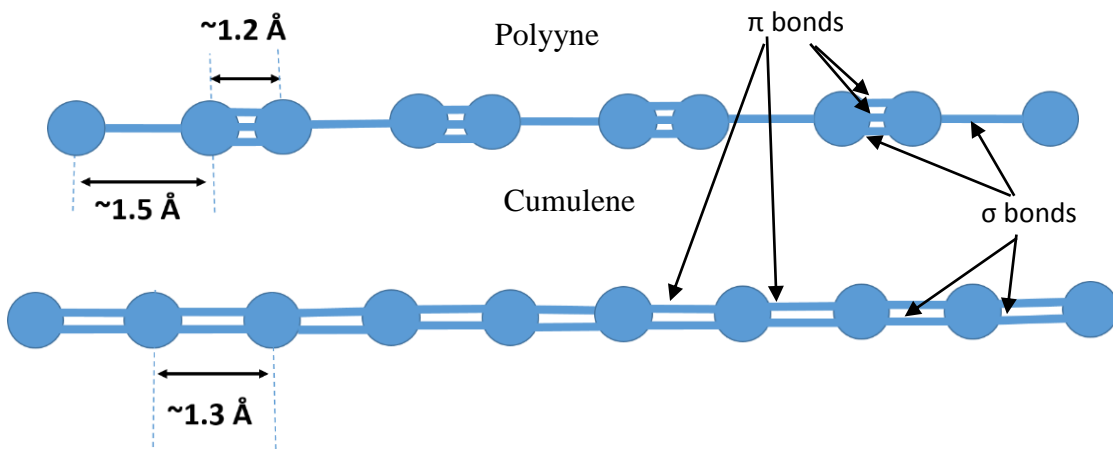


Figure 1.9. Schematics of carbyne composed of a 1D chain of carbon atoms. Top schematic is polyynes with alternating single and triple bonds and bottom schematic is cumulene with double bonds.

Despite the fact that cumulene and polyynes are 1D chains of carbon, they are different in their electronic properties and have different chemical bonds or structures [40]. For example, theoretical studies have predicted that polyynes exhibits semiconducting properties, while cumulene shows metallic behavior.

Also, polyynes and cumulene could coexist at appropriate experimental conditions [36]. This property enhances the feasibility of using them in many electronic devices. For example,

carbyne has  $\sigma$  and  $\pi$  bonds [36], [40]. In particular, there are two  $\sigma$  bonds along the axis, such as  $s$ - $p_x$  orbitals, and two degenerate  $\pi$  bonds from the perpendicular orbits, such as  $p_y$  and  $p_z$  orbitals. These orbitals are shown in Figure 1.10. In fact,  $\pi$  bond electrons are uniformly distributed along the double bonds in cumulene. On the other hand,  $\pi$  bond electrons are localized at the triple bonds in polyynes. Both  $\sigma$  bond and  $\pi$  bond are shown in Figure 1.11. Therefore, cumulene exhibits metallic properties and polyynes shows semiconducting behavior [36], [58].

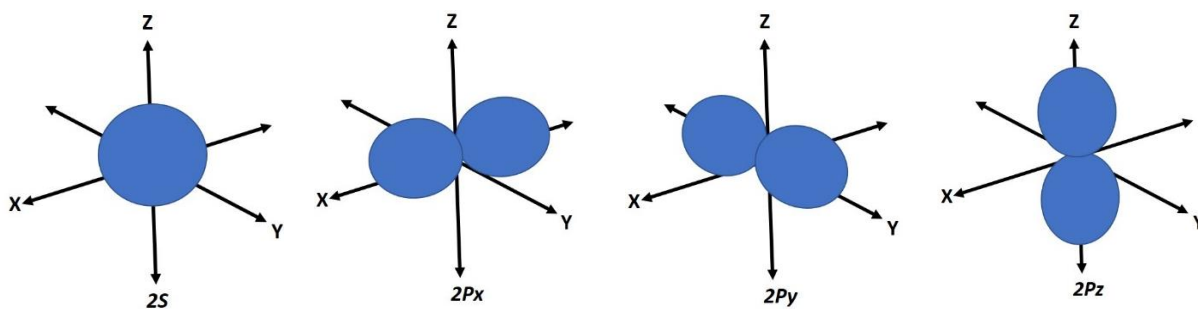


Figure 1.10.  $\sigma$  and  $\pi$  bonds are extended along orbitals  $s$  and  $p$ .

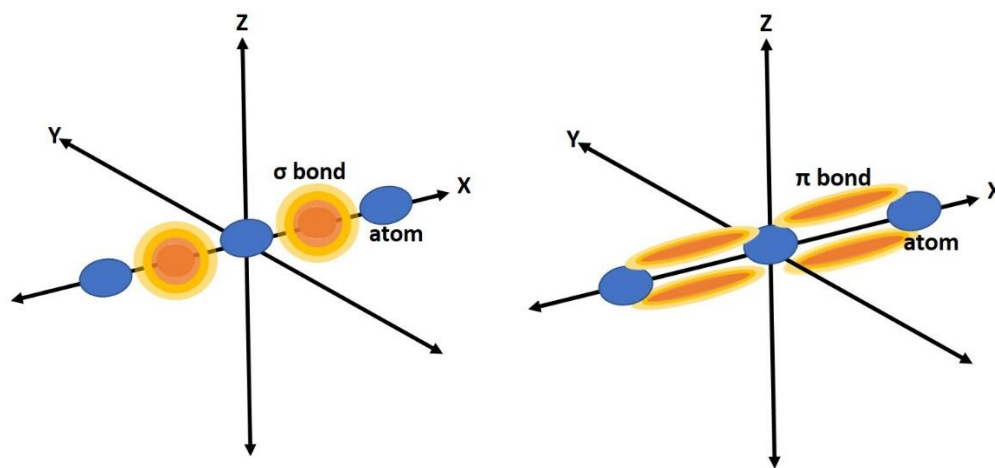


Figure 1.11. Schematics of  $\sigma$  bonds and  $\pi$  bonds between atoms.



Furthermore, it has been reported that carbyne as a 1D material exhibits Peierls's instability at low temperature [59]. Peierls's instability is a distortion of the periodic lattice structure of the 1D materials causing the distances between atoms to be nonsymmetrical. As an illustration, this distortion reduces the Fermi energy of the electrons resulting in the formation of electron pairs instead of electrons separated by equal distances [60]. As a result, an energy gap is created, and the density of electrons is different. Indeed, Peierls's instability lowers the energy of the electrons and changes the dimerization of ideal 1D chains.

More importantly, it has been reported that the effect of Peierls's instability on carbyne leads to the conversion of cumulene into polyene indicating that semiconductor behavior is transformed into metallic [36], [37]. One of the main consequences of such conversion is the change of the distances between atoms in a chain due to the oscillations of the atomic positions [59].

Moreover, carbyne has been found to be subject to zero-point vibrations (ZPV) [40]. ZPV is defined as the difference between the vibrational ground state energy and Born-Oppenheimer potential energy [61]. For example, the ground state energy is not zero according to quantum chemistry. This effect tends to appear in carbyne chains, and ZPV can be increased or decreased in a carbyne chain when it is under tension or strain [40]. One study that has been conducted by a group of researchers at Rice University has confirmed that ZPV eliminates Peierls's instability if the chain is free of strain. However, Peierls's instability increases and dominates ZPV when increasing the tension in the chain. The group justifies this physical phenomenon of carbyne by considering the threshold strain to be ~3%. Above 3% strain, carbyne shows the dominant effect of Peierls instability, while ZPV dominates below this threshold strain [40]. In addition, carbyne exhibits metallic properties below 3% strain, whereas it shows semiconducting behavior above it.

Thus, 3% strain is assumed as a switch between Peierls's distortion and ZPV and, hence, affects the quantum conductivity of carbyne sharply [40].

Furthermore, the odd and even number of atoms in a carbyne chain besides the chain length can impact the stability and conductivity of carbyne [36]. Moreover, finite and infinite 1D carbon chains tend to behave differently [60]. A study carried out using Density Functional Theory (DFT) has shown the effects of the chain ends as well as the odd/even number of carbon atoms on the electronic properties on atomic carbon chains [60]. According to this study, a chain that has an odd number of atoms has an even number of bonds; therefore, the center of the chain is at the central atom with two equivalent bonds on both sides. On the other hand, a chain that has an even number of atoms has an odd number of bonds indicating that the center of the chain is on the central bond. As a result, bond length alternation (BLA) approaches zero at the center of the chain for chains with an odd number of carbon atoms. In contrast, BLA is constant for chains with an even number of atoms [60]. BLA is defined as the "difference between the short and long bonds." [40]. A chain with an odd number of carbon atoms will have a singlet ground state, while a chain with an even number of carbon atoms will have a triplet state. These different electronic structures impact the electronic properties of the carbyne chains. Also, an infinite chain of carbon atoms has been found to act as a metal due to the free gas-like electrons. Mainly, these electronic properties affect the electron transport in such materials [60].

The mechanical properties of carbyne, such as deformations caused by strain, have been investigated by Nair and his group [57]. They reported that shorter carbyne chains are stronger and stiffer than longer chains because the number of bonds increases when increasing the number of atoms. The group concluded that higher order of vibrational modes is possible for longer chains when suggesting the usage of this material as a nanoscale resonator in many

applications. Therefore, the stability of carbyne relies on length of chain, number of atoms, ends of the chain or contacts, and other electronic and mechanical properties. Comparing carbyne with the other carbon-based materials emphasizes the significant differences and highly preferable properties of carbyne.

Carbyne has been produced experimentally via electrochemical synthesis, gas-phase deposition, epitaxial growth, and pulling the chain from graphene or CNTs [32], [37]. For example, carbon chains have been synthesized experimentally using a scanning tunneling microscopy (STM) tip in a transmission electron microscope (TEM) [36]. The 1D carbon chains were synthesized by unraveling them from few layers of graphene. It has been reported that the electrical conductivity of these chains is lower than what has been reported by theoretical studies of the electronic structure and quantum transport properties of carbyne chains. Also, the I-V characteristics obtained for these chains show nonohmic behavior [36].

Another experiment has been carried out using graphitic aggregations by metallic tip in TEM [58]. In this experiment, I-V characteristics show a combination of ohmic and S-shaped behavior at different voltages. According to this study, the contacts and mechanical strain show their clear influences on the electrical and transport properties of these 1D carbon chains.

Although several studies have focused on exploring carbyne mechanical and electrical properties, there has been no reported work on the interactions between carbyne and ssDNA bases. Sufficient knowledge of the electronic and transport properties associated with such interaction opens a wide range of potential applications for the next-generation electronic devices where carbyne/ssDNA structures can be used [62]. More specifically, an appropriate research on the electrical properties associated with the interaction between ssDNA bases and the truly one-dimensional carbon chain, carbyne, is essential. Thorough investigation of the electronic

structure and transport properties of carbyne/ssDNA structures is highly desired at this phase of discoveries.

### **1.3. Carbon Based Materials and ssDNA**

The electrical properties associated with the interaction between carbon based materials, such as graphene and CNT, and different ssDNA bases have been investigated intensely by several research groups [18], [26], [30], [32], [63]–[70]. The importance of such interaction stems from its effects on the sensing modality that uses the electrical property sensing as a probing mechanism for ssDNA bases.

There have been several experimental studies regarding the electrical and mechanical properties related to such interactions. In addition, some researchers investigate such interactions using numerical simulation methods. Some of these groups have used first principle simulation approaches, while others have considered using molecular dynamics simulations. For the electronic transport properties related to the interactions between ssDNA bases and the carbyne based materials, using density functional theory (DFT) and non-equilibrium Green's functions (NEGF) have been considered and achieved using a variety of codes.

The tunneling current through graphene nanoribbon of 1nm width has been calculated using DFT and NEGF [18]. According to this report,  $\pi$ - $\pi$  stacking interaction between graphene nanoribbon and the different ssDNA bases led to changes in the electrical properties of graphene nanoribbon. Hence, graphene nanoribbon produces distinct electrical signals associated with the different ssDNA bases. The simulation yields the transmission probability functions and the density of states. The code that has been used is NAMD, a simulation code that enables involving water and ions in the nanochannel when simulating such model systems. The

simulation approach is very efficient and produces good results. NAMD is also designed for very large model systems. However, such type of simulation for a large model system consumes memory [71], and it is costly.

Another group [43] has numerically simulated sequencing DNA passing through graphene nanopores. This group has used *ab initio* DFT to obtain the density of states. Their simulation has been performed by using Vienna Ab Initio simulations package [43]. The numerical results suggest that a graphene nanopore can be used as a sensing element and show variations in the electrical properties when graphene interacts with ssDNA bases. In their approach, it is assumed that the transmission probability function is equal to 1.0 for all energy states. The tunneling current in this study was calculated by integrating the density of states with respect to the energy. The calculated electrical current is in mA, which is considered to be high when compared with the electrical current for DNA sequencing devices which are in the range of  $\mu\text{A}$  to nA [43]. The study considered the flow of electrons through the graphene. Also, their simulated models were in vacuum where no water and ions were included in their simulation models. According to them, their simulation approach may result in such high electrical current.

The effort of embedding graphene and CNT in DNA sequencing devices has increased rapidly. Researchers have investigated the adsorption of different nucleobases on graphene and CNT. Their focus was to produce a single-molecule with high resolution and long-read-length DNA sequencing device. Hence, the high conductivity of graphene has been used in innovative manners for DNA sequencing devices. A report by McFarland and her group [72] investigated the interaction between graphene nanopore-based DNA sequencing by measuring the tunneling current through the nanoribbon. The simulation approach was based on using DFT and NEGF via Atomistic Toolkit (ATK) by Quantumwise. Their simulation results seem to indicate that

graphene based sequencing devices can distinguish the different ssDNA bases at 0.5 V, 1.3 V, and 1.6 V.

The strength of the interactions between graphene nanoribbon and different ssDNA bases has been investigated by a group of researchers [56]. The simulation method used is based on using DFT and NEGF. The group used SIESTA package and Smeagol code. The conclusion is that the interaction varies among the different bases and results in different electrical current associated with each base. The group found that different ssDNA bases are adsorbed to graphene nanoribbons differently due to  $\pi$ - $\pi$  stacking interactions. The difference in the adsorption of the four different bases to the graphene surface leads to the variations of the electrical properties.

Another group led by Ahmed [73] calculated the local density of states (LDOS) of different ssDNA bases when deposited on graphene nanoribbon. LDOS was obtained by the derivative of the electrical current with respect to the voltage. In their simulation approach, they used DFT without considering van der Waals interaction. According to their results, graphene shows differences for different bases. The study proposes that the identifications of the different ssDNA can be accomplished in laboratories via using scanning tunneling microscopy (STM) as a visual fingerprint of each base.

Another study conducted by Chen and his group used CNTs as semi-infinite electrodes [64]. They placed different ssDNA bases between two CNT electrodes separated by 6.6 Å. The simulation approach was based on using DFT and NEGF via SIESTA package and Smeagol code. Based on the obtained results, the electrical current increases at the positive and negative biasing voltages when placing base A between CNT electrodes. The increase in the electrical current is caused by  $\pi$ - $\pi$  interaction between the bases and CNT electrodes. The binding energy of ssDNA bases to graphene has been numerically investigated by Lee and his group [74]. The

study was conducted by using van der Waals energy-corrected DFT calculations. The study claims that including van der Waals interaction energy leads to accurately obtaining the binding energy of graphene. The obtained results predict weak hybridization between the molecular orbitals of ssDNA and  $\pi$  orbitals of graphene when including van der Waals energy. According to the study, the order of the binding of the four different bases to graphene is  $G > A > T > C$ .

The attractive properties of graphene and the reported simulation results have encouraged scientists to further proceed in experimentally measuring the electrical response of graphene when interacting with ssDNA bases and sensing their differences. The ionic blockage current has been measured through graphene nanopore through freestanding graphene membrane [75]. The study has reported large electrical signals caused by the interaction between graphene and the different bases. The group claimed that minimizing the nanopore diameter enhances the produced electrical signal caused by the interactions.

An experimental investigation of the interaction between graphene and ssDNA bases has been conducted by Akca et al [76]. The study uses graphite as a graphene surface and observes the  $\pi$ - $\pi$  interaction between graphene and ssDNA bases. The study claims that inter-base energy influences the binding energy and hence the interactions of ssDNA bases with graphene. Bases A and C show higher inter-base energy than binding energy to graphene, while bases G and T show higher binding energy to graphene than inter-base energy. The study shows the feasibility of experimentally investigating the interactions between graphene and ssDNA bases. These simulation approaches collectively show that using DFT and NEGF is the common method to investigate the electronic transport properties of carbon based materials for DNA sequencing devices. Hence, it is the simulation approach adopted in the research of this dissertation.

### 1.3.1. Carbyne and ssDNA Bases

Despite all the recognition that DNA sequencing technology has received, achieving the ultimate goal of low cost, label-free, high spatial resolution, ultrafast, and single-molecule detection has not been accomplished yet. Since the spacing between two nucleotides is 0.34 nm for ssDNA, sub-nanometer scale nanoelectrodes are required to properly sense the different nucleotides accurately [77], [78]. Carbyne can provide the required width of the sensing element that yields enough spatial resolution for single-molecule detection. The 1D chain of carbon atoms has an effective thickness (width) of about 0.772 Å which is comparable with the space between two sequential bases in ssDNA – 0.34 nm as shown in Figure 1.3. However, a theoretical study of the interaction between carbyne and ssDNA will be vital before implementing carbyne in sequencing devices.

Computer simulations act as a bridge that connects the experimental and theoretical studies. Numerical simulations are used by scientists and researchers to test their hypothesis. In addition, researchers attempt to inspect difficult or impossible experiments by carrying them out via computer simulations.

Numerical simulation studies associated with the interaction between carbyne chains and different ssDNA bases can be used to analyze all the characteristics related to such interaction, such as the structural and electronic transport properties. Numerical simulations are necessary to predict the possible designs and probable performances of carbyne devices as single nucleotide sensors. Thus, an investigation of the electrical properties associated with the interactions between carbyne chains and ssDNA can be a tool to possible embedding of carbyne in ssDNA sequencing devices. Schematics of the simulated model and 3D view of a carbyne DNA sequencer are presented in Figure 1.12.



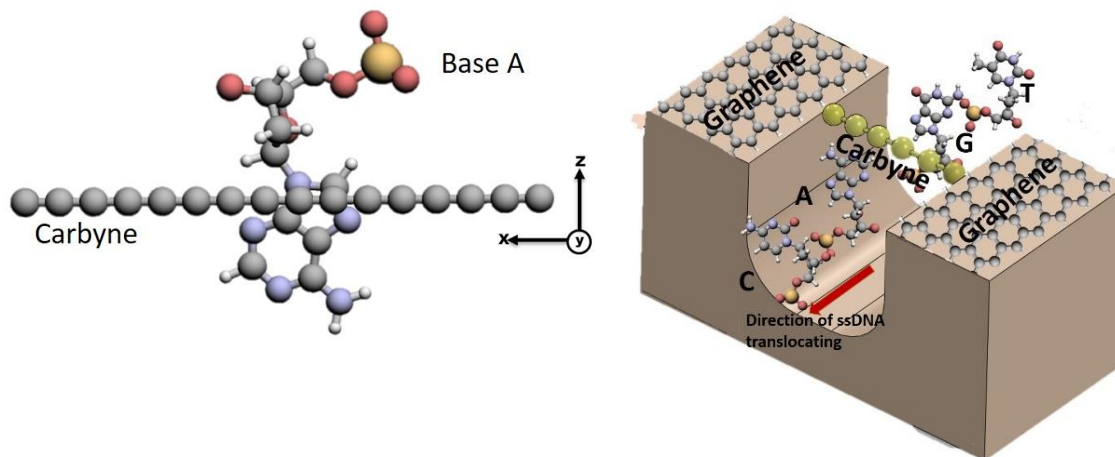


Figure 1.12. Schematics of an example of the simulated models and 3D view of a carbyne DNA sequencer.

#### 1.4. Primary Objectives of this Research

The primary objective of this research was to numerically investigate the electrical and transport properties associated with the interactions between carbyne chains and different ssDNA bases (carbyne/ssDNA) by using first-principle simulation method. The simulation approach was aimed to calculate the electrical properties for the simulated models in two cases. First, the electrical properties of the pure carbyne chain, control model, were calculated. Next, the electrical properties for the models that have single base of the different ssDNA with the carbyne chain were calculated. The differences in the electrical properties were analyzed and used to validate carbyne sensitivity to the presence of these different bases. The first-principle simulation method was based on using DFT and NEGF to calculate the electrical properties for the simulated models. These electrical properties included the density of states and the transmission probability functions. The density of states and the transmission probability functions were used

to calculate the electrical current for each simulated model. The codes used in this research were QUANTUM ESPRESSO and wannier90 [79]–[81]. The control model or first model was composed of a single chain of carbyne. Other models included the carbyne chain with one base of ssDNA placed at different orientations and locations with respect to the carbyne chain.

The novelty of this study lies in using a carbyne chain, the thinnest nanowire available in nature, as a sensing element of these different bases and then identifying each base based on the change in electrical properties caused by the interactions between carbyne and ssDNA. A brief description of the approach used in this study followed by the main aspects of first principle simulation are provided next.

#### **1.4.1. Specific Tasks**

The specific tasks associated with the simulation approach used in this study are listed below. The absence of substantial existing literatures associated with the electrical properties of the interaction between the carbyne chains and the different ssDNA bases provides an estimation of the contribution of this study to the existing knowledge of carbon based nanomaterials for bio-sensing applications.

The simulation approach was based on using DFT and NEGF to calculate the electrical properties associated with the interactions between the carbyne chain and different ssDNA bases. The individual tasks associated with the primary objective of this research in this dissertation are listed below.

1. Explore the electronic structure and transport properties of pure 1D carbon chains.
2. Investigate the changes in electronic and transport properties of 1D carbon chains in the presence of different ssDNA bases.

3. Determine the effects of different locations and orientations of different ssDNA bases on the electrical properties caused by the interactions between different ssDNA bases and 1D carbon chains.
4. Evaluate the differences between 1D carbon chains and graphene as sensing elements for DNA bases.
5. Determine the influence of having two graphene nanoribbons connected to the carbyne chain as contacts on the electrical properties of 1D carbon chains.

### **1.5. Dissertation Organization**

This dissertation is divided into four chapters. These chapters are: Simulation Method, Results and Discussion, Conclusion, and Future Work. Chapter Two explains the concept of first-principle simulation techniques and provides a brief description of the codes that were used in this study. Chapter Three presents and interprets the results of the simulation approach as well as compares the results with those reported in literature. Chapters Four and Five summarize the accomplishments and suggest new directions for future work.

## **CHAPTER TWO: SIMULATION METHODS**

### **2.1. First-Principle Simulation**

In this chapter, the theoretical background of DFT is discussed. The first part of this chapter deals with the electron transport in nanoscale devices. A review of DFT development and its important role in developing nanoscale electronic devices are deliberated. A detailed description of the calculation steps and equations solved by the codes used in this study is described.

#### **2.1.1. Electron Transport in Nanoscale Devices**

Nanoelectronics is one of the remarkably expanding fields in physics and chemistry [82]. The possibility of designing electronic devices on the basis of individual molecules has opened a new field of applications in bio-nanotechnology. Developing such devices requires essential understanding of the electrical properties of materials at the nanoscale. For macroscopic devices and conductors, Ohm's law can describe the molecular conductivity and the electronic transport processes based on the dimensions, carrier density, and mean free path. However, several factors that are ignored at large scales play significant roles when the dimensions become smaller. As a result, Ohm's law fails to describe the electronic transport properties and quantum effects at the nanoscale for several reasons.

First, electron scattering at the nanoscale is neglected due to having ballistic conductivity where the electrons do not diffuse. In addition, these electrons are subject to the quantized energy excitations at the single atomic levels. Therefore, the materials at the nanoscale have different electrical and chemical properties. On the other hand, the unique electromechanical properties of these materials have formed new disciplines of applications in the single molecule devices. In fact, molecular devices based on the electronic transport properties have great potential in many

industrial applications and have motivated researchers to actively study these electronic transport properties for a variety of systems [62].

In order to characterize and manipulate single molecule devices, sufficient and concrete theoretical understanding of the electromechanical properties and the electronic transport processes at the single molecule level is highly desired. Therefore, there are two major effects that one needs to consider when dealing with the molecular electronic devices for quantitative level of understanding.

The first effect is the electronic structure of the molecules included. The second effect is the interface to the external contacts [83]. To explain, the molecules or atoms can interchange energy and electrons with the electrodes, which leads to a change in the electronic structure of these molecules and atoms. As a consequence, accurate modeling of the electromechanical properties and electronic transport processes is required. The quantum chemical methods are one of the approaches that have been used to provide adequate knowledge when modeling the molecular electronic devices. Therefore, any investigations of the quantum transport phenomena are associated with the study of the electronic structures of the materials.

### **2.1.2. Density Functional Theory (DFT)**

The transport of electrons in the materials at the single molecule levels have been determined by the scattering property and occupations of the electronic eigenstates within the external applied potential [84]. Meanwhile, these electrons are confined in one or two directions in semiconductors. Moreover, the electronic and transport properties of the devices at such molecular dimensions rely on the atomic arrangements or structures when having external contacts. There have been several computational approaches to describe the electron transport

properties at the nanometer scale devices. Even though most of these methods have shown validity in explaining the electrical transport phenomena, accuracy and efficiency in modeling a wide range of quantum effects are some of the main concerns.

Density functional theory (DFT) has become one of the preferred theories in describing the electronic structures of atoms, molecules, materials, and complex chemical systems with cost efficiency [85]. The origin of DFT was in 1964-1965 based on Hohenberg-Kohn-Sham theoretical foundations [86]. According to the Web of Science analysis at the Tulane University, DFT was the most active field in physics during the time from 1980 to 2010. W. Kohn shared Nobel prize in chemistry with John Pople in 1998 [87].

DFT is favorable for its ability to counter on the static and dynamic electron correlations. To explain, there are two types of electron correlations: static correlation and dynamic correlation. Electrons repel each other instantaneously at short distances; therefore, avoiding each other results in an effect called the short-range effect or the dynamical correlation. This correlation can be seen in finite systems with two electrons or more and is accounted by a configuration wave function. At medium and large ranges, these electrons are further apart and, hence, experience an effect that is known as the static or the non-dynamical effect. The static effect is represented by configurations of wave functions that are nearly degenerate. DFT is accurate in including both parts of the electron correlations in its theoretical foundations of the electronic structures of materials [85].

In principle, the ground state properties of a system that has  $N$  electrons can be determined via the total electron density. The total electron density is the only essential parameter in this theory. To illustrate, the total electron density that is a scalar function of position determines any property and information associated with the ground and excited states of many body systems. According to Kohn-Sham DFT theory (KS-DFT), there is a single wave function to describe the

multi wave functions associated with the ground state of N electrons systems and constructed from a set of orbitals, which is the Slater determinant [88]. This wave function, Slater determinant, can uniquely and exactly determine all electron transport properties. To explain, determining this wave function guarantees knowing all the required information about the investigated system [88]. However, the external potential and degenerate ground states are not included, which causes underestimation of the electrical properties of the ground state of such N electrons system. Therefore, Kohn and Sham considered using vibrational principle and included exchange-correlation energy term in the total energy functional. Kohn-Sham proposed an exchange-correlation energy functional term to be added to the total energy of N electrons system such that DFT can deliver the density and total energy of any interacting correlated electronic system [87].

### **2.1.3. Non-Equilibrium Green's Function (NEGF)**

Non-equilibrium Green's function approach has been adopted by several researchers, and it is considered as a powerful tool to investigate quantum transport phenomena in nanodevices [84]. Also, numerically representing the N electrons system requires a mathematical framework in which the electromechanical properties of the system can be described quantitatively. Thus, Green's functions are one of the valuable tools that can be used for such representations. Some of the advantages of using Green's functions stem from its ease of use and efficiency when representing the quantum transport phenomena and electronic structures of materials.

Non-equilibrium Green's function (NEGF) is a representation method of describing nonequilibrium states [82]. To illustrate, the N electrons system is driven away from equilibrium when the charges, and hence the electrical current, start to flow through the device. Therefore, NEGF is needed when studying the electronic transport processes. NEGF is defined for each energy state and can be combined with DFT codes to calculate the probability transmission

functions as will be described later. Using NEGF approach allows one to benefit from the localizations of the energy states and enhances the possibility of studying the transport processes occurring at the single molecule levels where detailed descriptions of the electronic structure are necessary [84].

First-principle simulation approach used in this research is based on the combination of DFT and NEGF. Both DFT and NEGF are described later and more details are provided in the next section. First-principle simulations that are based on quantum mechanics are used to find the quantum conductance or the transmission probability functions and the density of states (DOS). The transmission probability functions and DOS are used to obtain the electrical current in this research.

#### **2.1.4. Calculating the Electrical Current**

The theory and mathematical equations that are used to calculate the electrical current flowing through the 1D carbon chain or along x axis are discussed in this section.

##### **2.1.4.1. Many Body States**

In quantum mechanics, the first step in gathering information about a system is to find the ground state wave functions and ground state energies. One of the common techniques that is adopted to find the ground state information is to solve Schrodinger's equation.

Schrodinger's equation is a total energy operator equation that is solved to find the ground state wave functions when the potential energy of the investigated system is precisely defined. By knowing the ground state wave functions, any other physical properties or phenomena can be found. Thus, the ground state wave functions and energy are the keys to obtain any other information related to the electronic and structural properties of the systems. For



the purpose of this study, the electrical current along the carbyne chain are derived after solving N electrons system problem by using DFT and NEGF. To start with, Schrodinger's equation is given in the following form [89]:

$$H\Psi(r) = \left( \underbrace{-\frac{\hbar^2}{2m}\nabla^2}_{\text{Kinetic energy}} + \underbrace{V(r)}_{\text{Potential energy}} \right) \Psi(r) = \underbrace{E\Psi(r)}_{\text{Total energy}} \quad (\text{Equation 2.1})$$

Here,  $H$  is the total Hamiltonian,  $\Psi$  is the wave function,  $\hbar = \frac{h}{2\pi}$  is Planck's constant,  $m$  is the mass of the particle,  $V(r)$  is the potential energy, and  $\nabla$  is the second derivative with respect to the space coordinates. The first part on left side of Equation 2.1 is the kinetic energy of the investigated system, and the second part is the potential energy. Thus, the Hamiltonian that is the total energy operator of a system is a combination of the kinetic and potential energy operators. Equation 2.1 demonstrates that the Hamiltonian is for a single particle and it describes time independent motion.

To include all the electrons or particles in the simulation, Equation 2.1 should be replaced by the non-relativistic Schrodinger's equation for a many particle system, which is known as a many-body problem. The total Hamiltonian for the many-body system changes in a way that not only the kinetic energy and potential energies of the particles are included, but also the interactions between these particles are considered. The term particles refer to charge carriers which are electrons and ions. When including all the possible types of interactions between electrons and ions in the many-body Hamiltonian operator, the form of the Hamiltonian becomes [89]:

$$H = -\frac{\hbar^2}{2m_e} \sum_i \nabla_i^2 - \sum_{i,l} \frac{z_l e^2}{|r_i - R_l|} + \frac{1}{2} \sum_{i \neq j} \frac{e^2}{|r_i - r_j|} - \sum_l \frac{\hbar^2}{2M_l} \nabla_l^2 + \frac{1}{2} \sum_{l \neq j} \frac{z_l z_j e^2}{|R_l - R_j|} \quad (\text{Equation 2.2})$$

The first term in Equation 2.2 represents the electron kinetic energy, the second term is the electron-ion Coulomb interaction energy, the third term shows electron-electron Coulomb interaction energy, the fourth part is the ion kinetic energy, and the last term represents the electron-ion Coulomb interaction energy.  $H$  is the Hamiltonian of the system,  $Z_{I,J}$  is the charge of ion  $I$  or  $J$ ,  $e$  is the charge of the electron,  $|r_i - R_I|$  is the distance between electron and ion,  $|r_i - r_j|$  is the distance between two electrons,  $M_I$  is the mass of an ion, and  $|R_I - R_J|$  is the distance between two ions. Equation 2.2 shows the types of interactions that one expects in a system of many electrons and ions which indicates how complicated many-body problems can be. The electrons are treated as quantum particles, and the nuclei are heavy compared with the electrons when dealing with the electronic transport properties. The electronic process is hence based on the interactions between the electrons themselves and the electrons with ions near them.

In DFT, the external potential and the number of electrons are the two elements that can solve the problem related to the system using quantum mechanics. As a result, the ground state wave functions can be found and used to determine the energy and other physical process parameters. In fact, the accuracy and reliability of obtaining the ground state information influence the accuracy of the theoretical predictions regarding the electronic properties and electron transport processes of many-body systems. Moreover, the density of electrons,  $n(r)$ , is used instead of the wave functions,  $\Psi$ , in determining the ground state wave functions. Based on the Kohn-Sham approximation in DFT, the total Hamiltonian of the system can be simplified as given in Equation 2.3 [90]. The Kohn-Sham approximation describes the system of many electrons and ions as a system that has electrons such that the ground state charge density is identical to the charge density of interacting electrons [91]. These electrons do not interact and are affected by external potential only.

$$H_{KS} = -\frac{\hbar^2}{2m}\nabla^2 + V_H(n(r)) + V_{xc}(n(r)) + V_{ion-electron}(n(r)) \quad (\text{Equation 2.3})$$

The first term of Equation 2.3 shows the kinetic energy of the system, the second term is Hartree potential, and the third part represents the exchange correlation potential. The last term of Equation 2.3 is the external potential in a form of ion-electron interaction potential. All terms in Equation 2.3 are functions of the electron density which is the reason for being called functional.

In Equation 2.3, the charge density is given by Equation 2.4 where  $i$  represents all the occupied states.

$$n(r) = \sum_i |\Psi_i(r)|^2 \quad (\text{Equation 2.4})$$

The Hartree energy that is defined as the electrostatic potential of the system is given by Equation 2.5 as follows:

$$V_H(n(r)) = \frac{\delta E[n(r)]}{\delta n(r)} = e^2 \int \frac{n(r')}{|r-r'|} dr' \quad (\text{Equation 2.5})$$

The exchange correlation potential can be expressed in the following equation:

$$V_{xc}(n(r)) = \frac{\delta E[n(r)]}{\delta n(r)} \quad (\text{Equation 2.6})$$

Finally,  $V_{ion-electron}(n(r))$  is the interaction potential between electrons and ions. KS-DFT views the N electrons system as a system of independent particles that move in an effective potential represented by the combination of three terms which are  $V_H$ ,  $V_{xc}$ , and  $V_{ion-electron}$ . Exchange correlation potential, which is given in Equation 2.6, can be written as two terms: exchange potential and correlation potential as given by Equation 2.7 [85].

$$V_{xc} = V_x + V_c \quad (\text{Equation 2.7})$$

In KS-DFT approximation, the electron dynamical correlation is included within the correlation potential. Electron static correlation is involved in the exchange potential term. If the exact form of the exchange correlation potential is known, the ground state energy and the density of states are exact. Otherwise, an approximation is needed for the exchange correlation potential. Examples of the approximations used are local density approximation (LDA) and generalized gradient approximation (GGA). These approximations are called DFT functional and will be discussed in the next section.

When using simulation codes, Equation 2.3 is substituted into Equation 2.1 to find the ground state wave functions that are used to find other physical processes by starting with trial wave functions and charge densities. However, one needs to introduce a basis set to describe the system being investigated before proceeding to the next step of the simulation process. Quantum ESPRESSO is the first-principle code used to simulate Equation 2.3.

#### **2.1.4.2. DFT Functional**

The simple form of DFT approximation for exchange-correlation energy is to consider the densities of the electrons only. This approximation is known as local density approximation (LDA) [85], [88]. In such case, neither the derivatives of the electron densities nor the non-local orbitals are accounted for. To explain, LDA assumes the atoms and molecules as uniform electron gases having local densities. LDA is considered as a simple approximation. The exchange potential in this approximation can be given by:

$$V_x = -\left(\frac{3}{4}\right)\left(\frac{3}{\pi}\right)^{\frac{1}{3}} \int n^{\frac{4}{3}}(r)dr \quad (\text{Equation 2.8})$$

In Equation 2.8, it is assumed that the number of electrons and the volume are very large and approach infinity; therefore, the density of electrons is constant. One of the drawbacks of LDA is

that the correlation energy can be found at high and low electron densities only. LDA can be used to describe systems at which the density of electrons fluctuates gradually. Small lattice constants and band gaps are other drawbacks of LDA. However, LDA can be used practically with the Monte Carlo simulation technique. In contrast, the approximation is called generalized gradient approximation (GGA) if the gradients of these electron densities are considered. Including the density gradient in the approximation increases the complexity of solving DFT. However, adding the gradient meets the requirements of having inhomogeneous electron densities and enhances the exchange energy functional in DFT [88].

The exchange potential in GGA is given by the following equation:

$$V_x = -\left(\frac{3}{4}\right)\left(\frac{3}{\pi}\right)^{\frac{1}{3}} \int n^{\frac{4}{3}}(r)f_x(s)dr \quad (\text{Equation 2.9})$$

In Equation 2.9,  $f_x(s)$  is called the exchange enhancement factor.  $s$  is a dimensionless or a reduced density gradient. According to this approximation, the electron density is homogenous near the atomic nuclei and inhomogeneous in the exponential tails.

It has been found that DFT with GGA can lead to very small gap between the highest occupied molecular orbits (HOMO) and the lowest unoccupied molecular orbits (LUMO), which is caused by the self-correlation and self-exchange potential. In fact, DFT with GGA and LDA can result in underestimation of the band gap in solids. Such phenomena lead to increase in the energy of the localized states and cause DFT to generate delocalized charge distributions. Such delocalized charge distributions can be due to the electron-electron interaction energy. The delocalization of the electron distributions affects the predicted properties of materials, such as expecting them to be metals instead of insulators. Some researchers have introduced practical methods to eliminate the effects of the self-correlation and self-exchange, such as including the

kinetic energy density in the exchange potential [85]. Both functional LDA and GGA are adopted widely by physicists and chemists to solve many challenging problems. There has been significant effort by researchers to approximate the exchange-correlation parameters to fit the experimental data obtained for electronic properties of atoms and molecules. One can find considerable literature on LDA and GGA and their different forms based on the continuous development of many software platforms that have been used to numerically solve many-body problems using DFT. Perdew, Burke, and Ernzerhof (PBE) in 1996 introduced an exchange GGA and correlation GGA by applying the following condition on total exchange-correlation energies [88]:

$$|V_{xc}| \leq 2.28 |V_x^{LDA}| \quad (\text{Equation 2.10})$$

The exchange functional parameters might fit for some N electron systems and might not be necessary for other systems. PBE approximates the exchange enhancement factor to fit the atomic data. It has been favored by many researchers as an exchange functional. As a result, these approximations or functionals, LDA and GGA, can be fitted to the investigated systems using experimental data and selected theoretical constraints.

### **2.1.4.3. Pseudopotential**

In atoms, electrons are arranged in shells or energy levels. These electrons can be classified into core electrons and valence electrons.

Filled atomic shells have core electrons, while valence electrons partially fill the atomic shells. Since the chemical bonds are formed by sharing electrons, the core electrons do not participate in the chemical bonding. In contrast, the valence electrons participate in the chemical bonding and hence affect the electronic structure of materials and their properties. Thus, DFT in

such approximation considers only the electrons that are affected by the chemical environment. To illustrate, the tightly bound core electrons are not considered in the calculations because the electrons in the inner shells of atoms do not contribute to the valence bonding; therefore, they are considered to be isolated and have no effect on the energy[91]. The main reason for reducing or eliminating the effects of the inner electrons is that their electronic wave functions can vary and expand intensively as they move closer to the core of the nuclei. The expansion of these electronic wave functions leads to prohibitive computational cost. Therefore, removing these electrons from the calculations is vital. Furthermore, introducing smooth wave functions that describe the valence electrons can result in decreasing the size of the calculations. The approach that considers the valence electrons and introduces smooth wave functions for these electrons is known as the pseudopotential approach.

Pseudopotential views the material as a combination of two elements: valence electrons and rigid ions. These rigid ions include the core electrons and nucleus that do not change the chemical environment of materials or are not involved in the chemical bonding. Therefore, pseudopotential plays the role of the external potential needed to find the ground state energies and wave functions, which is  $V_{ion-electron}$ . Ignoring the contribution of the rigid ions to the total interaction in the calculations leads to a decrease in the number of energy eigenvalues and wave functions required to solve a N electron system problem by having a smaller size of basis. This assumption may cause a decrease in the accuracy of the calculations. Nevertheless, the calculations are assumed to be effective and precise because many physical and chemical properties of materials are determined by valence electrons.

There are a few types of pseudopotential that have been used in DFT calculations. Norm-conserving and ultrasoft pseudopotentials are the most common pseudopotentials that have been

used widely by researchers. Both norm-conserving and ultrasoft pseudopotentials are based on the plane-wave electronic structures that enable lower cut-off radius of the basis for proper numerical convergence. This indicates that there is cut-off radius where the wave functions of the electrons are described. Hamann, Schlüter, and Chiang (HSC) in 1979 proposed norm-conserving pseudopotentials [91], [92]. Norm-conserving condition implies that the electrons outside the core region do not recognize any change in the charge distribution inside the core region when the total charge is the same. In a norm-conserving pseudopotential, the potential has two parts: local potential and non-local potential as given in the below equation:

$$V_{ion-electron} = V_{pseudo} = V_{local} + V_{non-local} \quad (\text{Equation 2.12})$$

Local potential is described by a radial wave function which depends on the position of electrons only. Whereas, non-local potential is the potential of all electrons inside the core. Each wave function inside the cut-off region that is produced by the norm-pseudopotential is identical to the all electrons wave functions. Also, these wave functions are identical outside the cut-off region [91], [92]. This can cause underestimation of the exchange-correlation energy when using DFT for N electrons systems. Ultrasoft pseudopotential releases the norm conservation condition and reduces the size of the basis further than the norm-conserving pseudopotential [93]. Ultrasoft pseudopotential divides the wave function into two parts. One part describes the electrons outside the core and the other part describes the charge distribution inside the core region. Having two parts for the wave function leads to having a wave function produced by the pseudopotential inside the cut-off radius and no wave function outside the cut-off radius [93]. In this research, ultrasoft pseudopotential is used.



#### 2.1.4.4. The Plane Waves Basis Set

Most of the first principle simulation codes require plane-wave basis functions that are periodic. The mathematical structure of such periodic plane-wave basis functions can be of the following form:

$$\Psi_n^k(r) = e^{ikr} \chi_n^k(r) \quad (\text{Equation 2.13})$$

Here,  $n$  represents the energy level or the band index,  $k$  is a wave number in the reciprocal unit cell or the crystal momentum,  $\chi_n^k(r)$  is the periodic part of the wave function, and  $e^{ikr}$  is the oscillating part of the wave functions  $\Psi_n^k(r)$ . The relationship between the energy and the wave number is known as the dispersion relation.

The resulting wave functions in Equation 2.13 are Bloch states at each point in the lattice, which are naturally delocalized. To explain, Bloch states have different values at different  $k$  points. In contrast, quantum conductance or the probability transmission functions requires localized orbitals. In fact, the transmission probability functions require Green's function representation that is localized.

Therefore, a way of enveloping these states into localized wave packet is required to obtain localized wave functions in real space. Large superpositions of Bloch states in  $k$  space can lead to a localized wave packet. However,  $k$  is a wave number in the reciprocal cell that is defined as a Brillouin zone. As a result, Wannier functions can be used to localize the wave packet and the states [94]. Figure 2.1 shows schematics of Bloch, Wannier, and the localized wave functions based on Nicola Marzari and his group's work [94]. Practically, a computational code is essential to convert these periodic functions represented by Equation 2.13 into localized functions in a real space basis set [85].

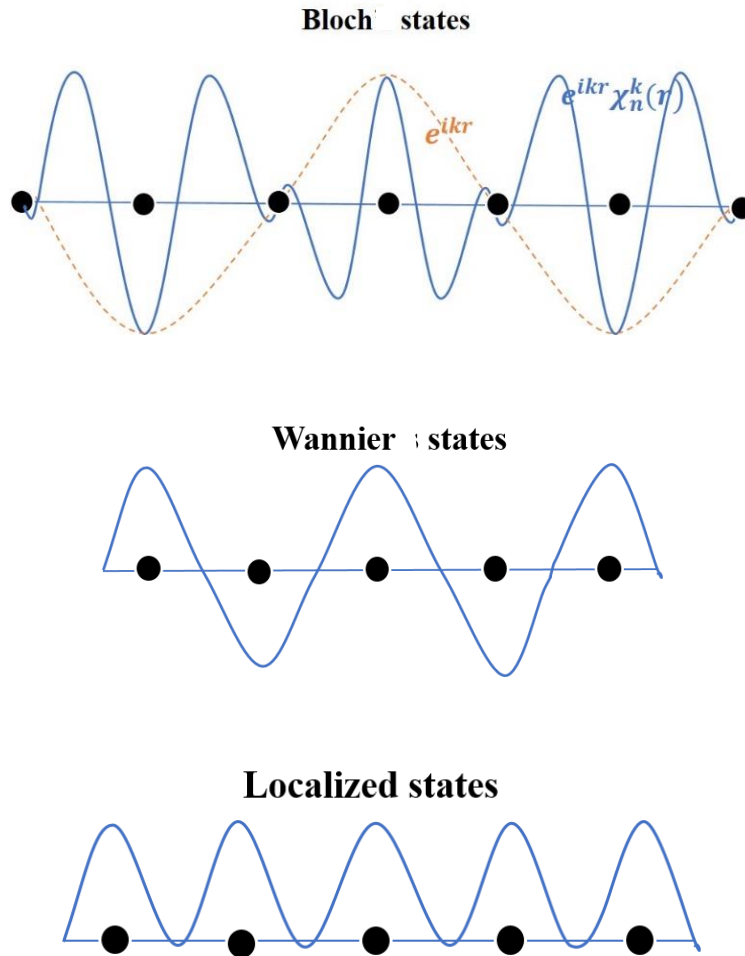


Figure 2.1. Schematics of Bloch, Wannier, and the localized states. Black dots represent the lattice vectors. Dashed orange line represents the envelop.

One of the functions used in calculating the quantum conductance and the transport properties is a Wannier function [85]. In this method,  $\Psi_n^k(r)$  will be converted into localized wave functions, Wannier functions, and hence converts Bloch functions using the smallest spatial distribution as illustrated in the following equation [90]:

$$w_{nR}(r) = \frac{V}{(2\pi)^3} \int_{BZ} \Psi_n^k(r) e^{-ik \cdot R} d^3k \quad (\text{Equation 2.14})$$

Here,  $w_{nR}(r)$  is Wannier function,  $R$  is the lattice vector,  $e^{-ik.R}$  is a phase factor that plays the role of translating Wannier functions by  $R$ ,  $v$  is the volume of the primitive cell in the real space, and  $BZ$ , Brillouin zone, can be defined as a special unit cell of the inverse lattice [90]. Wannier functions represent orthonormal basis functions of linear combinations of local functions [90].

There are some advantages of using Wannier functions. First, these functions are localized; i.e. their extension in space is very small compared with the plane waves. Also, Wannier functions provide the desired accuracy and efficiency when computing the ground state functions which are used to perform the electronic transport properties of the materials [95]. Equation 2.14 shows the integration within the BZ, Brillouin zone, which is a special unit cell of the inverse lattice [90] as mentioned earlier. In order to find the conductance,  $w_{nR}(r)$  resulting from Equation 2.14 are used to create the Hamiltonian that are solved for the lattice Green's function,  $G$ , as shown in the following equation:

$$(w_{nR} \pm i\eta - H)G(E) = I \quad (\text{Equation 2.15})$$

$I$  is the identity matrix,  $\pm i\eta$  is imaginary part that is added to satisfy the boundary conditions, and  $E$  is the energy. Equation 2.15 is solved to obtain two forms of Green's functions based on the sign of the  $i\eta$  term as shown in Equation 2.15 above. These functions are:

- Advanced Green's function,  $G^a$ , for positive  $i\eta$
- Retarded Green's function,  $G^r$ , for negative  $i\eta$

These two Green's functions can be used to calculate the transmission probability functions of the simulated system. For example, considering the coupling of the material to the electrode by Fisher and Lee, the transmission probability functions can be found using the following [90]:

$$T(E) = Tr[\Gamma_L G_C^r \Gamma_R G_C^a] \quad (\text{Equation 2.16})$$

Here,  $T(E)$  is the transmission factor,  $\Gamma_{L,R}$  are the functions that describe the coupling of the internal molecule to the left and right electrode leads, and  $G_C^{r,a}$  are the Green's functions of the molecule itself [80], [83], [96]. The transmission probability in Equation 2.16 describes the probability of the transport of electrons from the left side to the right side of the conductor and vice versa. The Landauer formula is the form that can be used to find the quantum conductance which is proportional to the probability transmission function assessed near the Fermi energy.

Landauer formula is given by [83]:

$$C = \frac{2e^2}{h} T(E_f) \quad (\text{Equation 2.17})$$

In Equation 2.17,  $C$  is the quantum conductance,  $T(E_f)$  is the transmission probability around Fermi energy,  $E_f$ ,  $h$  is Planck's constant, and  $e$  is the charge of an electron.

The total quantum conductance is found via summing the probability transmission functions through all the quantum channels as:

$$\mathcal{G}(E) = \frac{2e^2}{h} \sum_{i=1}^N T(E) \quad (\text{Equation 2.18})$$

Here,  $T(E)$  is the transmission probability function at energy  $E$ . The probability transmission function is the probability that an electron with energy  $E$  can be transmitted from one end to the other end of the electrode [94]. Equation 2.18 shows that the sum of the transition functions over all quantum channels,  $N$ , gives the total quantum conductance,  $\mathcal{G}(E)$ . DOS is the sum of all the states at each energy intervals.

The transverse electrical current can be found via the Landauer-Buttiker formula as given by the equation below:

$$I(V) = \frac{2e}{h} \int_{-E}^E dE' T(E') f(E') \quad (\text{Equation 2.19})$$

where  $I(V)$  is the transverse electrical current at voltage,  $V$ , and  $f(E')$  is the Fermi distribution function. In Equation 2.19, the energy  $E$  is in eV units and the voltage  $V$  is in units of volts. eV is  $1.602176487 \times 10^{-19}$  J [97]. The transverse electrical current shown in Equation 2.19 is directly proportional to the sum of the transmission peaks within the bias voltage,  $V$ .

The electrical quantum conductance and DOS obtained are associated with zero-bias voltage. However, the transverse electrical current shown in Equation 2.19 is directly proportional to the integration of the sum of the transmission probability peaks within the bias voltage,  $V$ .

In this research, the Fermi distribution function is assumed to be equal to the DOS obtained. This approximation has been adopted by other researchers when calculating the electrical current for DNA sequencing devices [98]. It has been also assumed that the transmission function has peaks associated with each base regardless of the values of the applied voltage [98]. Therefore, DOS is approximately equal to the Fermi distribution function in Equation 2.19 for this research. The estimated electrical current can be obtained via the numerical integration of the production of the quantum conductance,  $\mathcal{G}$ , and DOS. To illustrate, the calculated DOS and the transmission probability functions can be multiplied then integrated with respect to the energy  $E$  that is in units of eV to obtain the electrical current through the carbyne chain. eV is the required energy to move an electron through a potential of one volt [99]. Thus, both the voltage,  $V$ , and the energy,  $E$ , can be interchangeable in this dissertation. Equation 2.19 can be rewritten in the following form:

$$I(V) = \frac{2e}{h} \int_0^E dE' \rho(E - E') T(E') \quad (\text{Equation 2.20})$$

Here,  $\rho(E)$  represents the density of states, DOS. The integration to obtain the electrical current can be divided into two parts: the first part is for the positive biasing voltages and the second part is for the negative biasing voltages. Another electrical property that can be of interest is the differential conductance, which can be obtained by the derivative of the estimated electrical current obtained via Equation 2.20. The differential conductance,  $G(V)$ , is given by the following equation and it is called in some literature localized density of states (LDOS).

$$G(V) = \partial I(V)/\partial V \quad (\text{Equation 2.21})$$

### **2.1.5. DFT Simulation Using QUANTUM ESPRESSO and Wannier90**

QUANTUM ESPRESSO (QE) stands for quantum opEn-Source Package for Research in Electronic Structure, Simulation, and Optimization. It is a comprehensive package of open source codes that can be used to calculate the electronic-structure related properties of materials at the nanoscale using DFT, plane-wave (PW), and pseudopotentials. QE used in this work is version 5.1 which is available at Arkansas High Performance Computing Center (AHPCC). The codes that are included in QE can handle a variety of electronic-structure related calculations such as ground state, structural optimization, transition states and minimum energy paths, spectroscopic properties, response properties, and quantum transport.

Moreover, each one of these calculations is associated with more than one code with which a specific property can be evaluated. For example, quantum transport calculations include ballistic transport that can be calculated using PWCOND package, coherent transport from maximally localized Wannier functions that can be calculated using WanT code, and maximally localized Wannier functions and transport properties that can be calculated using wannier90

code. Therefore, QE has many very precise codes for specific properties. Several studies have reported using QE to calculate and predict the transport properties for many electronic devices at the nanoscale [80], [81].

The main components or namelists of the input data file for QE calculations are: control, system, electrons, ions, cells, atomic species, atomic positions, k\_ points, and cell\_ parameters. Each namelist has what is called cards to specifically introduce the data. Some of the data introduced in these namelists are mandatory and others are optional. The control namelist has all the data that controls the simulation. For example, users can identify the type of calculations such as relax, vc-relax, and other calculations that can be accomplished using pw.x code of QE. Also, the number of the calculation steps and forces or stresses that are applied on atoms and ions are specified in the control part of the input data file. Only calculation part is a mandatory variable within the control namelist. The system namelist has the structural information about the simulated system. Thus, the system namelist includes the Bravais-lattice index with which one can specifically describe the type of lattice that, when combined with the basis of atoms, forms the crystal structure of the material.

Furthermore, the number and type of atoms are defined in the system namelist of the input data file. Kinetic cut-off energy and charge cut-off energy are stated within the system namelist. These variables are mandatory in the system namelist. The maximum number of steps and mixing factor for self-consistency are defined in the electron namelist of the input file. When running relax and vc-relax calculations, the namelist ions plays an essential role in determining the algorithm by which the electronic structure can be examined.

There are several options to choose the way that the ions and cells are optimized. The choice is based on the models and the desired electronic properties. In relax and vc-relax

calculations, there are two algorithms: Broyden–Fletcher–Goldfarb–Shanno (BFGS) and damp. BFGS algorithm uses quasi-Newtonian mechanics to apply forces on atoms and ions. Damp uses Beeman dynamic to relax the structure. Both ion and cell dynamics have to be optimized using the same algorithm. These ion and cell namelists are optional in the input data file. Atomic species and positions namelists are specified in the input data file to determine the types and locations of atoms of the model. k point namelist defines the density of the mesh in reciprocal space. The dimensions of the simulation cell or the size of the cell is stated in a cell\_parameter namelist that is optional. An example of input data files can be found in Appendix A.

wannier90 is a code that is included in QE package of codes available at AHPCC. It is also open source code and is used mainly to calculate the transport properties of nanoscale materials [81], [100], [101]. As mentioned earlier, the main goal of using wannier90 is to convert the delocalized wave functions into localized functions that can be used to obtain the transport properties of nanostructures. There are some variables included in the input data file for wannier90 code. These parameters include the number of bands and number of wannier functions, which are mandatory. Also, the input data file includes atomic positions, cell size, initial projections, k-point grid with the path, Fermi energy, center of the unit cell, and other parameters. An example of a detailed wannier90 input file can be found in Appendix B.

### **2.1.6. Simulation Details**

As mentioned earlier, DFT is the approximation theory that was used in this research to deeply explore the electrical transport properties of electrons for the control system and other simulated models. In order to solve system-related quantum mechanics problems, pseudopotential is preferably used [81]. Pseudopotential is a scheme that is used as the external potential needed to determine the system-related electronic properties. First-principle simulations



based on DFT and NEGF were used for this research. As mentioned earlier in this chapter, QE [79] and wannier90 [81] were used to first simulate the transmission probability functions and DOS that were required to determine the I-V characteristics of the chain/ssDNA model systems.

The first set was the calculation of the ground states by QE. The outcomes of QE were the ground states in plane wave basis set. The second set used the Landaure formalism to calculate the transmission probability functions and DOS via wannier90 [90]. Landaure formalism relies on the electronic structure of the system under study and determines its transport properties by calculating the transmission probability functions. As discussed earlier, Landaure formalism requires Green's functions basis. Therefore, wannier90 code was used to convert the plane wave basis set that resulted from QE into a localized form that could be used in Landaure formalism. The simulation results of the second set were the transmission probability functions,  $T(E)$ , and DOS or  $\rho(E)$ . Here  $E$  is the energy. These first two sets of calculations were used to determine the electronic structure and transport properties at zero applied voltages. The third set of calculations was to integrate the product of DOS and the transmission probability functions to determine the I-V characteristics for each model. The 1D carbon chain electrical current,  $I$ , as well as the electrical current for all the simulated models were determined using the Landaure formalism as given in Equation 1.20. The numerical integrations were accomplished using OriginLab software Student Version. of wannier90 as shown in Figure 2.2. The first-principle simulation procedure included four steps of using QE and three steps. The code that was executed when using QE in all of the four steps was pw.x. The four steps in QE simulation included: (1) relax the simulated system by minimizing its energy to the lowest possible energy confirmation of the atoms in these simulated systems via Broyden– Fletcher–Goldfarb–Shanno (BFGS) algorithm; (2) variable cell relaxation (vc-relax) of the systems by optimizing the

simulation cell to the lowest possible confirmation; (3) self- consistent calculations to obtain the ground state wave functions; and, (4) non-self-consistent calculations. The work flow of the simulation process is presented in Figure 2.2.

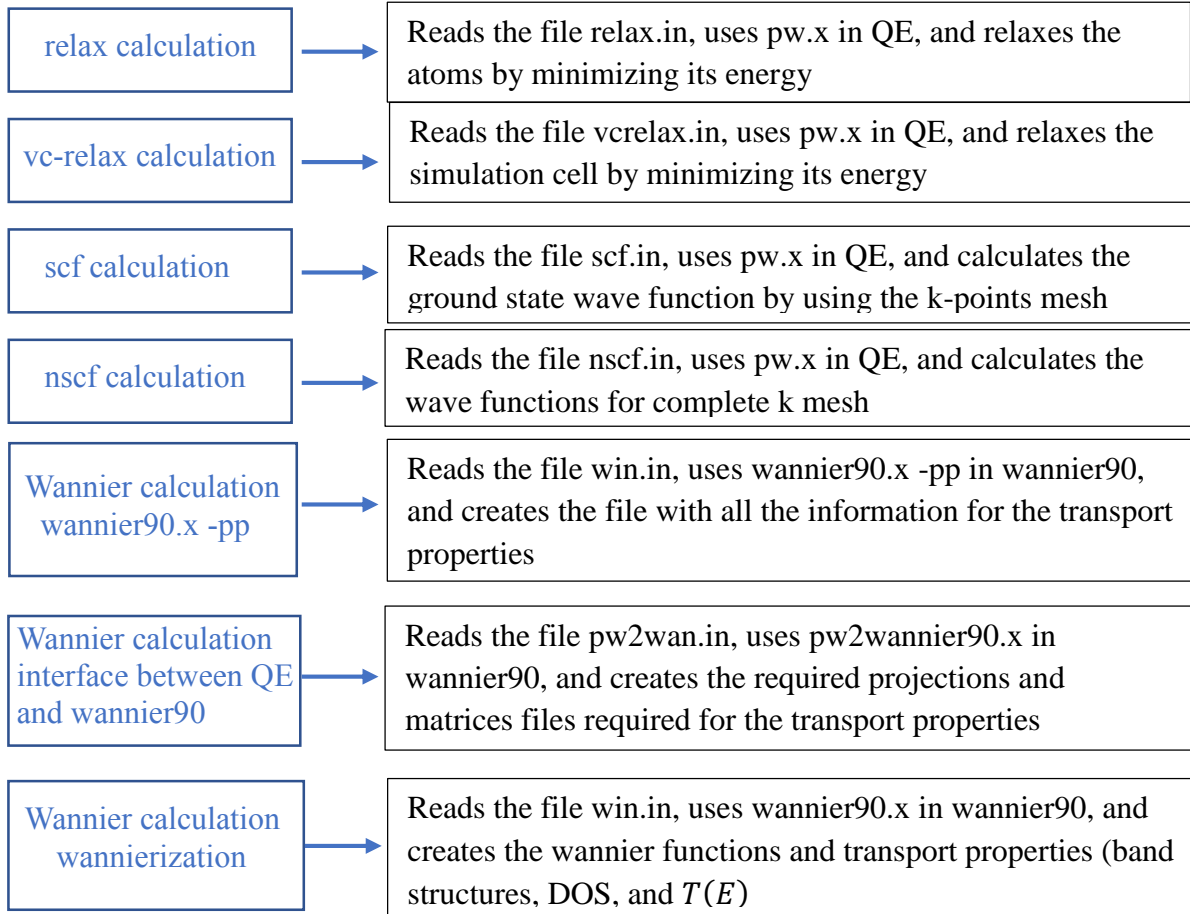


Figure 2.2. Work flow of the simulation process using QE and wannier90 codes.

The last step was using wannier90 to convert these delocalized states into localized functions and producing the transmission probability functions and DOS in three steps: (1) generating the projection file that had all the required information using wannier90.x -pp; (2)

interfacing between QE and wannier90 codes to create the required projections and matrices files required for the transport properties by using pw2wannier90.x in wannier90; and, (3) producing Wannier functions and the transport properties (DOS and  $T(E)$ ) using wannier90.x code. These properties were used to calculate the electrical current as discussed earlier.

The plane wave energy cutoff was 30 Ry and the Monkhorst-Pack  $k$  points were 8 x 1 x 1 for all the models that included a single chain of carbon atoms and ssDNA at different locations and orientations. For the 1D carbon chain attached to two graphene nanoribbons, the Monkhorst-Pack  $k$  points used were 4 x 2 x 2 in the presence and absence of ssDNA bases. Monkhorst-Pack  $k$  points were 8 x 1 x 1 for the graphene nanoribbon model systems investigated in this research. For the exchange and correlation interaction defined by the PBE functional and for the electron–core interaction [102], ultrasoft pseudopotentials with GGA [93] were used in this research.

## CHAPTER THREE: RESULTS AND DISCUSSION

This chapter includes the numerical simulation results and analysis for the first principle simulation approach used in this research. It is classified into sections. Each section presents the results and analysis of first-principle simulation for one of the simulated models and compares it with the available literature. Specifically, it describes the DOS and transmission probability functions obtained using QE and wannier90 codes. Also, the I-V characteristics and any analysis plots for the simulated models are plotted using OriginLab software.

### 3.1. First-Principle Simulation

DOS and quantum conductance or the transmission probability functions are presented for all the simulated models in this dissertation. I-V characteristics for all model systems are shown in each section.

#### 3.1.1. One-Dimensional Carbyne Chain

This section describes the first simulated model that is a one-dimensional (1D) chain of 16 carbon atoms and is located along the x direction. This chain, shown in Figure 3.1, was constructed to have a length of 21.6 Å using NanoEngineer1 [103].

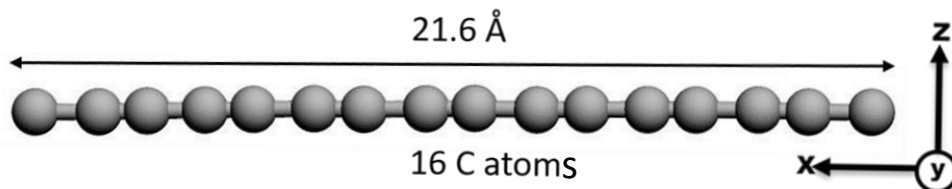


Figure 3.1. Schematic of the control model (polyyne) that is a chain of 16 carbon atoms along the x direction.

The geometrical optimizations were performed using Broyden–Fletcher–Goldfarb–Shanno (BFGS) algorithm until the forces were lower than 0.004 eV/Å. Ultrasoft pseudopotentials [93] with generalized gradient approximations were used for the exchange and correlation interactions defined by the PBE functional and the electron–core interactions [104]. The simulation cell was 23.1 Å along the x direction, while it was 25.0 Å along the y and z directions where sufficient vacuum was implemented. The plane wave energy cutoff was 30 Ry and the Monkhorst-Pack  $k$  points were 8 x 1 x 1.

A chain of the carbon atoms before the geometrical optimizations is polyene. It is constructed to have alternating single and triple bonds with length of ~1.55 Å and ~1.27 Å, respectively. As discussed in Chapter One, cumulene is considered as a metal due to having uniform distribution of  $\pi$  electrons around the chain, whereas polyene is a semiconductor due to having localized electrons at the triple bonds [58], [90], [105]–[107].

Moreover, polyene with alternating single and triple bonds has been reported to be slightly more stable than cumulene. Therefore, the 1D carbon that was constructed for this research was polyene. After the relaxing of the carbon chain and the simulation cell, the length of the bonds between the carbon atoms changes, and it was found to be approximately 1.32 Å for the single bond and 1.28 Å for the triple bonds. The total length of the chain after the geometrical optimization was 19.2 Å. A schematic of the 1D carbon chain after the relaxation process is shown in Figure 3.2. Hence, the chain is assumed to be a non-perfect polyene chain due to the changes in bond lengths after the geometrical optimizations. Similar behavior has been reported by several computational research groups when conducting the electronic transport properties of 1D carbon chains [90], [108]. The bond lengths after the geometrical optimization agree with the reported studies of the atomic carbon chains. The changes in the bond lengths are believed to

be due to Peierls's instability [36]. An unstrained chain is predicted to preserve cumulene and conserve metallic behavior, whereas a strained chain is predicted to show polyynic semiconducting behavior at room temperature [58], [105], [109]. Furthermore, the slight difference in energy between these two structures in a perfect system suggests the possibility of having cumulene and polyynic at some appropriate conditions.

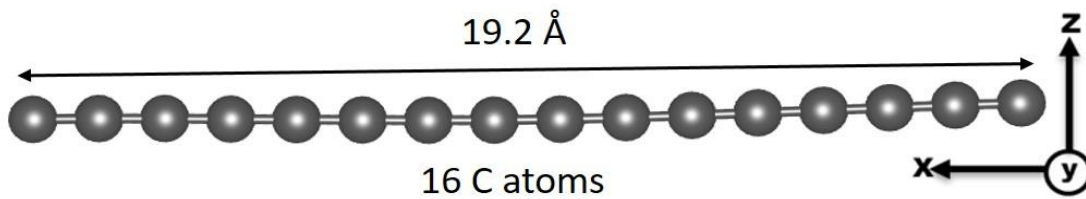


Figure 3.2. Schematic of the control model (polyynic) chain after the relaxation process.

The electronic transport properties of the carbon chains depend on the number of carbon atoms in the chain. The even number chains possess an odd number of bonds; therefore, the center of the chain is at the central bond. On the other hand, the chains with an odd number of carbon atom have their centers at the central atoms, which leads to zero BLA as discussed in Chapter One. BLA affects the electronic and structural properties of 1D systems [60]. BLA is defined as the difference between the long and short bonds as mentioned in Chapter One. As a result, the chain with an odd number of carbon atoms may possess higher energy than a chain with an even number of carbon atoms, which infers that odd-numbered chains are less stable than even-numbered chains. Since the stability of the chain is required, an even number of carbon

atoms was chosen in this research. The time required to minimize the energy of the system and achieve the convergence criteria increases when increasing the number of atoms in a simulated system. This is computationally costly. Thus, a chain of 16 carbon atoms was chosen.

The transmission probability functions and DOS for the control model are presented in Figure 3.3, while the electrical current and differential conductance are presented in Figure 3.4. The transmission probability functions or the quantum conductance spectra represented in Figure 3.3 shows that the carbyne chain exhibits a maximum of two quanta,  $2G_0$ , with  $G_0 = \frac{2e^2}{h}$ . The reason for having the two quanta is related to the two electronic structures of carbyne. The

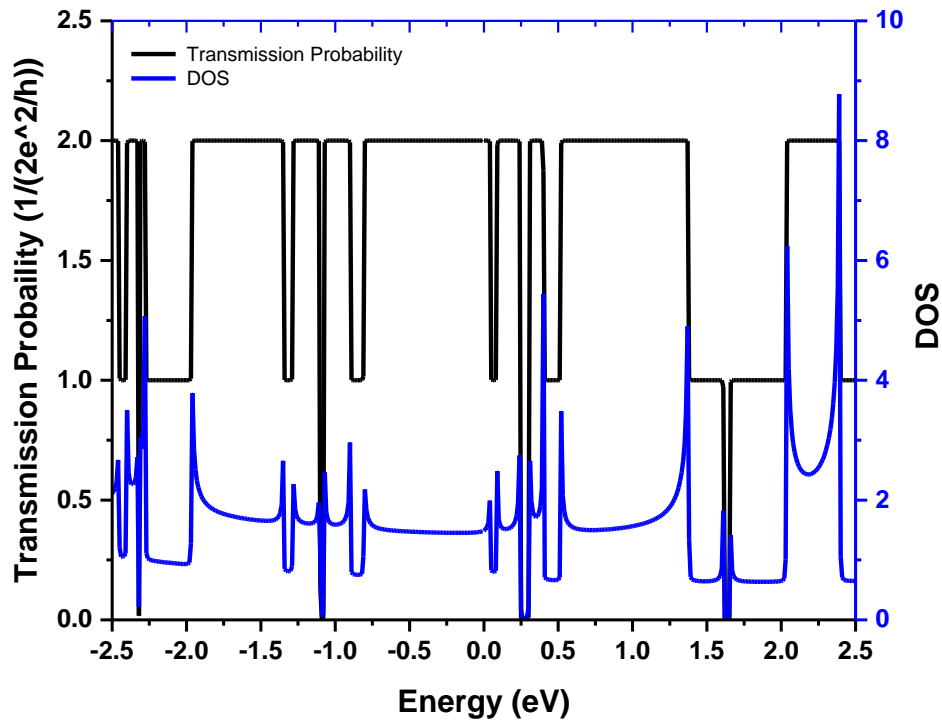


Figure 3.3. Transmission probability functions and DOS at positive and negative energies for the control model.

cumulene chain has two  $\sigma$ -bonds along  $s$ - $p_x$  orbitals and the two delocalized  $\pi$ - bonds along  $p_y$  and  $p_z$  orbitals as discussed in Chapter One. For example,  $\sigma$  states are in the middle of the bonds, while  $\pi$  states are centered around the carbon atoms. Thus, the electrons are uniformly distributed along the chain as mentioned earlier. The polyynes chain has two  $\sigma$ -bonds and two  $\pi$ - bonds. However, the distribution of these electronic states is different from the electronic distribution for the cumulene chain. For example,  $\sigma$  states are at each single and triple bond, while  $\pi$  states are localized at the triple bonds only in a polyynes chain. For a cumulene chain, there is one  $\sigma$  bond and  $\pi$  bond for each double bond. Thus, the electrons in a polyynes chain are localized at the triple bonds [36], [90], [105], meaning they are unevenly distributed along the chain. A degeneracy of bands has been reported to result in having a quantum conductance of two quanta in a cumulene. A polyynes chain exhibits two quanta of quantum conductance. Having two quanta indicates that the chain is characterized by the quantum channels associated with the electronic structure of the 1D chain [36], [62].

Furthermore, the quantum conductance or the transmission probability functions and DOS are different around zero energy. To illustrate, the range of energy in Figure 3.3 can be divided into two segments. The first segment is from 0.0 to 2.5 eV and the second is from 0.0 to -2.5 eV. The DOS showed a higher peak in the positive energy segment than in the negative energy segment. As mentioned earlier, Peierls's instability indicates that 1D systems are subject to loss of symmetry. Unstable electrons cause the loss of symmetry and lead to the lattice distortion. This distortion results in lowering the electron energies compared with their energies in a perfect crystal [105]. Hence, it is anticipated that Peierls's instability causes the distortion in the electronic structures of the one-dimensional carbon chain [36], [58], [105]. It is also obvious the transmission probability functions decrease from  $2G_0$  to  $G_0$  at 1.25 eV as can be seen in



Figure 3.3. The transmission functions or the quantum conductance is one quanta,  $G_0$ , within the range from 1.25 - 2 eV. More importantly, the transmission probability function is zero at 1.7 eV. In addition, there is a drop in the transmission probability functions at  $\sim -1.2$  eV. These drops in transmission probability functions or the quantum conductance and the DOS can be due to channel closing such that the electrons do not transport from one end of the chain to the other end [62].

Another factor that affects DOS is the gap between the highest occupied molecular orbits (HOMO) and the lowest unoccupied molecular orbits (LUMO). Chains with a larger gap are reported to be more stable than the ones with a smaller gap [60] as the semiconducting behavior shows for larger gaps compared with the metallic behavior that is displayed near zero band gap. In particular, the gap in the 1D carbon chain is reported to decrease when increasing the size of the chain [110], i.e., increasing the number of carbon atoms in the chain results in a decrease of the gap. Furthermore, the charge density distribution of the one-dimensional carbon chain is uneven along the chain due to having asymmetrical lengths of bonds [110]. Considering the uneven lengths of the bonds along the control model, it is speculated that the distribution of these electrons may differ at different energies.

To further understand the electronic transport properties of a 1D carbon chain, the electrical current and conductivity were obtained by numerically integrating the transport probability functions and DOS. The integration of the multiplications of the DOS and the transmission probability functions yields the estimations of the electrical current at various biasing voltages along the x direction as shown in Figure 3.4. The energy and the voltage in this research are assumed to be interchangeable as discussed in Chapter Two. The differential electrical conductance can be obtained by the derivations of the electrical current with respect to

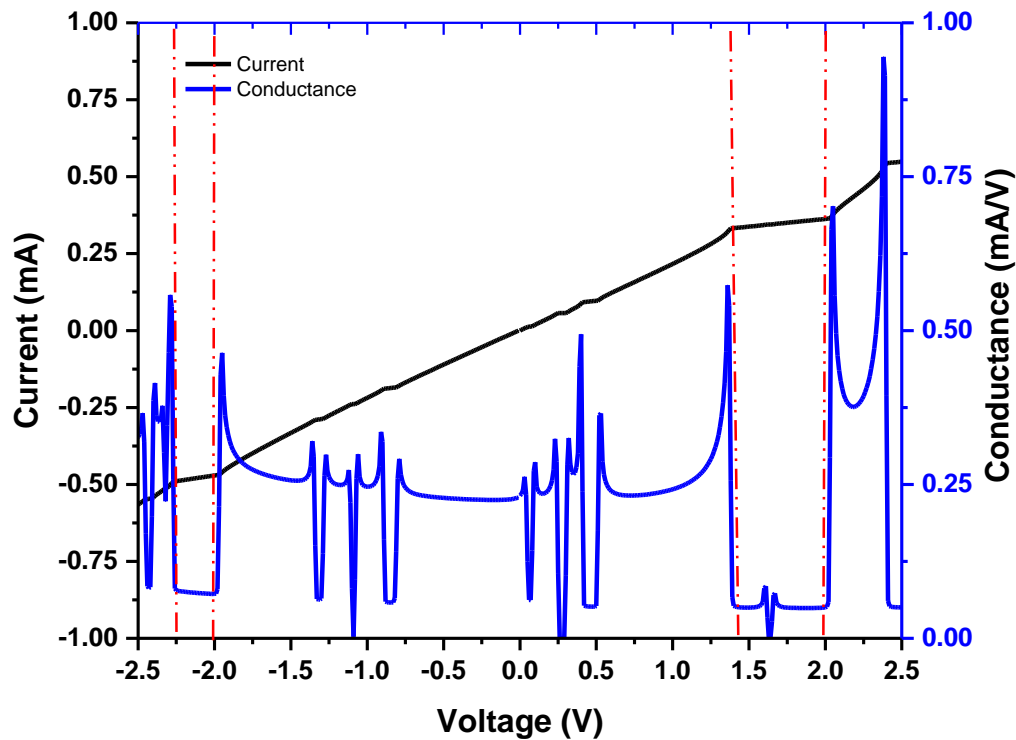


Figure 3.4. I-V characteristics and electrical conductivity for the control model at positive and negative biasing voltages.

the voltage as presented in Figure 3.4. The differential conductance was obtained via Equation 2.21 which can be found in Chapter Two. It is called the local density of states (LDOS) [73]. The I-V characteristics curve obtained for the control model at positive and negative biasing voltages shows a mostly linear increase in the electrical current when increasing the biasing voltages, positive and negative. Red dashed lines identify the different regions of the voltages on the I-V curve in Figure 3.4. The ohmic behavior or the linear I-V characteristics is expected for a perfect metallic chain. At the positive biasing voltages in Figure 3.4, the electrical current persists at a constant value within the range of 1.25 V to 2.0 V, and then starts to increase linearly again at 2.0 V. The same behavior can be seen at the range of -2.0 V to -2.25 V where the current starts to increase again in the reverse voltage region. The constant current that starts at 1.25 V and -2.0 V

indicates that the current is biasing independent, meaning the current stays constant despite the increase in the biasing voltages. The constant current regions are assumed to be caused by the drop in the transmission probability functions and DOS within these two ranges which can be seen in Figure 3.3. A first-principle study reported that the electrical current of an even number of carbon atoms ranging from 4 to 8 atoms in a chain do not change when increasing or changing the biasing voltages from approximately  $\sim 1.1$  V to  $\sim 1.7$  V [110]. Despite the fact that the constant current obtained in this research starts at  $\sim 1.25$  V for the positive biasing voltages, it is still within the range of  $\sim 1.1$  V to  $\sim 1.7$  V in [110]. Considering that the chains in the reported study are composed of about half the number of the carbon atoms compared with the research of this dissertation, the results obtained here are in good agreement with the reported study – increasing the number of atoms led to varying the electronic structure of the chain.

An experimental study reported a constant current segment and quasi-zero conductance at  $-1.2$  eV. The study claims quasi zero conductance at  $-1.2$  eV for a system that is nanoribbon-chain-nanotube [58]. Although the control model system investigated in this research is different, the behavior agrees with the experimental results obtained in Reference 58 by having a quasi-zero increase in the electrical current at negative biasing voltages.

The electrical current showed dependence of the biasing voltage within the range from  $-2.0$  V to  $1.5$  V. The I-V curve within this range is symmetrical and exhibits linear ohmic behavior as shown in Figure 3.4. The simulation approach used in this study does not include applying voltage, but the energy obtained can be used to represent the voltage. To explain, the energy is the potential required to transport the electrons. Therefore, Figure 3.3 and Figure 3.4 show the same scales for the energy and the voltage. It is anticipated that applying high biasing voltage leads to exciting the electrons at the high-energy levels, and these electrons can transport

through the chain. Furthermore, the applied voltage enhances the energy of the electrons and leads to a change in the gap. Also, high biasing voltage may lead to burning the 1D chain. Therefore, the range of the energy and voltage is within the range of 2.5 eV to -2.5 eV.

The carbon chains with an even number of carbon atoms are suggested to have higher electrical current and conductivity than the chains with odd number of carbon atoms [27], [30], [31]. Although this research does not include carbon chains with odd number of carbon atoms, the results obtained for the even-numbered chain of atoms are in good agreement with the reported numerical and experiment regarding the I-V characteristics for a single chain of carbon atoms [36], [58], [105], [110].

### **3.1.2. Atomic Carbon Chain as a Sensing Element for ssDNA**

The electronic transport properties are at the heart of the nanostructure functionalities for biomedical applications due to their small size and attractive quantum effects. Due to the remarkable mechanical and electrical properties of the 1D carbon chain besides its atomic thickness (width), it is anticipated that such a chain enhances the spatial resolution of the recent nanostructures detection devices when implemented in DNA sequencing devices. Thus, it was part of the interest in this research to further investigate the I-V characteristics and electrical conductivity of the 1D carbon chain in the presence of biomolecules such as ssDNA.

The effects of different ssDNA bases on the electrical properties of the single carbon chain were investigated in this research by including one base of the four different ssDNA bases individually. One base of adenine (A), cytosine (C), thymine (T), or guanine (G) was inserted normally to the chain to form four other different model systems. The molecular structures of these four different bases were downloaded from the Protein Data Bank (PDB) website [111].

The file had different bases originally. These bases were selected and saved as individual PDB file, while the rest of file was ignored.

The capability of detecting the DNA bases was demonstrated by analyzing the differences in quantum conductance or the transmission probability functions, DOS, and the electrical current values in the presence and absence of each base separately. All five systems including the control model were generated to be periodic along the x direction with enough vacuum along the y and z directions.

The 1D carbon chain was along the x direction. The electrical current was calculated along the x direction; whereas, the bases were inserted perpendicular to the chain. These four model systems had one ssDNA base placed normal to the chain as shown in Figure 3.5. After embedding each DNA base, the minimum energy structure was obtained by allowing the atoms to move along x then followed by cell optimization using Broyden–Fletcher–Goldfarb–Shanno (BFGS) algorithm until the forces were lower than  $0.004 \text{ eV}/\text{\AA}$ . Ultra-soft pseudopotentials [93] with generalized gradient approximations were used for the exchange and correlation interaction defined by the PBE functional and the electron–core interaction [104].

The size of the simulation cells and number of atoms are displayed in Table 3.1. Each of the different ssDNA bases included a base, a phosphate group, and a sugar backbone as shown in Figure 3.5. Plane wave cutoff energy was 30 Ry and the Monkhorst-Pack k points were  $8 \times 1 \times 1$ . The DOS and the transmission probability functions for the models of chain/ssDNA are presented in Figure 3.6 and Figure 3.7, respectively. The presence of these different bases caused noticeable changes in the DOS and the transmission probability functions as can be seen in Figures 3.6 and 3.7.

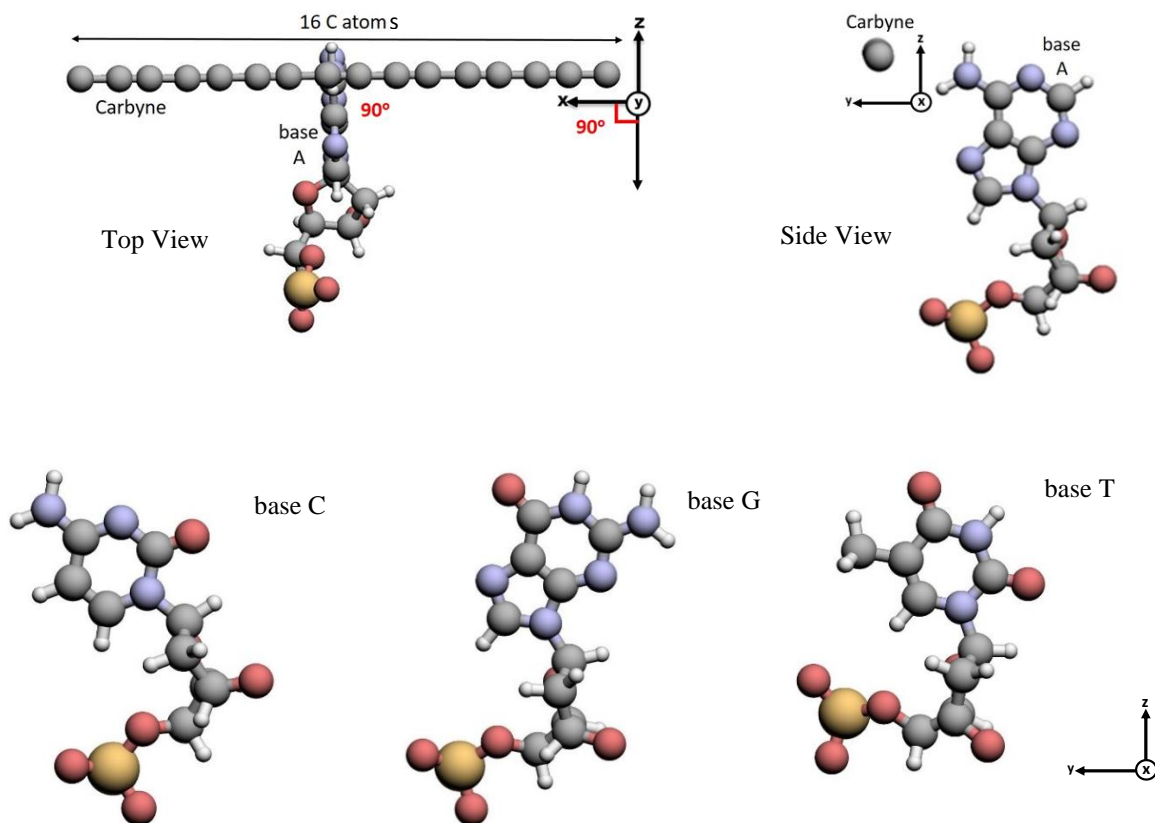


Figure 3.5. Schematics of the chain/A simulated model systems (top and side views). Schematics of the side view of bases C, G, and T. Gray spheres are the carbon atoms, red are the oxygen, yellow are the phosphorus, light purple are the nitrogen, and the white spheres are the hydrogen atoms.

Table 3.1. Number of atoms and size of the simulation cell for the model system chain/ssDNA

System	Number of atoms	Size of the simulation cell ( $\text{\AA}^3$ )
Carbyne/A	48	22.6×25.0×25.0
Carbyne/C	46	22.6×25.0×25.0
Carbyne/G	49	22.6×25.0×25.0
Carbyne/T	48	22.6×25.0×25.0

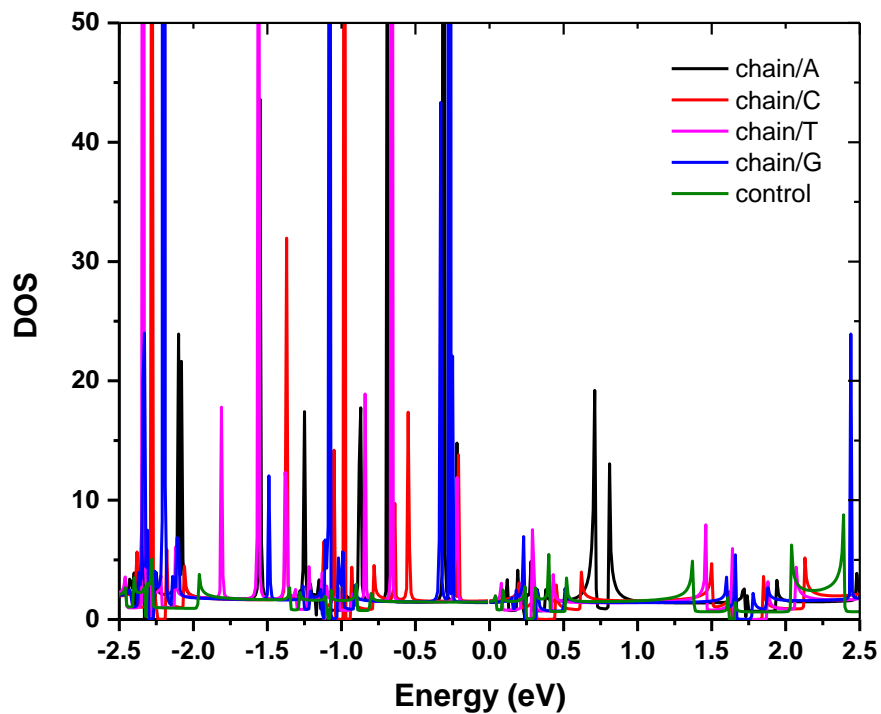


Figure 3.6. DOS for the chain/ssDNA simulated model systems compared with the control model.

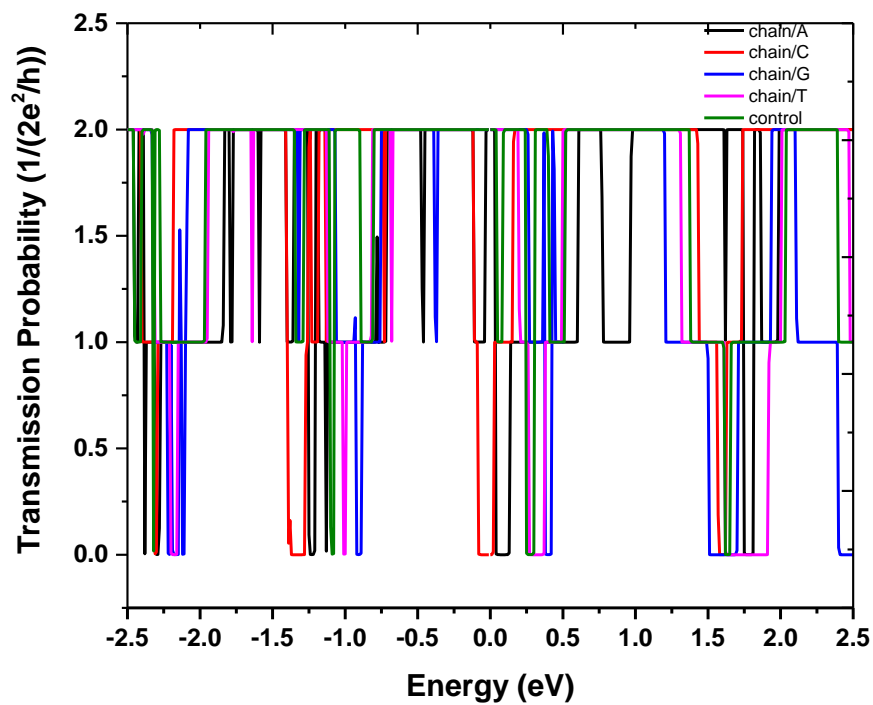


Figure 3.7. The transmission probability functions for the chain/ssDNA simulated model systems compared with the control model.

To recognize the 1D chain ability of distinguishing different ssDNA bases, I-V curves for five different model systems of chain/ssDNA compared with the pure carbon chain, control model, are presented in Figure 3.8. In general, the 1D carbon chain showed different behavior associated with different bases within the relevant energy ranges.

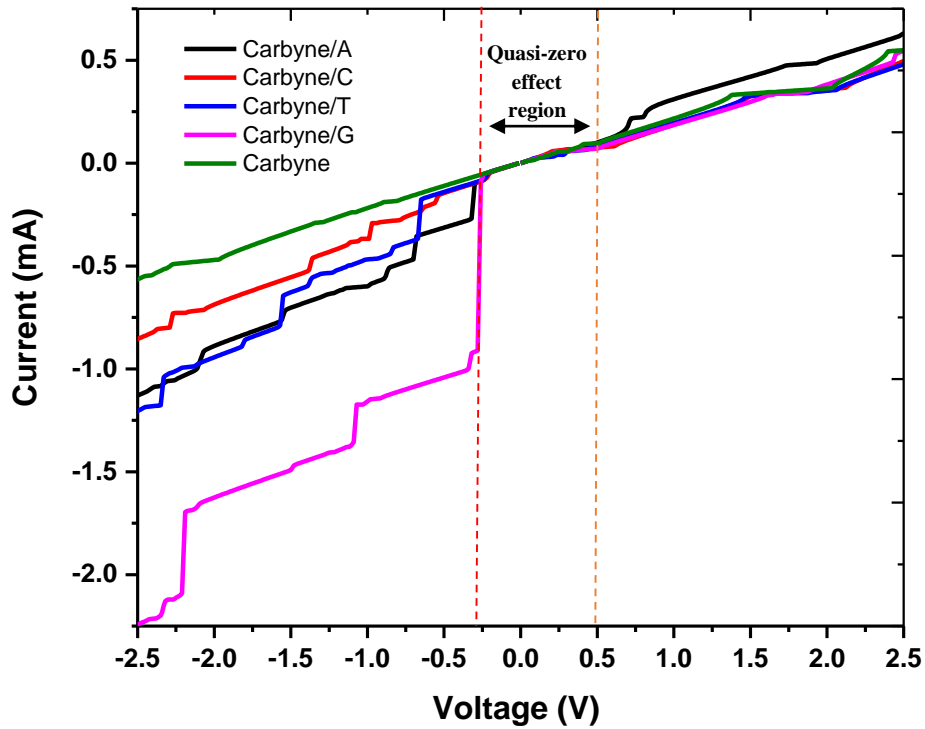


Figure 3.8. I-V characteristics of the chain/ssDNA model systems compared with the control model at positive and negative biasing voltages.

Comparing the DOS of the control model with DOS for the model systems chain/ssDNA, one can clearly observe that the number and height of the DOS peaks increased when the different bases were present normal to the carbon chain. In Figure 3.7, the maximum transmission probability remains two quanta with significant shifts of its values with the



existence of these different bases. The changes in DOS and the transmission probability functions indicate that different bases induce different electrical response in the carbyne chain at their presence. The DOS and the transmission probability functions for each model of different chain/ssDNA simulated models were used to obtain the electrical current. Since there were changes in these electrical properties, it was expected that the electrical current of the carbyne chain would vary differently with the existence of these different bases.

Figure 3.8 demonstrates the I-V characteristics for the chain/ssDNA simulated model systems compared with the control model at positive and negative energies. This curve can be discussed in terms of three regions of biasing voltages. These three regions are identified by red dashed lines to separate them as can be seen in Figure 3.8. First, positive biasing voltage started at 0.5 V to 2.5 V. This first region was extracted and is displayed in Figure 3.9. The second region started at -0.25 V to 0.5 V. Finally, negative biasing voltage started at -0.25 V to -2.5 V.

The first region of the I-V curve shows that the electrical current of chain/A model increased when base A was placed normal to the chain. On the other hand, the electrical current for the other simulated models, which are chain/C, chain/G, and chain/T, decreased compared with the control model. For example, the electrical current of chain/A model increased by about 27% at 1.3 V. In contrast, the current decreased by approximately 12%, 15 %, and 11% for chain/C, chain/G, and chain/T models, respectively. The change in the current was caused by the variations of the electrical properties of the single carbon chain in the presence of the different bases.

Specifically, the electrical current of the three simulated models that had bases C, G, and T showed similar trends at the positive voltages, while base A caused the carbon chain current to increase by approximately 0.2 mA as can be seen in Figure 3.9. The changes in the electrical

current of the carbon-based materials had been reported in other studies [8], [19], [56], [62], [64], [73], [112]–[114], [114]. For example, the adsorption of these different bases on the graphene nanoribbon is expected to be due to the  $\pi$ - $\pi$  interactions between the graphene sheet and different ssDNA bases [8], [56]. Such interactions or adsorption of ssDNA bases on the graphene surface results in inducing variations in the electrical current of the graphene.

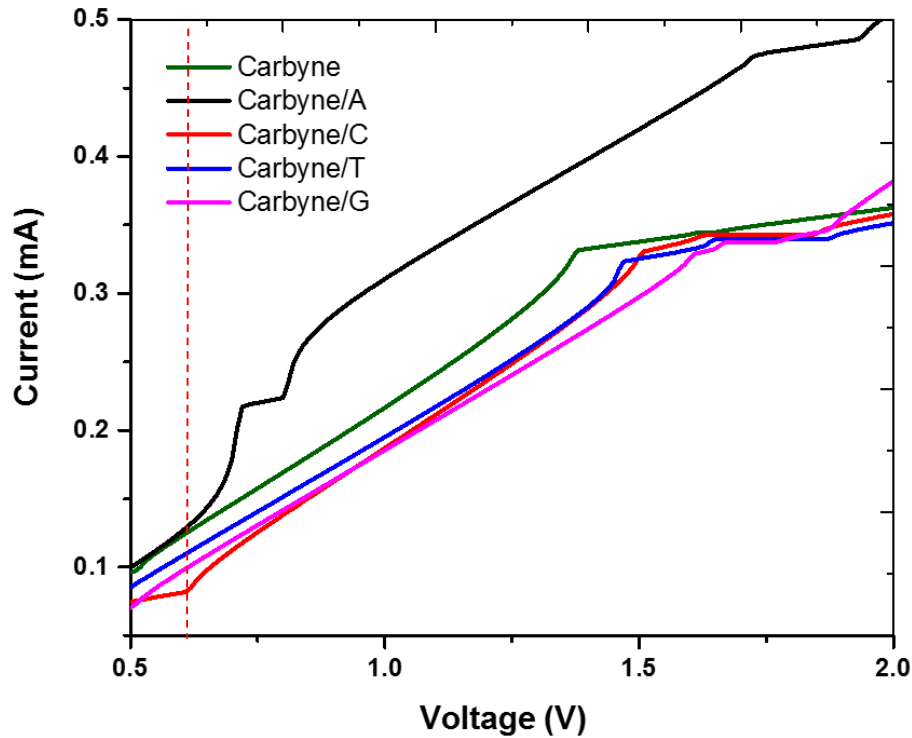


Figure 3.9. I-V curves for the different simulated models at positive biasing voltages.

Compared with the graphene nanoribbons, it was expected that  $\pi$ - $\pi$  interactions and the adsorptions of these different bases onto the carbyne surface could lead to changes in the electrical properties, the DOS and the transmission probability functions, of the 1D carbon chain. These changes suggest that the electrical current in the carbyne chain differs at the presence of

different bases. One of the reported studies claims that the electrical current through graphene nanoribbons increases slightly with an increase in the bias voltage from 0 to 0.6 V when bases C, G, and T are absorbed to the graphene nanoribbon surface. In contrast, the electrical current decreases when base A is present [56]. Thus, the obtained results in the research of this dissertation contradict the reported results for graphene nanoribbons. However, the differences in the simulation parameters, such as having the bases placed parallel to the graphene nanoribbons can lead to different effects on the graphene nanoribbon. Also, the bases in the reported graphene nanoribbons study include only those with no sugar and phosphate groups [56]. On the other hand, the base models simulated for this dissertation include the base, sugar group, and phosphate group. The variations in the chemical structures as well as the orientation of the bases are expected to lead to such disagreement.

Generally, there are several key factors and reasons that can affect the estimated single chain current. The locations and orientations of the bases with respect to the 1D chain are significantly important and could lead to changing the results drastically. The influence of different locations and orientations of the bases will be discussed later in Sections 3.1.3 and 3.1.4 of this chapter.

Another study reported that the adsorption of ssDNA bases on graphene armchair-edged nanoribbons leads to conductance drops caused by Fano resonance [30]. The drops in the conductance results in the decrease of the electrical current through the armchair-edged graphene nanoribbons. The main idea of Fano resonance is that a nucleobase acts as a resonator without bonding to the graphene nanoribbons. The study used DFT and NEGF to indicate the origin of the dips in the transmission probability functions. It concluded that there was a resonance effect between the nucleobase molecular orbitals and a continuum of energy states of a graphene

nanoribbon. Speculating based on the graphene nanoribbon study, Fano resonance and the orientations of the different bases with respect to the carbyne chain might be the reasons for such disagreement with the reported study on graphene in Reference 30.

In the second region of biasing voltage, the existence of different ssDNA base had no effects on the chain current. Such behavior has been reported by a group of researchers who investigated the adsorption of the different bases on the graphene nanoribbon surface. Song and his group found that different ssDNA bases are adsorbed to graphene nanoribbons differently due to  $\pi$ - $\pi$  stacking interactions [56]. The strength of these interactions varies among the different bases. The electrical current obtained in that study for different bases showed no difference below 0.3 V at the positive voltage region within the range 0.0 - 0.6 V [56]. This analogy of no-effect region can be applied to the strengths of the stacking interactions between the single carbon chain and the ssDNA bases. It is suspected that the interaction with each base is weak such that it cannot modulate the redistributions of the DOS and the transmission probability, and hence it is not sufficient to change the electrical current flowing through the chain. The results agree well with the observations of I-V curves in the results of this dissertation for biasing voltages below 0.25 V.

The third region of biasing voltages showed an increase in the chain current when different ssDNA bases were present. The electrical current increase was on the order of  $I_G > I_A > I_T > I_C$ . Obviously, the electrical current in the chain fluctuated when the different bases interact with the carbon chain. The electrical current obtained in this study was estimated by using DOS and the transport probability of electrons, and it was not via applying voltage as explained earlier. Therefore, the antisymmetric current behavior was associated with the energy of the states and not to an applied voltage on the chain. Furthermore, the Fermi energy for the control

model that was a chain of 16 carbon atoms in this study was found to be -5.079 eV, while it was -5.24 eV, -5.35 eV, -5.28 eV, and -5.12 eV when the bases present were A, C, T, and G, respectively. Therefore, these bases caused the Fermi energy to shift differently and, hence, led to a unique shift in the transverse electrical current associated with each base. This property can be used as another sensing mechanism for ssDNA bases.

As discussed earlier, the presence of different ssDNA bases leads to  $\pi$ - $\pi$  stacking interaction or the adsorption of ssDNA bases onto the chain surface. Several studies have reported that the binding energy of base G to graphene in solvents is the strongest compared with other bases [42], [74], [115]–[117]. The order of the binding energy is  $E_G > E_A > E_T > E_C$  in graphene via stacking interactions.

Another study has reported that the probability distribution of the electrical current is in order of base: G, A, T, and C, respectively [14]. The binding energy is directly proportional to the strength of the interactions between ssDNA bases and the sensing element, such as graphene and CNT [42]. Since there is no reported literature regarding the interaction and adsorption of the ssDNA bases to the 1D carbon chain, speculation based on the reported studies on graphene nanoribbons are presented in this dissertation.

Therefore, it was assumed that the  $\pi$ - $\pi$  interaction in the presence of base G was strong enough to cause the most drastic changes to the electrical properties of the chain and, hence, to increase the electrical current via increasing the DOS and the transmission probability. The strength of the interaction indicates that the binding energy of the G to the carbyne chain is the strongest compared with the other three bases.

### 3.1.2.1. Current of chain/ssDNA at 0.6 V and -0.85 V

To further analyze the resulting current for the different simulated models, the changes in the chain's current in the presence of different ssDNA bases are discussed for a biasing voltage of 0.6 V. Figure 3.9 shows the electrical current for the different model systems at the positive biasing voltages. The current at 0.6 V is represented by the red dashed line in Figure 3.9. Figure 3.10 represents the electrical current for the chain/ssDNA model systems compared with the control model at 0.6 V.

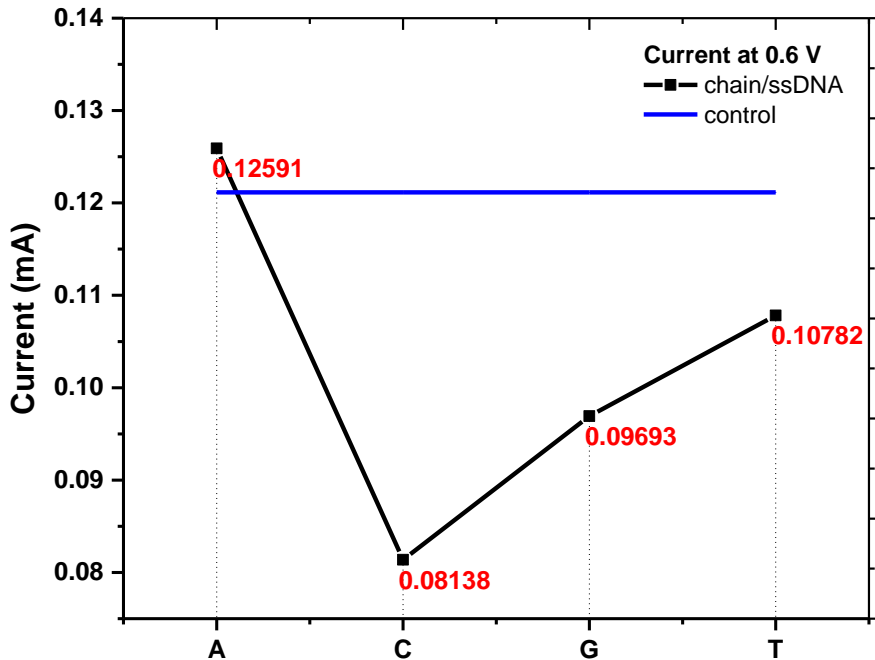


Figure 3.10. The current at 0.6 V for the chain/ssDNA model systems compared with the control model.

The voltage of 0.6 V has been used in a successful tunneling current measurement through platinum nanoelectrodes for DNA sequencing devices [118]. It produces a distinct

electrical signal when ssDNA bases are translocated through the nanogap. Thus, 0.6 V was used in this research to further investigate the carbyne sensitivity to the presence of different ssDNA bases. At 0.6 V, each base caused the electrical current in the carbyne chain to differ as shown in Figure 3.11. For example, the existence of base A leads to an increase in the electrical current flowing through the single carbon chain by 3.3  $\mu\text{A}$ . In contrast, the chain current decreased at 0.6 V by 41.1  $\mu\text{A}$ , 14.7  $\mu\text{A}$ , 25.6  $\mu\text{A}$ , when bases C, T, and G were present, respectively.

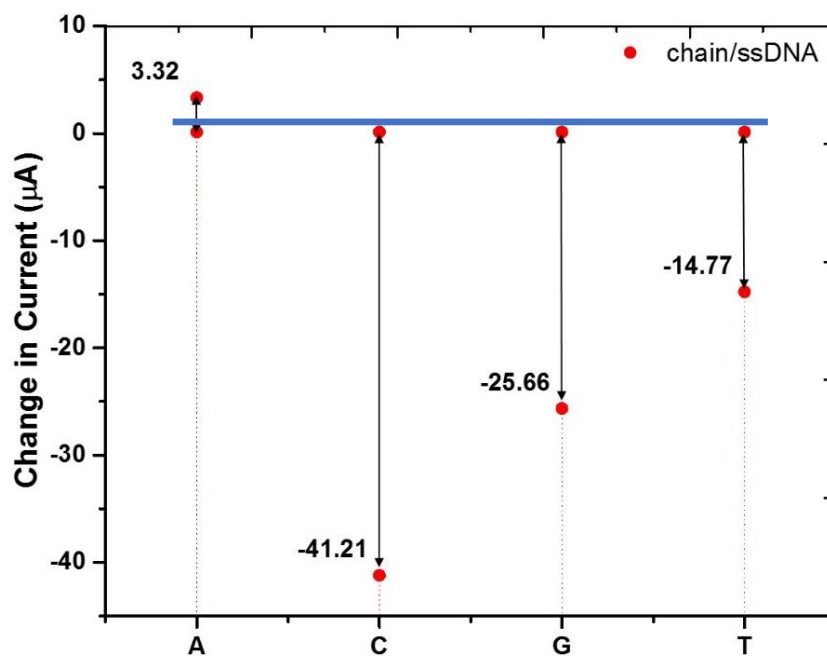


Figure 3.11. Change in the current for chain/ssDNA model systems compared with the control model at 0.6 V. Negative numbers refer to a decrease in the electrical current. The blue line is the chain current at 0.6 V (0.1225 mA).

The decrease in the electrical current is represented by the negative signs in Figure 3.11. Note that the decrease in the current values is given in  $\mu\text{A}$ , whereas the current in Figures 3.9 and 3.10 is given in mA. As discussed earlier, there are neither experimental nor computational

studies published regarding the interactions between 1D carbon chains and ssDNA bases to compare with the obtained results. However, a study has reported that the electrical current in graphene nanoribbons drops by  $0.5 \mu\text{A}$  when bases G, C, and T are present at  $0.6 \text{ V}$  [56]. On the other hand, base A is reported to be undetectable. That study concluded that the oxygen in G, C, and T bases modulates the electrical properties of graphene and produces a detectable response. Since base A does not have oxygen in its structure, it is undetectable based on the report [56]. Considering the differences in locations and orientations between the model systems in the reported study and this research, one can expect such disagreement between the obtained results in this dissertation and the reported results.

Figure 3.12a displays the current values and the percentage of changes in the electrical current at  $-0.85 \text{ V}$ . Figure 3.8 showed that the presence of base G led to the most significant increase in the electrical current at the negative biasing voltages. Figure 3.12b shows a 502% increase in the electrical current of the chain when base G was present. Base A induced a 171% increase in the electrical current through the chain. Bases C and T resulted in a about 51% and 137% increase in the electrical current of the carbyne chain, respectively.

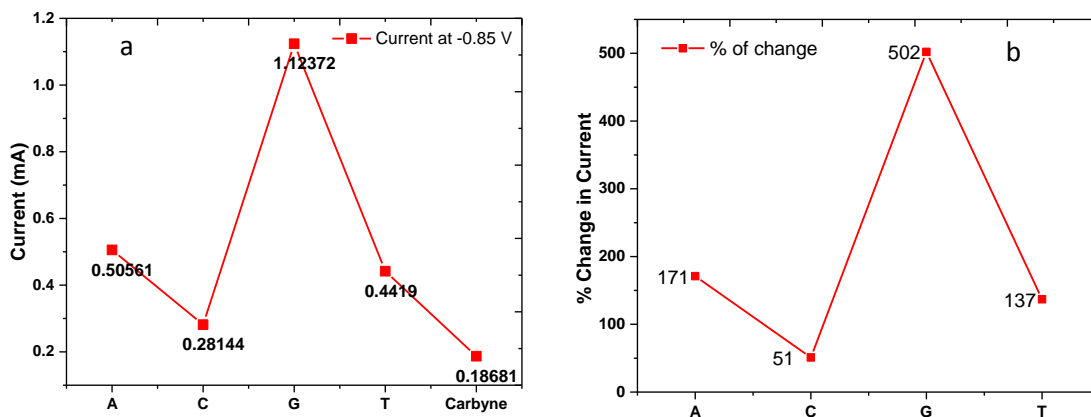


Figure 3.12. (a) Current for the chain/ssDNA model systems compared with the control model at  $-0.85 \text{ V}$ . (b) The percentage of change in the chain current with respect to the control model.



Choosing a single biasing voltage and measuring the percentage increase or decrease in the electrical current through the chain identifies the 1D chain sensitivity to the presence of the different bases. To further explore the electrical response of the 1D chain to the existence of bases A and G, visualizing the changes in DOS and transmission probability of the chain at the presence of these two bases can enhance the knowledge and represent a powerful tool to validate the implementation of the chain as a sensing element in DNA sequencing devices.

### **3.1.2.2. Carbyne/A Model**

The first model system used to visualize the changes in the electrical properties of the 1D carbon chain is chain/A. Figure 3.13 demonstrates the transmission probability functions and DOS of the model system chain/A compared with the transmission probability functions and DOS of the control model at the positive and negative energies. Particularly, transmission probability for the chain/A model showed drops at 0.25 eV, 1.75 eV, -1.25 eV, and -2.3 eV.

In addition, the transmission probability increased to 2.0 within the ranges 1.25 - 1.5 eV and -0.75 - -0.85 eV. The DOS demonstrated several peaks at different energies such as 0.75 eV, -0.25 eV, -0.6 eV, -0.8 eV, -1.25 eV, -1.5 eV, -2.15 eV, and -2.3 eV. Those drops and peaks in transmission probability and DOS can be associated with the changes in the gap between HOMO and LUMO or the location of Fermi energy for the simulated model in the presence of DNA bases [73]. To explain, the Fermi energy of the single chain of 16 carbon atoms or the control model for this research was found to be -5.079 eV, while it was found to be -5.24 eV at the presence of base A in the model chain/A. Therefore, base A caused the Fermi energy to shift by 0.161 eV. Such shift can lead to unique changes in the transmission probability and DOS and, hence, the electrical current. These significant changes in the electrical properties can be used as a sensing mechanism for base A.

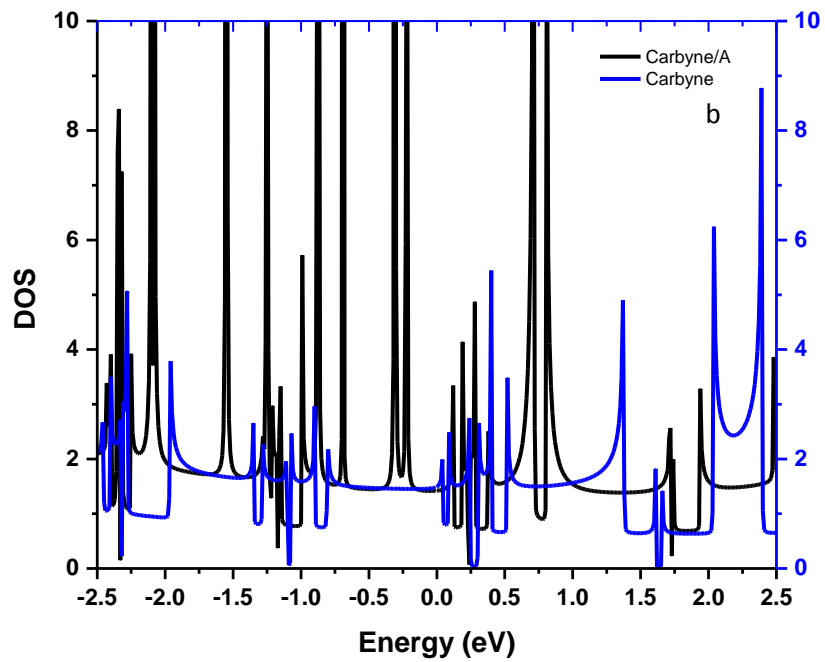
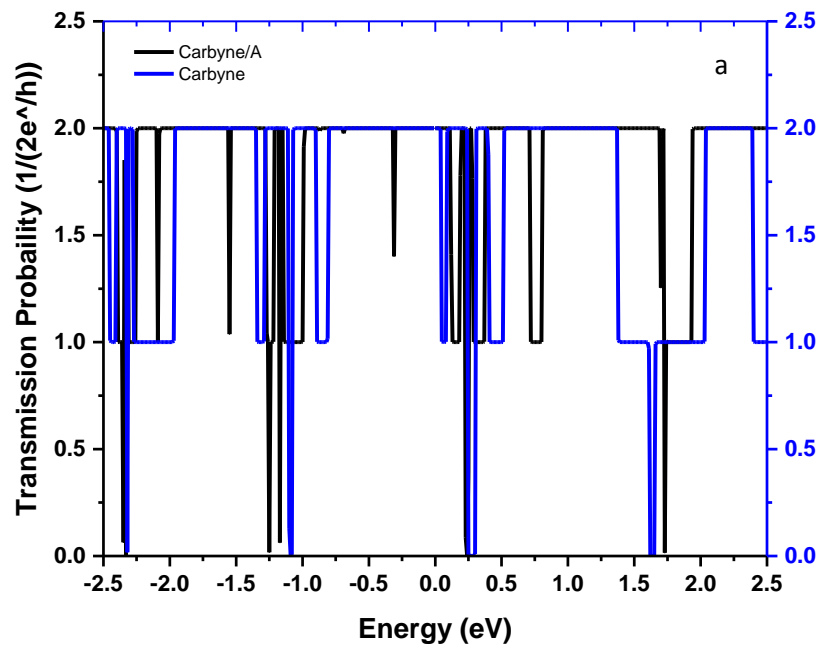


Figure 3.13. (a) Transmission probability functions and (b) DOS for chain/A compared with the control model at positive and negative biasing voltages.

The key factors that affect the electron transport properties are: molecular orbitals (MO), transmission probability, DOS, the locations of Fermi energy, and whether MO are localized or not [119]. To further investigate the chain sensitivity to the existence of base A, I-V characteristics curves were obtained as explained earlier and are presented in Figure 3.14.

At the positive biasing voltages, the presence of base A led to a clear increase in the single 1D carbon chain current. In fact, the current of the single carbon chain increased significantly when base A was placed normal to the chain as can be seen in the Figure 3.14.

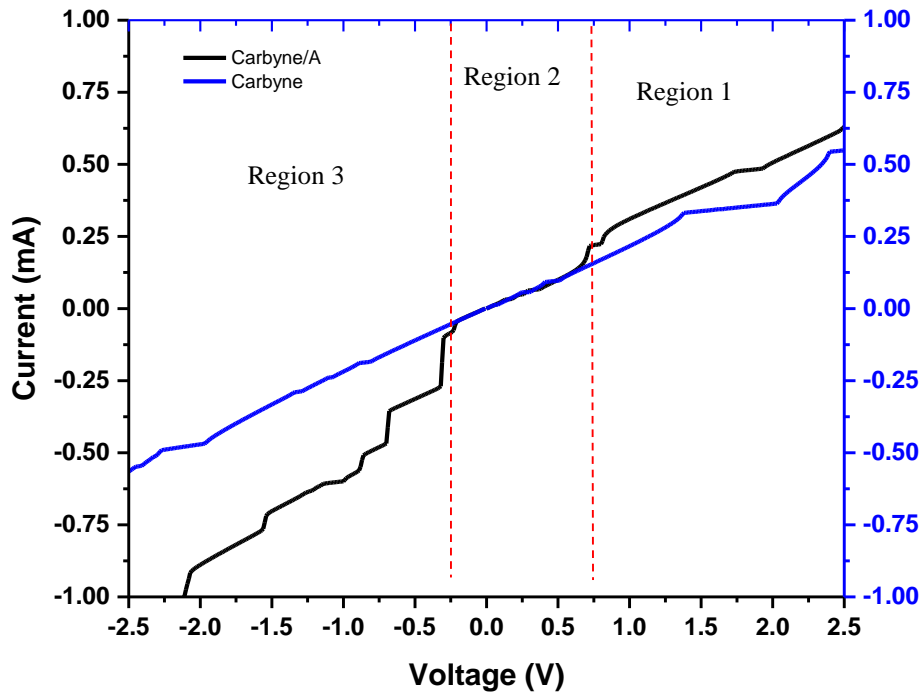


Figure 3.14. I-V characteristics of the chain/A model with the base normal to the chain compared with the control model at positive and negative biasing voltages.

The I-V curve for the chain/A model can be classified into three regimes. The first one starts at 0.75 V and goes to 2.5 V, the second is from -0.25 V to 0.75 V, and the last regime is

-0.25 V to -2.5 V. As discussed in Section 3.1.1, the 1D carbon chain showed mostly ohmic I-V characteristics with two bias independent regions that are 1.25 to 2.0 V and -2.0 to -2.25 V.

However, the adsorption of base A onto the chain surface led to an increase in the current of both positive and negative biasing voltages. The electrical current within -0.25 V to 0.75 V showed no difference when the base was adsorbed. At the negative biasing voltages, the current increased drastically as can be seen in Figure 3.14. However, base A has been reported to be the only base that causes the graphene nanoribbon current to reduce due to not having oxygen in its chemical structure [8], [56] as explained earlier. The location and orientation of base A with respect to the carbon chain could be the main reasons for such disagreement. The locations and orientations of ssDNA bases affect the interactions between the bases and the sensing element including  $\pi$ - $\pi$  interactions [64], [120]. A reported study has concluded that base A placed parallel to the graphene leads to a decrease in the electrical current of the graphene nanoribbon at 0.6 V [56]. The base in this research was located about 2 Å from the chain, and was placed perpendicularly along the z direction as was shown in Figure 3.4. Thus, it is expected that the different orientation of base A could lead to such disagreement with the reported study.

### 3.1.2.3. Carbyne/G Model

Another base that causes significant changes in the electrical current of the chain is base G. The transmission probability functions and DOS for the chain/G model compared with the control model are shown in Figure 3.15. The existence of base G results in changing the transport probability and DOS of the chain at positive and negative energies. These changes lead to a decrease in the electrical current and conductivity of the 1D carbon chain at the positive biasing voltages and an increase of them at negative voltages. The Fermi energy for the chain/G model was -5.12 eV, while it was -5.079 eV for the control model. The increase in Fermi energy by

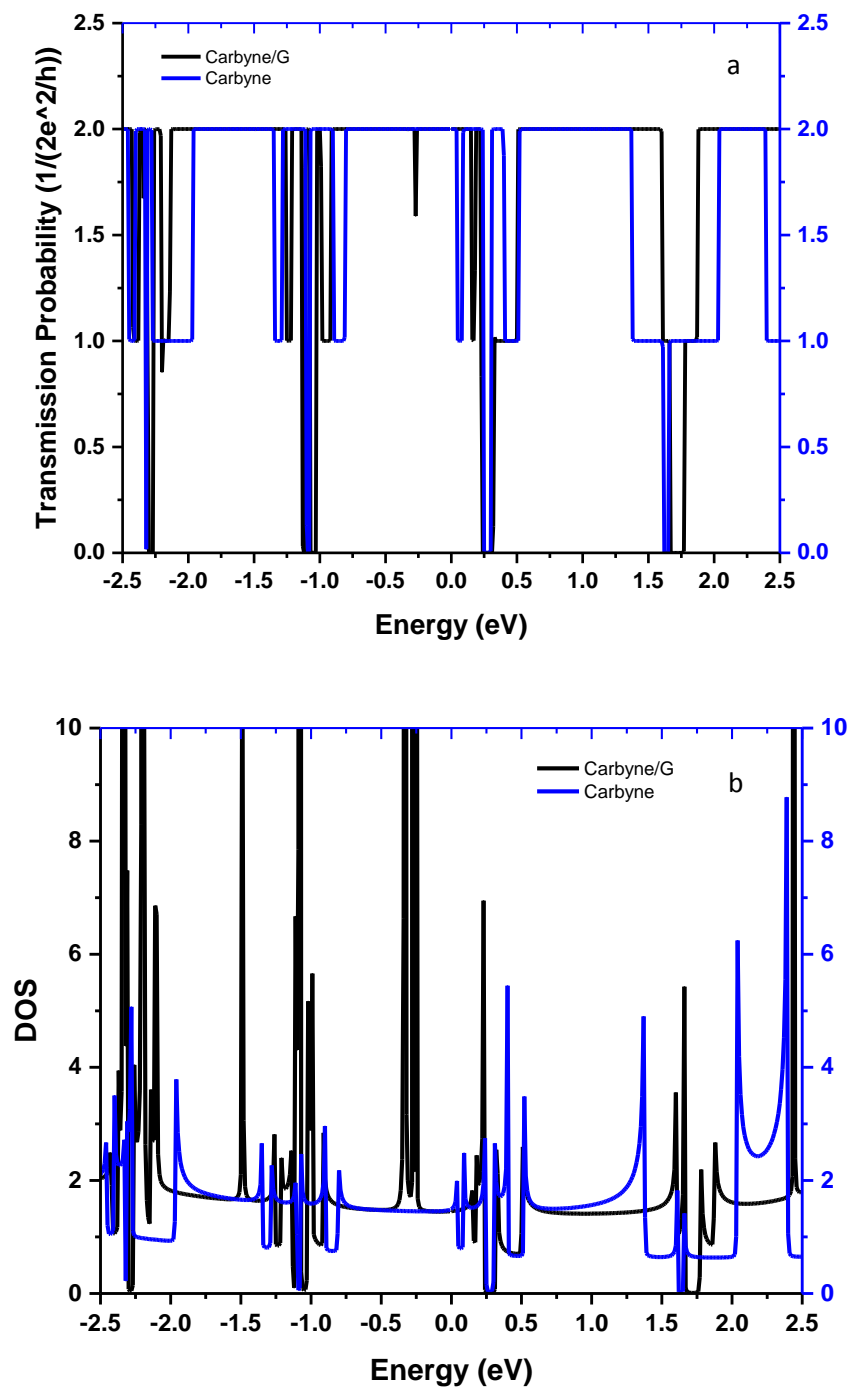


Figure 3.15. (a) Transmission probability and (b) DOS for the chain/G model compared with the control model.

0.041 eV could lead to change in the gap between the molecular orbitals (MO), and can cause splitting of the energy bands observed in the DOS as suggested by other studies [64].

In the presence of base G, the electrical current of the chain decreases at the positive biasing voltages. This is similar to the electrical response of the chain in the presence of bases C and T as was shown in Figure 3.9. Figure 3.8 showed a decrease in the electrical current for the chain/G model at positive voltages, whereas the chain current remarkably increased at the negative biasing voltages. Thus, the sensitivity of the single carbon chain to the presence of base G is distinguishable. The model for the chemical structure of base G was shown in Figure 3.4. As mentioned earlier, the binding energy of base G to the carbon-based materials, such as graphene and CNT, is the most significant compared with the other bases [42], [74], [115]–[117]. This binding energy is inversely proportional to the curvature of the sensing element [42]. To illustrate, the binding energy of graphene is higher than the binding energy of CNTs [42]. The reason for such behavior, according to the literature, is that the effects of  $\pi$  stacking on the surface increase when the curvature of the sensing element decreases [42]. Thus, the binding energy increases when the effects of  $\pi$ - $\pi$  interactions between carbon based materials and the ssDNA bases increase [42]. Calculations of the binding energy of chain/ssDNA simulated models are not part of this simulation approach. However, further analysis of the interaction between base G and carbyne can be discussed based on the reported studies.

Figure 3.16 shows the electrical current for the chain/G model compared with the electrical current of the control model. At the positive voltage, the chain current decreased in the presence of base G as discussed earlier. Furthermore, the ohmic behavior of I-V curve within the range from -0.25 V to 0.5 V was maintained. The drastic increase in the current can be seen at the negative biasing voltage in Figure 3.16. The increase in the electrical current of the chain

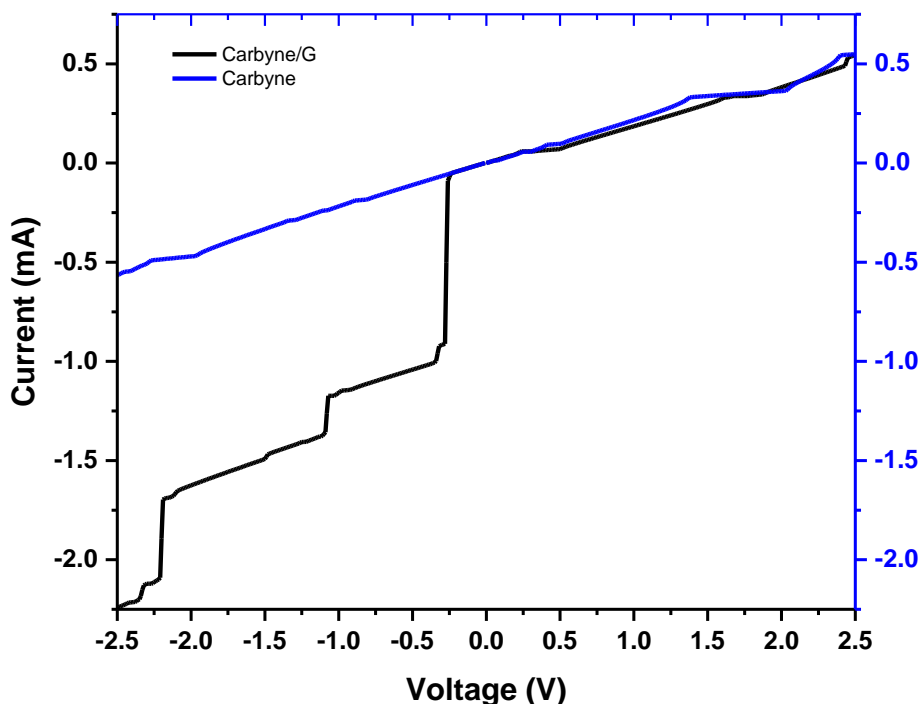


Figure 3.16. I-V characteristics of the carbyne/G model with the base normal to the chain compared with the control model at positive and negative biasing voltages.

induced by base G was about 2.0 mA at the negative biasing voltages. Based on the literature [42], [63], the binding energy of base G is the highest compared with the other three bases. Also, the high binding energy indicates a strong adsorption of G base on the chain surface at negative energies.

Base G has oxygen in its structure, which is reported to induce a high electrical response in the graphene due to the interaction between the base and graphene-based devices [56]. Thus, one can conclude that the geometry and the location of oxygen affect the current flowing through the chain. Particularly,  $\text{NH}_2$ ,  $\text{CH}_3$ , O, CO, and CH contribute via the  $\pi$ - $\pi$  stacking to the interactions between the different bases and carbon-based materials such as graphene and CNTs [42], [56], [64], [115]. The presence of these groups at sufficient distance from the sensing

elements is suspected to increase the interactions via the  $\pi$  stacking interactions leading to an increase in the electronic charge redistributions and the electronic transport probability. The stacking distance between the chain and oxygen in this carbyne/G simulated model is 3.5 Å, CH group is 2.7 Å, and NH<sub>2</sub> is 4.2 Å from the chain.

Considering the effects of these chemical groups and speculating based upon these studies, one should expect base G to influence the electrical properties and, hence, the electrical current. Thus, the adsorption of base G on the chain surface caused by the interaction between them via  $\pi$ - $\pi$  interaction induces modulation in the electrical properties of the chain at the negative biasing voltages. Such modulation results in noteworthy increase in electrical current. According to one study, oxygen forms a ‘carbon bond’ with a carbon atom. Such non-covalent bond is caused by the oxygen pulling the electrons or  $\sigma$  bond toward it causing a decrease in the number of electrons flowing through the material [121]. The pulling of the electrons leads to generating holes in the material, which can cause a decrease in electrons conductivity [121]. Consequently, it is expected that the oxygen in base G pulls the electrons toward it and leads to a decrease of the electrical current flowing through the chain due to such non-covalent bonding at the positive voltage reported in Reference 121.

Considering the four bases placed normally to the carbyne chain, each base influences the electrical properties of the carbyne chain and results in a significant effect on the electrical current. Such influence indicates the sensitivity of the carbyne chain to the presence of these bases. The work reported in this dissertation shows that the electrical current for the four carbyne/ssDNA model systems is different compared with the control model at the positive and negative biasing voltages. Therefore, carbyne can distinguish the different ssDNA bases. In fact, the presence of each base induces a unique electrical response in the single carbon chain.



### 3.1.3. Orientations of the ssDNA Bases

One of the considerations in this research was to investigate the effects of the different orientations of ssDNA bases with respect to the 1D carbon chain. Hence, three different orientations of base A were included.

#### 3.1.3.1. Orientations of Base A

The first orientation is when base A is placed normal to the carbyne chain, which was discussed in the previous section. The second orientation is when base A is tilted by  $45^\circ$  with respect to the chain. Thirdly, base A can be placed parallel to the carbyne chain at the same location with respect to the chain. Figure 3.17 shows schematics of the three different orientations of base A with respect to the chain.

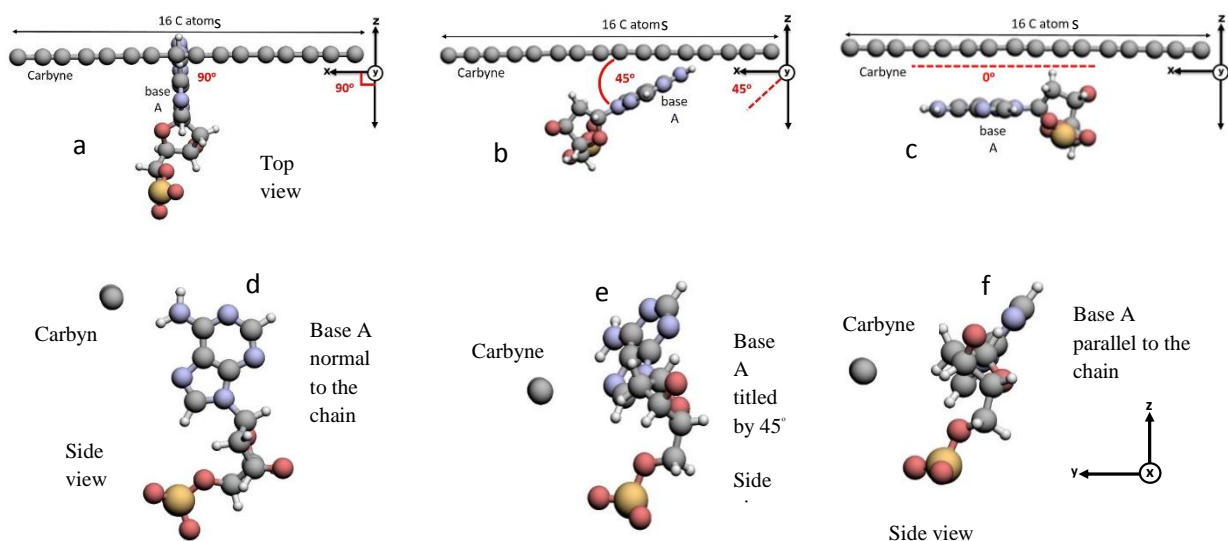


Figure 3.17. Schematics of the three models for oriented base A.

The DOS and the transmission probability functions for the model chain/A at the three different orientations are displayed in Figure 3.18 and Figure 3.19. Figure 3.20 shows the I-V curves for the model chain/A associated with the three different orientations. The different orientations are obtained by the rotations of base A around y axis as shown in Figure 3.17. Figures 3.18 and 3.19 indicate that the different orientations of base A induce different electrical responses in the chain. In general, the changes in DOS and the transport probability functions are asymmetric in negative and positive voltages. The changes below zero energy are most significant compared with the changes at the positive voltages. As discussed earlier, the energy and voltage in the approach used for this research were the same. Thus, the voltage in the I-V curves shown in Figure 3.20 can be represented as the energy of the states. Due to the changes in the DOS and the transport probability functions caused by the different orientations, the calculated electrical current was expected to differ at positive and negative voltages.

Generally, the electrical current at the positive voltage was the highest for the normal base A with respect to the chain. The presence of base A at  $45^\circ$  and  $0^\circ$  with respect to the chain led to a decrease in the electrical current at the positive voltage as shown in Figure 3.20. On the other hand, the three different orientations caused the current to increase at the negative voltage. The variations in the electrical response of the chain when altering the orientation and locations of the groups  $\text{NH}_2$  and  $\text{CH}$  with respect to the chain can be justified by the interactions between the base and the chain.

The orientations of DNA bases have been of great importance to researchers. Many DNA sequencing investigations have included different angles of the different ssDNA bases [8], [43], [64], [70], [73], [114], [120], [122], [123]. The importance of investigating different orientations stems from the nature of the interactions between ssDNA bases and the sensing elements.

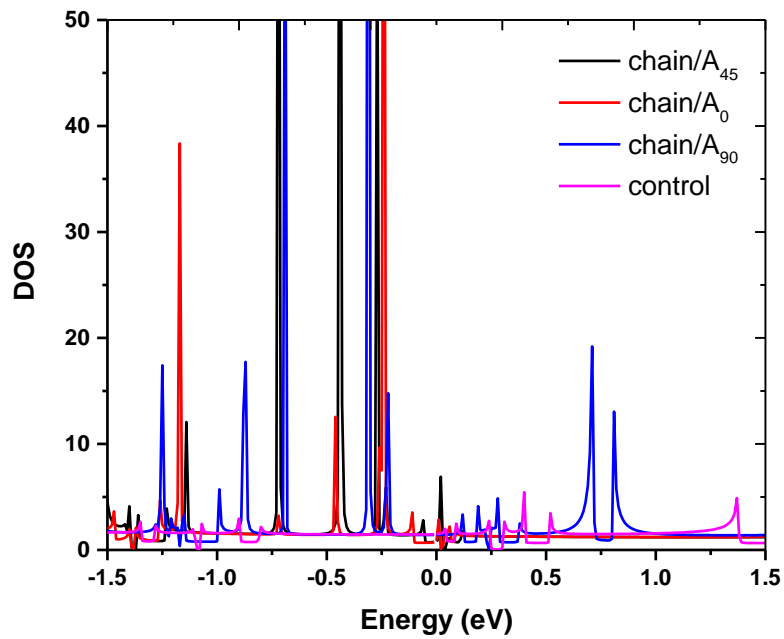


Figure 3.18. DOS for the models with base A at three different orientations.

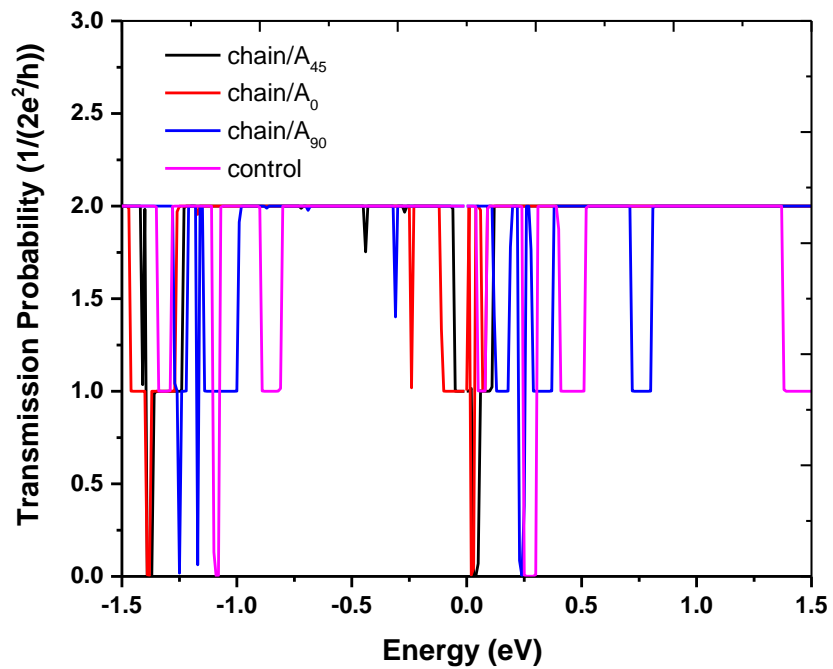


Figure 3.19. Transmission probability functions for the models with base A at three different orientations.

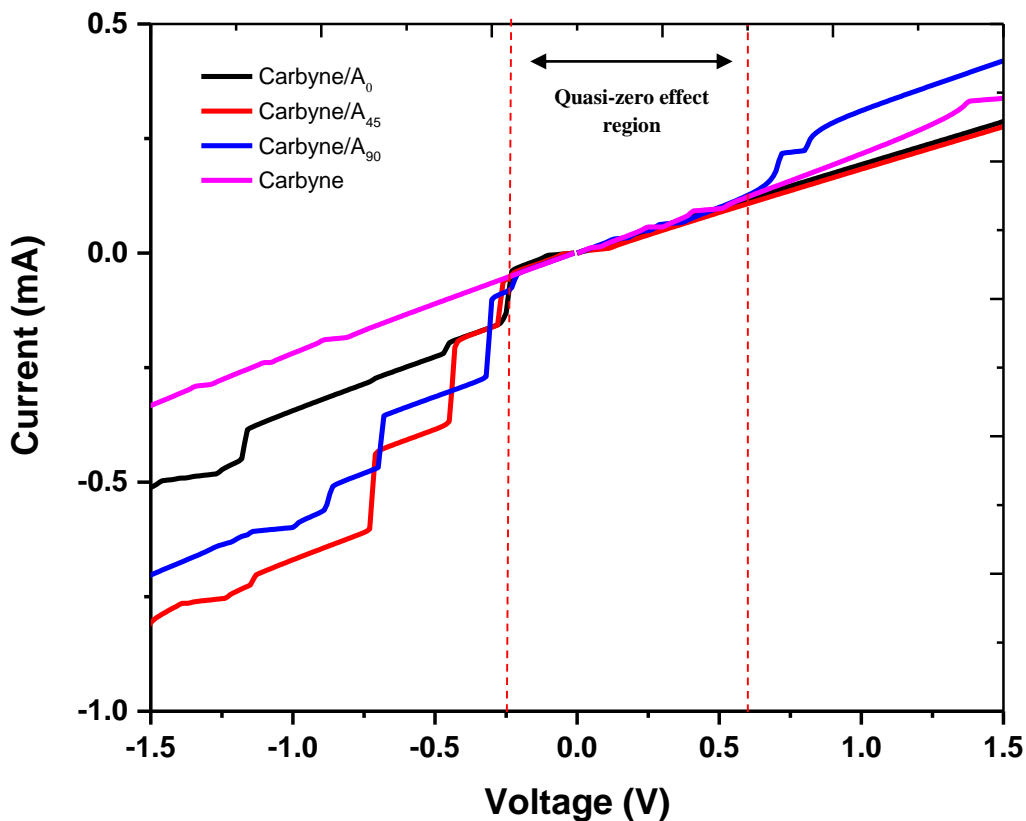


Figure 3.20. I-V characteristics for the carbyne/A model at three different orientations with respect to the chain compared with the control model.

Generally, the backbone strains and fluctuations make ssDNA bases tilted in the practical situations. Therefore, different orientations of base A with respect to the carbyne have been considered in this research. The main interaction that involves DNA bases is the  $\pi$ - $\pi$  interaction [18], [56], [114], [124], [125]. There are three geometrical configurations that represent the  $\pi$ - $\pi$  interactions. These three geometrical configurations are: face to face  $\pi$ -stacked, edge on or T-shaped geometry, and offset  $\pi$ -stacked geometry [126]. The three geometrical arrangements are shown in Figure 3.21.

Particularly, the  $\pi$ - $\pi$  interaction depends on the electronic properties at the point of contact and not on the electronic properties of the whole system [126]. Thus, the distance and geometrical configurations between the two interacting atoms affect this  $\pi$ - $\pi$  interaction between them as mentioned earlier. As a result, the distance between the base and the chain as well as the base orientations with respect to the chain are speculated to influence the strength of the interactions between them. Specifically, there are two  $\sigma$  bonds and two  $\pi$  bonds for the 1D carbon chain as discussed earlier in Chapter One. DNA bases are described as  $\pi$  systems [8],

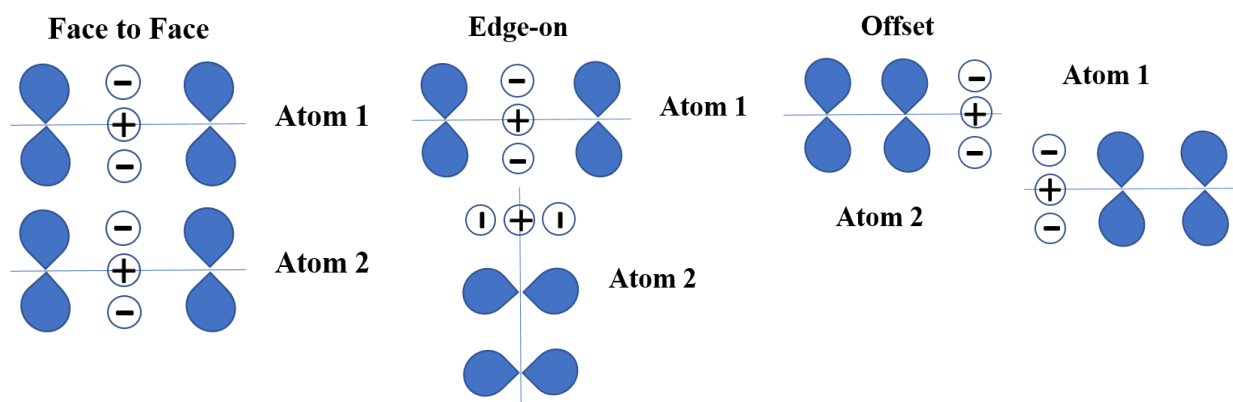


Figure 3.21. Geometrical arrangements for  $\pi$ - $\pi$  interactions.

[32], [56], [73], [74]; therefore, they interact with the sensing elements via  $\pi$ - $\pi$  interactions.

As an illustration, the  $\text{NH}_2$  group in the base is  $\text{sp}^3$  hybridized [127]. The chain in this research is constructed to have alternating  $\text{sp}$  and  $\text{sp}^3$  hybridization. The carbon and nitrogen atoms in the base are  $\text{sp}^2$  hybridized. If it is assumed that the chain after the geometrical organization is  $\text{sp}^2$  hybridized, the chain has two  $\pi$  bonds associated with each atom.  $\pi$  bonds are normal to the surface of the atoms. Therefore, the chain possesses  $\pi$  bonds and can interact with the base via  $\pi$ - $\pi$  interaction. Figure 1.12 and Figure 1.13 in Chapter One demonstrated the  $\pi$

bonds for the carbyne chain. Comparing the three arrangements shown in Figure 3.17 with the three different orientations investigated for base A, one can conclude that the  $\pi$ - $\pi$  stacking interaction between  $\text{NH}_2$  and  $\text{CH}$  groups and the 1D chain is the main interaction and contributes to the total interaction between them.

Offset  $\pi$ -stacked geometry is in fact  $\sigma$ - $\pi$  attraction. Face to face is  $\pi$ - $\pi$  repulsion electronic interaction and preferred by van der Waals interaction [126]. Any rotation between  $0^\circ$  to  $90^\circ$  is considered as  $\pi$ - $\sigma$  attraction at small offset; i.e. it is edge-on or T-shaped geometry. Also, any rotation between  $90^\circ$  to  $180^\circ$  is assumed as small offset  $\pi$ - $\sigma$  repulsion; i.e. it is face to face  $\pi$ -stacked interactions. It is also ruled that the effects of  $\pi$ - $\pi$  interactions are within a distance that is limited to  $3.5 \text{ \AA}$  [126]. To apply these rules to the orientations of base A and its locations with respect to the 1D carbon chain, face to face and T-shaped geometry for stacked  $\pi$  interactions are expected. Figure 3.22 shows the geometrical configurations of the expected interaction between the chain and the base considering the locations and orientations of  $\text{NH}_2$  and  $\text{CH}$  groups with

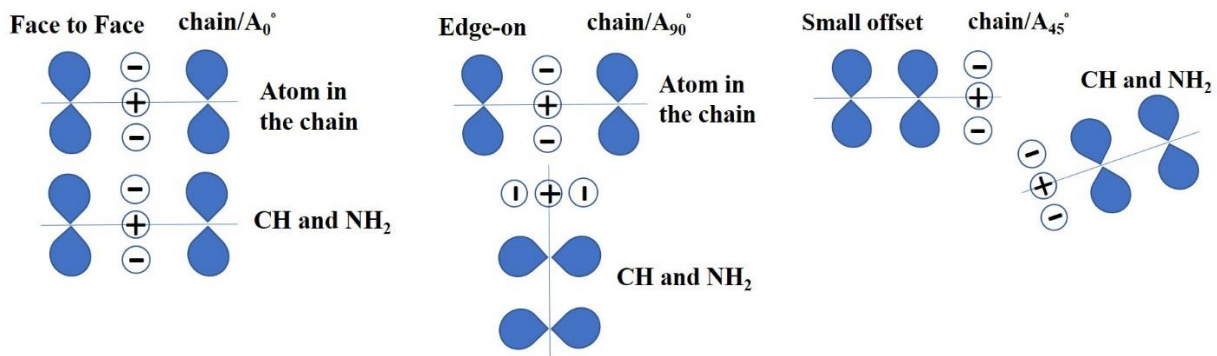


Figure 3.22. Geometrical arrangements of the  $\text{NH}_2$  and  $\text{CH}$  groups with respect to the chain.

respect to the chain. Hence,  $\pi$ - $\pi$  interaction is anticipated to impact the electrical response of the chain to base A at different orientations. Figure 3.20 showed three different regions of I-V curves

for the three different orientations. Those three regions are separated by red dashed lines to recognize them. The first region is from 0.6 V to 1.5 V, the second region is within the range -0.25 V to 0.6 V, and the third region is from -0.25 V to -1.5 V. As discussed earlier, the second region shows little difference among the three different orientations compared with the control model. The first region reflects a significant difference in current. For the simulated model that has base A orientated at  $90^\circ$ , the chain current increases by about 0.15 mA. On the other hand,  $0^\circ$  and  $45^\circ$  orientations show decrease in the electrical current of the chain. Finally, the chain current increases for all three orientations compared with the control model at the negative voltages.

The locations of  $\text{NH}_2$  and CH groups at these three orientations in Figure 3.17 were close to the chain. For example, the distance between  $\text{NH}_2$  group and the chain was 3.1 Å when the base was  $45^\circ$  oriented, while it was at 2.6 Å from the chain at  $90^\circ$  orientation. In fact, this difference in current indicates that the interactions between  $\text{NH}_2$  and CH groups and the one-dimensional chain increase the total interactions energies and lead to higher modulations in electrical response of the chain to the ssDNA bases.

Further analysis of the obtained current at the three different orientations included plotting the relative current at different voltages. The current values of the pure chain model at different voltages were subtracted from the current values for the model chain/A at the different orientations and then divided by the maximum difference value within the biasing voltage ranges. Figure 3.23 shows the relative electrical current for the investigated models versus biasing voltages. Previously in Figure 3.20, the current for chain/A model did not show any difference compared with the pure chain model within the range -0.25 V to 0.5 V. Thus, the range of voltage -0.15 V to 0.5 V is eliminated and not shown in Figure 3.23. The variations in the relative current values were caused by the differences in the actual current values for the

models compared with the control model at different biasing voltages. These observations can be explained based on the maximum differences of the electrical current associated with the three different orientations. To explain, the orientation of  $90^\circ$  shows a clear increase in the electrical current with respect to the control model at positive and negative voltages. The difference in the

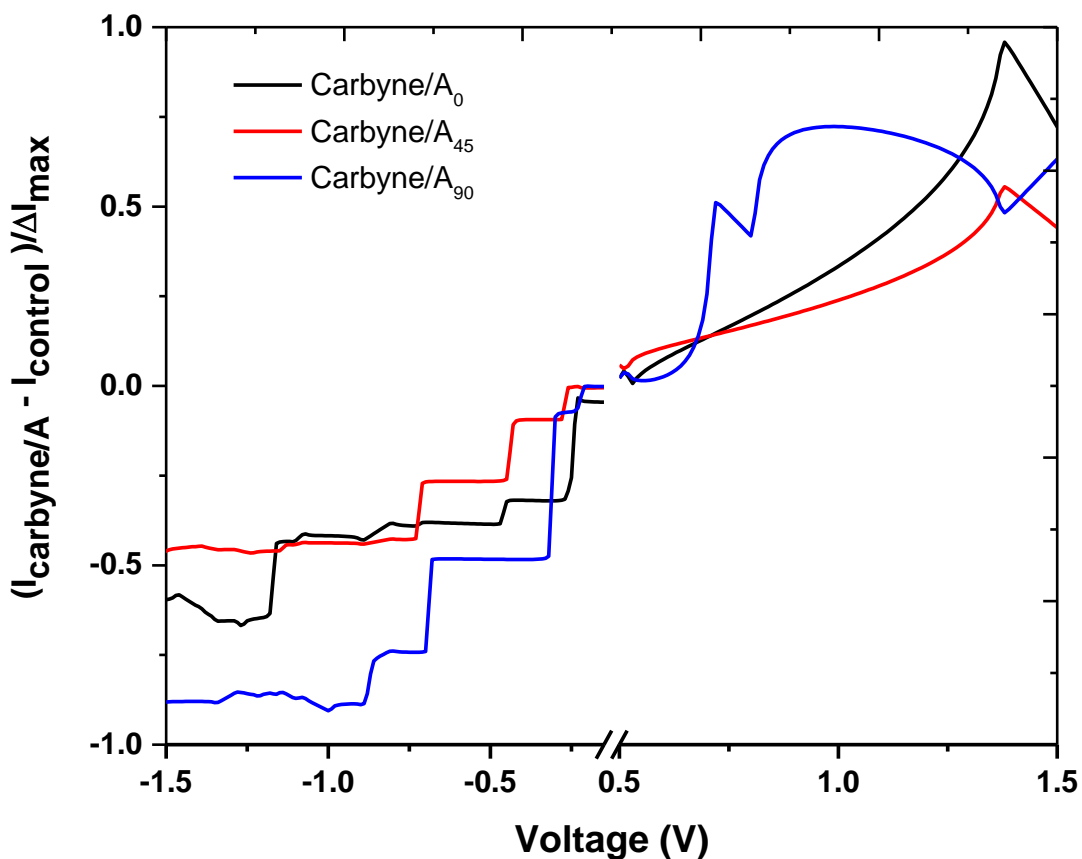


Figure 3.23. Relative current for the chain/A model with base A at three different orientations with respect to the chain at positive and negative voltages.

electrical current is approximately 0.15 mA as discussed earlier. This difference represents up to ~ 60 % to 70% alteration in the chain current with respect to the maximum difference. In



contrast, 45° orientation shows the minimum relative current, which is ~10% alteration in the pure chain current relative to the maximum difference. However, there is 40% to 50% difference in the chain current with respect to the maximum at the negative voltages for 45° orientation.

Finally, 0° orientation is mainly different from the other two orientations. It has been reported that the interaction between CNT and NH<sub>2</sub> group in base A is significant when base A is planar to a CNT [114]. A CNT is sp<sup>2</sup> hybridized, which indicates that it can interact with ssDNA bases via the  $\pi$ - $\pi$  stacking interactions. When the base is absorbed onto a CNT plane, a charge redistribution occurs and leads to positive charges being induced on the base plane. Therefore, the electrons accumulate near the base plane, and a depletion region is revealed near the CNT. As a result, there is a net charge transferred to the CNT from the base when base A is parallel to the CNT [114]. Recalling the previous discussion regarding the  $\pi$ - $\pi$  stacking geometrical configurations represented in Figure 3.22, the parallel orientation is the face-to-face interaction with the base. However, the distance between NH<sub>2</sub> and the chain is 3.8 Å at the parallel orientation. Therefore, it is expected that the distance affected the  $\pi$ - $\pi$  interaction between the chain and the base and led to such disagreement with the reported study for CNTs. Overall, the 1D carbon chain is sensitive to the different orientations of base A.

### 3.1.3.2. Parallel ssDNA Bases

Investigating the three different orientations for base A led to a desire to investigate the effects on the electrical properties of 1D carbon chains caused by different ssDNA bases placed parallel to the chain. As mentioned earlier, ssDNA bases can be at any orientation in the practical situation. Considering the one-dimensional chain sensitivity to the three different orientations of base A, it was expected that the parallel ssDNA bases can have different effects on the electrical current of the chain. The different ssDNA bases were placed at 0° with respect to the chain's axis.

Each base was within  $\sim 2 \text{ \AA}$  distance below the chain, which is where  $\text{NH}_2$ ,  $\text{O}$ , and  $\text{CH}_3$  groups for the different bases were located. For the sake of consistency, all the simulation parameters and details for the model systems that have the bases normal to the chain were kept the same.

Figure 3.24 represents schematics of the chain/ssDNA model systems where the bases are parallel to the chain. Figures 3.25 and 3.26 show the DOS and the transmission probability functions for these different models. Figure 3.27 shows I-V curves for the simulated models. Note that parallel indicates  $0^\circ$  orientation and normal is  $90^\circ$ . Figure 3.25 and Figure 3.26 show variations in the DOS and the transmission probability functions when the different ssDNA bases were placed parallel to the single carbon chain.

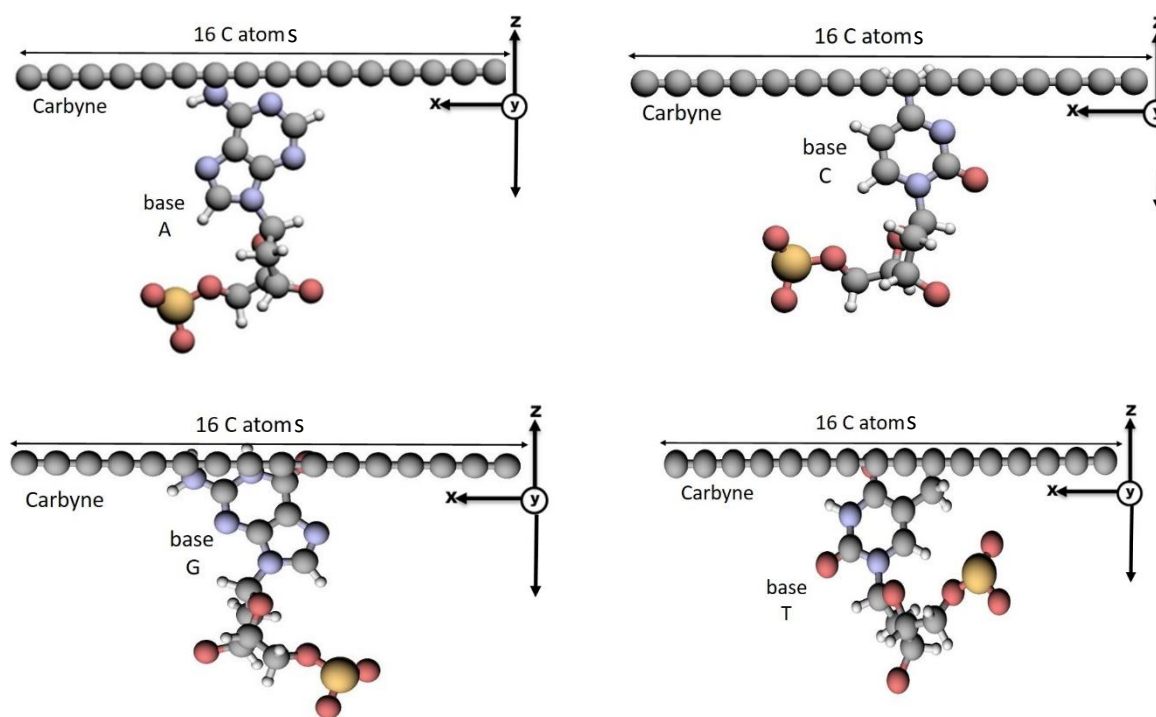


Figure 3.24. Schematics of the carbyne/ssDNA model systems with each base parallel to the chain.

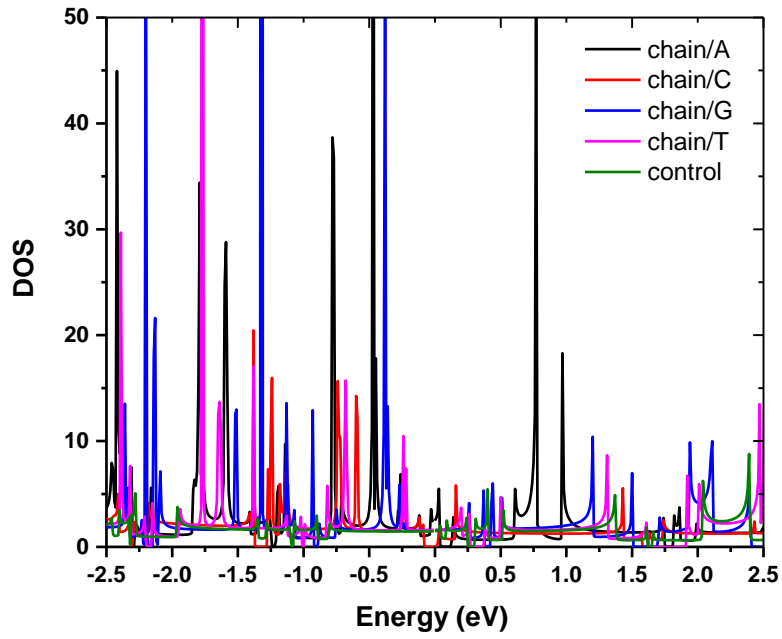


Figure 3.25. DOS for the models with the bases parallel to the chain.

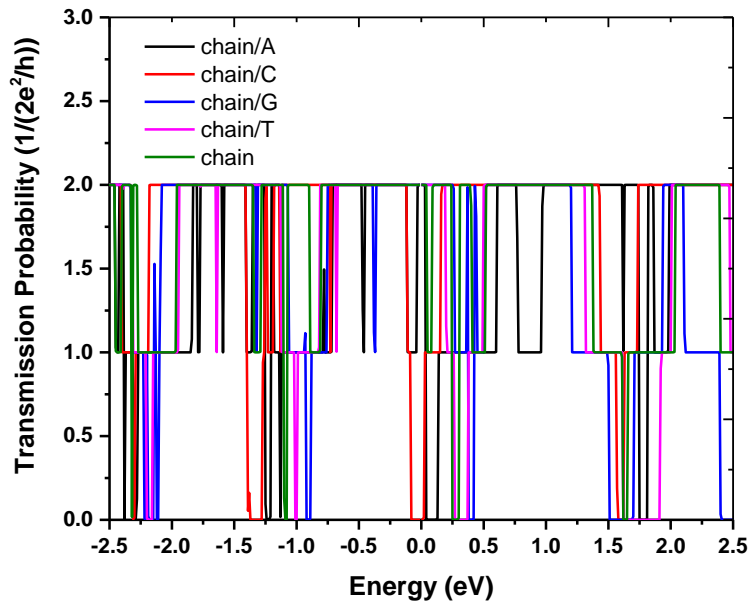


Figure 3.26. Transmission probability functions for the models with the bases parallel to the chain.

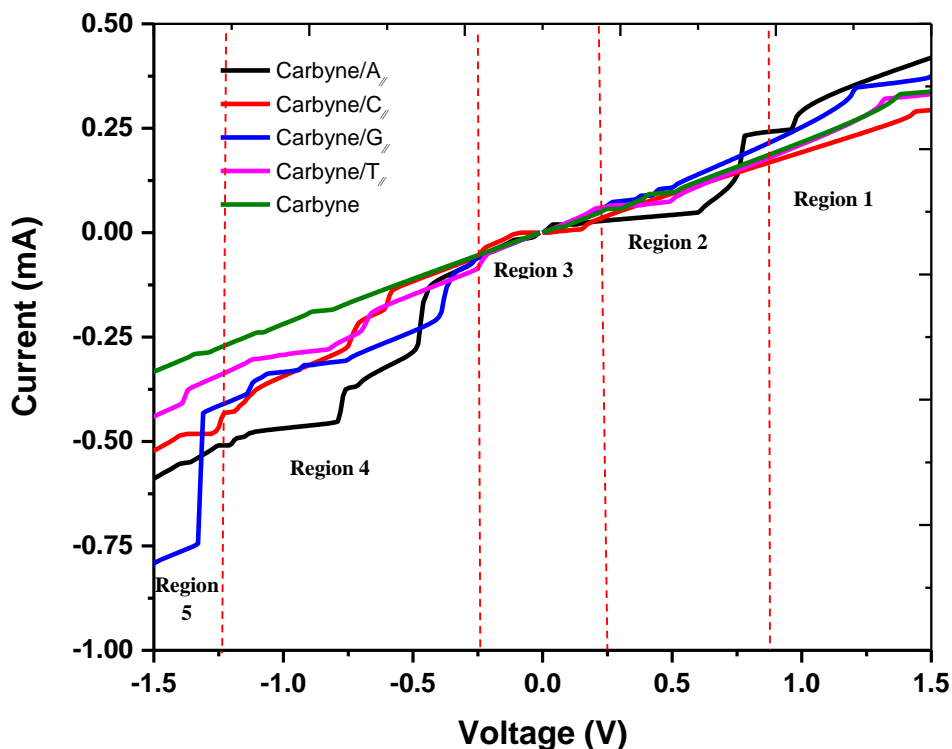


Figure 3.27. I-V characteristics of the models with the bases parallel to the chain compared with the control model at positive and negative voltages.

These variations were expected to lead to differences in the electrical current of the chain. I-V curves for the chain/ssDNA model systems where the bases were parallel compared with the control model are displayed in Figure 3.27. In Figure 3.27, five different regions of voltage can be recognized. Also, these five regions are identified by red dashed lines to separate them as shown in Figure 3.27. The first region is 0.9 V to 1.5 V, the second region is 0.25 V to 0.9 V, the third region is -0.25 V to 0.25V, the fourth region is -0.25 V to -1.25 V, and the final region is -1.25 V to -1.5 V. The electrical current was asymmetrical among the different regions as shown in Figure 3.27. The first region shows clear changes in the chain current caused by the presence of different ssDNA bases. The electrical current of the chain in the first region was in the order

of  $I_A > I_G > I_T > I_C$ . When the bases are parallel to the chain or at  $0^\circ$  orientation, they interact by face-to-face  $\pi$ -stacked interactions as shown in Figure 3.22. It is suspected that the different locations of  $\text{NH}_2$ ,  $\text{CH}$ , and  $\text{O}$  groups from the chain play significant roles in inducing electrical response and current for the 1D chain.

In the first region in Figure 3.27, the presence of base A led to an increase in the electrical current of the chain. This could be due to the interaction between base A and the 1D chain at this range of energy. The existence of base G also caused the electrical current in the base to increase. However, this increase in the electrical current was less than the current increase caused by the presence of base A. This result can be justified based on the strength of the interaction between the different bases and the chain. For example, the adsorption of base G onto the chain surface induced less electrical response in the chain properties compared with the changes induced by the presence of base A. Base T displays quasi-zero effect on the chain properties, while base C caused the current to decrease slightly within the range 0.9 V to 1.5 V.

The second region, which is the low positive basing voltage, shows the current in the order  $I_G > I_C \sim I_T > I_A$ . Base A caused a clear decrease in current. Bases G, C, and T maintained the same effect, which is no significant modulation in the electrical properties and, hence, no change in the electrical current. The third region reflects no effect on the electrical current of the chain by the presence of all the bases when compared with the control model despite the slight change in current caused by the existence of base C. The fourth region shows the electrical current of the chain increased in the presence of base A with fluctuations in the current within the range of -0.25 V to -0.4 V. The fifth region shows domination of the electrical current caused by the existence of base G with the order of  $I_G > I_A > I_C > I_T$ . The changes in the electrical current are expected for several reasons that involve the different locations of the different groups which

interact with the chain. Fano-resonance is caused by discrete energy states of DNA and continuous energy states for graphene [8] as discussed earlier. In fact, a study has reported the fluctuations of the electrical current and conductance and has anticipated such fluctuations to be caused by quantum phenomena, such as Fano-resonance in graphene nanoribbons [66]. The study also concluded that such effect can lead to no detection of ssDNA bases. The rotations of the different bases in that study were from  $-30^\circ$  to  $30^\circ$ . The only base that was detectable in their approach was G at positive voltages. Thus, it is expected that Fano-resonance might affect the electrical current of the chain in the presence of these different bases.

A study conducted by Min and his group [18] examined the orientation effects on graphene nanoribbons while ssDNA was passing through the nanochannel that was 1 nm below the graphene nanoribbon. They used base A to inspect the effect of a tilted geometry by rotating the base  $10^\circ$  around the stacked axis. According to their conclusion, there are no significant effects of the rotations of the ssDNA bases on the electrical current and the transport properties of the graphene nanoribbon.

These reported studies have shown no significant changes in the electrical current of the graphene sequencing devices when the orientations of different bases vary. In contrast, the 1D carbon chain in this study showed clear distinctions among the different bases at different orientations. The 1D carbon chain is about one atom width and is equivalent to the distance between two sequential ssDNA bases. Thus, it is expected that the 1D carbon chain reflects remarkable sensitivity to any orientation or change in the chemical environment. Further investigation of the effects of ssDNA orientations on the electrical transport properties of the 1D carbon chain was done by visualizing the electrical current for different models at  $0^\circ$  and  $90^\circ$  orientations compared with the control model. Figure 3.28 displays the I-V curves for the

chain/ssDNA model systems compared with the control model and the average current of the two orientations as error bars.

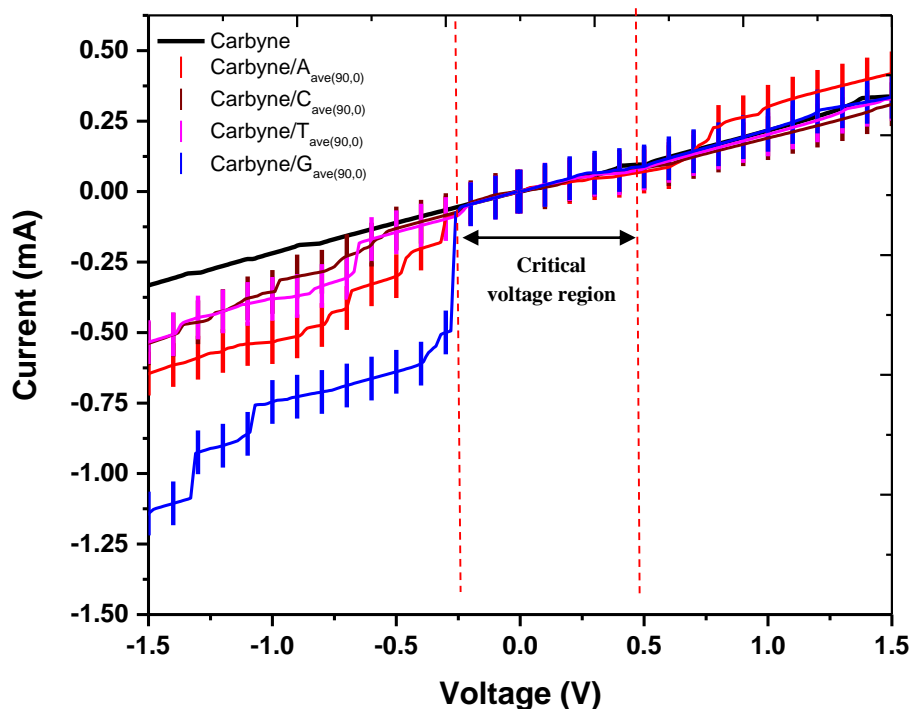


Figure 3.28. I-V characteristics of the models shows two orientations of ssDNA with respect to the chain compared with the control model at positive and negative voltages.

The figure sums up the two orientations and shows clearly the effectiveness of using a 1D carbon chain as a sensing element. Similar to I-V curves in previous discussions, the current of the chain show no difference in the presence of different ssDNA bases within the range of -0.25 V to 0.5 V, which has been reported in several studies including graphene nanodevices for DNA sequencing [72]. According to the literature [72], this range of voltage is described as the critical voltage that a sensing element, such as graphene, has to overcome to start its conductivity and identify the different bases. This critical voltage is normally associated with the energy barrier. It

is 1.0 V for graphene and is reduced when different ssDNA bases are present [72]. Figure 3.28 shows obvious sensitivity to bases A and G at positive and negative biasing voltages. Base T is distinguishable at the negative biasing voltages. Base C shows slight effect on the chain current at the negative biasing voltages and virtually no effect at the positive biasing voltages. Similar behavior has been reported regarding the binding of base C and its rotation effects on other materials. Base C has been reported to have no effect on the graphene nanoribbon current when tilted [18], [43]. Also, several studies have reported that base C binds the least to the carbon-based materials [42]. Therefore, the relative current of base C with respect to the control model was calculated and is shown in Figure 3.29.

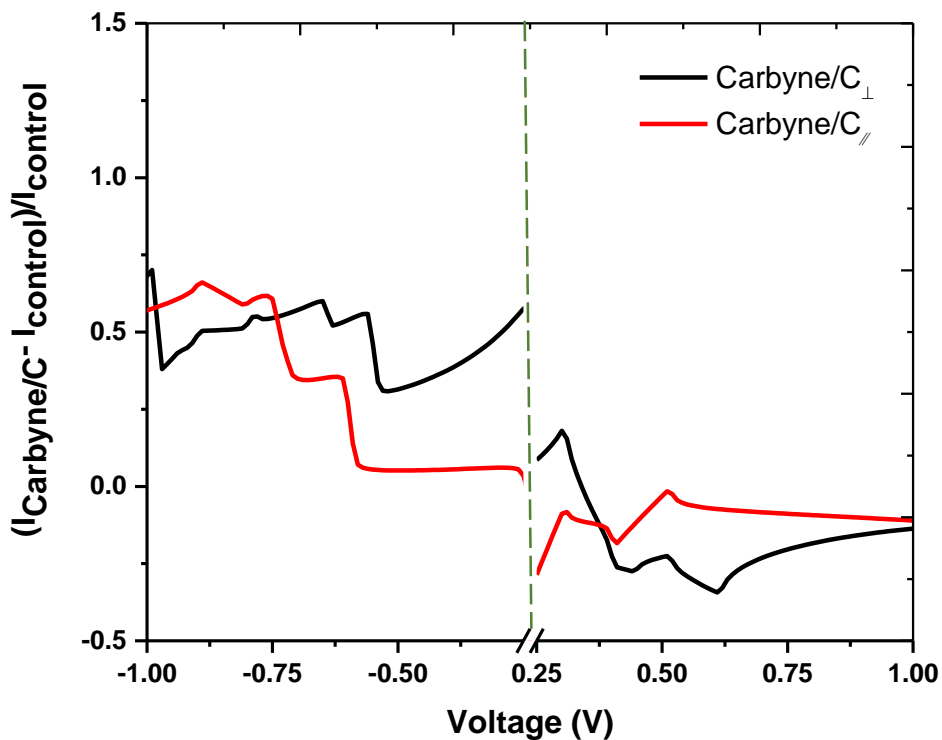


Figure 3.29. Relative current for the chain/C model with base C parallel ( $0^\circ$ ) and normal ( $90^\circ$ ) to the chain at positive and negative biasing voltages.



In Figure 3.29, the relative current is eliminated at certain voltage ranges. The reason is to highlight the ranges of voltage that the chain can respond to the existence of base C. The relative current fluctuated within three ranges of biasing voltages. Starting from -0.75 V to -1.0 V, the relative current associated with the  $0^\circ$  or parallel orientation was higher than the relative current associated with the  $90^\circ$  orientation. This behavior was similar to the relative current within the range from 0.35 V to 1.0 V. At the ranges of -0.75 V to -0.15 V and 0.25 V to 0.35 V, the relative current associated with the  $90^\circ$  orientation was higher than the relative current associated with the  $0^\circ$  orientation. The relative current behavior reflects the decrease in the electrical current of the chain in the presence of base C at the positive and negative biasing voltages. This decrease was higher for  $0^\circ$  orientation at -0.75 V to -1.0 V and 0.35 V to 1.0 V. Whereas it was higher for  $90^\circ$  orientation at the low biasing voltages within  $\sim$  -0.75 V to 0.25 V.

To sum up the changes in the electrical current caused by the presence of base C, one can expect that  $0^\circ$  orientation induces higher changes in the electrical properties of the chain at higher biasing voltages. In contrast, the  $90^\circ$  orientation induces higher changes in the electrical properties of the chain at low biasing voltages. Even though the decrease in the electrical current caused by the presence of base C was small, the 1D carbon chain revealed electrical changes when base C was present compared with graphene and CNT. Graphene nanoribbon devices have demonstrated no effects to different orientations of base C as mentioned earlier. For example, the study that was conducted by Min and his group showed that the orientation of the bases has no effect on the graphene nanoribbon current at the positive and negative biasing voltages [18].

Another study reported that the presence of base C parallel to the graphene nanoribbon leads to increase in the electrical current of the graphene nanoribbons [56]. However, the results of the research of this dissertation contradict the reported results. The 1D carbon chain showed a

decrease in the electrical current at the presence of base C. This decrease in electrical current of the 1D carbon chain could be due to several reasons. The decrease indicates that the presence of base C may lead to the adsorption of the base onto the chain surface due to the  $\pi$ - $\pi$  stacking interactions that enhance the electrical response of the chain to the presence of the base. The atomic width of the one-dimensional carbon chain may lead to increase in the sensitivity to any electrical variations caused by the existence of different ssDNA bases. In addition, the reported studies included the base only in their simulation model systems while in this research, the base with the sugar and phosphate groups was included. Also, the location and orientation of base C with the respect to the 1D chain is different from the those for the reported studies. Therefore, different electrical modulation was expected.

Further analysis of the electrical response of the 1D carbon chain included a comparison between two electrical current values at  $90^\circ$  and  $0^\circ$  for the four simulated model systems of chain/ssDNA. Figure 3.30 demonstrates the current for these models at 0.6 V. The two different orientations of the bases resulted in different electrical current in the presence of these different bases in the model systems. This difference was the most significant for bases A, G, and C, respectively. Base T did not show significant effect on the chain current at the different orientations. This may have been due to the structure of base T and to having a  $\text{CH}_3$  group near the chain in both orientations. As an illustration, the distance between the  $\text{CH}_3$  group in T base and the chain is  $3.2 \text{ \AA}$  for  $90^\circ$  orientation. On the other hand, the distance is  $3.15 \text{ \AA}$  for  $0^\circ$  orientation. Thus, it is expected that the interaction between  $\text{CH}_3$  and the chain is nearly equivalent for both orientations. As such, the electrical current differed by 0.00305 mA. The change in current was essentially insignificant for base T. Base A caused the highest shift that is 0.0776 mA. That was a significant shift in the electrical current of the chain. Specifically,  $\text{NH}_2$

group for base A was at 2.6 Å for 90° orientation and 4.6 Å for 0° orientation. There was a weaker interaction with the chain for 0° orientation due to having NH<sub>2</sub> group at a further distance than it was at 90° orientation. Bases G and C induced modulations of 0.0426 mA and 0.0325 mA in the electrical current, respectively.

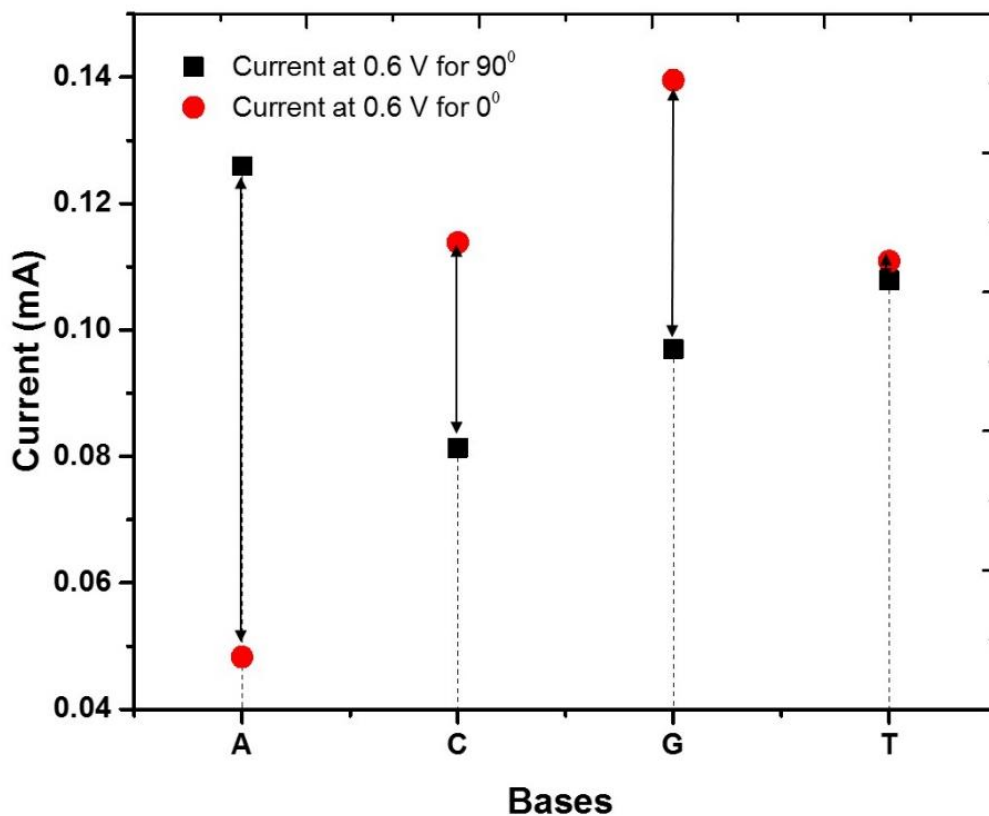


Figure 3.30. The current for the different model systems with the bases A, C, G, and T at two different orientations (0°, 90°) with respect to the chain at 0.6 V.

As previously described, the distance between the NH<sub>2</sub>, CH, and O groups in base G and the chain for the 90° orientation is 3.7 Å, 3.7 Å, and 4.8 Å, respectively. For the 0° orientation,

the NH<sub>2</sub>, CH, and O groups are at 3.6 Å, 3.7 Å, and 3.7 Å, respectively. As a result, the interaction was stronger for 0° orientation due to the equivalent contribution of these groups to the total energy. This increase in the strength of the interactions led to higher electrical current in the chain when base G was parallel compared with the model where base G was normal to the chain. In fact, the same analogy can be used to justify the increase in the electrical current of the chain when base C was parallel to it. For example, the distance between NH<sub>2</sub> group in base C and the chain is 3.7 Å for 90° orientation. The groups CH and O are at 3.9 Å and 6.3 Å, respectively. At 0° orientation, NH<sub>2</sub> is at 3.8 Å. Whereas, CH and O are at 3.8 Å and 4.4 Å, respectively. The contributions of these groups to the interaction energy at 0° orientation were higher and caused an increase in the electrical current compared with base C at 90° orientation.

The current at 0.6 V at two different orientations is shown in Figure 3.30. The figure indicates that when the orientation of base A cannot be controlled, the electrical current is within the range of 0.05 – 0.126 mA. Also, the electrical current is within the range of 0.08 – 0.114 mA for base C and 0.1 – 0.14 mA for G, respectively. For base T, the electrical current range is from 0.108 mA to 0.11 mA.

As mentioned earlier, the orientations of the different bases cannot be controlled in the practical situation which may lead to overlapping in the electrical signals produced by the chain at the presence of these different bases. However, using the electrical current ranges for each base, the base can be identified. For example, the base can be A, C, G, or T if the measured current is 0.08 mA, i.e. the bases are non-distinguishable. If the electrical current is 0.14 mA, the base is G. The base is A if the measured electrical current is 0.07 mA. Therefore, bases A and G can be identified at 0.6 V for the two different orientations. To differentiate base C from base T, the base is C if the electrical current is 0.09 mA.

It can be concluded that these shifts or variations in the electrical current confirm that the 1D carbon chain is very sensitive to the presence of different ssDNA bases. The presence of these bases at two different orientations induces distinguishable electrical modulations and produces different electrical current that can be caused by  $\pi$ - $\pi$  stacking interaction between the chain and ssDNA bases. Therefore, the 1D carbon chain has demonstrated significant electrical response to different orientations of the ssDNA bases.

#### **3.1.4. Bases A and C at Different Locations from the Chain**

In order to investigate the actual interaction between different ssDNA bases and the 1D carbon chain, moving the bases to different locations was of great interest for this research. Thus, bases A and C were placed at five different locations along z-axis, while the chain is along x-axis. Each one of these bases were moved by about  $\sim 1.0$  Å to  $2.0$  Å along the z direction with respect to its previous location. The base was below the chain as shown in Figure 3.31. As the base was moved to different distance from the chain, different groups present at different locations and are expected to contribute to the interactions with the chain besides  $\pi$ - $\pi$  interaction differently at each location. Figure 3.31 shows schematics of the five different locations of bases A and C with respect to the carbon chain. For the sake of consistency, all simulation parameters and details were kept the same for all models when changing the locations. Specifically, the size of the simulation cells for all the model systems at the five different locations was  $22.6$  Å x  $25.0$  Å x  $25.0$  Å. The DOS and the transmission probability functions at the five different locations of bases A and C are represented by Figure 3.32, Figure 3.33, Figure 3.35, and Figure 3.36, respectively. Different I-V curves associated with the five different distances between the bases A and C with respect to the chain are shown in Figure 3.34 and Figure 3.37, respectively. The DOS and the transmission probability functions for base A in Figure 3.32 and 3.33 show clear

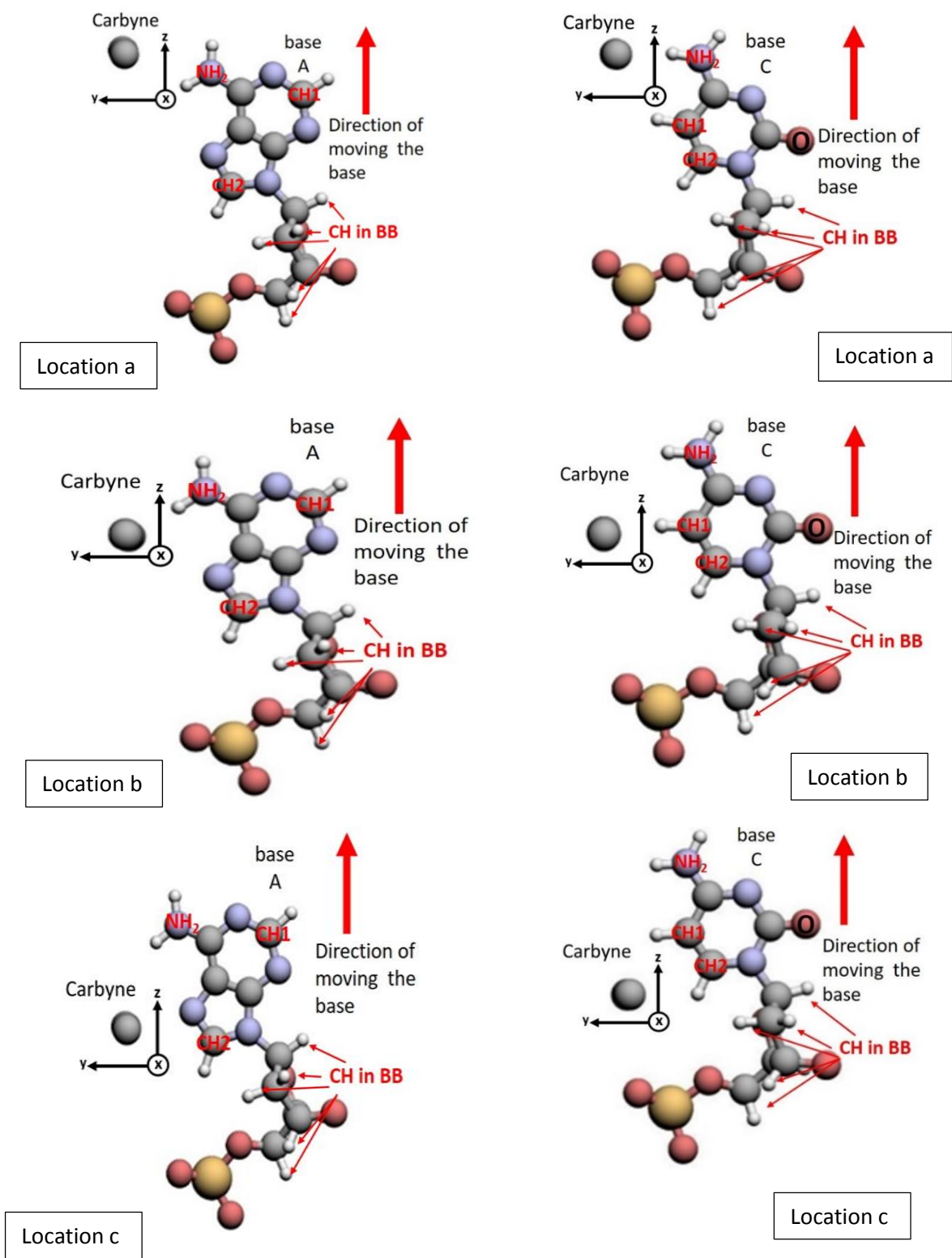


Figure 3.31. Schematics show the five different locations of bases A and C with respect to the chain.

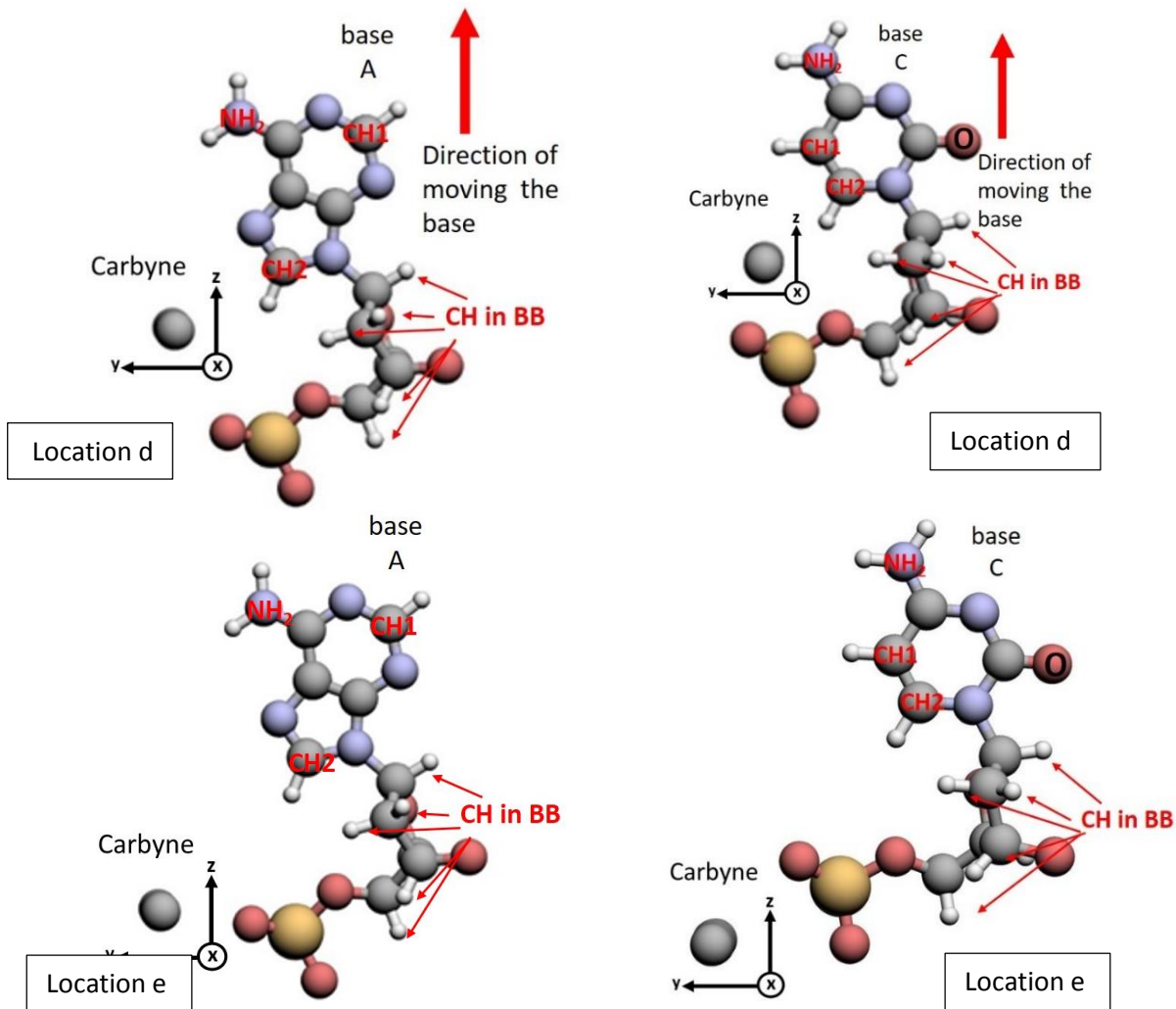


Figure 3.31. Cont.

variations at the five different locations. Similarly, the electrical properties of the chain with the existence of base C at five different locations with respect to the chain indicate changes in the DOS and the transmission probability functions as shown in Figures 3.35 and 3.36. Several noticeable peaks in the DOS can be seen at the negative energies for both chain/A and chain/C model systems. Regarding the transmission probability functions, there were few dips in the transmission probability functions as shown in Figure 3.33 for base A model.

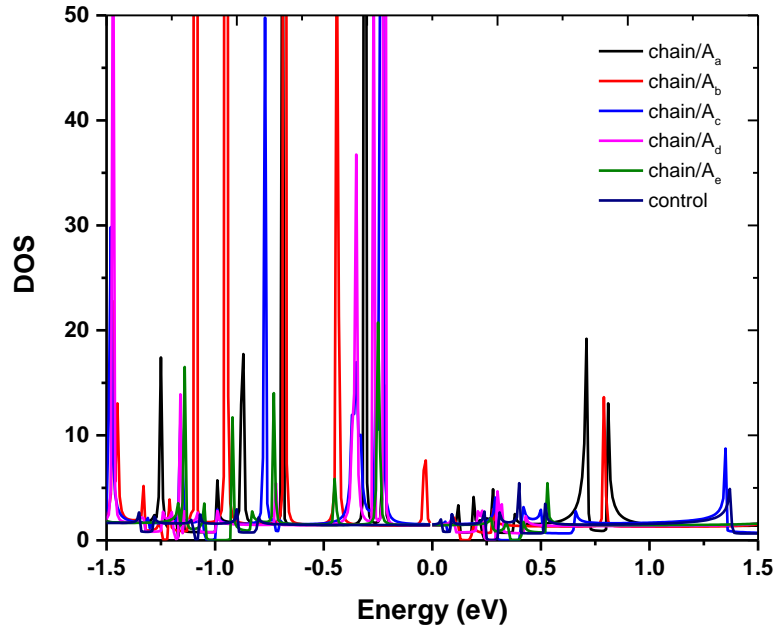


Figure 3.32. DOS for the models with base A at five different locations from the chain compared with the control model.

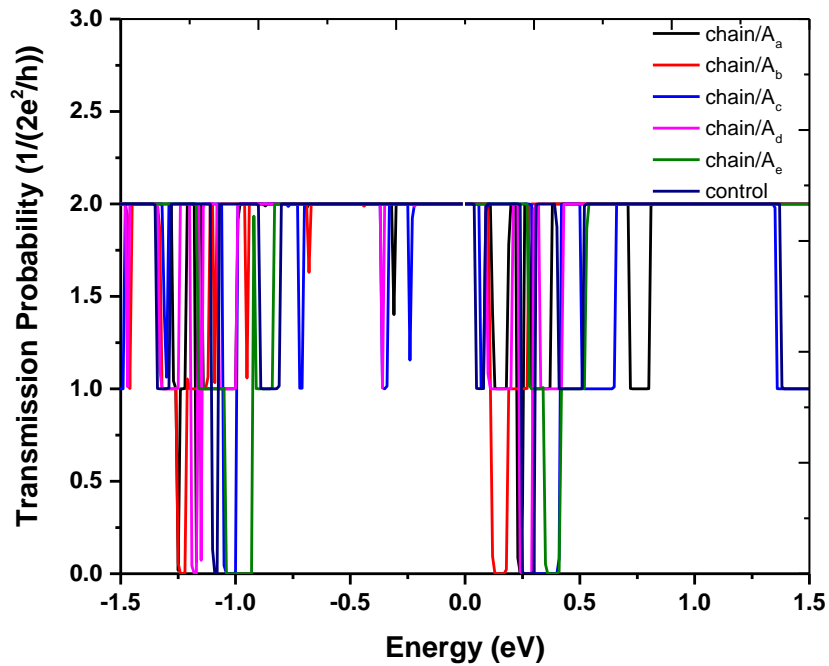


Figure 3.33. Transmission probability functions for the models with base A at five different locations from the chain compared with the control model.



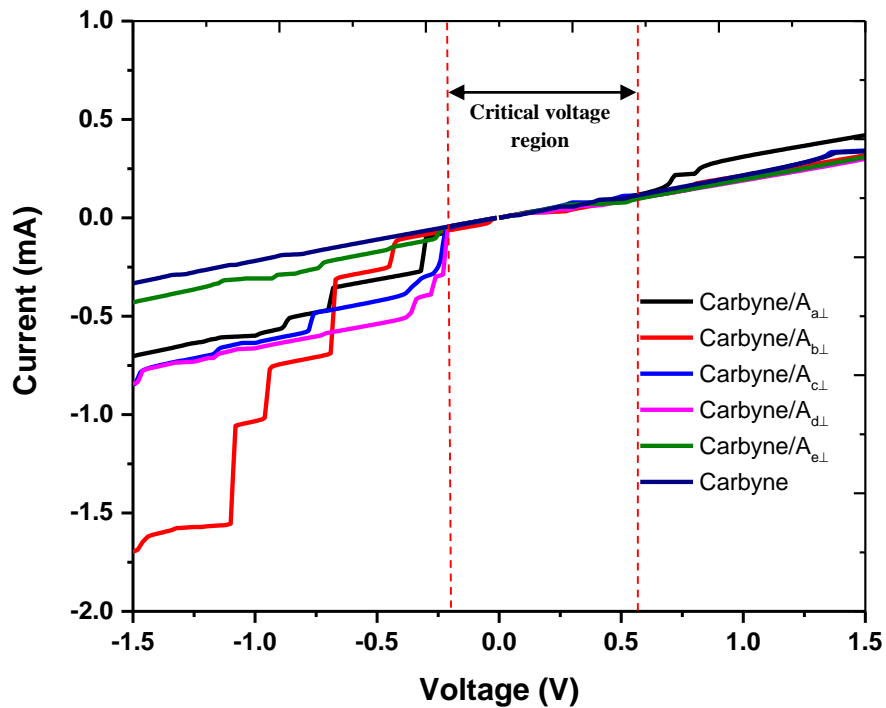


Figure 3.34. I-V characteristics of the chain/A model with the base placed at five different locations with respect to the chain compared with the control model.

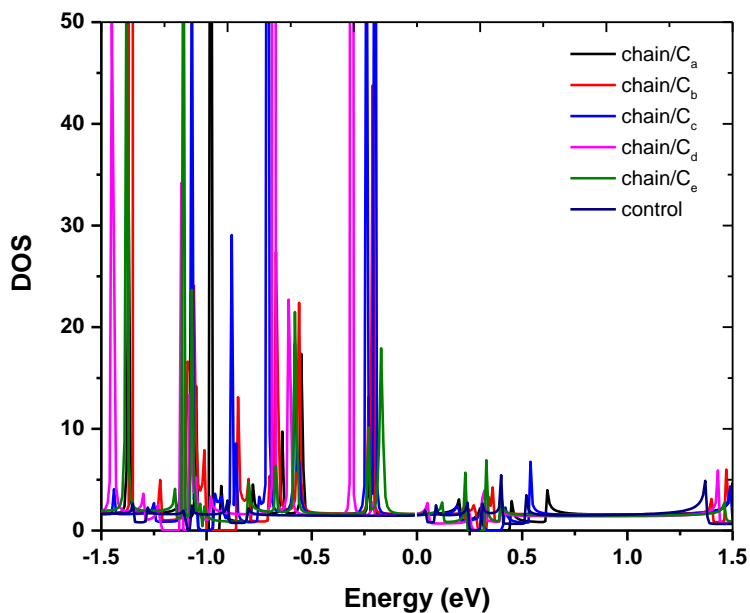


Figure 3.35. DOS for the models with base C at five different locations from the chain compared with the control model.

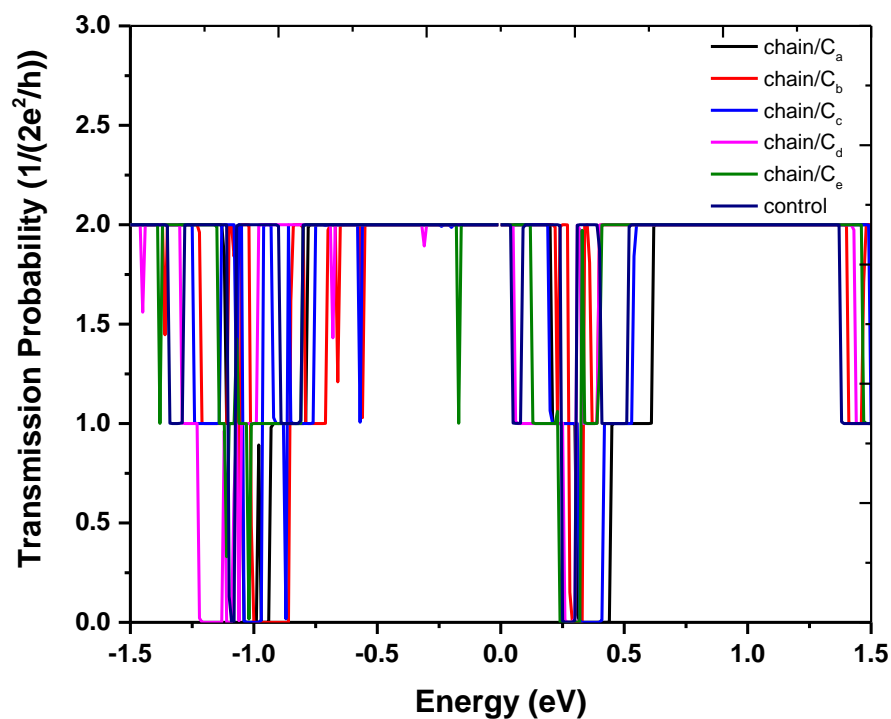


Figure 3.36. Transmission probability functions for the models with base C at five different locations from the chain compared with the control model.

Similarly, there were few dips in the transmission probability for base C model as shown in Figure 3.35. These dips are suspected to have been caused by the interactions between the bases and the carbon chain. This interaction induced different electrical responses which could cause the gap between HOMO and LUMO to be different [42]. The change or difference in the gap leads to a change in the DOS and the transmission probability functions. In fact, such dips in the transmission probability functions have been reported in a study regarding the adsorption of the different bases onto a graphene based sequencing device [30]. That study was about an investigation of the origin of dips in the transmission probability function graphs when different ssDNA bases are adsorbed to the graphene based sequencing device. According to the study, these dips are caused by Fano resonance between the molecular orbitals (MO) of a base and the

continuous energy states of graphene nanoribbons. More importantly, the study claimed that the size of the dip depends on the rotation and the distance between a base and the graphene nanoribbon [30].

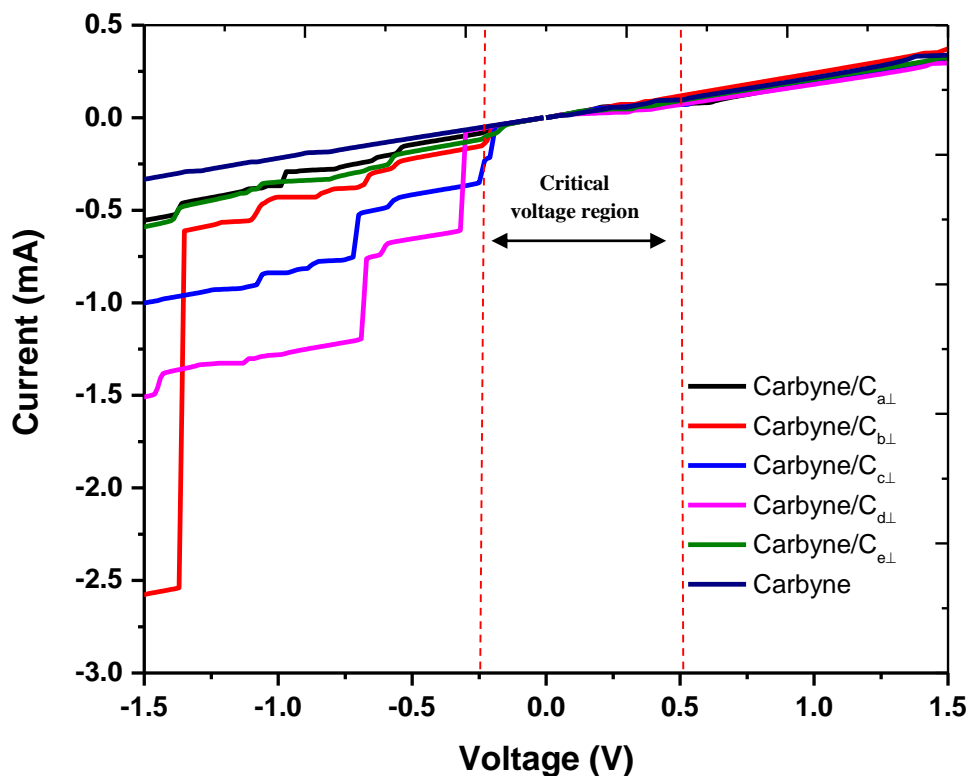


Figure 3.37. I-V characteristics of the chain/C model with the base C placed at five different locations with respect to the chain compared with the control model.

Therefore, the geometrical configuration of the model affects the strength and type of interactions between the different ssDNA bases and the sensing element which can be graphene nanoribbons or, 1D carbon chain for the research of this dissertation. The electrical current for the chain/A and chain/C model systems was obtained at five different locations. Figure 3.34 and Figure 3.37 show the I-V characteristics for the chain/A and chain/C model systems, respectively.

At the five different locations or distances from the chain, both bases induced small effects on the electrical current of the chain at the positive biasing voltages. Each I-V curve can be classified into three main regions. These three regions represent the positive voltage region, the critical voltage region, and the negative voltage region. The three regions are separated by red dashed lines as shown in Figure 3.34 and Figure 3.37. As discussed earlier, the presence of the bases A and C seemed to cause insignificant effects on the electrical properties of the chain and, hence, the electrical current within the range of -0.25 V to 0.5 V. This range may be described as the critical region at which the carbyne chain needs to overcome certain voltage to distinguish the different bases as mentioned earlier. This analogy of the critical voltage region is based on the same behavior that has been reported for graphene-based sequencing devices [72].

In the second region, the only shift in the electrical current that was seen was at the first location of base A, shown in the positive voltage region of Figure 3.34. On the other hand, both bases caused significant changes in the electrical current of the chain at the negative biasing voltages. The negative voltage or the negative energy region shows clear differences in the electrical current of the simulated model systems associated with the five different locations. The interaction between the sensing element and ssDNA is mainly due to the  $\pi$ - $\pi$  stacking interaction. This interaction includes the contribution of NH<sub>2</sub>, CH, and O to the total interaction force between them. The interaction of these different groups with the carbon-based materials is based on the  $\pi$  bond geometrical configuration of the carbon-based materials and ssDNA as explained earlier.

Moving these bases to different distances, where NH<sub>2</sub>, CH, and O are located at different distances from the chain, can enhance the knowledge and lead to better understanding of the origin of the different electrical responses of 1D chain to the existence of different bases. To the

author's knowledge, there has not been a mathematical model to describe the contributions of these different chemical groups to the strength of the interaction forces between the sensing element and the different ssDNA bases. The actual mathematical forms of such forces and their contributions to the electrical modulations of materials have not been provided elsewhere although the different geometrical configurations of  $\pi$ - $\pi$  interactions have been well identified. The different geometrical configurations of  $\pi$ - $\pi$  interactions were discussed earlier in Section 3.1.3.1 of this chapter and were shown in Figure 3.21 and Figure 3.22. Based on the geometrical configurations shown in these figures, the orientations and locations of different  $\pi$  bonds can enhance or reduce the strength of the interaction force and, hence, the adsorption of the different ssDNA bases with the chain.

#### **3.1.5.1. Force Model**

A model to express the changes in the electrical current induced by the presence of these bases at different locations from the chain was needed. Thus, a proof-of-concept model to describe the expected strength of the interaction forces between the chain and  $\text{NH}_2$ , CH, and O was developed. To have consistent effects produced by  $\text{NH}_2$ , CH, and O initiated at different distances, the orientations of bases A and C were kept the same at the different locations as shown in Figure 3.31. Therefore, the only parameter that was intended to change was the distance between the chain and  $\text{NH}_2$ , CH, and O. The force model that represents the contributions of  $\text{NH}_2$ , CH, and O to the total interaction force was established based on the types of the non-covalent intermolecular forces between atoms. The main objective of developing this model was to gain better understanding of these different group contributions to the strength of the interaction force between the 1D carbon chain and ssDNA bases. The force trend was compared with the electrical current trend at these different locations. Table 3.2 and Table 3.3

show the locations of these groups with respect to the chain for bases A and C, respectively. The distances were measured using vesta visualizing software [128]. These are the distances between each one of the groups (NH<sub>2</sub>, CH, O) from the chain along the z direction. In Table 3.2 and Table 3.3, CH1 and CH2 are the first and the second in location with respect to NH<sub>2</sub> group. To illustrate, CH1 is the CH group that was located closest to NH<sub>2</sub>. CHs are the three CH groups in the backbone of the base. Base A does not have oxygen in its structure and, hence, there is no term associated with oxygen in the force calculations for base A model.

Table 3.2. Locations of different groups in base A with respect to the chain.

NH <sub>2</sub> (Å)	CH1 (Å)	CH2 (Å)	CHs in backbone (Å)
2.6	6.5	8.7	11.2
3.6	4.9	7.2	8.91
4.8	3.9	7.4	7.91
6.2	2.9	8.8	6.19
8.8	4.99	11.32	8.03

Table 3.3. Locations of different groups in base C with respect to the chain.

NH <sub>2</sub> (Å)	CH1 (Å)	CH2 (Å)	CHs in backbone (Å)	O (Å)
3.7	3.1	5.47	9.12	7.7
4.99	2.84	4.33	7.88	7.9
5.66	2.99	3.03	6.4	7.2
6.0	3.37	2.91	5.51	6.8
10.9	8.2	7.1	8.51	11.35

Intermolecular forces can be of several types. However, there are mainly three common types of forces between small molecules in a vacuum [129]. These three main forces of interactions are: dipole-dipole, London or dispersion, and dipole-induced interactions. As discussed in Chapter One, the  $\sigma$  bond is normally centered between the atoms. In contrast,  $\pi$  bonds are normally non-uniformly distributed around the atoms as was shown in Figure 1.4 in Chapter One. The intermolecular interaction energies are inversely proportional to the distance between the centers of the two interacted molecules. To explain, the explicit expressions of these interaction energies can be found in Reference 129 and can be simplified to the following forms based on their purpose for this dissertation:

$$E_{dipole-dipole} \propto \left( A \frac{f(\theta, \phi)}{r^3} + B \frac{1}{KT r^6} \right) \quad (\text{Equation 3.1})$$

$$E_{dispersion} \propto \frac{C}{r^6} \quad (\text{Equation 3.2})$$

$$E_{dipole-induced dipole} \propto \left( D \frac{f'(\theta, \phi)}{r^6} + G \frac{1}{r^6} \right) \quad (\text{Equation 3.3})$$

In the above equation,  $A$ ,  $B$ ,  $C$ ,  $D$ , and  $G$  are constants.  $f(\theta, \phi)$  and  $f'(\theta, \phi)$  are functions of the angles between atoms for each molecule,  $K$  is Boltzmann constant, and  $T$  is temperature. The distance between the centers of the molecules is  $r$ . Specifically, the first term of Equation 3.1 describes the interaction energy between two molecules when the atoms are fixed, while the second term represents the freely moving atoms.

Similarly, the first term of Equation 3.3 displays the dipole-induced dipole interaction energy for fixed atoms and the second term is for freely moving atoms. The fixed atoms term indicates that the angles between the atoms in a molecule do not change during the interaction process. On the other hand, the freely moving atoms term represents atoms that can move and,

hence, their angles can change during the interaction process. Equation 3.2 represents the dispersion energy. This energy is not included in DFT calculations of this research. Therefore, it is not considered in the force model developed in this study.

The forces are normally the derivative of the interaction potential energies,  $E$ , as follows [129]:

$$F = -\frac{dE}{dr} \quad (\text{Equation 3.4})$$

Thus, the expressions of the forces associated with each type of the interaction energies given in Equations 3.1 and 3.3 will have the following forms:

$$F = F_{dipole-dipole} + F_{dipole-induced\ dipole} \quad (\text{Equation 3.4})$$

$$F_{dipole-dipole} \propto (A' \frac{f(\theta, \phi)}{r^4} + B' \frac{1}{kTr^7}) \quad (\text{Equation 3.5})$$

$$F_{dipole-induced\ dipole} \propto (D' \frac{f'(\theta, \phi)}{r^7} + G' \frac{1}{r^7}) \quad (\text{Equation 3.6})$$

$A'$ ,  $B'$ ,  $D'$ , and  $G'$  are constants.

The main interest of this force calculation is to obtain a general expression of the total force that can describe the electrical current at a given biasing voltage. The angles between atoms at each molecule in the simulated models were fixed; therefore, the second terms of Equations 3.5 and 3.6 are ignored. In addition, the calculations of the electrical properties of the modeled systems do not take the temperature into considerations. Thus, the total force is approximated as:

$$F_{total} \propto (\beta \frac{1}{r^4} + \gamma \frac{1}{r^7}) \quad (\text{Equation 3.7})$$



$\beta$  and  $\gamma$  are the new constants and are assumed to be 1.0 for simplicity. The second term of Equation 3.7 takes into account the first part of the dipole-induced dipole force. The contributions of the groups  $\text{NH}_2$ ,  $\text{CH}$ , and  $\text{O}$  to the total force of interaction for the chain/A and chain/C model systems can be obtained using Equation 3.7. The given distances in Tables 3.3 and 3.4 are assumed as the distances between the centers of the interacting molecules. At each distance of these different groups, Equation 3.7 is used to estimate the interaction force. Adding these forces together, the total force for each model is obtained. Figures 3.38 and 3.39 show the total force trend for each simulated model compared with the electrical current at -0.85 V. The resulting total force trend for each model shows similar behavior to the trend of the electrical current values at -0.85 V.

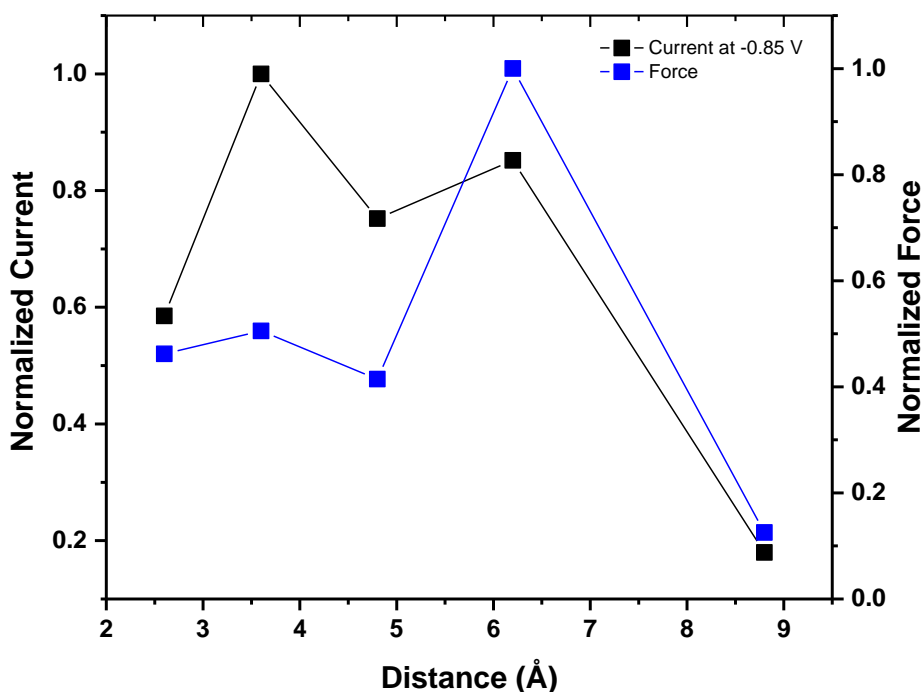


Figure 3.38. Force trend and current for the 1D chain/A model at -0.85 V.

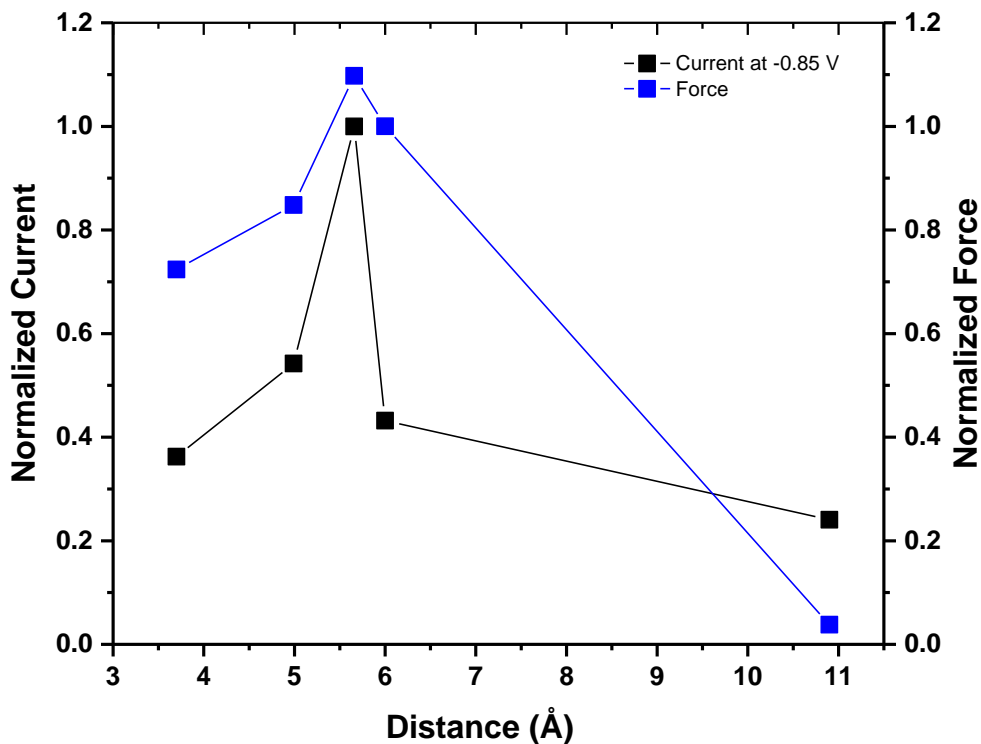


Figure 3.39. Force trend and current for the 1D chain/C model at -0.85 V.

The force trend shown in Figures 3.38 and 3.39 has peaks and drops similar to the electrical current. For example, one CH group can possibly be close to one of the carbon atoms in the chain, while another CH is further away from it. Also,  $\pi$ - $\pi$  interaction is affected by the orientation of these groups as discussed earlier. These different orientations may induce an attraction force with one of these groups and a repulsive force with another group due to their different geometrical orientations with respect to the chain. Therefore, the attraction and the repulsion forces are based on the geometrical configurations discussed previously and displayed in Figures 3.21 and 3.22. The force trend may not perfectly match the trend of the electrical current; however, they show similar performance. One way that could improve the quality of

these trends is to obtain each angle between the atoms at each molecule and calculate precisely each term of the estimated total force.

The developed theoretical model is a proof-of-principle that estimates the contribution of each group to the interactions between ssDNA bases and the 1D carbon chain. In fact, it reflects the high sensitivity of the 1D carbon chain to each of these groups. It is concluded that the geometrical configurations of these groups in different ssDNA bases strongly influence the electrical response of the chain to the presence of each base uniquely.

### **3.1.5.2. Current at 0.6 V**

Additional confirmation of the electrical current obtained in this study was desirable. To examine the one-dimensional carbon chain ability to distinguish a single base, the electrical current at one biasing voltages for the models of bases A and C at five different locations was plotted.

One way to further analyze the I-V curves for the models that have bases A and C at the different locations was to extract the I-V characteristics at the positive biasing voltages and choose one voltage to determine the sensitivity of carbyne to the change in the locations of the different bases.

Figure 3.40 shows I-V curves for both models at the positive biasing voltages. Clearly, Figure 3.40 demonstrates the differences in the electrical current for these models at the positive biasing voltage. One voltage (0.6 V) within the positive biasing voltage range was chosen to demonstrate the sensitivity of carbyne at the different locations. Figure 3.41 shows the current for the chain/A and chain/C model systems at five different locations with respect to the chain at 0.6 V. The figure reflects distinction between the two bases at the five different locations. The

electrical current for chain/A and chain/C models fluctuates at the different locations. For example, the first location of the current trend reflects higher current associated with base A compared with base C.

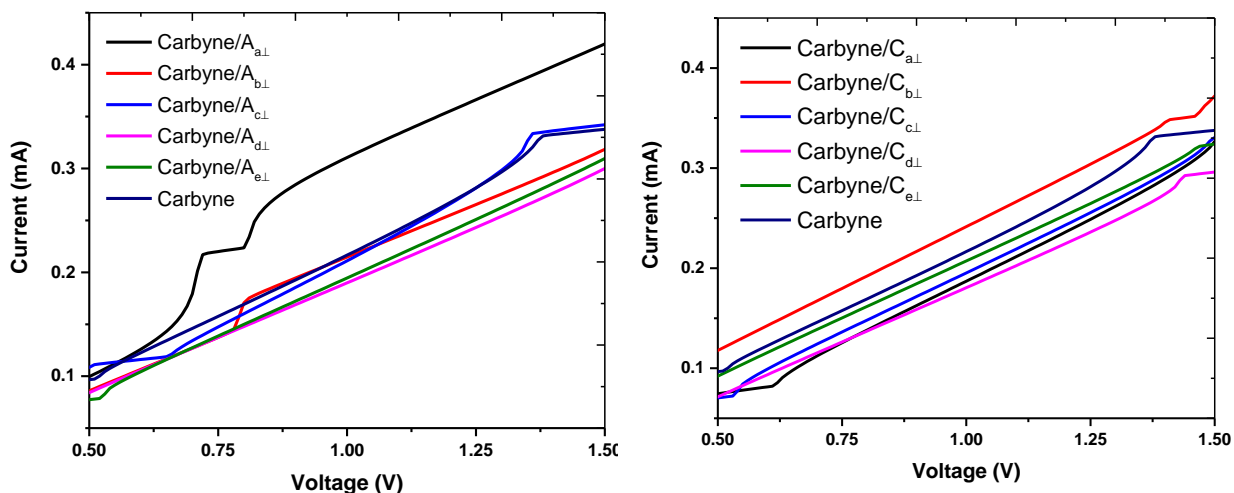


Figure 3.40. I-V curves for the chain/A and chain/C model systems at the five different locations for the positive biasing voltages.

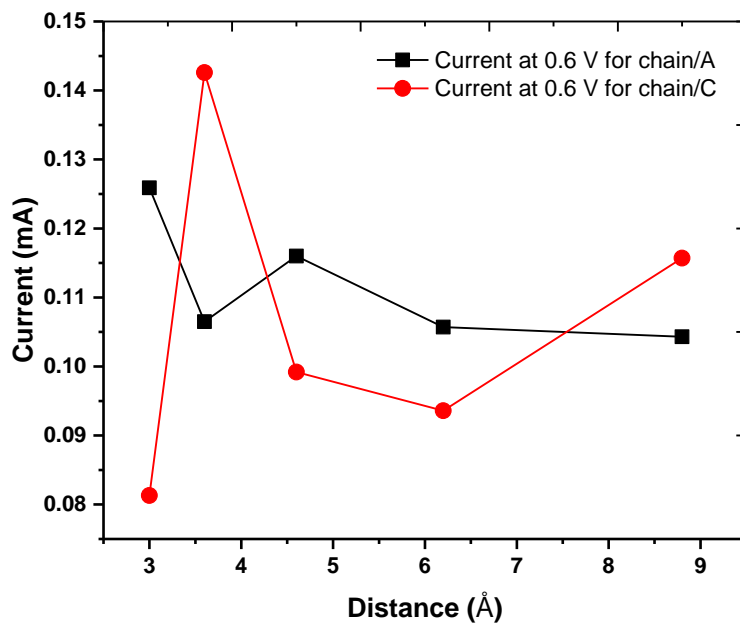


Figure 3.41. Current as a function of the base distance from the chain for the chain/A and chain/C models at 0.6 V.

By looking at the distances of different groups provided in Tables 3.2 and 3.3, one can see that  $\text{NH}_2$  in base A has its maximum influence on the chain at first location as shown in Figure 3.40. In contrast, the electrical current produced in the presence of base C at the second location is higher than the current in the presence of base A. This can be explained by having  $\text{CH}_1$  of base C closest in location to the chain as was shown in Figure 3.31. The electrical current at other locations is believed to be a combination of the effects of the different groups.

In brief, this result is remarkable. Indeed, the one-dimensional carbon chain induces unique electrical response to different groups in the different bases. The first-principle approach did not include time or speed of travel for ssDNA bases. In experimental situations, ssDNA travels or moves with speed. Thus, it is part of the considerations of this research to estimate the time associated with the translocations of the bases at different locations. Hence, the resulting electrical current for the chain/A and chain/C simulated model systems was used to validate the conclusion regarding the effects of different groups on the electrical current through the chain at different voltages.

Figure 3.42 represents the current with respect to an estimated translocation time. The estimation of the translocation time was calculated based on a simple assumption. Since the translocation speed of ssDNA is  $0.1 \mu\text{m/s}$  at  $0.6 \text{ V}$  when using an AFM tip [118], it is assumed that bases A and C travel at this speed below the carbon chain. To find the current, the distance of each base from the chain at the five different locations was used. Using the simple formula for speed and distance in physics, the time was found. The distance in this part of the calculations represents the distance between the closest atom in the base to the chain. The electrical current as a function of time is plotted in Figure 3.42. Figure 3.42 indicates that the carbyne chain can distinguish the different bases at different time if the bases translocate at  $0.1 \mu\text{m/s}$  at  $0.6 \text{ V}$ .

Therefore, it is considered a feasible analysis. This result infers that single base resolution is a possibility when using a truly atomic thickness carbon chain.

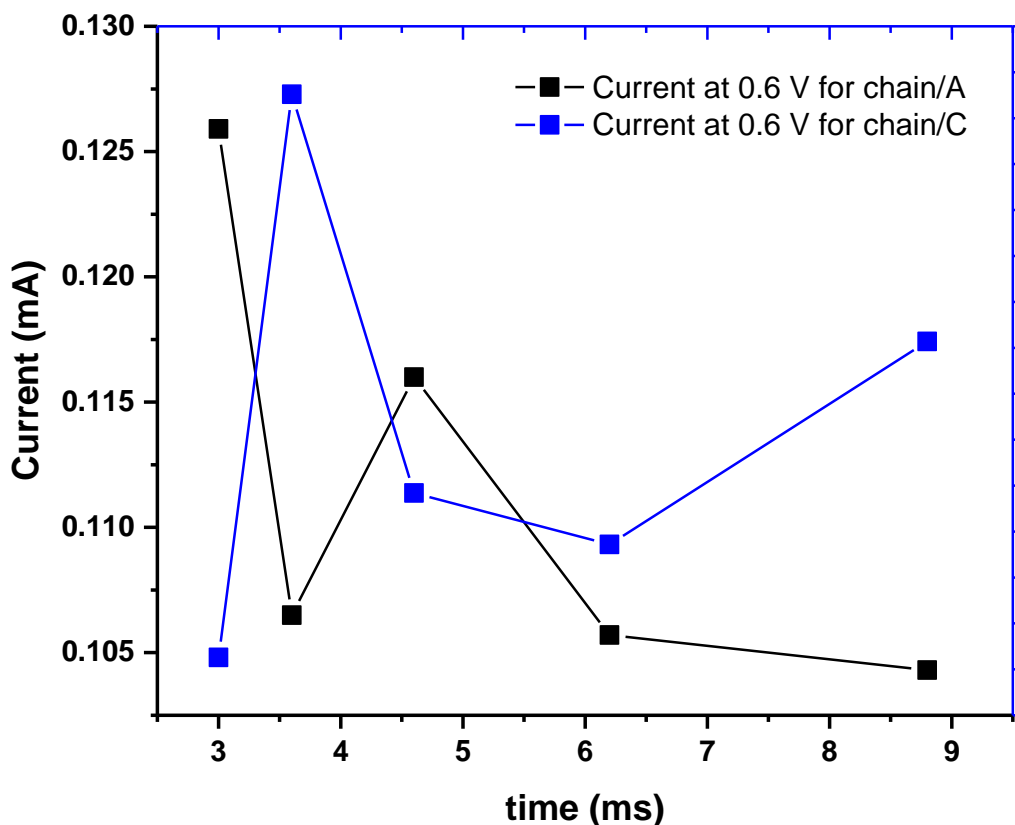


Figure 3.42. Current as a function of time calculated by assuming bases A and C move with a speed of  $0.1 \mu\text{m/s}$  at  $0.6 \text{ V}$ .

In brief, the 1D carbon chain capability to distinguish the different groups in a base when they are located at different distances is a powerful tool that can be used in ssDNA sequencing devices. The sensitivity of the atomic width carbon chain is altered due to the different interactions with different groups in a base. Hence, this result does not only prove that carbyne is sensitive to the different orientations, but it also shows significant changes in its electrical

response and its interactions to different chemical groups in different ssDNA bases. This result is unlike graphene-based sequencing devices which show no difference for different ssDNA orientations.

### **3.1.6. 1D Carbon Chain Between Graphene Nanoribbons**

The 1D carbon chain that is mainly considered in this study is a single chain of 16 carbon atoms with anti-symmetric bond lengths between the atoms as explained in Section 3.1.1. However, a 1D carbon chain can be of different structures based on the reported experimental investigations [36], [58]. To explain, cumulene and polyyne can co-exist under appropriate experimental conditions as mentioned in Section 1.2.2. It has been reported that a chain of 1D carbon atoms attached to two graphene nanoribbons can be used in many potential applications for nanodevices [62]. One of the advantages of such a structure is that it can be experimentally possible to produce via scanning tunneling microscopy (STM) tip in a transmission electron microscopy stage (TEM) as reported by Reference 37. The group indicated the possibility of producing a one-dimensional carbon chain successfully in situ where graphene serves as a precursor for the formation of a 1D carbon chain.

#### **3.1.6.1. Control Model**

The type of contact used has been reported to influence the electrical conductivity of the 1D carbon chain due to having different junction properties and the change in Fermi energy [58]. Therefore, a control model of the 1D carbon chain with alternating single and triple bonds attached to two zigzag-edge graphene ribbons on both sides was constructed using *NanoEngineer1* software [103]. A schematic of the model is shown in Figure 3.43. The total number of carbon atoms in the single carbon chain was 16 atoms and the total number of atoms

for the whole model was 58 atoms. The distances between the carbon atoms in the constructed carbon chain was about 1.55 Å for single bonds and about 1.28 Å for triple bonds. However, after allowing the atoms to relax along the x direction, the distances become about 1.38 Å for the single bonds and about 1.25 Å for the triple bonds.

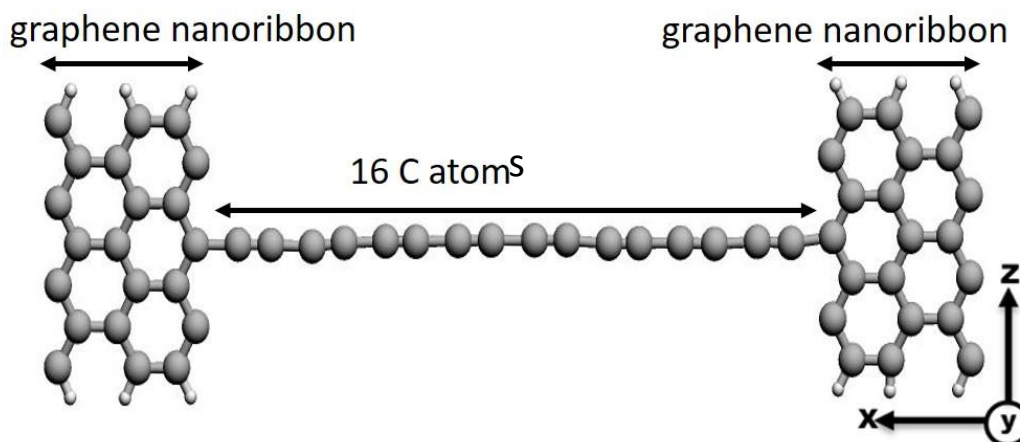


Figure 3.43. Schematic of the model that has a single chain of carbon atoms attached to graphene nanoribbons on both sides.

Therefore, it is assumed that the chain was asymmetric and not a perfect polyene chain after the geometrical optimization. The distance between the carbon atoms in the honeycomb graphene ribbons remains 1.43 Å after relaxation.

Different ssDNA bases were incorporated within this 1D carbon chain to investigate the electrical response of such a nanostructure to the presence of different ssDNA bases. Each base model consisted of a single DNA base placed normal to the 1D carbon chain where each base was about 2 Å above the chain. The reason for choosing such distance was to consider the short-range interactions between the chain and different DNA bases only. van der Waals interaction was neglected by the DFT calculations adopted in this work. After embedding each DNA base,



the minimum energy structure was obtained by allowing the atoms to move along x without any further cell optimization. These ssDNA bases were the same bases that have been used elsewhere in this dissertation research for the sake of consistency. As described previously, each DNA model included a base, a phosphate group, and a sugar backbone.

The plane wave cutoff energy used was 30 Ry and the Monkhorst-Pack k points were  $4 \times 2 \times 2$ . For the exchange and correlation interactions defined by the PBE functional and for the electron–core interaction [104], Ultrasoft pseudopotentials with generalized gradient approximations were used [93]. For geometrical optimization, the Broyden–Fletcher–Goldfarb–Shanno (BFGS) algorithm was used until the forces were lower than  $0.04 \text{ eV}/\text{\AA}$ . Water molecules were not included in the simulation to minimize the computation time. The dimensions of the simulation cell were  $34.2 \text{ \AA} \times 33.0 \text{ \AA} \times 33.0 \text{ \AA}$ . The electrical properties including transmission probability functions and DOS are shown in Figure 3.44. Figure 3.45 shows the I-V curve associated with this control model. The transmission probability functions for a single chain attached to graphene nanoribbons (Fig 3.44) had a maximum value of 1.0. On the other hand, the maximum value for the transmission probability obtained for the single carbon chain of 16 carbon atoms in a vacuum is 2.0, which was shown in Figure 3.2. This result indicates that there was less transport probability that the electrons would move from one end to the other end of the chain when the chain was attached to two graphene nanoribbons on both ends. Specifically, there are fewer open quantum channels that the electrons can transport through. The variation of the transmission probability between these two structures could be due to the graphene nanoribbons attached on both ends.

As mentioned previously, the type of contact used influences the electrical properties of the one-dimensional carbon chains. It was recently reported that the conductivity of one-

dimensional carbon chains synthesized experimentally decreases progressively when one end of the chain is attached to a closed end of a single-walled nanotube [58]. The reduction in the transmission probability function is expected for such systems and agrees with the transmission probability results obtained for this work.

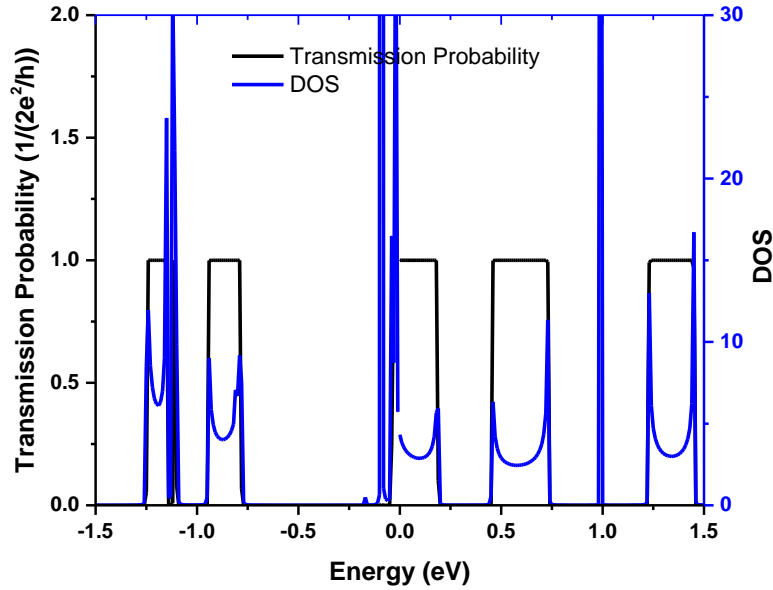


Figure 3.44. Electrical properties for a single chain attached to graphene nanoribbons on both sides at positive and negative energies.

Another study has considered the electronic transport of a 1D carbon chain between two graphene nanoribbons [62]. The study included that the 1D chain attached to two graphene nanoribbons: armchair-edged and zigzag-edged. According to the study, the maximum transmission probability of a 1D carbon chain is 1.0 regardless of the type of edge for the graphene nanoribbons. The report claims that the electronic structure of the graphene nanoribbons and the scattering from the middle region are the two reasons for such effects on the transport properties of the 1D carbon chain. In particular, the quantum conductance is  $2ne^2/h$ , where  $n$  is the number of the quantum channels and  $h$  is Planck's constant. The number of the

quantum channels depends on the electronic structure of the graphene nanoribbons. These channels can be off/on and accordingly lead to decrease or increase in the transport probability. Also, the study indicates that a 1D carbon chain with zigzag-edged graphene nanoribbons has non-zero transmission probability and non-zero DOS at 0 eV. It is caused by the scattering at the middle region of the chain [62]. This is another good agreement with this work as can be seen in Figure 3.44.

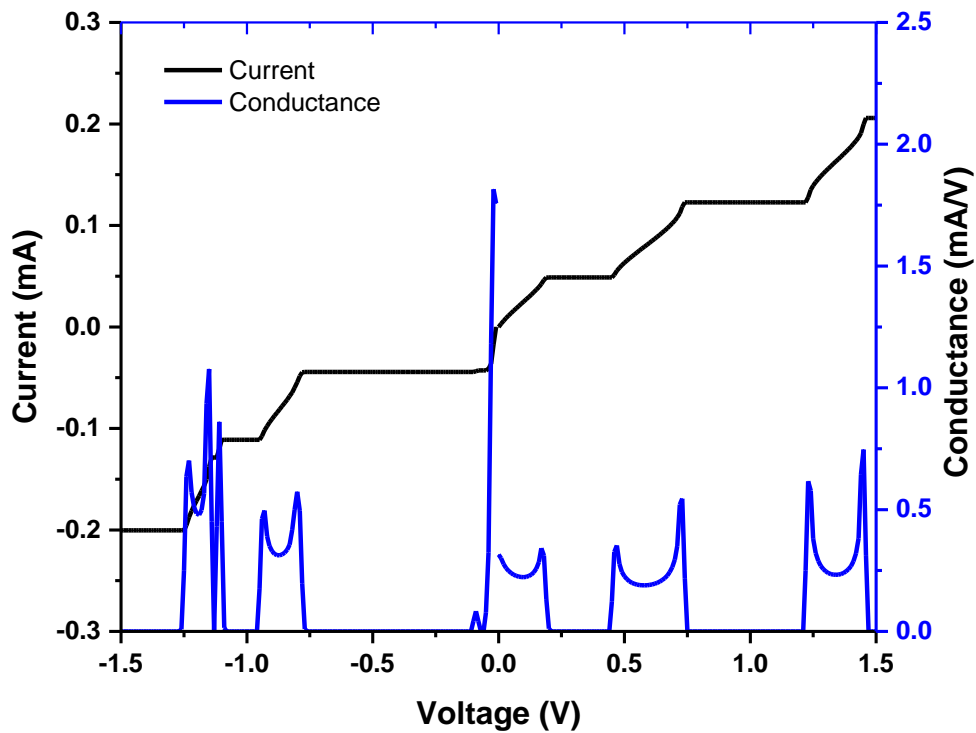


Figure 3.45. Electrical current and conductance for the model that has a 1D chain attached to graphene nanoribbons on both sides at positive and negative voltages.

Comparing the DOS obtained for the single carbon chain shown in Figure 3.2 with the DOS obtained for the carbon chain between two graphene nanoribbons shown in Figure 3.44, it seems that increasing the number of carbon atoms results in increasing of the DOS peaks at specific energy values. For example, Figure 3.44 displays main peaks of DOS at three energies,

which are about 1.0 eV, 0 eV, and -1.1 eV. In contrast, the DOS for a single chain of carbon atoms displayed in Figure 3.2 showed wider and smaller peaks. The results in this dissertation are in good agreement with the reported study in Reference 62. It is explained in terms of the scattering region at the middle of the chain and the electronic structure of the two contacts, which are the graphene nanoribbons [62]. For each energy band, there are many energy states. These energy states can increase or decrease based on the electronic structures. The DOS represents these states packed together. Thus, the peaks of the DOS are higher and sharper when increasing the number of states. As a result, there will be more states at each energy value.

Moreover, the DOS is higher and sharper when the number of carbon atoms in the chain increases. The reported work in Reference 62 examines three different lengths of chain: 9, 12, and 15 carbon atoms. Increasing the number of carbon atoms causes the DOS and the transmission probability functions to be sharper for longer chains due to the resonance transmission. Although the number of the carbon chain in this study is 16, it agrees with the DOS and the transmission probability reported.

Another study has investigated numerically the structure nanoribbons-chain-nanotube [58]. The DOS was calculated and found to have many sharp peaks. The study suggests that these sharp peaks are the result of the localized energy states contributed by the bare zigzag edge of the nanoribbon and the nanotube. In order to envision a full picture of the electronic properties of such structure, the electrical current was obtained. Figure 3.45 shows the I-V curve and the differential conductance for the carbon chain attached to the two graphene nanoribbons. Figure 3.3 represented the electrical current and conductance of a single chain of carbon atoms.

The electrical current for a single chain was higher than the electrical current for a 1D chain attached to two graphene nanoribbons. Also, the electrical current for the single chain was

mostly ohmic with two regions that showed current independency of the biasing voltage as discussed earlier. However, the electrical current for the chain with two graphene nanoribbons represents step-like current. The nonohmic behavior of I-V characteristics have been reported [36]. The 1D carbon chain in that report was produced via unraveling of the carbon chain from the graphene layer. The study assumed the large fluctuations in the electrical current through the 1D carbon chain were caused by the separation of the chain from graphene. Also, the study suggested that the presence of Peierls's instability and the loss of symmetry are two factors that can cause the asymmetric configuration [36] as discussed in Section 3.1.1. The energy and voltage in this study are interchangeable, i.e. they basically represent the energy of electronic states as discussed in Section 3.1.1 of this chapter. In addition, the presence of the sharp peaks in DOS and on/off quantum channel fluctuations contributed to the nonohmic behavior of the electrical current. Considering the differences in the two structures, the type of contact is a very effective factor that impacts the conductivity of 1D carbon chains as discussed earlier.

The behavior of the I-V curve when different contacts are present was reported experimentally [58]. That report claims that the chain acts as Schottky diode with I-V curve being asymmetric. Furthermore, they indicate that a depletion of  $\pi$ - electrons at the chain-nanotube contact region is expected. The study also proves that the reduction in the transmission probability and electrical current can be caused by the resonance or the resonant tunneling transport through the chain [58]. In fact, the resonance leads to closing the quantum channels that the electrons can transport through. As an illustration, the 1D carbon chain and the graphene nanoribbons should open the quantum channels for the electrons to transport at the same energy [58], [62]. Therefore, one may anticipate that having graphene nanoribbons attached to the carbyne chain affects the electronic structures and reduces the number of quantum channels for

the 1D chain which leads to decrease in its conductivity. The significant decrease in the transmission probability results in decreasing of the electrical current and the molecular conductance. This progressive decrease in the transport probability functions or the quantum conductance is caused by the electronic structure of the graphene nanoribbons and the resonance as well as the scattering effects at the middle region of the chain.

### 3.1.6.1. Carbon Chain Attached to Graphene Nanoribbons as a Sensing Element for ssDNA

Since such a carbyne structure is part of this research, placing different ssDNA bases was considered for this dissertation. Therefore, a ssDNA base was placed normally to the 1D chain with the graphene nanoribbons. The electrical properties of the resulting structure were calculated via following the same approach that was used for the single carbon chain. Figure 3.46 shows schematics of base A placed normally to the chain. The DOS and the transmission

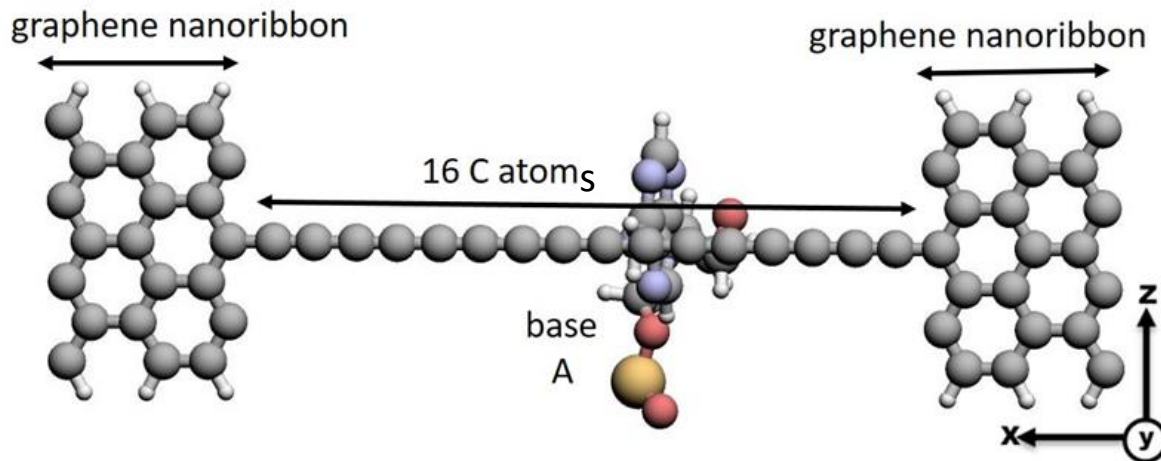


Figure 3.46. Schematic of the model that has single chain of carbon atoms attached to graphene nanoribbons on both sides with base A placed normal to the chain.

functions are presented in Figures 3.47 and 3.48. I-V characteristics are displayed in Figure 3.49. In the figure, the electrical current at positive and negative biasing voltages is shown. The main reason for including the negative biasing voltages was to highlight the structural distortion in the chain as reported by several studies [36] and to predict its influences on the chain sensitivity to different ssDNA bases.

By examining the simulation results for all model systems that had the carbyne chain attached to two graphene nanoribbons and one base, one could conclude that the presence of those bases caused the electrical properties of the carbyne chain to alter. The DOS and the transmission probability functions of the chain shown in Figure 3.47 and Figure 3.48 demonstrate changes with the presence of the bases. In particular, the number of peaks or dips in the DOS increased and became sharper with the presence of the different ssDNA bases.

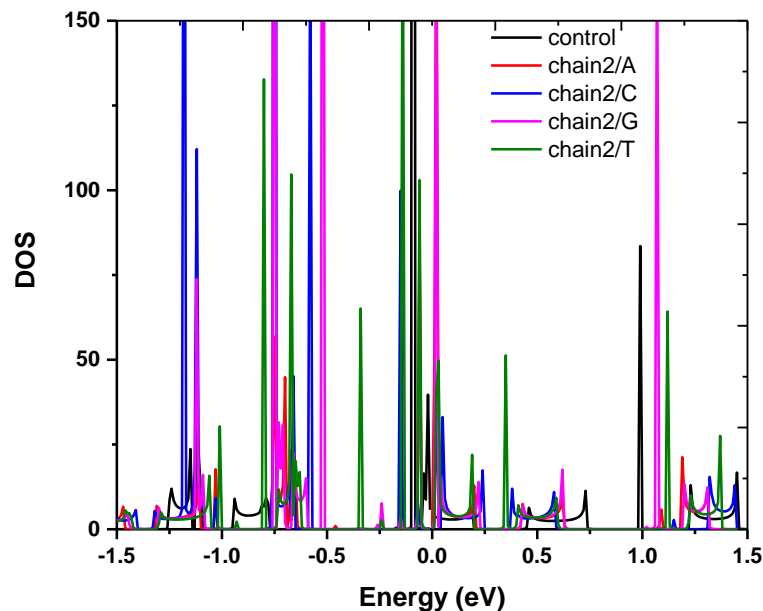


Figure 3.47. DOS for the chain2/ssDNA model compared with the control model.

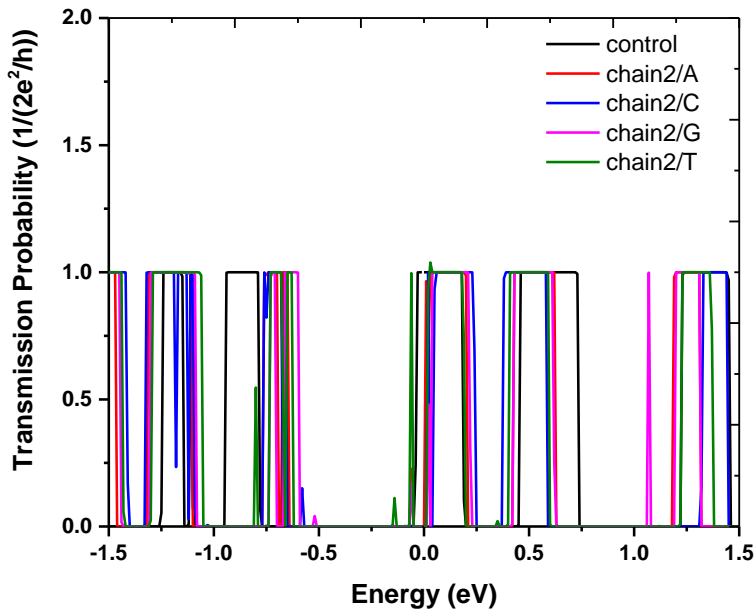


Figure 3.48. Transmission probability functions for the chain2/ssDNA models compared with the control model.

In addition, the transmission probability functions also changed with the presence of different bases. The changes in the DOS and the transmission probability were expected to lead to substantial changes in the electrical current of the chain. The electrical current of the chain increased for both positive and negative biasing voltages except within the range from 0 to -0.8 V. Also, there was a clear domination of the electrical current with the presence of base A compared with the other three bases. This result differs from that obtained for the single chain shown in Figure 3.7. As an illustration, the variations in the electrical properties and, hence, the electrical current of the 1D chain when placing the different ssDNA bases  $90^\circ$  with respect to the chain could be due to the differences in the DOS, the quantum conductance or the number of the open channels, and the electronic properties of the contact. These differences could be caused by the adsorption of the ssDNA bases onto the chain surface. The existence of different ssDNA bases resulted in modulation of the electrical response through the chain and induced changes in



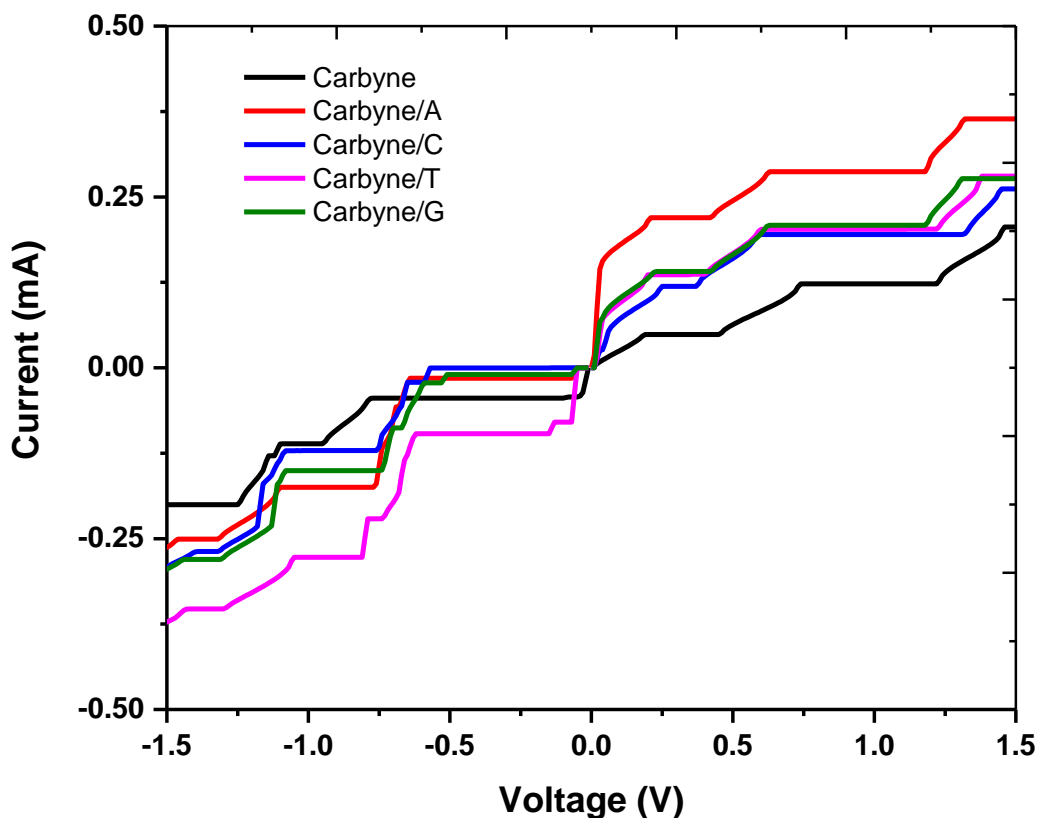


Figure 3.49. I-V characteristics for the chain2/ssDNA models compared with the model that has carbon chain attached to graphene ribbons on both sides at positive and negative voltages.

its electrical properties accordingly. These electrical modulations can be justified by the structural distortion in the chain. The 1D chain of carbon atoms is subject to Peierls's instability [36] as mentioned earlier. Consequently, the electronic and structural properties of 1D carbon chain, including the location of Fermi energy, differ and they are anticipated to alter with the presence of ssDNA bases. The structural and the electronic properties are associated with the locations of Fermi level as well as the locations of the lowest unoccupied molecular orbitals (LUMO) and highest occupied molecular orbitals (HOMO). To explain, all simulated models

with different bases and the control model had their Fermi energies within the range of -4.6 to -5.0 eV. Particularly, Fermi energy for the control model was -4.65 eV. Fermi energies were -4.89 eV, -4.86 eV, -4.90 eV, and -4.91 eV for models of the 1D chain with bases A, C, G, and T, respectively. Thus, their different ssDNA bases were adsorbed onto the chain surface. Fermi levels were located around the same energy with a small difference compared with the control model. Comparing the Fermi energies with the one of the control model, the presence of DNA bases changed the chemical environment of the carbyne chain causing the Fermi level to shift by about 0.2 eV. This led to variation in the electronic features of the models.

This increase in Fermi energy caused by the presence of different ssDNA bases has been reported for graphene nanoribbons [43]. Furthermore, it has been reported that the gap between HOMO and LUMO of isolated DNA bases is about 5 eV. Having similar electronic properties near this gap may raise difficulty in identifying the individual bases [73]. However, the locations of the HOMO of DNA bases can overlap with LUMO when these bases are adsorbed on graphene nanoribbon surfaces due to the interaction between graphene and the DNA bases which leads to an increase in the number of DOS peaks [119]. This overlapping can cause the movement of the electronic charges and the flow of electrical current, which indicates that the quantum channels have their off/on state at the same energy. The effect of adsorption of DNA bases onto the graphene surface permits the distinction of these bases [119].

Thus, having DNA bases adsorbed onto the 1D chain surface allows more electrons to transport through the 1D carbon chain prompting changes in its electronic properties and causing the current to increase. When including more atoms in a model system, the number of electrons and the number of energy states increase. Hence, the presence of different ssDNA bases enhances the transport process by providing more conductance channels that the electrons

transport through from one side of the chain to the other. As a result, the current for the 1D chain attached to the graphene nanoribbons increases when DNA bases are absorbed onto its surface. This increase in the current is the largest for base A at a positive biasing voltage and base T at a negative voltage.

As mentioned earlier, the DOS for the model systems at positive biasing voltages was different from DOS for these systems at negative biasing voltages. To explain, the electrical current increases when the transmission probability functions increased accompanied by an increase in DOS and vice versa. The voltage here represents the electronic state energy as mentioned in previous sections. Therefore, the increase in current was different at positive and negative biasing voltages, meaning the current behavior at the positive voltage was different from its behavior at the negative voltage. This property demonstrates that the 1D carbon chain is sensitive to different bases which can be originated from the variations in the electronic transport properties with the presence of different bases. Consequently, it is suggested that the one-dimensional carbon chain distinguishes different bases at different positive and negative biasing voltages. This provides an additional advantage of using a carbon chain in DNA sequencers.

For further investigation of the chain sensitivity to DNA bases, two different biasing voltages were chosen, -0.85 Volt and 1.3 Volt. At these two different voltages, one can recognize the significant difference in the electrical current through the 1D chain as shown in Figure 3.50a. In addition, a percentage increase in the chain current for different DNA bases at these particular voltages was determined in order to more deeply investigate the effects of the different DNA bases on the electrical current. Figure 3.50b shows the increase in the electrical current of the 1D chain for different DNA bases. In general, the simulations showed that the chain current increased when DNA bases were adsorbed onto its surface. As discussed earlier, this percentage

of increase was different for all the bases at positive biasing voltages and negative voltages. For example, there was 265% increase in the current for base A model at 1.3 V and also 270% for base T model at -0.85 V. At other voltages, the increase was 133% for base A model at -0.85 V and 111% for base T model at 1.3 V. Base C model showed 55% increase in the current at 1.3 V and 62% at -0.85 V. Base G model showed 101% and 158% at -0.85 V and 1.3 V, respectively. This indicates the possibility of an efficient 1D carbon chain DNA sequencer. In fact, a 1D carbon chain demonstrates sufficient sensitivity to different DNA bases.

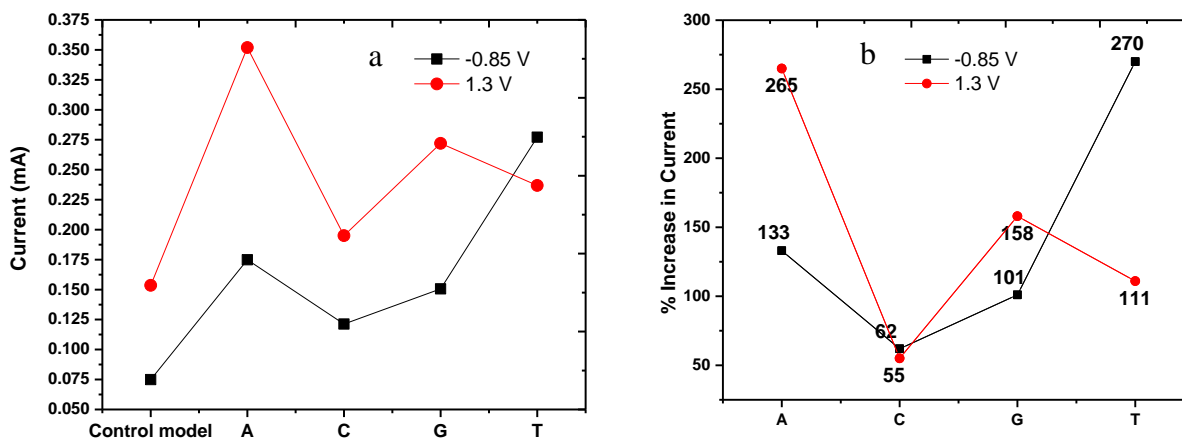


Figure 3.50. (a) The electrical current for the chain/ssDNA models at two different biasing voltages (-0.85 V and 1.3 V) and (b) the percentage increase in current associated with the presence of ssDNA bases at -0.85 V and 1.3 V.

A final consideration was to compare the electrical current obtained when different ssDNA bases were placed normally to the single chain with the chain of carbon atoms attached to the graphene nanoribbons in the presence of the different ssDNA bases. The differences between the two structures of the 1D carbon chain can be inspected in many ways. One of the

ways, which has been used in previous sections, was to find the differences in the electrical current and divide it by the maximum difference. This approach provides estimations of the percentage differences between the two models. Figure 3.51 shows the relative current for these systems at positive and negative biasing voltages. Generally, the relative current fluctuated at

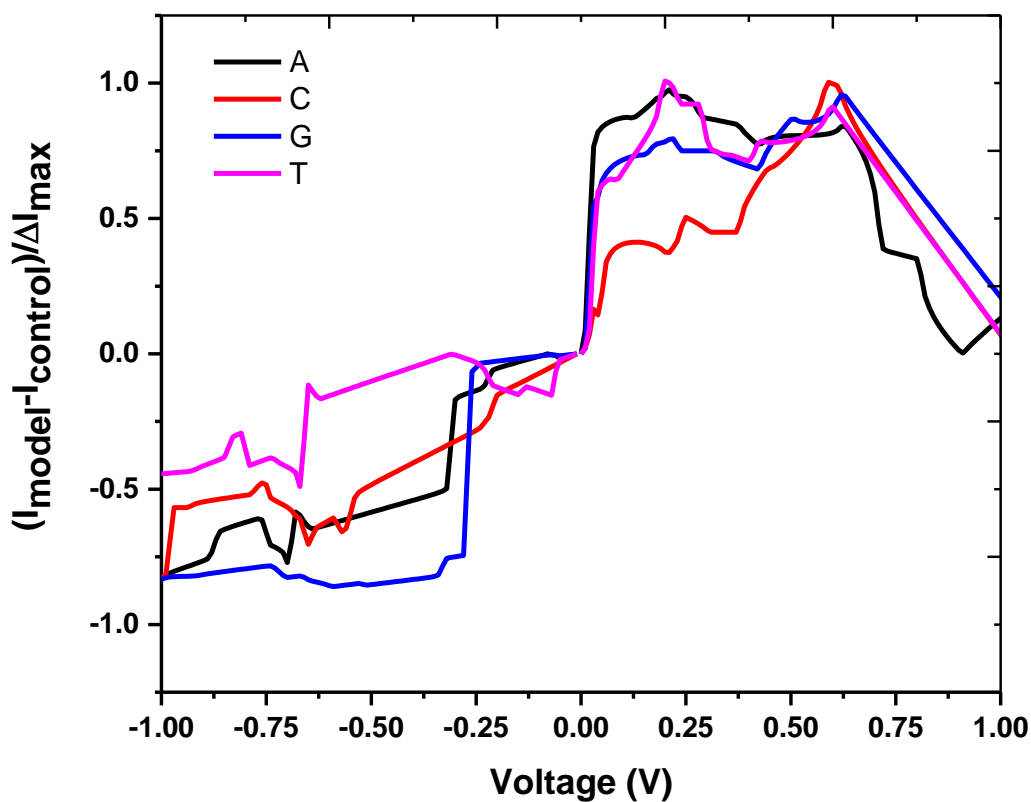


Figure 3.51. The relative current for the two different models or structures of chain in the presence of ssDNA.

both positive and negative voltages. At the positive biasing voltages, the relative current increased when increasing the voltage up to about 0.6 V at which the relative current decreased when increasing the voltage. Base C shows the least relative current within the range from 0 to

0.6 V. On the other hand, base A indicates the least relative current starting from 0.6 V to 1.0 V. Base G and T present the highest and least relative current at the neagtive voltages, respectively.

More specifically, two different voltages were chosen, 1.3 V and -0.85 V. The sensivity to the presence of different ssDNA bases at these two different voltages was calculated and shown in Figure 3.50b. It has been established that the 1D carbon chain attached to two graphene nanoribbons is sensitive at these two voltages. Thus, comparing the sensivity of the 1D chain attached to graphene nanoribbons model with the 1D chain model at these voltages can provide a valid evaluation. The percentage of change in the current for the 1D chain model at -0.85 V was shown in Figure 3.12b. Also, the percentage of change in the current for the 1D chain model at 1.3 V was discussed in Section 3.1.2. At 1.3 V, the 1D chain of carbon atoms was 238% less sensitive to base A than the chain with the two graphene nanoribbons. Also, it was 44% and 100% smaller in its ability to detect bases C and T, respectively. For base G, the 1D chain was 143% less sensitive to the presence of base G. At -0.85 V, the single chain of carbon atoms showed very high sensivity to the presence of base G, which could also be seen in Figure 3.7 and Figure 3.12. Particularly, the 1D chain was 401% more sensitive to the presence of base G than the chain attached to the graphene nanoribbons. Also, the sensitivity of the 1D chain was 37% higher to the presence of base A than the chain attached to the graphene nanoribbons at -0.85 V, which is significant. Also, its sensivity was less by 11% in the presence of base C and 134% in the presence of base T than the chain attached to the graphene nanoribbons.

In brief, the single chain of carbon atoms showed higher sensivity to the presence of different ssDNA bases compared with the chain attached to two graphene nanoribbons at -0.85 V. However, it is less sensitive at 1.3 V compared with the chain attached to the graphene. These two structures of one-dimensional carbon chain were indeed very sensitive to each base of

ssDNA. The atomic width of these chains could result in as high sensitivity as 401% with the presence of base G at -0.85V and as low as 143% at 1.3V. Such differences in sensitivity are a valuable tool in DNA sequencing devices that can implement carbyne as a sensing element. These simulation results collectively demonstrate the effectiveness of 1D carbon chains as nanowire sensors for ultra-sensitive electrical based measurements of individual DNA molecules.

### **3.1.7. Graphene and Carbyne**

As discussed earlier, the truly 1D feature of carbyne and its high sensitivity to any chemical and geometrical changes have placed carbyne as a fascinating material for numerous sensing devices at the nanometer scale including bio sensors. One of the main goals of the research for this dissertation was to propose a reliable and robust sensing element that maintains single molecule resolution. Thus, comparison of carbyne with graphene as a sensing element for different ssDNA bases is provided in this section.

First, the electrical properties for the model systems that have carbyne chain with the absence and presence of base A are compared with the electrical properties for the model systems that have graphene with the absence and presence of base A. More specifically, two graphene models are considered in this dissertation: graphene of width 7.1 Å represented by graphene 1 and graphene of width 9.3 Å represented by graphene 2. The main goal of choosing two different widths is to demonstrate the effect of the width of the sensing element in DNA sequencer on the detection mechanism. The graphene nanoribbons are zigzag-edged. For the sake of consistency and better evaluation, the simulation parameters and techniques for the model systems that have the single carbon chain were kept the same for all the model systems.

The single chain of carbon atom has 16 carbon atoms with alternating single and triple bonds as discussed in previous sections. When inserting base A, it was located at the same location with respect to the chain and the two graphene nanoribbons models. In fact, the carbyne/A model that was used in this part was the same as the chain/A model where the base was located at location (c) in Figure 3.31. The base was placed about 2 Å above the carbyne chain and the two graphene models. Table 3.4 shows the number of atoms and the size of the simulation cells for the model systems of carbyne and graphene.

Table 3.4. The simulation parameters for model systems of carbyne and graphene.

System	Number of atoms	Size of the simulation cell (Å)
Carbyne	16	22.6×25.0×25.0
Carbyne/A	48	22.6×25.0×25.0
Graphene 1	70	22.6×25.0×25.0
Graphene 1/A	102	22.5×25.0×25.0
Graphene 2	94	23.8×25.0×25.0
Graphene 2/A	126	23.6×25.0×25.0

The carbon atoms at both ends of graphene were fixed when placing the base by applying constraints on their locations. The hydrogen atoms were attached to the carbon atoms on both sides to overcome any issue might occur due to the dangling bonds. Figure 3.52 shows schematics of these model systems of graphene nanoribbons with two different widths. Hydrogen atoms are attached to the graphene nanoribbons as can be seen in the figure. The geometrical optimizations were performed using the Broyden–Fletcher–Goldfarb–Shanno (BFGS) algorithm until the forces were lower than 0.0045 eV/Å. The electrical current for the



graphene nanoribbon models was higher than the one-dimensional carbon chain's current. The DOS and the transmission functions are displayed in Figures 3.53 and 3.54. Figure 3.55 shows I-V curves for the three simulated models compared at positive and negative biasing voltages. The electrical current for the model system that has a carbon chain in vacuum is the lowest compared with the graphene models at the positive voltage within the range  $\sim 0.2$ - $1.1$  V. Having a thickness (width) of a single molecule makes the resistance of the single carbon chain the highest.

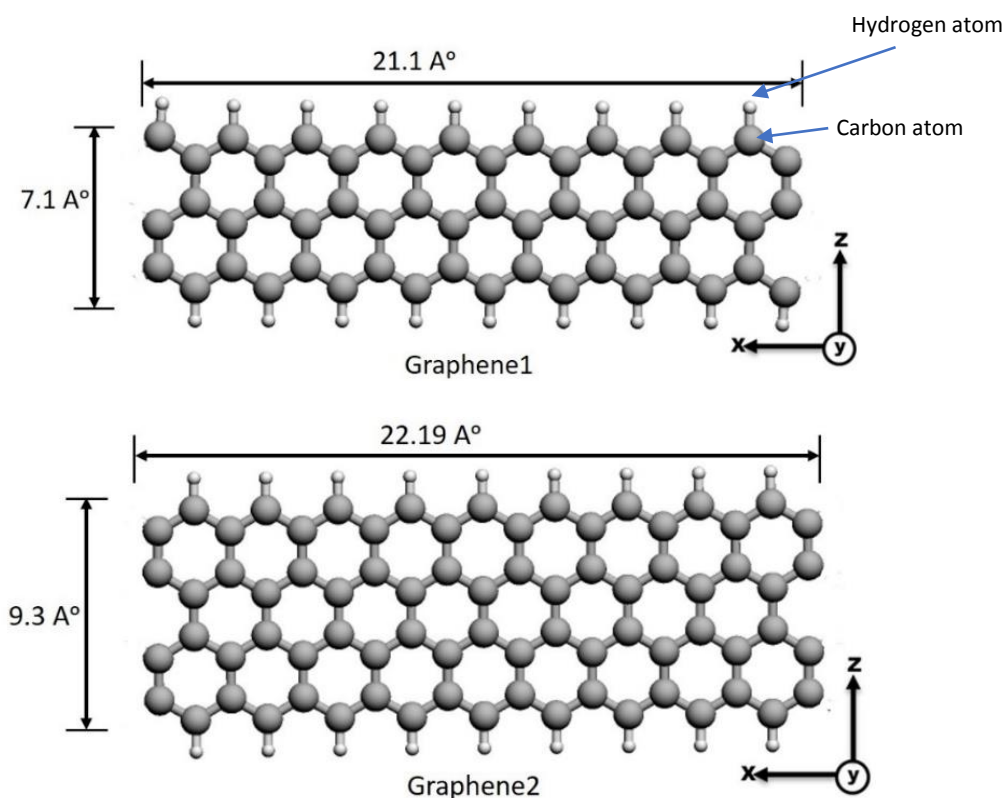


Figure 3.52. Schematics for the top view of the simulated models of graphene with two different widths. Gray spheres are the carbon atoms and the white spheres are the hydrogen atoms.

However, the electrical current of the carbyne chain model is higher than the current for the graphene of  $7.1 \text{ \AA}$  width and lower than the current for the graphene of  $9.3 \text{ \AA}$  width in the negative voltage region. Moreover, graphene of width  $7.1 \text{ \AA}$  had the highest in current compared

with the single carbon chain and the graphene nanoribbon of width 9.3 Å at the positive voltage although there was an overlap in the current for graphene models with width 7.1 Å and 9.3 Å.

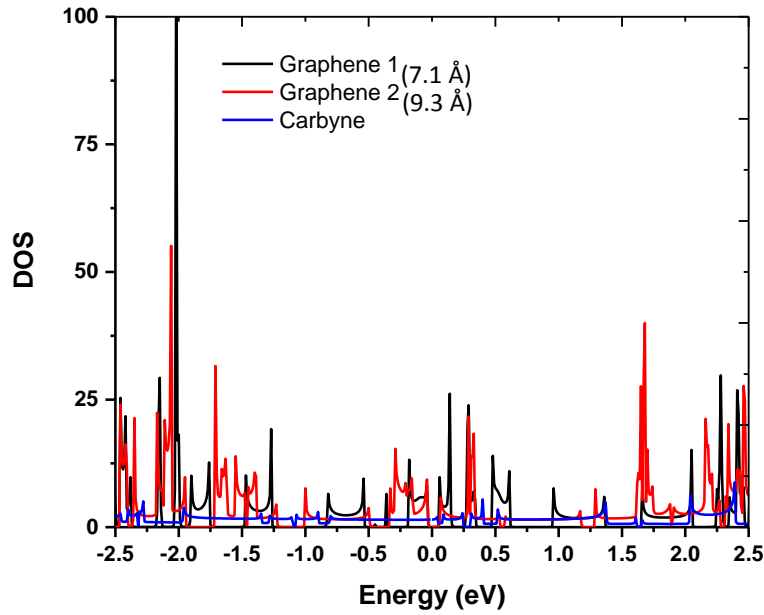


Figure 3.53. DOS for the two models of graphene compared with the single chain of carbon.

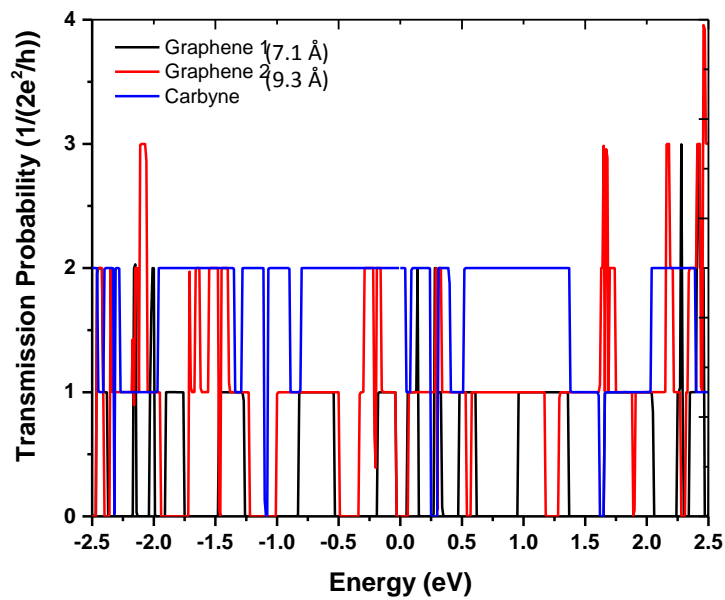


Figure 3.54. Transmission probability functions for the two models of graphene compared with the control model.

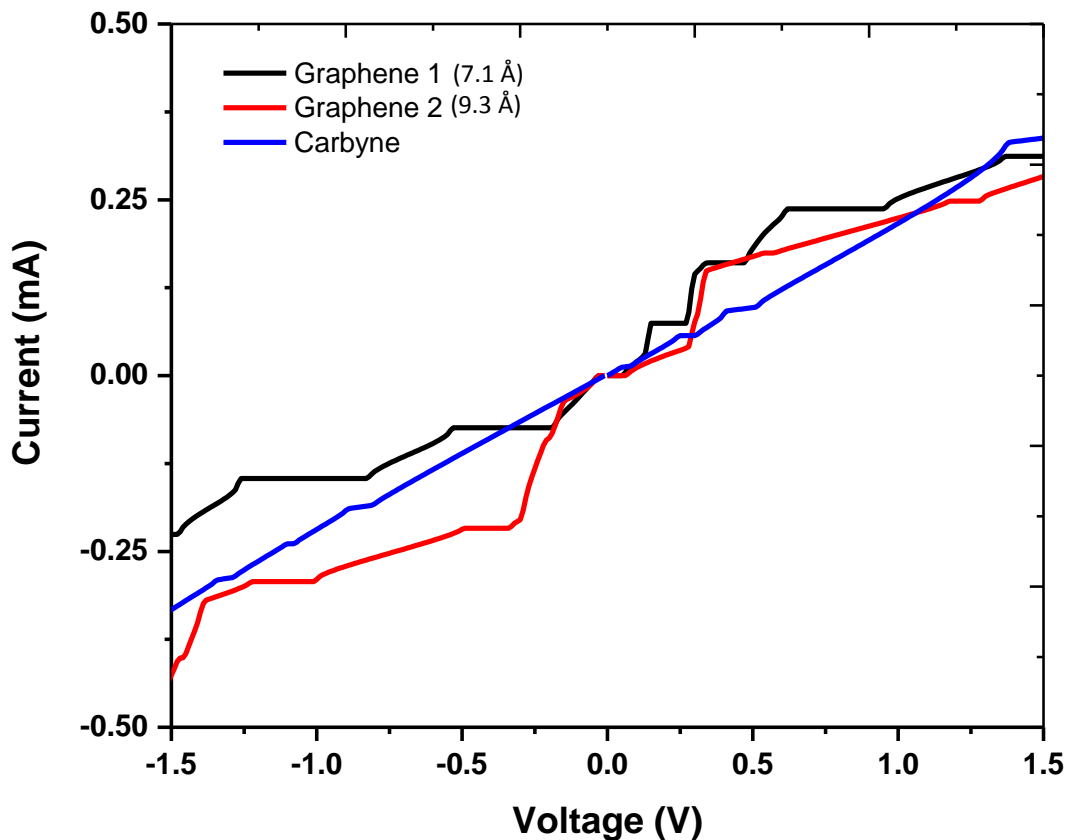


Figure 3.55. I-V characteristics of the graphene models compared with the carbon chain model in the absence of base A at positive and negative voltages.

This result agrees with the results reported by Reference 58, which concluded that the 1D carbon chain shows lower current compared with the nanotubes and graphene nanoribbons. The suspicious part of the I-V curves for the three model systems was at the positive voltage higher than 1.1 V. At 1.1 V, the electrical current of the model that had the carbyne chain increased and dominated at voltages of 1.25 V. This behavior can be seen in Figure 3.55. At the negative voltages, the electrical current for the model system that had the graphene nanoribbon of 9.3 Å width was the highest compared with the model that had the carbyne chain and the model that had the graphene nanoribbon of 7.1 Å width. Graphene is a gapless semiconductor whose

properties are dependent on its structure. For example, zigzag-edged graphene has been reported to be a metallic, while armchair-edged is reported to exhibit semiconducting properties [8].

In order to emphasize the advantages of using a truly one-dimensional carbon chain over graphene as a sensing element in DNA sequencing devices, base A was placed normal to the single carbon chain and graphene models. The electrical current was calculated along the x direction, whereas, base A was oriented along the z direction. Base A was inserted perpendicular at the center of the carbyne chain and graphene model systems. The base model that was used included the base, the phosphate group, and the sugar group.

Figure 3.56 shows a schematic of the model that has a graphene nanoribbon of width 9.3 Å with base A placed normal to it. The other two models had base A placed similarly at the center of them. Next, the electrical properties of carbyne and graphene models with the presence of base A were calculated. Figure 3.57 shows the DOS and Figure 3.58 represents the transmission probability functions for carbon chain and graphene nanoribbon model systems when placing base A normal to them.

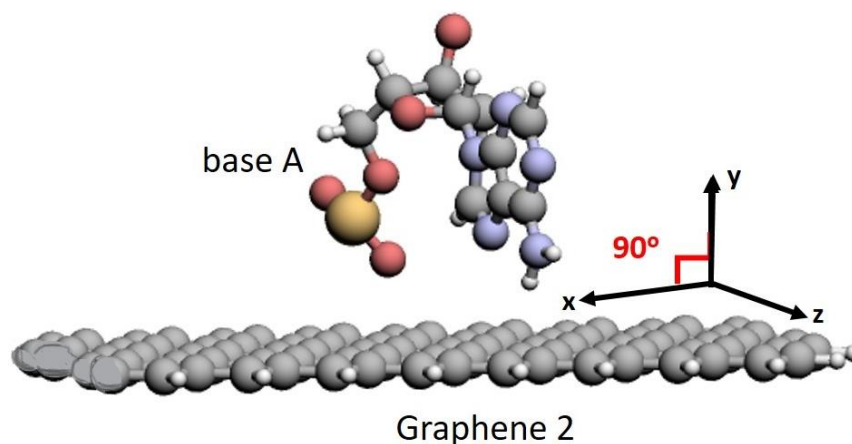


Figure 3.56. Schematic of the model with base A placed normal to the graphene nanoribbon with width 9.3 Å.

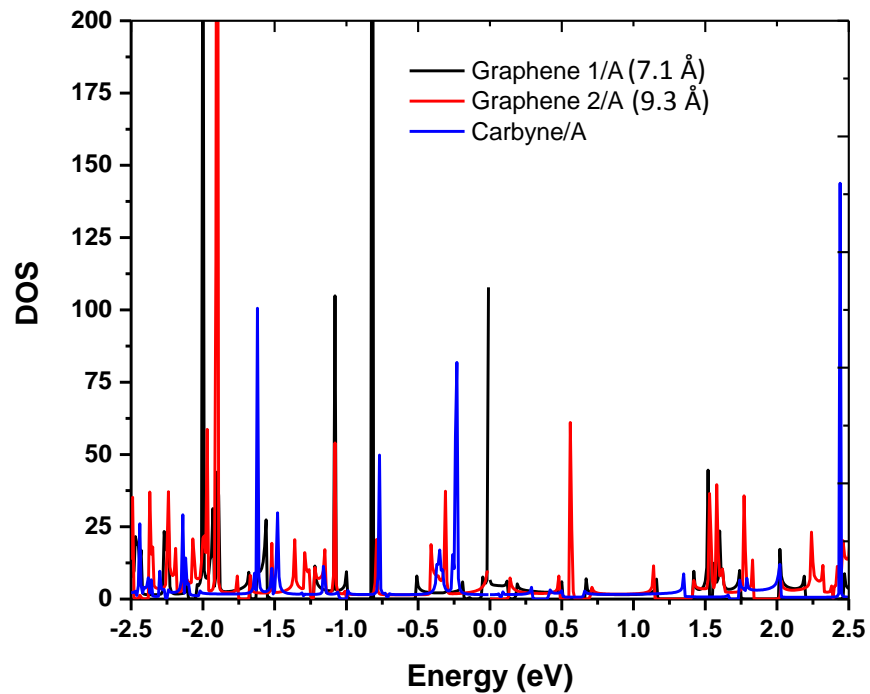


Figure 3.57. DOS for the two models of graphene compared with the control model in the presence of base A.

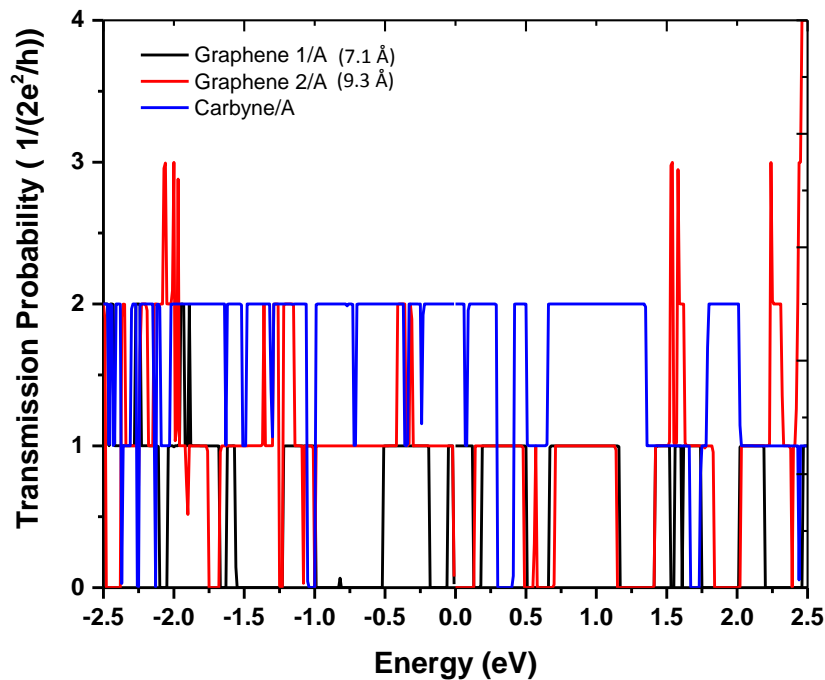


Figure 3.58. Transmission probability functions for the two models of graphene nanoribbons compared with the control model in the presence of base A.

Figure 3.59 shows the electrical current for the different simulated models at positive and negative biasing voltages. It is obvious from Figures 3.57 and 3.58 that the presence of base A caused changes in the DOS and transmission probability functions. In Figure 3.59, the electrical

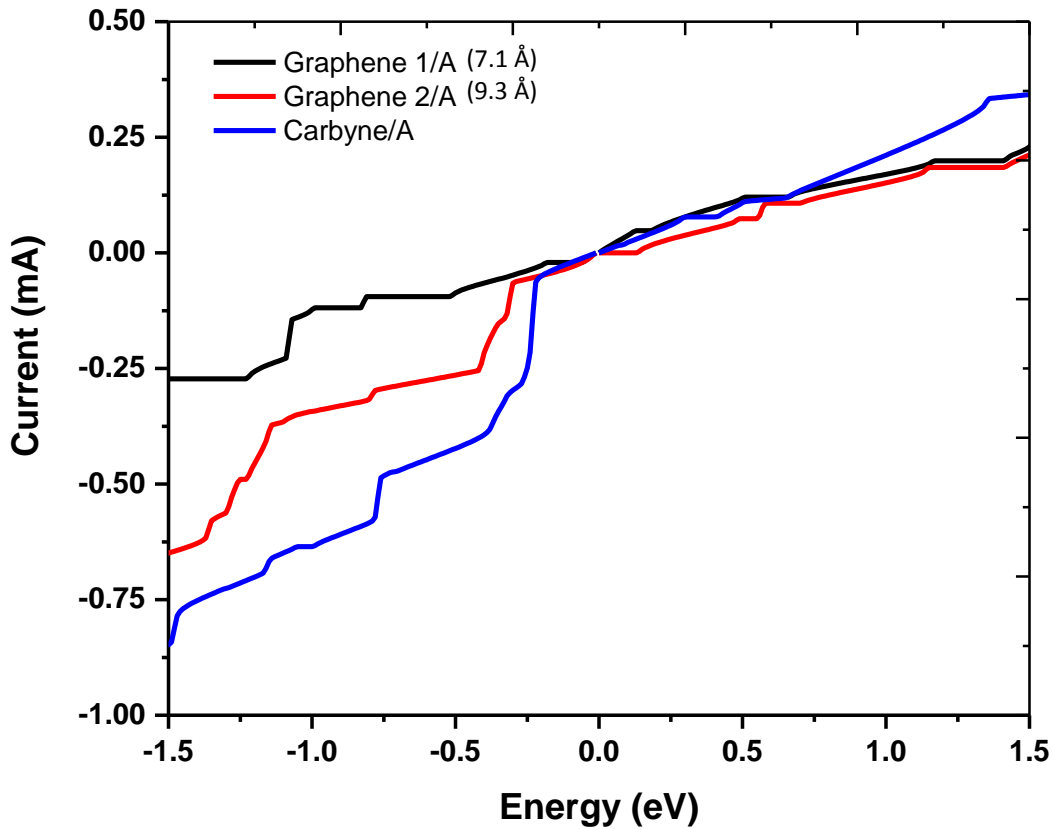


Figure 3.59. I-V characteristics of the graphene models of thickness 7.1 Å and 9.3 Å compared with the carbon chain model at the presence of base A.

current decreases in the presence of base A for the graphene models at positive biasing voltages. The decrease in the electrical current in graphene nanoribbons when base A is present has been reported by [56]. Compared with the case of a single chain of carbon atoms, the simulated model presented in this section is equivalent to the model of the single base where base A was located at location c in Figure 3.31. In fact, this result indicates that the technique that was adopted in

this dissertation yields good agreement with the work by Song et al. [56]. In the research of this dissertation the electrical current increased for all the simulated models at the negative biasing voltages with the presence of base A. Furthermore, the electrical current for the model system that had the single chain of carbyne with base A showed the highest current at the negative voltages. On the other hand, the model system that has the graphene nanoribbon of 7.1 Å width showed lower current compared with the model that had graphene nanoribbon of 9.3 Å. The voltage in this study is in unit of volts and the energy is in units of eV.

Although the current for all the simulated models that include the single carbon chain and graphene show differences with the presence of base A, these I-V curves do not provide enough insight of the efficiency of carbyne compared with graphene. Therefore, two ways of identifying the differences were used. The first method was choosing one biasing voltage to compare the percentage of decrease in the electrical current, and the second method was to plot the relative current.

Figure 3.60a shows the current values and Figure 3.60b shows the percentage of the increase in the presence of base A at -0.6 V. At -0.6 V, the presence of base A caused the electrical current to increase for all simulated models. This increase in current was the most for the single carbon chain and the least for graphene of width 7.1 Å as can be seen in Figure 3.60b. Thus, the presence of base A led to a significant increase in the single carbon chain current at -0.6 V. In general, the size and curvature of the sensing element plays a central role in non-covalent interactions. The presence of the nucleobases results in redistribution of DOS and transmission probability functions. The redistribution of the charge density and the change in the electrical properties of graphene and carbon chain are mainly caused by the interactions between graphene or single chain with ssDNA bases. Consequently, the non-covalent interactions are

demonstrated by nucleobases adsorption to the graphene or the single chain surface resulting in a detectable perturbation in the electrical properties. The decrease in the electrical current with the existence of DNA nucleotides was reported in graphene nanodevices used in sequencing [8].

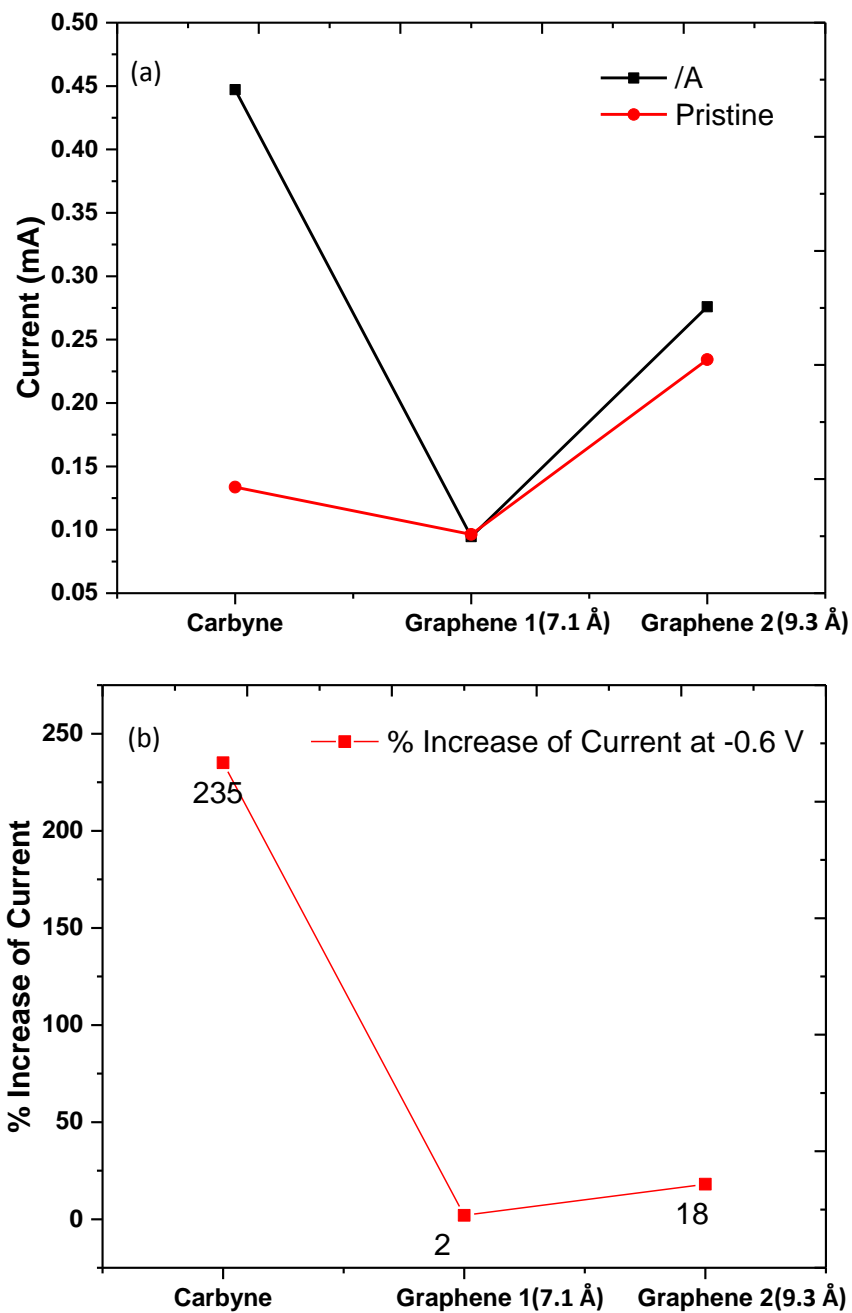


Figure 3.60. (a) Current for the models with graphene 1, graphene 2, and carbyne (b) The percentage of the increase in current in the presence of base A compared at -0.6 V.



The group of researchers investigated graphene nanoribbon sensitivity to different ssDNA bases. According to their results, graphene nanoribbons show an indistinct scheme of detecting base A at the positive voltage. However, the work in this study shows that the single carbon chain is remarkably sensitive to the presence of base A and its current increased by 0.31359 mA at -0.6 V. This increase in current is equivalent to 235% increase in the current as shown in Figure 3.60b. Compared with graphene of 9.3 Å width and 7.1 Å width, the electrical current increased by 0.04158 mA and 0.00189 mA for the two different widths of graphene nanoribbons, respectively. This indicates that the percentage of the increase in the electrical current is 2% and 18% for graphene of 9.3 Å width and 7.1 Å width, respectively. Hence, the small width of single carbon chain shows significant increase in the electrical current of the chain at -0.6 V, which proves that the 1D chain is sensitive to the presence of ssDNA bases. The second way of recognizing the differences between graphene and carbon chain as sensing elements is by considering the differences between the single chain and graphene current. The approach used was to subtract the single chain current, which is considered as the control model, from graphene current and then divide by the maximum difference between them.

Figure 3.61 represents the relative current for the two models of graphene with respect to the control model which was the carbon chain with the presence of base A. The plot can be divided into three main regions based on the range of the biasing voltages. The first region is within the range from 0.2 V to 1.5 V. The second region is from -0.2 V to 0.2 V, and the third is from -1.5 V to -0.2 V. Clearly the second region shows similarity in graphene nanoribbon current for the two different widths. It also reflects that the difference between the single carbon chain and graphene current within this range is very small compared with the maximum difference, which can also be seen in Figure 3.61. The small graphene current at voltages below 0.2 V with

base A present is similar to the behavior of graphene nanoribbon current reported in Reference 56. According to that study, the trend of graphene nanoribbon current with the presence of ssDNA bases does not show differences below 0.3 V and starts to demonstrate clear differences above 0.3 V. That is in good agreement with the results obtained in this study shown in Figure 3.60 and Figure 3.61.

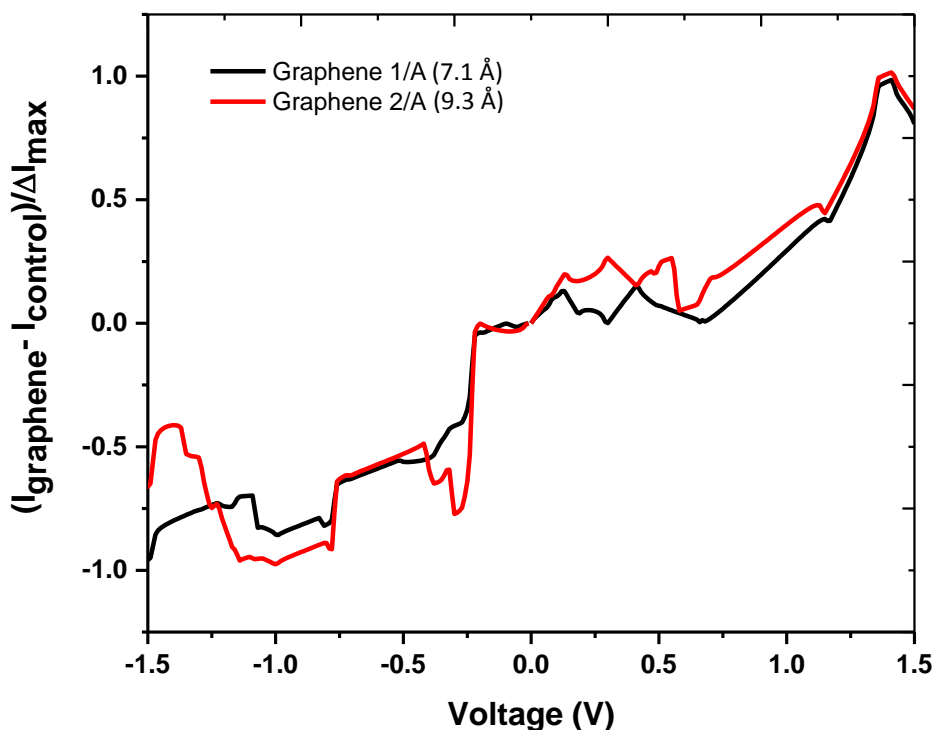


Figure 3.61. Normalized graphene current with respect to the single chain control model current.

In Figure 3.61, the positive biasing voltage region 0.15 – 1.1 V indicates that the electrical current for the two different models of graphene nanoribbons differs and yields a distinct scheme. In contrast, the relative electrical current of the graphene nanoribbon of 9.3 Å width was the same as the relative current of the graphene nanoribbon of 7.1 Å. The relative current at the negative biasing voltage fluctuated due to the maximum difference between the

control model current and the graphene nanoribbon model current being different. As discussed earlier, the electrical current of graphene with the smaller width was lower than the graphene nanoribbon with the larger width as can be seen in Figure 3.59 at the negative voltage.

Particularly, it is suspected that the change in current for the simulated models was caused by the adsorption of the base onto graphene or carbon chain surfaces as mentioned earlier. As an illustration, the presence of base A caused a modulation in the electrical properties of the single carbon chain. These modulations result in more significant electrical effects on the chain than on the graphene nanoribbons.

Comparing the 1D carbon chain with the other carbon-based materials as discussed in Chapter One emphasizes the significant differences and highly preferable properties of carbyne. Although several studies have focused on exploring its mechanical and electrical properties, there have been no reported investigations regarding the interactions between carbyne and biomolecules, such as ssDNA. Hence, having a sensing element with truly single atom thickness that shows an idealistic conductor behavior is certainly an advantage for ultimate nanodevices for DNA sequencing.

## CHAPTER FOUR: CONCLUSION

The electrical properties associated with the interaction between 1D carbon chain, carbyne, and ssDNA were numerically investigated in two cases 1) in the absence of ssDNA 2) in the presence of ssDNA. The differences between the two cases were analyzed to determine the effects of these different bases onto the carbyne. The differences in the electrical properties of the carbon chain indicated that there were interactions between the carbon chain and different ssDNA. Such interactions influenced electrical modulations in the chain and led to different responses for different ssDNA bases.

The numerical simulation approach conducted were based on the first principle simulation. In first principle simulation, the electrical properties were investigated in this study. These properties included DOS and the transmission probability functions, and they were integrated to obtain the electrical current. All simulated model systems investigated using first principle approach were in vacuum, meaning no water or solvents were included.

The total number of simulated models was 25. The control models or first models were composed of a single chain of carbyne with two different structures using *NanoEngineer1* software. The first model had a chain of 16 carbon atoms along the x direction and the second model had a chain of 16 carbon atoms attached to two graphene nanoribbons along the x direction. Visualizing and measuring the distances between atoms were accomplished by using *vesta* software. The density of states and transport probabilities for the control models were calculated using QUANTUM ESPRESSO and wannier90 codes.

The density of states and transport probability functions were used to calculate the electrical current for these models. The next 8 models included these carbon chains with one base

of ssDNA placed at about  $2.0 \text{ \AA}$  below the chain with  $90^\circ$  orientations of the bases with respect to the chain. The density of states and transport probability functions as well as the electrical current with the presence of these bases were calculated and the differences between the presence and absence of ssDNA were analyzed. Clear distinctions among the different bases were obtained. At  $0.6 \text{ V}$ , base A was found to increase the current by  $3.3 \text{ \mu A}$ . The other bases caused a decrease in current by  $41.1 \text{ \mu A}$ ,  $14.7 \text{ \mu A}$ , and  $25.6 \text{ \mu A}$  for bases C, T, and G, respectively. This result contradicted the reported study for graphene nanoribbons based DNA sequencing device [56]. The orientations of the different bases in this dissertation were different from the orientations of the bases in the reported study.

Another two models included one of the chains, which is the single chain, and base A with different orientations. Differences in the electrical properties were found when base A was placed at  $0^\circ$ ,  $45^\circ$ , and  $90^\circ$  with respect to the chain. Thus, different ssDNA bases were placed parallel to the chain and the differences in the chain's electrical properties were calculated. 1D carbon chains were found to be sensitive to the different orientations of the bases. The differences in the electrical properties at different orientations were suggested to be due to the interactions between the base and the carbon chain. The interaction was mainly  $\pi$ - $\pi$  interaction. The orientations of ssDNA were of great interest for this study. Models where the bases were placed parallel to the carbon chain were also investigated. Base A caused a decrease in the chain current, while base G caused an increase in the chain current at  $0.6 \text{ V}$  for parallel orientation. The result compared well with the graphene nanoribbon device.

To investigate the effects of different chemical groups of these bases in the total interaction, bases A and C were placed at 5 different locations at which the bases were moved by about  $1.0$  to  $2.0 \text{ \AA}$  along the  $z$  direction for every location. A force model to estimate the strengths of the

interactions between these groups and the chain was developed and compared with the current trend. The force trend matched well with the current trends when compared at -0.85 V. There is no reported literature for comparison.

The second structure of carbon chain was examined in terms of its sensitivity to the presence of ssDNA bases. The result showed approximately 265% increase in current for base A model at 1.3 V. The presence of base T caused the current to increase by about 111%. Base C showed 55.3% increase in current, while base G resulted in about 158% increase in current at 1.3 V. There was no reported studies to compare with these results.

Finally, carbyne is expected to be more sensitive to the presence of DNA bases. Thus, the electrical current of the carbyne model was compared with the electrical current of the graphene nanoribbons that had widths of 7.1 Å and 9.3 Å. It was found that carbyne current was mostly linear compared with graphene nanoribbons and its sensitivity to the presence of base A was higher at -0.6 V.

Overall, the approach of calculating the carbyne electrical current with the presence of DNA bases may be idealistic for several reasons. First, water molecules or any solvents were not considered in this study. Second, ignoring the effects of electron scattering and van der Waals interactions in the first principle simulation part of this study can lead to underestimation of DOS, transmission probability functions, energy gaps, etc. Also, actual devices that include carbyne as a sensing element will have a substrate which can affect the electronic properties associated with the interaction between carbyne and DNA bases.

Furthermore, the carbyne current represents the current caused by the transport of electrons. Since the electrons are faster than ions due to having less mass-to-charge ratio and long

scattering lengths, it is anticipated that electrical current is higher than the ionic current obtained in nanopore based DNA sequencer.

Even though the adopted method may underestimate the interactions between carbyne chains and DNA bases, the results suggest the possibility of using a 1D carbon chain as a sensing element. The small width of the carbyne chain enables stronger interactions with the DNA bases because the atomic thickness of the 1D carbon chain is about the same distance between the sequential DNA bases. This property of the 1D carbon chain enhances its sensitivity to differentiate DNA bases. Success of the current study is expected to lead to the development of new electrical measurement based bio-sensing devices for a variety of biomedical applications including DNA sequencing. More importantly, this work contributes to the knowledge of the third-generation DNA sequencing technique and enable further progress toward ultrafast, low cost, label-free, and high-resolution DNA sequencing devices.

## **CHAPTER FIVE: FUTURE WORK**

Based on the results obtained from this study, future research can be directed into two numerical approaches and experimental work.

### **5.1. First Principle Simulation**

- Single chain of carbon atoms and ssDNA: Bases G and T at different locations can be tested similar to bases A and C.
- Single chain of carbon atoms attached to two graphene nanoribbons and ssDNA: Different orientations and locations of the bases with respect to the chain would be beneficial to be tested and compared with the results obtained for a single chain and ssDNA bases.

### **5.2. Molecular Dynamic (MD) Simulation**

- Single chain of carbon atoms and ssDNA: Connecting bases A, C, G, and T at different locations and locations from the chain would be useful for experimental research.
- Single chain of carbon atoms attached to two graphene nanoribbons and ssDNA: Connecting bases A, C, G, and T at different locations and locations from the chain could be very valuable for experimental investigation.

### **5.3. Experimental**

Experimental study of the model systems tested in this dissertation would serve as a guide for potential applications.



## REFERENCES

- [1] V. Pokropivny, I. Hussainova, and S. Vlassov, "Introduction to nanomaterials and nanotechnology," *Introd. Nanomater. Nanotechnol.*, pp. 1–138, 2007.
- [2] R. Chau, S. Datta, M. Doczy, B. Doyle, B. Jin, J. Kavalieros, A. Majumdar, M. Metz, and M. Radosavljevic, "Benchmarking nanotechnology for high-performance and low-power logic transistor applications," *IEEE Trans. Nanotechnol.*, vol. 4, no. 2, pp. 153–158, 2005.
- [3] R. Martel, T. Schmidt, H. R. Shea, T. Hertel, and P. Avouris, "Single- and multi-wall carbon nanotube field-effect transistors," *Appl. Phys. Lett.*, vol. 73, no. 17, pp. 2447–2449, 1998.
- [4] N. G. Portney and M. Ozkan, "Nano-oncology: Drug delivery, imaging, and sensing," *Anal. Bioanal. Chem.*, vol. 384, no. 3, pp. 620–630, 2006.
- [5] R. H. Scheicher, A. Grigoriev, and R. Ahuja, "DNA sequencing with nanopores from an ab initio perspective," *J. Mater. Sci.*, vol. 47, no. 21, pp. 7439–7446, 2012.
- [6] J. C. T. Eijkel and A. van den Berg, "Nanofluidics: What is it and what can we expect from it?," *Microfluid. Nanofluidics*, vol. 1, no. 3, pp. 249–267, 2005.
- [7] Y. Yang, R. Liu, H. Xie, Y. Hui, R. Jiao, Y. Gong, and Y. Zhang, "Advances in Nanopore Sequencing Technology," *J. Nanosci. Nanotechnol.*, vol. 13, no. 7, pp. 4521–4538, 2013.
- [8] S. J. Heerema and C. Dekker, "Graphene nanodevices for {DNA} sequencing," *Nat. Nanotechnol.*, vol. 11, no. 2, pp. 127–136, 2016.
- [9] NHGRI, "DNA Sequencing Costs\_ Data - National Human Genome Research Institute (NHGRI)," 2015. [Online]. Available: <https://www.genome.gov/sequencingcostsdata/>. [Accessed: 30-May-2015].
- [10] L. Liu, Y. Li, S. Li, N. Hu, Y. He, R. Pong, D. Lin, L. Lu, and M. Law, "Comparison of next-generation sequencing systems," *J. Biomed. Biotechnol.*, vol. 2012, 2012.
- [11] "Polymerase Chain Reaction (PCR)." [Online]. Available: <https://www.ncbi.nlm.nih.gov/probe/docs/techpcr/>. [Accessed: 08-May-2017].

- [12] M. Gužvić, “The History of DNA Sequencing,” *J. Med. Biochem.*, vol. 32, no. 4, pp. 301–312, 2013.
- [13] M. Di Ventura and M. Taniguchi, “Decoding {DNA}, {RNA} and peptides with quantum tunnelling,” *Nat. Nanotechnol.*, vol. 11, no. 2, pp. 117–126, 2016.
- [14] J. Lagerqvist, M. Zwolak, and M. Di Ventura, “Fast {DNA} squencing via transverse electronic transport,” vol. 6, no. 4, pp. 779–782, 2006.
- [15] D. R. Duckett, A. I. H. Murchie, R. M. Clegg, G. S. Bassi, M. J. E. Giraudpanis, and D. M. J. Lilley, “Nucleic Acid Structure and Recognition,” *Biophys. Chem.*, vol. 68, no. 1–3, pp. 53–62, 1997.
- [16] D. Fologea, J. Uplinger, B. Thomas, and D. S. Mcnabb, “Slowing DNA Translocation in a Solid-State Nanopore,” *Nano Lett.*, vol. 5, no. 9, pp. 20–23, 2005.
- [17] A. J. Storm, J. H. Chen, H. W. Zandbergen, and C. Dekker, “Translocation of double-strand DNA through a silicon oxide nanopore,” *Phys. Rev. E - Stat. Nonlinear, Soft Matter Phys.*, vol. 71, no. 5, pp. 1–10, 2005.
- [18] S. K. Min, W. Y. Kim, Y. Cho, and K. S. Kim, “Fast DNA sequencing with a graphene-based nanochannel device,” *Nat. Nanotechnol.*, vol. 6, no. 3, pp. 162–165, 2011.
- [19] M. Zwolak and M. Di Ventura, “Electronic signature of DNA nucleotides via transverse transport,” *Nano Lett.*, vol. 5, no. 3, pp. 421–424, 2005.
- [20] M. Tsutsui, Y. He, M. Furuhashi, S. Rahong, M. Taniguchi, and T. Kawai, “Transverse electric field dragging of DNA in a nanochannel,” *Sci. Rep.*, vol. 2, p. 394, 2012.
- [21] D. R. Tobergte and S. Curtis, “Design and Fabrication of Nanofluidic Systems with Integrated Sensing Electrodes for Rapid Biomolecule Characterization,” *J. Chem. Inf. Model.*, vol. 53, no. 9, pp. 1689–1699, 2013.
- [22] C. Hyun, H. Kaur, R. Rollings, M. Xiao, and J. Li, “Threading immobilized DNA molecules through a solid-state nanopore at >100  $\mu$ s per base rate,” *ACS Nano*, vol. 7, no. 7, pp. 5892–5900, 2013.
- [23] D. Deamer, M. Akeson, and D. Branton, “Three decades of nanopore sequencing,” *Nat.*

- Biotechnol.*, vol. 34, no. 5, pp. 518–524, 2016.
- [24] Y. Feng, Y. Zhang, C. Ying, D. Wang, and C. Du, “Nanopore-based fourth-generation DNA sequencing technology,” *Genomics, Proteomics and Bioinformatics*, vol. 13, no. 1, pp. 4–16, 2015.
- [25] M. Zheng, A. Jagota, E. D. Semke, B. A. Diner, R. S. McLean, S. R. Lustig, R. E. Richardson, and N. G. Tassi, “DNA-assisted dispersion and separation of carbon nanotubes,” *Nat. Mater.*, vol. 2, no. 5, pp. 338–342, 2003.
- [26] H. Rokadia, S. Tung, and D. Spearot, “Experimental characterization of DNA/CNT hybrid structures with atomic force microscope,” in *2008 8th IEEE Conference on Nanotechnology*, 2008, pp. 255–258.
- [27] J. Wang, Y. Hernandez, M. Lotya, J. N. Coleman, and W. J. Blau, “Broadband nonlinear optical response of graphene dispersions,” *Adv. Mater.*, vol. 21, no. 23, pp. 2430–2435, 2009.
- [28] Y. Cho, S. K. Min, J. Yun, W. Y. Kim, A. Tkatchenko, and K. S. Kim, “Noncovalent Interactions of DNA Bases with Naphthalene and Graphene,” *J. Chem. Theory Comput.*, vol. 9, no. 4, pp. 2090–2096, 2013.
- [29] N. Varghese, U. Mogera, A. Govindaraj, A. Das, P. K. Maiti, A. K. Sood, and C. N. R. Rao, “Binding of DNA nucleobases and nucleosides with graphene,” *ChemPhysChem*, vol. 10, no. 1, pp. 206–210, 2009.
- [30] Y. Cho, S. K. Min, W. Y. Kim, and K. S. Kim, “The origin of dips for the graphene-based DNA sequencing device,” *Phys. Chem. Chem. Phys.*, vol. 13, no. 32, pp. 14293–6, 2011.
- [31] E. Paulechka, T. A. Wassenaar, K. Kroenlein, A. Kazakov, and A. Smolyanitsky, “Nucleobase-functionalized graphene nanoribbons for accurate high-speed DNA sequencing,” *Nanoscale*, vol. 8, no. 4, pp. 1861–1867, 2016.
- [32] W. Qin, L.-N. Wu, X.-Y. Zhang, C.-Q. Dong, Y.-P. Yang, X. Li, and J.-Y. Qi, “Nature of DNA-graphene Interaction System: An Theoretic Account,” *J. harbin Inst. Technol.*, vol. 20, no. 6, pp. 123–128, 2013.

- [33] J. W. Kim, J. H. Kim, and R. Deaton, "DNA-linked nanoparticle building blocks for programmable matter," *Angew. Chemie - Int. Ed.*, vol. 50, no. 39, pp. 9185–9190, 2011.
- [34] E. Winfree, F. Liu, L. A. Wenzler, and N. C. Seeman, "Design and self-assembly of two-dimensional DNA crystals," *Nat.*, vol. 394, pp. 539–544, 1998.
- [35] M. R. Jones, R. J. Macfarlane, B. Lee, J. Zhang, K. L. Young, A. J. Senesi, and C. a Mirkin, "DNA-nanoparticle superlattices formed from anisotropic building blocks.," *Nat. Mater.*, vol. 9, no. 11, pp. 913–917, 2010.
- [36] O. Cretu, A. R. Botello-Mendez, I. Janowska, C. Pham-Huu, J. C. Charlier, and F. Banhart, "Electrical transport measured in atomic carbon chains," *Nano Lett.*, vol. 13, no. 8, pp. 3487–3493, 2013.
- [37] M. Liu, V. I. Artyukhov, H. Lee, F. Xu, and B. I. Yakobson, "Carbyne from first principles: Chain of c atoms, a nanorod or a nanorope," *ACS Nano*, vol. 7, no. 11, pp. 10075–10082, 2013.
- [38] L. Shi, P. Rohringer, K. Suenaga, Y. Niimi, J. Kotakoski, J. C. Meyer, H. Peterlik, M. Wanko, S. Cahangirov, A. Rubio, Z. J. Lapin, L. Novotny, P. Ayala, and T. Pichler, "Confined linear carbon chains as a route to bulk carbyne," *Nat. Mater.*, vol. 15, no. 6, 2016.
- [39] C. Dekker, "Carbon Nanotubes as Molecular Quantum Wires," *Technology*, vol. 52, no. 5, pp. 22–28, 1999.
- [40] V. I. Artyukhov, M. Liu, and B. I. Yakobson, "Mechanically Induced Metal – Insulator Transition in Carbyne," *Nano Lett.*, vol. 14, no. 8, pp. 4224–4229, 2014.
- [41] K. Liu, J. Feng, A. Kis, and A. Radenovic, "Atomically thin molybdenum disulfide nanopores with high sensitivity for dna translocation," *ACS Nano*, vol. 8, no. 3, pp. 2504–2511, 2014.
- [42] D. Umadevi and G. N. Sastry, "Quantum mechanical study of physisorption of nucleobases on carbon materials: Graphene versus carbon nanotubes," *J. Phys. Chem. Lett.*, vol. 2, no. 13, pp. 1572–1576, 2011.

- [43] T. Nelson, B. Zhang, and O. V. Prezhdo, “Detection of nucleic acids with graphene nanopores: Ab initio characterization of a novel sequencing device,” *Nano Lett.*, vol. 10, no. 9, pp. 3237–3242, 2010.
- [44] Y. He, R. H. Scheicher, A. Grigoriev, R. Ahuja, S. Long, Z. Ji, Z. Yu, and M. Liu, “Fast DNA sequencing via transverse differential conductance,” *Int. Conf. Simul. Semicond. Process. Devices, SISPAD*, pp. 313–316, 2010.
- [45] F. Schedin, A. Geim, S. Morozov, E. Hill, P. Blake, M. Katsnelson, and K. Novoselov, “Detection of individual gas molecules adsorbed on graphene,” *Nat. Mater.*, vol. 6, no. 9, pp. 652–655, 2007.
- [46] A. K. Geim and K. S. Novoselov, “The rise of graphene,” *Nat. Mater.*, vol. 6, no. 3, pp. 183–191, 2007.
- [47] A. a Balandin, S. Ghosh, W. Bao, I. Calizo, D. Teweldebrhan, F. Miao, and C. N. Lau, “Superior Thermal Conductivity of Single-Layer Graphene 2008,” *Nano Lett.*, vol. 8, pp. 902–907, 2008.
- [48] C. Lee, X. Wei, J. W. Kysar, and J. Hone, “Measurement of the Elastic Properties and Intrinsic Strength of Monolayer Graphene,” *Science (80-. )*, vol. 321, no. 5887, pp. 385–388, 2008.
- [49] V. M. Pereira, A. H. Castro Neto, and N. M. R. Peres, “Tight-binding approach to uniaxial strain in graphene,” *Phys. Rev. B - Condens. Matter Mater. Phys.*, vol. 80, no. 4, pp. 1–9, 2009.
- [50] R. R. Nair, P. Blake, a. N. Grigorenko, K. S. Novoselov, T. J. Booth, T. Stauber, N. M. R. Peres, and a. K. Geim, “Fine Structure Constant Defines Visual Transparency of Graphene,” *Science (80-. )*, vol. 320, no. 5881, pp. 1308–1308, 2008.
- [51] A. K. G. S.V. Morozov, K. S. Novoselov, M. I. Katsnelson, F. Schedin, D.C. Elias, J.A. Jaszczak, “Giant Intrinsic Carrier Mobilities in Graphene and Its Bilayer S.V.,” *Phys. Rev. Lett.*, vol. 100, no. 1, p. 016602, 2008.
- [52] A. C. Ferrari, F. Bonaccorso, V. Falco, K. S. Novoselov, S. Roche, P. Bøggild, S. Borini, F. Koppens, V. Palermo, N. Pugno, J. a. Garrido, R. Sordan, A. Bianco, L. Ballerini, M.

- Prato, E. Lidorikis, J. Kivioja, C. Marinelli, T. Ryhänen, A. Morpurgo, J. N. Coleman, V. Nicolosi, L. Colombo, A. Fert, M. Garcia-Hernandez, A. Bachtold, G. F. Schneider, F. Guinea, C. Dekker, M. Barbone, C. Galiotis, A. Grigorenko, G. Konstantatos, A. Kis, M. Katsnelson, C. W. J. Beenakker, L. Vandersypen, A. Loiseau, V. Morandi, D. Neumaier, E. Treossi, V. Pellegrini, M. Polini, A. Tredicucci, G. M. Williams, B. H. Hong, J. H. Ahn, J. M. Kim, H. Zirath, B. J. van Wees, H. van der Zant, L. Occhipinti, A. Di Matteo, I. a. Kinloch, T. Seyller, E. Quesnel, X. Feng, K. Teo, N. Rupesinghe, P. Hakonen, S. R. T. Neil, Q. Tannock, T. Löfwander, and J. Kinaret, “Science and technology roadmap for graphene, related two-dimensional crystals, and hybrid systems,” *Nanoscale*, vol. 7, no. 11, pp. 4598–4810, 2014.
- [53] D. Branski, “Density Functional Theory Calculations for the Monolayer–Bilayer Graphene Heterojunctions,” *Friderico Alexandrinae Sicillvm Academiae*, 2014.
- [54] Y. Hu, F. Li, D. Han, and L. Niu, “Biocompatible Graphene for Bioanalytical Applications,” vol. 2, pp. 11–34, 2015.
- [55] M. Aydin and D. L. Akins, “Geometric and Spectroscopic Properties of Carbon Nanotubes and Boron Nitride Nanotubes,” in *Electronic Properties of Carbon Nanotubes*, 2011, pp. 157–210.
- [56] B. Song, G. Cuniberti, S. Sanvito, and H. Fang, “Nucleobase adsorbed at graphene devices: Enhance bio-sensorics,” *Appl. Phys. Lett.*, vol. 100, no. 6, pp. 6–10, 2012.
- [57] A. K. Nair, S. W. Cranford, and M. J. Buehler, “The minimal nanowire: Mechanical properties of carbyne,” *EPL (Europhysics Lett.)*, vol. 95, no. 1, p. 16002, 2011.
- [58] A. La Torre, A. Botello-Mendez, W. Baaziz, J.-C. Charlier, and F. Banhart, “Strain-induced metal-semiconductor transition observed in atomic carbon chains,” *Nat. Commun.*, vol. 6, no. 6, p. 6636, 2015.
- [59] J. P. Pouget, “The Peierls instability and charge density wave in one-dimensional electronic conductors,” *Comptes Rendus Phys.*, vol. 17, no. 3–4, pp. 332–356, 2016.
- [60] X. Fan, L. Liu, J. Y. Lin, Z. Shen, and J. L. Kuo, “Density functional theory study of finite carbon chains,” *ACS Nano*, vol. 3, no. 11, pp. 3788–3794, 2009.

- [61] K. K. Irikura, “Experimental vibrational zero-point energies: Diatomic molecules,” *J. Phys. Chem. Ref. Data*, vol. 36, no. 2, pp. 389–397, 2007.
- [62] G. P. Zhang, X. W. Fang, Y. X. Yao, C. Z. Wang, Z. J. Ding, and K. M. Ho, “Electronic structure and transport of a carbon chain between graphene nanoribbon leads,” *J. Phys. Condens. Matter*, vol. 23, no. 2, p. 025302, 2011.
- [63] S. Akca, A. Foroughi, D. Frochtzwajg, and H. W. C. Postma, “Competing interactions in dna assembly on graphene,” *PLoS One*, vol. 6, no. 4, pp. 4–7, 2011.
- [64] X. Chen, I. Rungger, C. D. Pemmaraju, U. Schwingenschlogl, and S. Sanvito, “First-principles study of high-conductance DNA sequencing with carbon nanotube electrodes,” *Phys. Rev. B*, vol. 85, no. 11, p. 115436, 2012.
- [65] T. Ohshiro, K. Matsubara, M. Tsutsui, M. Furuhashi, M. Taniguchi, and T. Kawai, “Single-molecule electrical random resequencing of DNA and RNA,” *Sci. Rep.*, vol. 2, p. 501, 2012.
- [66] H. Jeong, H. Seul Kim, S. H. Lee, D. Lee, Y. Hoon Kim, and N. Huh, “Quantum interference in DNA bases probed by graphene nanoribbons,” *Appl. Phys. Lett.*, vol. 103, no. 2, 2013.
- [67] S. Banerjee, J. Wilson, J. Shim, M. Shankla, E. A. Corbin, A. Aksimentiev, and R. Bashir, “Slowing DNA transport using graphene-DNA interactions,” *Adv. Funct. Mater.*, vol. 25, no. 6, pp. 936–946, 2015.
- [68] N. S. Green and M. L. Norton, “Interactions of DNA with graphene and sensing applications of graphene field-effect transistor devices: A review,” *Anal. Chim. Acta*, vol. 853, no. 1, pp. 127–142, 2015.
- [69] X. Qiu, F. Ke, R. Timsina, C. Y. Khripin, and M. Zheng, “Attractive Interactions Between DNA-Carbon Nanotube Hybrids in Monovalent Salts,” *J. Phys. Chem. C*, vol. 120, no. 25, pp. 13831–13835, 2016.
- [70] A. A. Kletsov, E. G. Glukhovskoy, A. S. Chumakov, and J. V. Ortiz, “Ab initio electron propagator calculations of transverse conduction through DNA nucleotide bases in 1-nm nanopore corroborate third generation sequencing,” *Biochim. Biophys. Acta - Gen. Subj.*,

- vol. 1860, no. 1, pp. 140–145, 2016.
- [71] “NAMMD 2.11 Release Notes.” [Online]. Available: <http://www.ks.uiuc.edu/Research/namd/2.11/notes.html>. [Accessed: 29-Apr-2017].
- [72] H. L. McFarland, T. Ahmed, J. X. Zhu, A. V. Balatsky, and J. T. Haraldsen, “First-Principles Investigation of Nanopore Sequencing Using Variable Voltage Bias on Graphene-Based Nanoribbons,” *J. Phys. Chem. Lett.*, vol. 6, no. 13, pp. 2616–2621, 2015.
- [73] T. Ahmed, S. Kilina, T. Das, J. T. Haraldsen, J. J. Rehr, and A. V. Balatsky, “Electronic fingerprints of DNA bases on graphene,” *Nano Lett.*, vol. 12, no. 2, pp. 927–931, 2012.
- [74] J. H. Lee, Y. K. Choi, H. J. Kim, R. H. Scheicher, and J. H. Cho, “Physisorption of DNA nucleobases on h -BN and graphene: VdW-corrected DFT calculations,” *J. Phys. Chem. C*, vol. 117, no. 26, pp. 13435–13441, 2013.
- [75] S. Garaj, W. Hubbard, a Reina, J. Kong, D. Branton, and J. a Golovchenko, “Graphene as a subnanometre trans-electrode membrane.,” *Nature*, vol. 467, no. 7312, pp. 190–193, 2010.
- [76] S. Akca, A. Foroughi, D. Frochtzwaig, and H. W. C. Postma, “Competing interactions in dna assembly on graphene,” *PLoS One*, vol. 6, no. 4, 2011.
- [77] Y. Shamoo, “Single-stranded DNA-binding Proteins,” *Encyclopedia of Life Sciences*. John Wiley & Sons, Ltd, pp. 1–7, 2002.
- [78] G. V. Soni and A. Meller, “Progress toward ultrafast DNA sequencing using solid-state nanopores,” in *Clinical Chemistry*, 2007, vol. 53, no. 11, pp. 1996–2001.
- [79] P. Giannozzi and C. Cavazzoni, “Large-scale computing with quantum ESPRESSO,” *Nuovo Cim. della Soc. Ital. di Fis. C*, vol. 32, no. 2, pp. 49–52, 2009.
- [80] P. Giannozzi, S. Baroni, N. Bonini, M. Calandra, R. Car, C. Cavazzoni, D. Ceresoli, G. L. Chiarotti, M. Cococcioni, I. Dabo, A. Dal Corso, S. de Gironcoli, S. Fabris, G. Fratesi, R. Gebauer, U. Gerstmann, C. Gougoussis, A. Kokalj, M. Lazzeri, L. Martin-Samos, N. Marzari, F. Mauri, R. Mazzarello, S. Paolini, A. Pasquarello, L. Paulatto, C. Sbraccia, S. Scandolo, G. Sclauzero, A. P. Seitsonen, A. Smogunov, P. Umari, and R. M.



- Wentzcovitch, “QUANTUM ESPRESSO: a modular and open-source software project for quantum simulations of materials.,” *J. Phys. Condens. Matter*, vol. 21, no. 39, p. 395502, 2009.
- [81] A. A. Mostofi, J. R. Yates, Y.-S. Lee, I. Souza, D. Vanderbilt, and N. Marzari, “Wannier90: A Tool for Obtaining Maximally-Localised Wannier Functions,” no. February 2008, pp. 1–27, 2007.
- [82] W. Y. Kim and K. S. Kim, “Carbon nanotube, graphene, nanowire, and molecule-based electron and spin transport phenomena using the nonequilibrium Green’s function method at the level of first principles theory,” *J. Comput. Chem.*, vol. 29, no. 7, pp. 1073–1083, 2008.
- [83] Y. Xue, S. Datta, and M. A. Ratner, “First-principles based matrix Green’s function approach to molecular electronic devices: general formalism,” *Chem. Phys.*, vol. 281, no. 2–3, pp. 151–170, 2002.
- [84] Y. Xue, S. Datta, and M. a Ratner, “First-Principles Based Matrix-Green’s Function Approach to Molecular Electronic Devices: General Formalism,” *Chem. Phys.*, vol. 281, pp. 151–170, 2001.
- [85] C. J. Cramer and D. G. Truhlar, “Density functional theory for transition metals and transition metal chemistry.,” *Phys. Chem. Chem. Phys.*, vol. 11, no. 46, pp. 10757–10816, 2009.
- [86] E. J. Baerends, “Perspective on ‘Self-consistent equations including exchange and correlation effects,’” *Theor. Chem. Acc.*, vol. 103, no. 3, pp. 265–269, 2000.
- [87] A. K. Rajagopal and J. Callaway, “Inhomogeneous electron gas,” *Phys. Rev. B*, vol. 7, no. 5, pp. 1912–1919, 1973.
- [88] A. D. Becke, “Perspective: Fifty years of density-functional theory in chemical physics,” *J. Chem. Phys.*, vol. 140, no. 18, p. 18A301, 2014.
- [89] “The Many-Electron Schrödinger Equation.” [Online]. Available: [http://cmt.dur.ac.uk/sjc/thesis\\_mcg/node7.html](http://cmt.dur.ac.uk/sjc/thesis_mcg/node7.html). [Accessed: 28-Jul-2017].

- [90] A. Calzolari, N. Marzari, I. Souza, and M. Buongiorno Nardelli, “Ab initio transport properties of nanostructures from maximally localized Wannier functions,” *Phys. Rev. B*, vol. 69, no. 3, p. 035108, 2004.
- [91] D. Hamann, M. Schlüter, and C. Chiang, “Norm-Conserving Pseudopotentials,” *Phys. Rev. Lett.*, vol. 43, no. 20, pp. 1494–1497, 1979.
- [92] L. Kleinman and D.M. Bylander, “Efficacious Form for Model Pseudopotentials,” *Phys. Rev. Lett.* 17, vol. 59, no. 7, pp. 807–811, 1987.
- [93] D. Vanderbilt, “Soft self-consistent pseudopotentials in a generalized eigenvalue formalism,” *Phys. Rev. B*, vol. 41, no. 11, pp. 7892–7895, 1990.
- [94] N. Marzari, A. A. Mostofi, J. R. Yates, I. Souza, and D. Vanderbilt, “Maximally localized Wannier functions: Theory and applications,” *Rev. Mod. Phys.*, vol. 84, no. 4, pp. 1419–1475, 2012.
- [95] M. Shelley, N. Poilvert, A. A. Mostofi, and N. Marzari, “Automated quantum conductance calculations using maximally-localised Wannier functions,” *Comput. Phys. Commun.*, vol. 182, no. 10, pp. 2174–2183, 2011.
- [96] S. Mallajosyula, J. Lin, D. Cox, S. Pati, and R. Singh, “Sequence Dependent Electron Transport in Wet DNA: Ab initio and Molecular Dynamics Studies,” *Phys. Rev. Lett.*, vol. 101, no. 17, p. 176805, 2008.
- [97] “electron volt.” [Online]. Available: <https://www.unitjuggler.com/convert-energy-from-eV-to-J.html>. [Accessed: 06-Jun-2017].
- [98] H. Zhang, H. Xu, X. Ni, S. L. Peng, Q. Liu, and F. P. Ouyang, “Detection of nucleic acids by graphene-based devices: A first-principles study,” *J. Appl. Phys.*, vol. 115, no. 13, 2014.
- [99] “definition of an electron volt | Science Mission Directorate.” [Online]. Available: [https://science.nasa.gov/science-news/science-at-nasa/2001/comment2\\_ast15jan\\_1](https://science.nasa.gov/science-news/science-at-nasa/2001/comment2_ast15jan_1). [Accessed: 06-Jun-2017].
- [100] I. Souza, N. Marzari, and D. Vanderbilt, “Maximally localized Wannier functions for

- entangled energy bands,” *Phys. Rev. B*, vol. 65, no. 3, p. 035109, 2001.
- [101] A. A. Mostofi, J. R. Yates, G. Pizzi, and Y. Lee, “An updated version of wannier90 : A Tool for Obtaining Maximally-Localised Wannier Functions,” *Comput. Phys. Commun.*, vol. 185, no. 8, pp. 2309–2310, 2014.
- [102] J. Perdew, K. Burke, and M. Ernzerhof, “Generalized Gradient Approximation Made Simple.,” *Phys. Rev. Lett.*, vol. 77, no. 18, pp. 3865–3868, 1996.
- [103] “nanoengineer-1 download | SourceForge.net.” [Online]. Available: <https://sourceforge.net/projects/nanoengineer-1/>. [Accessed: 24-Jul-2017].
- [104] J. P. Perdew, K. Burke, and M. Ernzerhof, “Generalized Gradient Approximation Made Simple [Phys. Rev. Lett. 77, 3865 (1996)],” *Phys. Rev. Lett.*, vol. 78, no. 7, pp. 1396–1396, 1996.
- [105] X. Liu, G. Zhang, and Y. W. Zhang, “Tunable mechanical and thermal properties of one-dimensional carbyne chain: Phase transition and microscopic dynamics,” *J. Phys. Chem. C*, vol. 119, no. 42, pp. 24156–24164, 2015.
- [106] S. Yang and M. Kertesz, “Bond length alternation and energy band gap of polyyne,” *J. Phys. Chem. A*, vol. 110, no. 31, pp. 9771–9774, 2006.
- [107] Á. Ruzsnyák, V. Zólyomi, J. Kürti, S. Yang, and M. Kertesz, “Bond-length alternation and charge transfer in a linear carbon chain encapsulated within a single-walled carbon nanotube,” *Phys. Rev. B - Condens. Matter Mater. Phys.*, vol. 72, no. 15, pp. 1–6, 2005.
- [108] B. Song, S. Sanvito, and H. Fang, “Anomalous I-V curve for mono-atomic carbon chains,” *New J. Phys.*, vol. 12, 2010.
- [109] P. Xie, Q. Xiong, Y. Fang, Q. Qing, and C. M. Lieber, “Local electrical potential detection of {DNA} by nanowire-nanopore sensors,” *Nat. Nanotechnol.*, vol. 7, no. 2, pp. 119–125, 2012.
- [110] B. Song, S. Sanvito, and H. Fang, “Anomalous I – V curve for mono-atomic carbon chains,” *New J. Phys.*, vol. 12, no. 10, p. 103017, 2010.
- [111] W. Ren, H. Chen, Q. Sun, X. Tang, S. C. Lim, J. Huang, and H. Song, “Structural Basis of

- SOSS1 Complex Assembly and Recognition of ssDNA,” *Cell Rep.*, vol. 6, no. 6, pp. 982–991, Mar. 2014.
- [112] S. Chang, S. Huang, J. He, F. Liang, P. Zhang, S. Li, X. Chen, O. Sankey, and S. Lindsay, “Electronic signatures of all four DNA nucleosides in a tunneling gap,” *Nano Lett.*, vol. 10, no. 3, pp. 1070–1075, 2010.
- [113] Z. J. Qi, C. Daniels, S. J. Hong, Y. W. Park, V. Meunier, M. Drndic, and A. T. C. Johnson, “Electronic transport of recrystallized freestanding graphene nanoribbons,” *ACS Nano*, vol. 9, no. 4, pp. 3510–3520, 2015.
- [114] M. Sheng, P. Maragakis, C. Papaloukas, and E. Kaxiras, “DNA nucleoside interaction and identification with carbon nanotubes,” *Nano Lett.*, vol. 7, no. 1, pp. 45–50, 2007.
- [115] S. Gowtham, R. H. Scheicher, R. Ahuja, R. Pandey, and S. P. Karna, “Physisorption of nucleobases on graphene: Density-functional calculations,” *Phys. Rev. B - Condens. Matter Mater. Phys.*, vol. 76, no. 3, pp. 2–5, 2007.
- [116] D. Le, A. Kara, E. Schröder, P. Hyldgaard, and T. S. Rahman, “Physisorption of nucleobases on graphene: a comparative van der Waals study,” *J. Phys. Condens. Matter*, vol. 24, p. 424210, 2012.
- [117] A. Das, A. K. Sood, P. K. Maiti, M. Das, R. Varadarajan, and C. N. R. Rao, “Binding of nucleobases with single-walled carbon nanotubes: Theory and experiment,” *Chem. Phys. Lett.*, vol. 453, no. 4–6, pp. 266–273, 2008.
- [118] B. Ma and S. Tung, “AFM Assisted DNA Sequencing Based on Electronic Tunneling,” in *17th annual IEEE-NANOMED*, 2017, pp. 392–397.
- [119] A. D. Bobadilla and J. M. Seminario, “Assembly of a Noncovalent DNA junction on graphene sheets and electron transport characteristics,” *J. Phys. Chem. C*, vol. 117, no. 50, pp. 26441–26453, 2013.
- [120] R. Zikic, “Characterization of the tunneling conductance across DNA bases,” *Phys. Rev. E*, vol. 74, p. 11919, 2006.
- [121] S. P. Thomas, M. S. Pavan, and T. N. Guru Row, “Experimental evidence for ‘carbon

- bonding' in the solid state from charge density analysis.," *Chem. Commun. (Camb)*., vol. 50, no. 1, pp. 49–51, 2014.
- [122] M. Hjort and S. Stafström, "Band resonant tunneling in DNA molecules.," *Phys. Rev. Lett.*, vol. 87, p. 228101, 2001.
- [123] J. Li, Y. Zhang, J. Yang, K. Bi, Z. Ni, D. Li, and Y. Chen, "Molecular dynamics study of DNA translocation through graphene nanopores," *Phys. Rev. E*, vol. 87, no. 6, p. 062707, 2013.
- [124] P. Mignon, S. Loverix, J. Steyaert, and P. Geerlings, "Influence of the  $\pi$ - $\pi$  interaction on the hydrogen bonding capacity of stacked DNA/RNA bases," *Nucleic Acids Res.*, vol. 33, no. 6, pp. 1779–1789, 2005.
- [125] A. L. Ringer, A. Senenko, and C. D. Sherrill, "Models of S / p interactions in protein structures : Comparison of the H<sub>2</sub>S – benzene complex with PDB data," *Protein Sci.*, vol. 16, pp. 2216–2223, 2007.
- [126] C. A. Hunter and J. K. M. Sanders, "The nature of .pi.-.pi. interactions," *J. Am. Chem. Soc.*, vol. 112, no. 14, pp. 5525–5534, 1990.
- [127] R. C. Neuman, "Chapter 1 Organic Molecules and Chemical Bonding from Organic Chemistry," in *Organic Chemistry*, 1999, pp. 1–23.
- [128] K. Momma, F. Izumi, IUCr, P. C. J., H. P. J., C. S. J., P. M. C., N. T., and K. Y., "VESTA 3 for three-dimensional visualization of crystal, volumetric and morphology data," *J. Appl. Crystallogr.*, vol. 44, no. 6, pp. 1272–1276, Dec. 2011.
- [129] J. N. Israelachvili, *Intermolecular and surface forces*. Academic Press, 2011, pp. 71-122.

## Appendix A: Example of Input File for QUANTUM ESPRESSO Calculation

&CONTROL

calculation = 'scf',

restart\_mode= 'from\_scratch',

verbosity = 'high'

pseudo\_dir = '/share/apps/espreso/espreso-5.1/wannier90-1.2/pseudo',

outdir = './',

prefix = '5cc',

tstress = .f.,

tprnfor = .t.,

/

&SYSTEM

ibrav = 0,

cosbc = 0.,

cosac = 0.,

cosab = 0.,

nat = 5,

ntyp = 1,

ecutwfc = 30.,

ecutrho = 240.,

occupations = 'smearing',

smearing = 'gauss',

```

degauss = 0.03,

nspin = 1,

/

&ELECTRONS

mixing_beta = 0.4

electron_maxstep = 1000,

conv_thr = 1.D-10,

/

CELL_PARAMETERS {angstrom}

6.520 0.00 0.00

0.00 1.304 0.00

0.00 0.00 1.304

ATOMIC_SPECIES

C 12.0107 C.pz-vbc.UPF

ATOMIC_POSITIONS {angstrom}

C -14.700 2.190 0.000

C -13.380 2.190 0.000

C -11.946 2.190 0.000

C -10.626 2.190 0.000

C -9.1920 2.190 0.000

K_POINTS {automatic}

10 5 5 0 0 0

```

## Appendix B: Example of Input File for wannier90 Calculation

```
num_bands    = 14
num_wann     = 10
num_iter     = 100

dis_num_iter = 100
dis_win_max  = 10.0
dis_froz_max = 7.5
dis_froz_min = -12.84750

guiding_centres = .true.
mp_grid        = 10 5 5
iprint         = 2
num_dump_cycles = 100
num_print_cycles = 10
transport      = true
transport_mode = bulk
one_dim_axis   = x
dist_cutoff    = 5.5
tran_win_min   = -6.5
tran_win_max   = 6.5
tran_energy_step = 0.01
fermi_energy   = 2.3476
```



```
dist_cutoff_mode = one_dim
translation_centre_frac = 0.0 0.0 0.0

bands_plot = true
bands_plot_format = gnuplot
!search_shells = 50

begin kpoint_path
G 0.00000 0.00000 0.00000 F 0.00000 0.50000 0.00000
end kpoint_path

begin projections
C:sp
end projections

begin unit_cell_cart
Ang
6.312024015 0.000000000 0.000000000
0.000000000 3.245715713 0.000000000
0.000000000 0.000000000 3.245716112
end unit_cell_cart
```

begin atoms\_cart

Ang

C -14.111718038 0.710814132 0.000000000

C -12.849324565 0.710811473 0.000000000

C -11.587001610 0.710807482 0.000000000

C -10.324782002 0.710811141 0.000000000

C -9.062260470 0.710814477 0.000000000

end atoms\_cart

Begin KPoints

0.00000000 0.00000000 0.00000000

0.00000000 0.00000000 0.20000000

0.00000000 0.00000000 0.40000000

0.00000000 0.00000000 0.60000000

0.00000000 0.00000000 0.80000000

0.00000000 0.20000000 0.00000000

0.00000000 0.20000000 0.20000000

0.00000000 0.20000000 0.40000000

0.00000000 0.20000000 0.60000000

0.00000000 0.20000000 0.80000000

0.00000000 0.40000000 0.00000000

0.00000000 0.40000000 0.20000000

0.00000000 0.40000000 0.40000000

0.00000000 0.40000000 0.60000000  
0.00000000 0.40000000 0.80000000  
0.00000000 0.60000000 0.00000000  
0.00000000 0.60000000 0.20000000  
0.00000000 0.60000000 0.40000000  
0.00000000 0.60000000 0.60000000  
0.00000000 0.60000000 0.80000000  
0.00000000 0.80000000 0.00000000  
0.00000000 0.80000000 0.20000000  
0.00000000 0.80000000 0.40000000  
0.00000000 0.80000000 0.60000000  
0.00000000 0.80000000 0.80000000  
0.10000000 0.00000000 0.00000000  
0.10000000 0.00000000 0.20000000  
0.10000000 0.00000000 0.40000000  
0.10000000 0.00000000 0.60000000  
0.10000000 0.00000000 0.80000000  
0.10000000 0.20000000 0.00000000  
0.10000000 0.20000000 0.20000000  
0.10000000 0.20000000 0.40000000  
0.10000000 0.20000000 0.60000000  
0.10000000 0.20000000 0.80000000  
0.10000000 0.40000000 0.00000000

0.10000000 0.40000000 0.20000000  
0.10000000 0.40000000 0.40000000  
0.10000000 0.40000000 0.60000000  
0.10000000 0.40000000 0.80000000  
0.10000000 0.60000000 0.00000000  
0.10000000 0.60000000 0.20000000  
0.10000000 0.60000000 0.40000000  
0.10000000 0.60000000 0.60000000  
0.10000000 0.60000000 0.80000000  
0.10000000 0.80000000 0.00000000  
0.10000000 0.80000000 0.20000000  
0.10000000 0.80000000 0.40000000  
0.10000000 0.80000000 0.60000000  
0.10000000 0.80000000 0.80000000  
0.20000000 0.00000000 0.00000000  
0.20000000 0.00000000 0.20000000  
0.20000000 0.00000000 0.40000000  
0.20000000 0.00000000 0.60000000  
0.20000000 0.00000000 0.80000000  
0.20000000 0.20000000 0.00000000  
0.20000000 0.20000000 0.20000000  
0.20000000 0.20000000 0.40000000  
0.20000000 0.20000000 0.60000000

0.20000000 0.20000000 0.60000000  
0.20000000 0.20000000 0.80000000  
0.20000000 0.40000000 0.00000000  
0.20000000 0.40000000 0.20000000  
0.20000000 0.40000000 0.40000000  
0.20000000 0.40000000 0.60000000  
0.20000000 0.40000000 0.80000000  
0.20000000 0.60000000 0.00000000  
0.20000000 0.60000000 0.20000000  
0.20000000 0.60000000 0.40000000  
0.20000000 0.60000000 0.60000000  
0.20000000 0.60000000 0.80000000  
0.20000000 0.80000000 0.00000000  
0.20000000 0.80000000 0.20000000  
0.20000000 0.80000000 0.40000000  
0.20000000 0.80000000 0.60000000  
0.20000000 0.80000000 0.80000000  
0.30000000 0.00000000 0.00000000  
0.30000000 0.00000000 0.20000000  
0.30000000 0.00000000 0.40000000  
0.30000000 0.00000000 0.60000000  
0.30000000 0.00000000 0.80000000  
0.30000000 0.20000000 0.00000000

0.30000000 0.20000000 0.20000000  
0.30000000 0.20000000 0.40000000  
0.30000000 0.20000000 0.60000000  
0.30000000 0.20000000 0.80000000  
0.30000000 0.40000000 0.00000000  
0.30000000 0.40000000 0.20000000  
0.30000000 0.40000000 0.40000000  
0.30000000 0.40000000 0.60000000  
0.30000000 0.40000000 0.80000000  
0.30000000 0.60000000 0.00000000  
0.30000000 0.60000000 0.20000000  
0.30000000 0.60000000 0.40000000  
0.30000000 0.60000000 0.60000000  
0.30000000 0.60000000 0.80000000  
0.30000000 0.80000000 0.00000000  
0.30000000 0.80000000 0.20000000  
0.30000000 0.80000000 0.40000000  
0.30000000 0.80000000 0.60000000  
0.30000000 0.80000000 0.80000000  
0.40000000 0.00000000 0.00000000  
0.40000000 0.00000000 0.20000000  
0.40000000 0.00000000 0.40000000  
0.40000000 0.00000000 0.60000000

0.40000000 0.00000000 0.80000000  
0.40000000 0.20000000 0.00000000  
0.40000000 0.20000000 0.20000000  
0.40000000 0.20000000 0.40000000  
0.40000000 0.20000000 0.60000000  
0.40000000 0.20000000 0.80000000  
0.40000000 0.40000000 0.00000000  
0.40000000 0.40000000 0.20000000  
0.40000000 0.40000000 0.40000000  
0.40000000 0.40000000 0.60000000  
0.40000000 0.40000000 0.80000000  
0.40000000 0.60000000 0.00000000  
0.40000000 0.60000000 0.20000000  
0.40000000 0.60000000 0.40000000  
0.40000000 0.60000000 0.60000000  
0.40000000 0.60000000 0.80000000  
0.40000000 0.80000000 0.00000000  
0.40000000 0.80000000 0.20000000  
0.40000000 0.80000000 0.40000000  
0.40000000 0.80000000 0.60000000  
0.40000000 0.80000000 0.80000000  
0.50000000 0.00000000 0.00000000  
0.50000000 0.00000000 0.20000000

0.50000000 0.00000000 0.40000000  
0.50000000 0.00000000 0.60000000  
0.50000000 0.00000000 0.80000000  
0.50000000 0.20000000 0.00000000  
0.50000000 0.20000000 0.20000000  
0.50000000 0.20000000 0.40000000  
0.50000000 0.20000000 0.60000000  
0.50000000 0.20000000 0.80000000  
0.50000000 0.40000000 0.00000000  
0.50000000 0.40000000 0.20000000  
0.50000000 0.40000000 0.40000000  
0.50000000 0.40000000 0.60000000  
0.50000000 0.40000000 0.80000000  
0.50000000 0.60000000 0.00000000  
0.50000000 0.60000000 0.20000000  
0.50000000 0.60000000 0.40000000  
0.50000000 0.60000000 0.60000000  
0.50000000 0.60000000 0.80000000  
0.50000000 0.80000000 0.00000000  
0.50000000 0.80000000 0.20000000  
0.50000000 0.80000000 0.40000000  
0.50000000 0.80000000 0.60000000  
0.50000000 0.80000000 0.80000000



0.60000000 0.00000000 0.00000000  
0.60000000 0.00000000 0.20000000  
0.60000000 0.00000000 0.40000000  
0.60000000 0.00000000 0.60000000  
0.60000000 0.00000000 0.80000000  
0.60000000 0.20000000 0.00000000  
0.60000000 0.20000000 0.20000000  
0.60000000 0.20000000 0.40000000  
0.60000000 0.20000000 0.60000000  
0.60000000 0.20000000 0.80000000  
0.60000000 0.40000000 0.00000000  
0.60000000 0.40000000 0.20000000  
0.60000000 0.40000000 0.40000000  
0.60000000 0.40000000 0.60000000  
0.60000000 0.40000000 0.80000000  
0.60000000 0.60000000 0.00000000  
0.60000000 0.60000000 0.20000000  
0.60000000 0.60000000 0.40000000  
0.60000000 0.60000000 0.60000000  
0.60000000 0.60000000 0.80000000  
0.60000000 0.80000000 0.00000000  
0.60000000 0.80000000 0.20000000  
0.60000000 0.80000000 0.40000000

0.60000000 0.80000000 0.60000000  
0.60000000 0.80000000 0.80000000  
0.70000000 0.00000000 0.00000000  
0.70000000 0.00000000 0.20000000  
0.70000000 0.00000000 0.40000000  
0.70000000 0.00000000 0.60000000  
0.70000000 0.00000000 0.80000000  
0.70000000 0.20000000 0.00000000  
0.70000000 0.20000000 0.20000000  
0.70000000 0.20000000 0.40000000  
0.70000000 0.20000000 0.60000000  
0.70000000 0.20000000 0.80000000  
0.70000000 0.40000000 0.00000000  
0.70000000 0.40000000 0.20000000  
0.70000000 0.40000000 0.40000000  
0.70000000 0.40000000 0.60000000  
0.70000000 0.40000000 0.80000000  
0.70000000 0.60000000 0.00000000  
0.70000000 0.60000000 0.20000000  
0.70000000 0.60000000 0.40000000  
0.70000000 0.60000000 0.60000000  
0.70000000 0.60000000 0.80000000  
0.70000000 0.80000000 0.00000000

0.70000000 0.80000000 0.20000000  
0.70000000 0.80000000 0.40000000  
0.70000000 0.80000000 0.60000000  
0.70000000 0.80000000 0.80000000  
0.80000000 0.00000000 0.00000000  
0.80000000 0.00000000 0.20000000  
0.80000000 0.00000000 0.40000000  
0.80000000 0.00000000 0.60000000  
0.80000000 0.00000000 0.80000000  
0.80000000 0.20000000 0.00000000  
0.80000000 0.20000000 0.20000000  
0.80000000 0.20000000 0.40000000  
0.80000000 0.20000000 0.60000000  
0.80000000 0.20000000 0.80000000  
0.80000000 0.40000000 0.00000000  
0.80000000 0.40000000 0.20000000  
0.80000000 0.40000000 0.40000000  
0.80000000 0.40000000 0.60000000  
0.80000000 0.40000000 0.80000000  
0.80000000 0.60000000 0.00000000  
0.80000000 0.60000000 0.20000000  
0.80000000 0.60000000 0.40000000  
0.80000000 0.60000000 0.60000000

0.80000000 0.60000000 0.80000000  
0.80000000 0.80000000 0.00000000  
0.80000000 0.80000000 0.20000000  
0.80000000 0.80000000 0.40000000  
0.80000000 0.80000000 0.60000000  
0.80000000 0.80000000 0.80000000  
0.90000000 0.00000000 0.00000000  
0.90000000 0.00000000 0.20000000  
0.90000000 0.00000000 0.40000000  
0.90000000 0.00000000 0.60000000  
0.90000000 0.00000000 0.80000000  
0.90000000 0.20000000 0.00000000  
0.90000000 0.20000000 0.20000000  
0.90000000 0.20000000 0.40000000  
0.90000000 0.20000000 0.60000000  
0.90000000 0.20000000 0.80000000  
0.90000000 0.40000000 0.00000000  
0.90000000 0.40000000 0.20000000  
0.90000000 0.40000000 0.40000000  
0.90000000 0.40000000 0.60000000  
0.90000000 0.40000000 0.80000000  
0.90000000 0.60000000 0.00000000  
0.90000000 0.60000000 0.20000000

0.90000000 0.60000000 0.40000000

0.90000000 0.60000000 0.60000000

0.90000000 0.60000000 0.80000000

0.90000000 0.80000000 0.00000000

0.90000000 0.80000000 0.20000000

0.90000000 0.80000000 0.40000000

0.90000000 0.80000000 0.60000000

0.90000000 0.80000000 0.80000000

End KPoints

## **Appendix C: Description of Research for Popular Publication**

### **A Numerical Study of the Interaction Between One Dimensional Carbon Chain and Single Stranded DNA**

The ability to sequence the human genome rapidly and inexpensively is of great demand around the world. One hope is to precisely sequence the whole genome as a part of routine medical processes at clinics and health centers for less than \$1000. Several universities and laboratories in the United States, United Kingdom, France, Germany, Japan, and China have put much efforts into such goal. Zeina Salman who is a PhD student in Microelectronics-Photonics program at the University of Arkansas is one of many who have been working to accomplish such a goal.

The question is why is sequencing the human genome important? Why all this interest or effort? Simply, the genome is described as a book that has all the information about the history of organisms. This information is inherited. If one can read the historical information in this book and combine it with the present, one can make predications for the future. This is very useful in curing and predicting or possibly preventing diseases. One way of reading the information is using electrical measurement based sensors. These sensors monitor the current passing through the sensing element when DNA passes through a nanofluidic channel. DNA is a part of the genome and has four different bases with 0.34 nm space between them. The different bases are guanine (G), adenine (A), thymine (T), and cytosine (C). The length of a DNA depends on the number of bases included. Each of these four bases generates a unique electrical signal when they are pulled through the channel. Now, is there any device in the market? The answer is yes. There are some devices, but they have issues like limited accuracy or resolution. The resolution of the electrical sensors depends on the width of the sensing element. For high

resolution, the sensing element should be of a width that is comparable with the distance between two sequential bases. Zeina has been working under the guidance of Dr. Steve Tung and Dr. Arun Nair for about four years on examining a material that can be used in such a device. Specifically, the goal of her research is to investigate the possibility of using a one-dimensional carbon chain known as carbyne as a sensing element in nanofluidic devices that can sequence the genome. Before investing energy and resources into using such low dimensional material, Zeina numerically explored whether the interactions between carbyne and different DNA bases would produce distinguishable electrical signals DNA detection. According to Ms. Salman, *“It is motivating to work on such nanoscale material that could have huge impact on society.”*

For the last four years, Zeina has been using simulation codes that are available at the High-Performance Computing Center at the University of Arkansas (AHPCC). The codes that have been used are QUNATUM ESPRESSO and wannier90. The idea is to calculate the electrical current for the simulated models in two cases. The first case is the control model that consists of a chain of 16 carbon atoms. The second case is the control model with one base of the four bases. Analyzing the differences in the electrical current can be used to uniquely sense each base. Each base is placed about 2 Å below the chain. The angle between the base plane and the chain is considered as 0° for one study and 90° for another study. Also, the research includes five different distances between base A or C and the chain to investigate the strength of the interaction force between the bases and the chain. The research involves examining a different structure of the carbyne. The second structure has a chain of 16 carbon atoms with two sheets of graphene attached on both sides. Graphene is a two-dimensional sheet of carbon atoms that form a hexagonal structure. Different ssDNA bases are placed individually within the model to test its

effects on the electrical signal produced by carbyne. Carbyne is also compared with graphene to examine its sensitivity compared with graphene when the width is reduced.

This project has shown that carbyne may be used as a sensing element in the electrical sensors to sequence DNA. The four different bases induced distinguishable electrical signals at different orientations and distances from the chain. Zeina expects that carbyne would serve as a highly sensitive element in DNA sequencing devices. Having such sequencing devices available at clinics, health professionals will be able to personalize patient treatment based on their genome sequence. The impact of this project is not limited to identifying and curing genetic diseases, but it can also detect cancer cells at early stages.



## **Appendix D: Executive Summary of Newly Created Intellectual Property**

The newly created intellectual property during this research include the following items and should be considered from both a patent and commercialization perspective:

1. A numerical simulation method to simulate the interaction between the one-dimensional carbyne chain and ssDNA bases.
2. The electrical properties associated with the interaction between the one-dimensional carbyne chain and ssDNA bases.

## **Appendix E: Potential Patent and Commercialization Aspects of Listed Intellectual Property Items**

### **E.1. Patentability of Intellectual Property**

The newly created intellectual property items listed in Appendix D cannot be patented as the mathematical formulas, models, and algorithms are not patentable.

### **E.2. Commercialization Prospects**

Not applicable

### **E.3 Possible Prior Disclosure of IP**

Not applicable

## **Appendix F: Broader Impact of Research**

### **F.1 Applicability of Research Methods to Other Problems**

Carbyne chains can be used in many electrical measurement based bio-sensing devices for a variety of biomedical applications including DNA sequencing. The knowledge of the electrical properties associated with the interaction between DNA and carbyne contributes toward further improvement of sequencing devices. One of several applications of DNA sequencing is cancer diagnosis at early stages. A sensing element as narrow as the carbyne chain could distinguish with high resolution the cancerous cells from the healthy cells based on the electrical signals produced by them. Also, precisely uncovering the information of individuals' genes using a device that includes carbyne could help health professionals select the most appropriate drugs for them. The feasibility of truly using such a one-dimensional nanowire in DNA sequencing devices would provide the health industry with fast and cost-effective sequencing devices for cancer detections and personalized drug prescriptions.

### **F.2 Impact of Research Results on U.S. and Global Society**

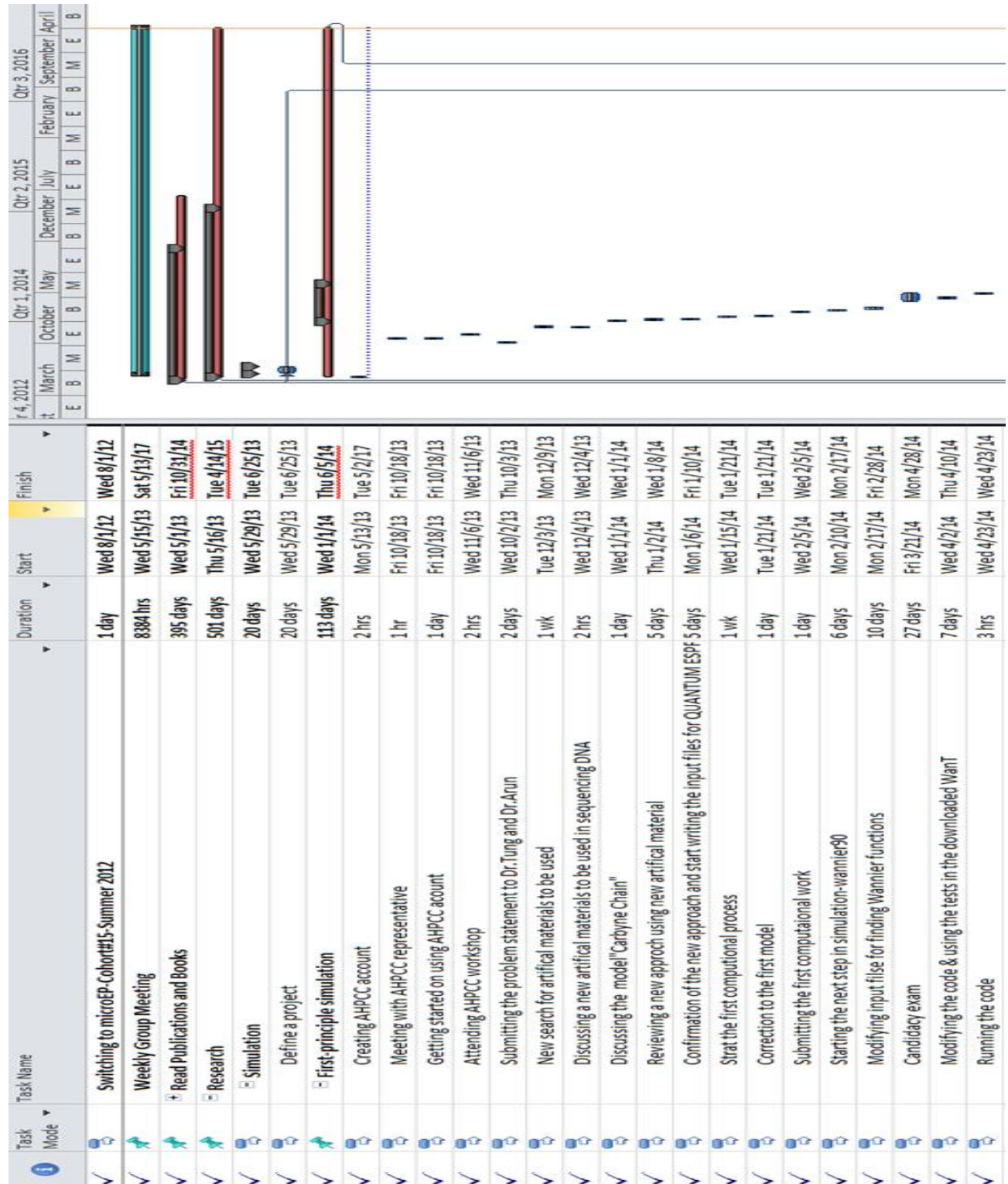
Having a sequencing device with high resolution would lead to significant development in the health industry. This research provides valuable information for experimentalists who have been searching for nanoscale material that can be used as a sensing element for DNA sequencing devices. Being able to extract the genetic information of an individual could lead to better cures for different diseases as well as early diagnosis for a variety of illnesses such as diabetes and cancer. Improvements in this research could lead to the development of robust, accurate, cost effective, and rapid sequencing devices which would revolutionize the health systems around the globe.

### **F.3 Impact of Research Results on the Environment**



























This research has no harmful effects on the environment. The research focuses on numerically investigating the interaction between carbyne and different ssDNA bases. Since carbyne can be produced experimentally via unraveling graphene nanoribbons, carbyne can be considered as a graphene based nanomaterial. Graphene based nanomaterials and devices could be toxic and might escalate environmental concerns regarding the waste associated with it when produced in large scales [1].

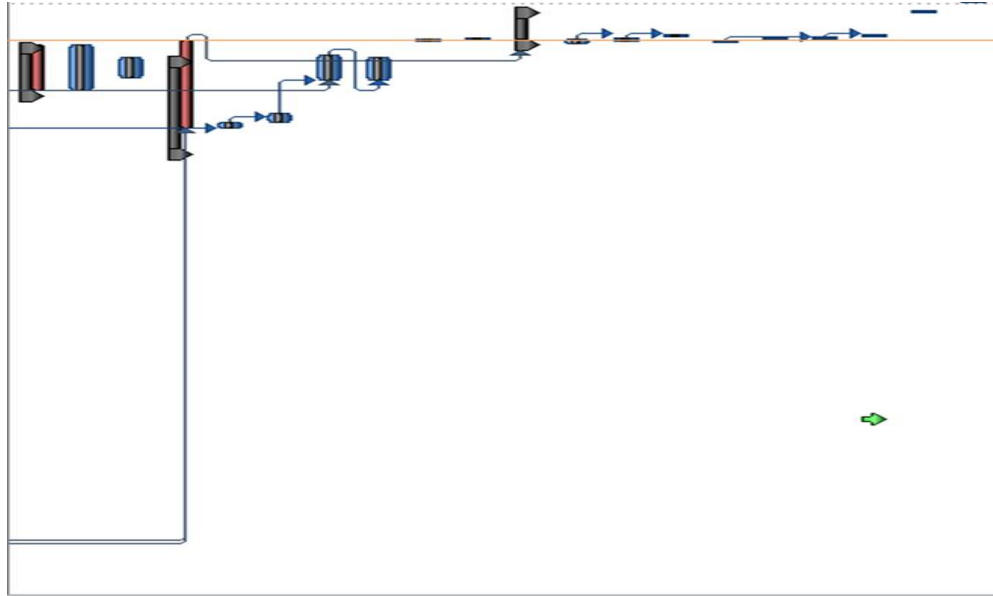
1. R. Arvidsson, S. Molander, and B. A. Sandén, “Review of Potential Environmental and Health Risks of the Nanomaterial Graphene,” *Hum. Ecol. Risk Assess. An Int. J.*, no. November 2011, p. 130313080735004, 2013.

## Appendix G: Microsoft Project for PhD MicroEP Degree Plan



✓		Debugging the code to rerun it	4 wks	Mon 6/2/14	Fri 6/27/14	
✓		<input type="checkbox"/> Milestone one: First principle simulation ( Minimum Goal)	376 days	Thu 10/30/14	Thu 4/7/16	
✓		<input type="checkbox"/> Task one: Calculating the tunneling currents	376 days	Thu 10/30/14	Thu 4/7/16	
✓		<input type="checkbox"/> Subtask one: Many body wave functions	376 days	Thu 10/30/14	Thu 4/7/16	
✓		Scf & nscf parts of the plane wave functions was found for 4 carbon atoms cahi	3 days	Thu 10/30/14	Mon 11/3/14	
✓		Converting the plane wave functions into wannier localized wave functions	4 mons	Fri 11/21/14	Thu 3/12/15	
✓		Comparing the resulted wave functions and tunneling current to published o	4 mons	Fri 11/21/14	Thu 3/12/15	
✓		Inserting bases on ssDNA into different structures of carbyne chains	3 mons	Mon 8/3/15	Fri 10/23/15	
✓		Comparing and analysing the differences between quantum conductance whe	12 days	Fri 10/9/15	Mon 10/26/15	
✓		Contacting the code's owners to verify the method required to insert ssDNA w	18 mons	Fri 11/21/14	Thu 4/7/16	
✓		<input type="checkbox"/> Subtask two: Plane wave basis set & tunneling currents	25 days	Thu 3/12/15	Wed 4/15/15	
✓		Comparing and analysing the resulted data	5 wks	Thu 3/12/15	Wed 4/15/15	
✓		<input type="checkbox"/> Milestone two: MD simulation	132 days	Tue 9/1/15	Wed 3/2/16	
✓		<input type="checkbox"/> Task one: Defining the simulation cell and boundary conditions	353 days	Tue 9/1/15	Tue 1/3/17	
✓		Collecting more information about software	7 days	Tue 9/1/15	Wed 9/9/15	
✓		Attending workshop in Atlanta for computational biophysics codes	7 days	Mon 11/14/16	Tue 11/22/16	
✓		Downloading all software required for workshop and MD simulation	1 day	Thu 10/20/16	Thu 10/20/16	
✓		<input type="checkbox"/> Task two: Defining the number of atmos	7 days	Thu 9/10/15	Fri 9/18/15	
✓		Defining the structure of the modeling systems that are simulated	7 days	Thu 9/10/15	Fri 9/18/15	
✓		<input type="checkbox"/> Task three: Defining the interactions	14 days	Mon 9/21/15	Thu 10/8/15	
✓		Use available and simple interactions and software to generate the structures fo	30 days	Mon 9/21/15	Fri 10/30/15	
✓		Task four: Minimizing the energy	1 wk	Fri 10/14/16	Thu 10/20/16	
✓		Task five: Choosing the thermodynamic ensemble	2 days	Fri 10/21/16	Mon 10/24/16	
✓		Task six: Running the simulation	2.5 mons	Tue 10/25/16	Fri 12/30/16	
✓		Task seven: Analysis the data	10 days	Mon 1/2/17	Fri 1/13/17	

✓		<input type="checkbox"/> MD simulation using MS	103 days	Sat 11/19/16	Sat 4/8/17
✓		Running the same model systems used earlier in first principle simulation	784 hrs	Thu 12/1/16	Sat 4/15/17
✓		Comparing the results with published results	9.2 wks	Fri 1/6/17	Sat 3/11/17
✓		<input type="checkbox"/> Write Dissertation	194 days	Wed 6/1/16	Fri 2/24/17
✓		Chapter 1: Background of area	3 wks	Sat 8/13/16	Sat 9/3/16
✓		Chapter 2: Description of Project	4.4 wks	Thu 9/1/16	Fri 9/30/16
✓		Chapter 3: Results	55 days	Mon 1/2/17	Sat 3/18/17
✓		Chapter 4: Analysis	50 days	Mon 1/2/17	Fri 3/10/17
✓		Chapter 5: Conclusion	1 day	Thu 4/27/17	Thu 4/27/17
✓		Appendix	1 day	Mon 5/1/17	Mon 5/1/17
		<input type="checkbox"/> END GAME	70 days	Mon 4/17/17	Thu 7/20/17
✓		Review by Major Professor	2.4 wks	Mon 4/17/17	Tue 5/2/17
✓		Correct issues found	5 days	Thu 4/27/17	Wed 5/3/17
✓		Final approval by Major Professor	2 days	Wed 5/10/17	Thu 5/11/17
		Send Title, Abstract & Scheduling Information to MicroEP	1 day	Mon 4/24/17	Mon 4/24/17
		Send dissertation to committee members	1 day	Thu 5/4/17	Thu 5/4/17
		Public Presentation Event	1 day	Thu 5/4/17	Thu 5/4/17
		Defense-Committee	1 day	Fri 5/12/17	Fri 5/12/17
		Graduate School Dead Line	1 day	Thu 7/20/17	Thu 7/20/17
		Graduate	1 day	Mon 8/14/17	Mon 8/14/17



## **Appendix H: Identification of All Software Used in Research and Dissertation Generation**

### Computer # 1

Computer Name: MEEG-RTNG764C

Model: DH57DD

MAC Address: E0:69:95:90:40:24

Location: ENRC3402

Owner: University of Arkansas

There are no serial number and model number associated with this computer because several parts of it have been replaced after being damaged. Therefore, the serial number and model number are shown as “not available” when viewing them.

### Software # 1

Name: NanoEngineer1 (open source)

Downloaded by: Zeina Salman

### Software # 2

Name: vesta (open source)

Downloaded by: Zeina Salman

### Software # 3

Name: Microsoft Office 2016

Purchased by: University of Arkansas

### Computer # 2: Personal laptop

Model Name: 20270

Serial Number: 0807870291

Owner: Zeina Salman

### Software # 1

Name: OriginPro 2016 Student Version

Purchased by: Zeina Salman

Serial Number: GA3S4-6089-7212389

### Software # 2

Name: NanoEngineer1 (open source)



Downloaded by: Zeina Salman

Software # 3

Name: vesta (open source)

Downloaded by: Zeina Salman

Software # 4

Name: Microsoft Office 2016

Purchased by: University of Arkansas via Zeina Salman's student account

## Appendix I: All Publications Published, Submitted and Planned

- **Published**

- Zeina Salman, Arun Nair, and Steve Tung, " Electromechanical Properties of One Dimensional Carbon Chains," 2015 9th IEEE International Conference on Nano/Molecular Medicine & Engineering (NANOMED) IEEE-NANOMED 2015 Conference, 2015.  
Pages: 35 - 38, DOI: [10.1109/NANOMED.2015.7492501](https://doi.org/10.1109/NANOMED.2015.7492501)

- **Submitted**

- Zeina Salman, Arun Nair, and Steve Tung, " One-Dimensional Carbon Chains as Electrical Sensors for Single-Stranded DNA," IEEE-NEMS 2017 Conference, 2017. April 9-12. Los Angeles, CA

- **Planned**

- " Carbyne Chains as Electrical Sensors for DNA Sequencing" is planned to be submitted to Nano Letter. The title is subject to change
- " Modeling of 1D Carbon Chains as Electrical Sensors" is planned to be submitted to Modeling and Nanofabrication of 1D and 2D Materials. The title is subject to change

## Appendix J: Research Abstract in Arabic

### محاكاة رقمية للخصائص الكهربائية المتعلقة بالتأثيرات بين مواد الكربون الأحادية الأبعاد (carbyne) وجزيئات الـ DNA

تعتبر دراسة التأثيرات المتبادلة بين مواد الكربون والجزيئات البيولوجية من مجالات البحوث النشطة في الوقت الحالي. إن لهذه التأثيرات مجالات تطبيق متعددة منها المتحسسات البيولوجية (biosensors) ومتحسسات الـ DNA (sequencers). تلعب الإشارات الكهربائية الصادرة من المتحسس دوراً مهماً وفعالاً عند وجود جزيئات الـ DNA وهي تعتمد على التأثيرات المتبادلة بين المتحسس وجزيئات الـ DNA. يؤثر سمك (عرض) العنصر المتحسس على دقة وجودة الإشارة الصادرة منه عند تصميم أجهزة (DNA sequencers).

إن الغرض من هذا البحث هو دراسة الخصائص الكهربائية المرتبطة والتأثيرات أو التفاعلات بين مواد الكربون الأحادية الأبعاد (كما تسمى الكرباين-carbyne) وجزيئات الـ DNA بطريقة المحاكاة الرقمية. تم حساب الخصائص الكهربائية لمادة الكرباين (carbyne) أولاً ومن ثم إضافة جزيئة واحدة من جزيئات الـ DNA للنظام وحساب الخصائص الكهربائية بعد الإضافة. أدى تحليل ومقارنة النتائج لكلا الحالتين إلى تحديد تأثير جزيئات الـ DNA على الخصائص الكهربائية لمادة الكرباين (carbyne).

اعتمدت طريقة المحاكاة الرقمية في هذا البحث على استخدام First-principle simulation وهي طريقة تعتمد على حل نظرية دوال الكثافة (density functional theory- DFT) ودوال كرين غير المناظرة (non-equilibrium Green's functions-NEGF). شملت الخصائص الكهربائية كل من كثافة مستويات الطاقة ودوال احتمالية الانتقال وأستخدم كليهما لحساب التيار الكهربائي. أثبتت الدراسة أن الخصائص الكهربائية لمادة الكرباين (carbyne) مختلفة عند وجود جزيئات الـ DNA. أزداد التيار الكهربائي بمقدار 3.3 مايكروأمبير عند وجود الجزيئة A في حين أنه تناقص بمقدار 41.1 مايكروأمبير، و14.7 مايكروأمبير، و25.6 مايكروأمبير عند وجود الجزيئات G, T, C على التوالي.

كما أظهرت النتائج أن وضع هذه الجزيئات على مسافات مختلفة من الكرباين (carbyne) يؤدي إلى صدور إشارات كهربائية مختلفة نتيجة اختلاف الخصائص الكهربائية له بسبب وجود المجاميع O, NH<sub>2</sub>, CH الموجودة في تركيب الـ DNA على مسافات مختلفة منه. وشمل البحث أيضاً تطوير نموذج يمثل قوة التأثيرات المتبادلة بين جزيئات الـ DNA والمتحسس (carbyne). كان اتجاه وشكل نموذج القوة مطابق لاتجاه وشكل التيار الكهربائي عند الفولتية -0.85 فولت.

شمل البحث دراسة تأثيرات زوايا الدوران لجزيئات الـ DNA على الخصائص الكهربائية للكرباين (carbyne). أظهرت النتائج أن وضع جزيئات الـ DNA باتجاه طويل يؤدي إلى الحصول على تيار كهربائي مختلف عما يتم الحصول عليه عند وضعهم باتجاه عرضي بالنسبة لسلسلة carbyne حيث اختلف التيار بمقدار 0.0776 ملي أمبير عند وضع الجزيئة A بينما اختلف بمقدار 0.0325 ملي أمبير، و0.0426 ملي أمبير، و0.00305 ملي أمبير عند وضع كل من T, G, C على التوالي عند 0.6 فولت.

يُساهم هذا البحث بشكل فعال في زيادة المعرفة في تطوير أجهزة DNA sequencing ويُمكن من التعجيل في عملية التطور نحو أجهزة فائقة السرعة رخيصة الثمن وذات دقة عالية.